AFRL-RX-WP-TR-2013-0052

CONSORTIUM FOR NANOMATERIALS FOR AEROSPACE COMMERCE AND TECHNOLOGY (CONTACT)

Daniel M. Mittleman, Jun Lou, Junichiro Kono, and Wade Adams
William Marsh Rice University

FEBRUARY 2013
Final Report

AIR FORCE RESEARCH LABORATORY
MATERIALS AND MANUFACTURING DIRECTORATE
WRIGHT-PATTERSON AIR FORCE BASE, OH 45433-7750
AIR FORCE MATERIEL COMMAND
UNITED STATES AIR FORCE

NOTICE AND SIGNATURE PAGE

Using Government drawings, specifications, or other data included in this document for any purpose other than Government procurement does not in any way obligate the U.S. Government. The fact that the Government formulated or supplied the drawings, specifications, or other data does not license the holder or any other person or corporation; or convey any rights or permission to manufacture, use, or sell any patented invention that may relate to them.

Qualified requestors may obtain copies of this report from the Defense Technical Information Center (DTIC) (http://www.dtic.mil)

AFRL-RX-WP-TR-2013-0052 HAS BEEN REVIEWED AND IS APPROVED FOR PUBLICATION IN ACCORDANCE WITH ASSIGNED DISTRIBUTION STATEMENT.

//SIGNATURE//
LAURA S. REA, Program Manager
Soft Matter Materials Branch
Functional Materials Division
Materials & Manufacturing Directorate

//SIGNATURE//
KATIE E. THORP, Chief
Soft Matter Materials Branch
Functional Materials Division
Materials & Manufacturing Directorate

//SIGNATURE//
KAREN R. OLSON, Deputy Chief
Functional Materials Division
Materials & Manufacturing Directorate

This report is published in the interest of scientific and technical information exchange and its publication does not constitute the Government's approval or disapproval of its ideas or findings.

REPORT DOCUMENTATION PAGE

Form Approved
OMB No. 0704-0188

1. REPORT DATE *(DD-MM-YY)*	2. REPORT TYPE	3. DATES COVERED *(From - To)*
February 2013	Final	4 October 2007 – 5 February 2013

4. TITLE AND SUBTITLE
CONSORTIUM FOR NANOMATERIALS FOR AEROSPACE COMMERCE AND TECHNOLOGY (CONTACT)

5a. CONTRACT NUMBER
FA8650-07-2-5061

5b. GRANT NUMBER

5c. PROGRAM ELEMENT NUMBER
62102F

6. AUTHOR(S)
Daniel M. Mittleman, Jun Lou, Junichiro Kono, and Wade Adams (William Marsh Rice University)

5d. PROJECT NUMBER
4347

5e. TASK NUMBER

5f. WORK UNIT NUMBER
X02Z (11500200)

7. PERFORMING ORGANIZATION NAME(S) AND ADDRESS(ES)
William Marsh Rice University
6100 Main St
Houston, Texas 77005-1892

8. PERFORMING ORGANIZATION REPORT NUMBER

9. SPONSORING/MONITORING AGENCY NAME(S) AND ADDRESS(ES)
Air Force Research Laboratory
Materials and Manufacturing Directorate
Wright-Patterson Air Force Base, OH 45433-7750
Air Force Materiel Command
United States Air Force

10. SPONSORING/MONITORING AGENCY ACRONYM(S)
AFRL/RXAS

11. SPONSORING/MONITORING AGENCY REPORT NUMBER(S)
AFRL-RX-WP-TR-2013-0052

12. DISTRIBUTION/AVAILABILITY STATEMENT
Approved for public release; distribution is unlimited.

13. SUPPLEMENTARY NOTES
Approved by 88ABW Public Affairs Office: Case number 88ABW-2013-1682 on 03 APR 13. Report contains color.

14. ABSTRACT

CONTACT was launched in November 2006 under the leadership of Senator Kay Bailey Hutchison. This cooperative research program consisted of AFRL and seven Texas universities including University of Houston, University of Texas at Arlington, University of Texas at Austin, University of Texas at Brownsville, University of Texas at Dallas, University of Texas Pan American, and Rice University. CONTACT was developed to advance research and commercialization of nanomaterials to address the needs of the AFRL and defense and aerospace industry. Four areas of research were identified by the Air Force: 1) Adaptive Coatings and Surface Engineering, 2) Nano Energetics, 3) Electromagnetic Sensors, and 4) Power Generation and Storage. Projects were selected that focused in one or more of these areas. CONTACT began with nine research projects in October 2007 and expanded to 18 projects at its conclusion in February 2013. Other achievements of the program include: fostering a long-term partnership with AFRL; developing relationships with industry through the Industrial Advisory Committee; bolstering student research through the Student Travel Grant Program; and providing general support for participants and their universities in a broad range of activities.

15. SUBJECT TERMS
Consortium for Nanomaterials for Aerospace Commerce and Technology (CONTACT), nanomaterials, nanocomposites, solar cell, Carbon Nanotube (CNT), armchair quantum wire

16. SECURITY CLASSIFICATION OF:			17. LIMITATION OF ABSTRACT:	18. NUMBER OF PAGES	19a. NAME OF RESPONSIBLE PERSON (Monitor)
a. REPORT	b. ABSTRACT	c. THIS PAGE			Laura S. Rea
Unclassified	Unclassified	Unclassified	SAR	166	19b. TELEPHONE NUMBER *(Include Area Code)* (937) 528-8735

REPORT DOCUMENTATION PAGE Cont'd

6. AUTHOR(S)

Karen Lozano, Mircea Chipara, Dumitru Caruntu, and Horacio Vasquez (University of Texas-Pan American)
Venkat Ganesan, Brian Korgel, Allen Bard, Ananth Dodabalapur, and David Vanden Bout (University of Texas at Austin)
Karen Martirosyan, Andreas Hanke, and Malik Rakhmanov (University of Texas at Brownsville)
Dan Luss and Paul Chu (University of Houston)
Weidong Zhou, Zeynep Celik-Butler, and Donald Butler (University of Texas at Arlington)
Anvar Zakhidov, John Ferraris, and Julia Hsu (University of Texas at Dallas)

7. PERFORMING ORGANIZATION NAME(S) AND ADDRESS(ES)

University of Texas-Pan American
1201 W University Drive
Edinburg, TX 78539

University of Texas at Austin
Austin, Texas 78712

University of Texas at Brownsville
80 Fort Brown
Brownsville, Texas 78520

University of Houston
4800 Calhoun Rd.
Houston, TX 77004

University of Texas at Arlington
701 S. Nedderman Drive
Arlington, TX 76019

University of Texas at Dallas
800 W. Campbell Road
Richardson, Texas 75080-3021

TABLE OF CONTENTS

LIST OF FIGURES

LIST OF TABLES

ABSTRACT

The Consortium for Nanomaterials for Aerospace Commerce and Technology (CONTACT) was launched in November 2006 under the leadership of Senator Kay Bailey Hutchison. This cooperative research program comprised of the Air Force Research Laboratory (AFRL) and seven Texas universities including University of Houston, University of Texas at Arlington, University of Texas at Austin, University of Texas at Brownsville, University of Texas at Dallas, University of Texas Pan American, and Rice University. CONTACT was developed to advance research and commercialization of nanomaterials to address the needs of the AFRL and the defense and aerospace industry. Four areas of research were identified by the Air Force: 1) Adaptive Coatings and Surface Engineering, 2) Nano Energetics, 3) Electromagnetic Sensors, and 4) Power Generation and Storage. Projects were selected that focused in one or more of these areas. CONTACT began its first year with nine research projects in October 2007 and expanded to 18 projects at its conclusion in February 2013. Other achievements of the program include: fostering a long-term partnership with AFRL; developing relationships with industry through the Industrial Advisory Committee; bolstering student research through the Student Travel Grant Program; and providing general support for participants and their universities in a host of nanotechnology-related activities.

EXECUTIVE SUMMARY

The Consortium for Nanomaterials for Aerospace Commerce and Technology (CONTACT) began in November 2006 through a $1.4 million Department of Defense grant as a result of U.S. Senator Kay Bailey Hutchison's leadership. CONTACT was created to develop nanotechnology research solutions for current challenges faced by the Air Force and aerospace industry. This cooperative research program involved a collaboration between the Air Force Research Laboratory (AFRL) and seven Texas Universities which included Rice University, University of Houston, and five campuses of University of Texas (Arlington, Austin, Brownsville, Dallas, and Pan American). The program concluded on February 5, 2013.

CONTACT was successful in procuring funding that went to support an increase in research activity and the number of research projects steadily from year to year. The program expanded from the initial nine projects doubling to 18 projects at a funding level of $3.6 million during this final year.

The CONTACT Student Travel Grant program was successful in awarding 74 grants to 52 students at 8 Texas universities. Students from both CONTACT and non-CONTACT schools across the state of Texas have been supported in this program and benefited from the state-of-the-art facilities available at the CONTACT universities.

The CONTACT Industrial Advisory Committee also sustained steady growth with a final membership of 35 participants. These organizations have been an integral part of the program through their participation and contribution in meetings, white paper reviews, and collaborative projects.

CONTACT Annual Review Meetings were organized at various venues including CONTACT university campuses and Wright Patterson Air Force Base. These events were instrumental in reinforcing and strengthening the relationship between CONTACT PIs, Industry members and the Air Force.

The "Nano-at-the-Border" initiative involved the development of the nanotechnology programs in the two CONTACT universities in the South, UT Brownsville and UT Pan American. UT Brownsville experienced the expansion of their physics facilities while receiving significant funding from the National Science Foundation and Department of Defense. UT Pan American was successful in creating start-up companies.

The community of CONTACT Program members and associates is broad and substantial. The program has provided the groundwork for numerous collaborations and new relationships and enterprises to emerge.

1.0 INTRODUCTION

The CONTACT Program or Consortium for Nanomaterials for Aerospace Commerce and Technology was launched in November 2006 through the leadership of Senator Kay Bailey Hutchison. This cooperative program included a partnership between the Air Force Research Laboratory (AFRL) and seven universities in Texas (see Figure 1).

- University of Houston
- University of Texas at Arlington
- University of Texas at Austin
- University of Texas at Brownsville
- University of Texas at Dallas
- University of Texas Pan American
- Rice University

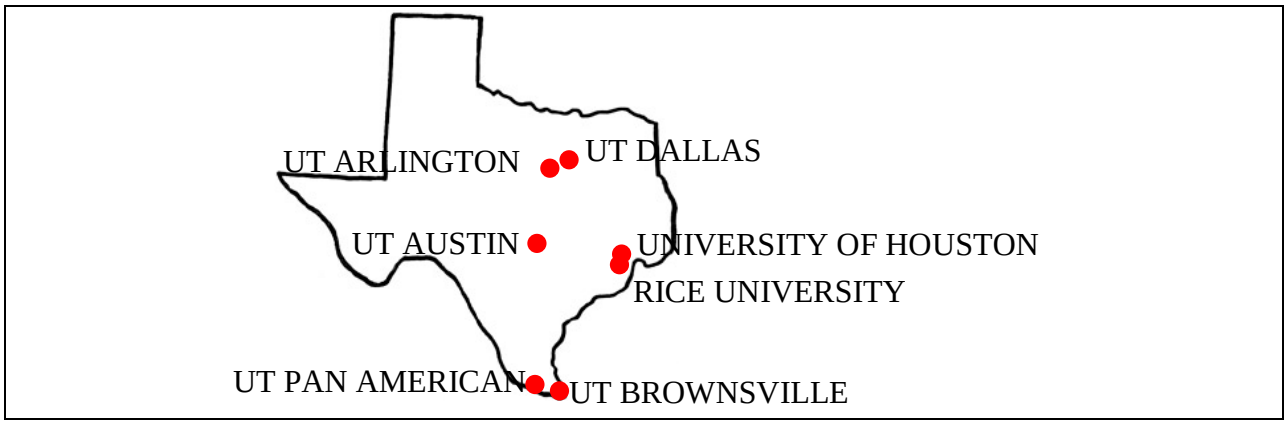

Figure 1. CONTACT Program universities

The CONTACT Director and Executive Committee members along with the AFRL program manager provided the leadership and direction for the program. Principal Investigators and Industrial Advisory Committee members were also vital constituents to the program and were welcomed to participate in the steering meetings. The six universities were subcontractors to Rice University where the Director's office subsisted.

CONTACT aimed to develop nanotechnology applications to address the current challenges facing the Air Force and aerospace industry. Its predecessor program SPRING or the Strategic Partnership for Research in Nanotechnology, was a four-year program with $37.5 million in federal funding aimed to establish nanotechnology infrastructure at Texas universities. The success of SPRING enabled subsequent research programs such as CONTACT to materialize.

CONTACT was successful in procuring steady funding over the course of the four-year program (see Figure 2). The award for the first year (October 2007-2008) was $1.3 million which provided initial support for nine projects to be launched. The following year, the award was increased to $2.4 million which allowed full funding for existing projects and three new projects including an AFRL-funded project for a total of 12 projects. In the third year, CONTACT received $2.4 million again, enough to fund 13 projects. Finally, an exceptional funding increase to $3.6 million was secured in the fourth year permitting an additional five new projects, two of which were separately funded, for a total of 18 projects at the program's conclusion. Despite the

general budgetary challenges during these past years, CONTACT had not only sustained but expanded its research program progressively.

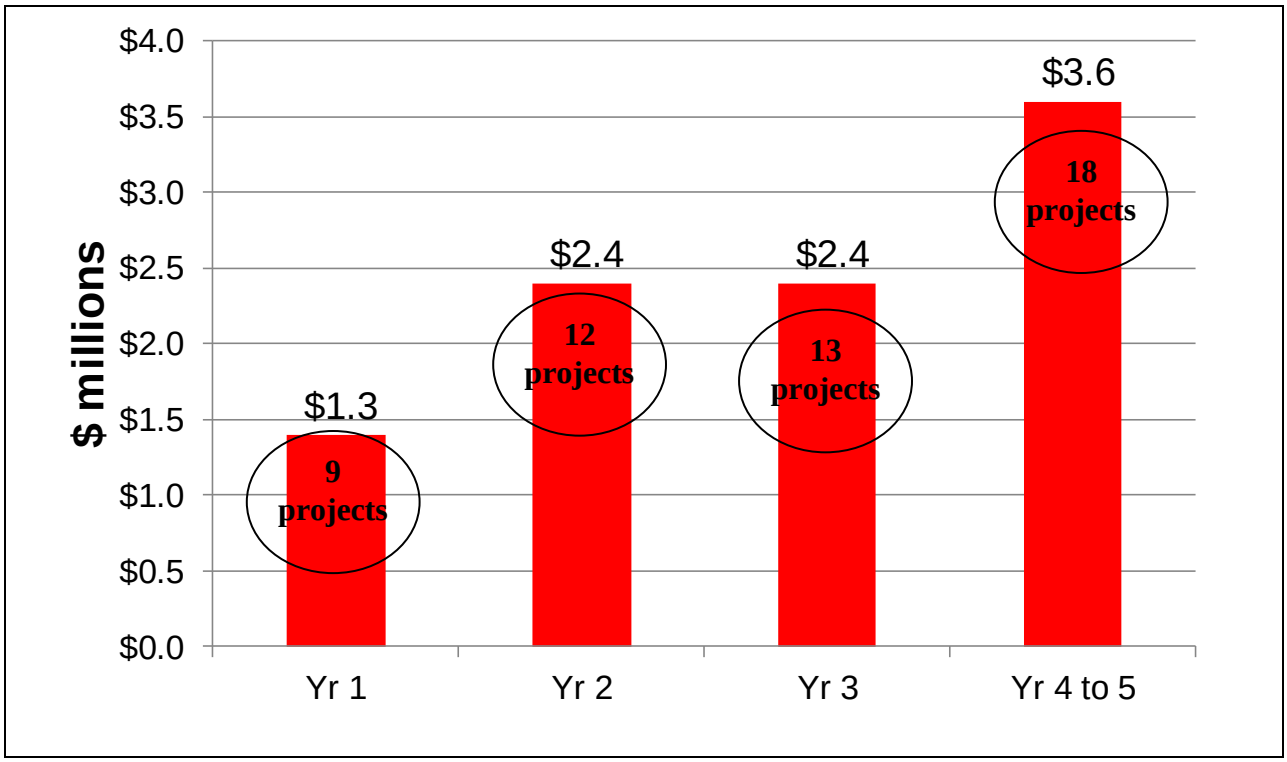

Figure 2. CONTACT funding per year

1.1 Fabulous Four

AFRL identified four areas of research which provided the basis for the CONTACT projects (Table 1). Over 30 white papers from professors from the CONTACT universities were collected and reviewed. Each year, new funding would prompt a review of potential projects from this list and new white papers to be considered for new research projects based on the Air Force's interest.

Table 1. Four areas of research

AREA OF RESEARCH and DESCRIPTION
1. Adaptive Coatings and Surface Engineering
▪ Nanostructured coatings (resist corrosion, reduce drag, repair cracks) ▪ Thermal control, space environment resistant satellites
2. Nano Energetics
▪ High energy propellants and explosives ▪ Use nanoparticles to control the burn rate
3. Electromagnetic Sensors
▪ Devices for optical sensing, communications ▪ Ultraviolet, visible, infra-red, terahertz frequencies
4. Power Generation and Storage
▪ Solar cells, magnets, next generation batteries, capacitors ▪ Enable directed energy weapons, compact power generators

The following describe the Fabulous Four areas in more depth.

1. Adaptive Coatings and Surface Engineering

Nanomaterials provide a technological foundation for the development of adaptive, multifunctional coatings systems. Current nanostructured coatings provide enhanced corrosion protection for aluminum alloys, and have enabled tribological coatings that actively change their mode of lubrication based on the environment. These adaptive coatings utilize different protection mechanisms in the humid air of terrestrial environments and the dry vacuum of space. From these initial successes, a range of enabling new capabilities is possible.

Nanoscience and fabrication will enable coatings that are self cleaning (lotus effect) and self-repairing, and that provide improved corrosion protection, enhanced thermal control, protection from the space environment, and enhanced lubricity. These coatings revolutions arise from the ability of nanostructured materials to modify surface properties and to incorporate diverse functionality and compositions in nano-encapsulated structures.

Nanoscopic materials have marked surface interaction effects, illustrated by two extremes in the behavior of biological systems. The gecko is able to adhere to almost all surfaces (especially when completely inverted) due to the multiple, flexible cilia-like setae which cover their feet. Geckos can adhere to smooth glass surfaces, even when rendered either hydrophobic or hydrophilic. This is sharply contrasted with the nanoscale waxy bifurcations on the surface of a lotus leaf. In this case, the surface resists wetting and adhesion to such a degree that water droplets merely roll from the surface (ultrahydrophobicity). These two disparate results are the likely result of the complex interplay of forces that are size and distance dependent. For example, non-specific attractive forces compete with specific forces at this particular size scale, giving the net result of previously undiscovered surface properties. Nanostructured materials also enable compartmentalization of reactive constituents, such as a bio-decontamination agent, a compound to mediate corrosion or heal material damage.

2. Nano Energetics

Energetic materials are stable compounds that exothermically release energy at an extremely rapid rate in deflagration or detonation reactions upon an initiation stimulus or input. These materials are critical for several AF applications, including munitions, air-breathing propulsion, and spacelift. Nanotechnology has the potential to provide revolutionary capabilities for these applications by using the energetic nanostructure to control the reaction energies, products, and rates. In particular, reactive metal nanoparticles have shown promise in changing the reaction rates for munitions applications while nanoparticle-based fuel additives could provide enhanced capabilities in thermal transport, signature control, efficiency, and reaction rates. Nanostructured propellants have the potential to improve the specific impulse and efficiency of spacelift engines with significant advantages in performance, safety, cost, and structural properties.

3. Electromagnetic Sensors

Quantum Confined Optical Sensors

This topic includes development of quantum engineered materials and devices for high performance optical sensing and communication. Materials utilizing quantum effects from electrons confined in 1, 2 or 3 dimensions, on scales of 100 nm or less, offer new capabilities in optical detector design and performance. Quantum based semiconductor materials can be designed to selectively cover a large portion of the optical spectrum, from ultraviolet wavelengths (10 to 400 nm) to very long infrared wavelengths (15 to 30 μm). These materials could also potentially find uses in the cross over region, from photon detection to electromagnetic wave detection, which occurs at terahertz (THz) frequencies. Quantum confinement based materials enable the ability to manipulate and enhance the optical, electrical, thermal and noise mechanisms to optimize device performance. Photon detectors based on quantum wells, quantum wires, quantum dots, superlattices and carbon nanotubes provide revolutionary new capabilities, such as high sensitivity in a narrow wavelength band, higher operating temperatures in the very long wavelength infrared range, polarization selectivity, and multiple wavelength bands in the same detector pixel. These capabilities reduce costs, system power requirements, radically improve performance, and allow for better tracking, targeting, and identification (ID) of threats. Quantum confined detectors are envisioned for applications in intelligence, surveillance and reconnaissance (ISR), situational awareness, threat warning and tracking, and secure communications.

4. Power Generation and Storage

Nanoscience and technology approaches are being pursued to advance a number of power technologies, such as solar cells; superconducting generator windings, permanent magnets for power generation and utilization, power conditioning devices; energy storage devices; and energy harvesting through thermoelectric/thermionic and piezoelectric means. By taking advantage of the novel and unique optical and electrical properties of nanoparticle hybrid systems and by learning to control the nanoscale morphologies of these systems, significant improvements in device efficiencies for a variety of power system applications can be achieved. Expected benefits include higher power conversion efficiencies of solar cells, higher power and energy densities of next-generation batteries, lighter-weight alternatives to high energy density capacitor systems, more efficient fuel cell systems and “self-powered” load-bearing structures with integrated energy harvest/storage capabilities. These approaches will enable new capabilities for the Air Force and will provide reduced cost and size of power conditioning

devices; enhanced safety and improved reliability of batteries for ground, air and space; compact power for high power applications; higher power for satellites, and dramatic improvements in system-level efficiency.

Table 2 shows all the projects that were operative during the CONTACT program.

Table 2. CONTACT projects, PIs, and active years grouped by Fabulous Four areas

CONTACT PROJECTS and PRINCIPAL INVESTIGATORS	PROGRAM YEAR			
1. Adaptive Coatings and Surface Engineering				
▪ Nanocomposite as Structural Materials Jun Lou, Rice University	1	2	3	4
▪ Electrorheological Properties of Nano-Laden Systems Karen Lozano, UT Pan American; Venkat Ganesan, *UT Austin*	1	2	3	
▪ Investigation of Hybrid Materials for the Development of Sensors and Actuators Karen Lozano and Mircea Chipara, *UT Pan American*				4
▪ Dispersion and Electromechanical Properties of Nano-Laden Systems Venkat Ganesan, *UT Austin*	1	2	3	4
2. Nano Energetics				
▪ Nanoenergetic "Gas-Generator" Karen Martirosyan, *UT Brownsville;* Dan Luss, University of Houston	1	2	3	4
3. Electromagnetic Sensors				
▪ Spectrally-Selective Photonic Infared Sensors for Gas Sensing Weidong Zhou, *UT Arlington*	1	2	3	4
▪ Plasma-Enhanced Terahertz Near-Field Sensing Dan Mittleman, *Rice University*	1	2	3	4
▪ Microarry-Based Hybridization Technology for Biosensors Andreas Hanke, *UT Brownsville*	1	2		
▪ Design and Control of the Electromagnetic Casimir Force in Nanomechanical Systems Andreas Hanke, *UT Brownsville*			3	4
▪ Photothermal/Photopyro/Photoacoustic Effects in Nanowires Paul Chu, University of Houston		2	3	4
▪ Nonuniform Resonator Sensors for Enhanced Sensitivity Dumitru Caruntu and Horacio Vasquez, *UT Pan American*			3	4
▪ Light Storage and Amplification in Photonic Crystal Nanocavities Malik Rakhmanov, *UT Brownsville*			3	4
▪ Spectroscopy of InAs/GaSb Superlattices for the Development of High-Operating Temperature Infrared Detectors Junichiro Kono, *Rice University*				4
▪ Integrated Flexible Sensors (Smart Skin) for Structural Health Monitoring Zeynep Celik-Butler, *UT Arlington*				4
4. Power Generation and Storage				
▪ Photovoltaics - Electronic Devices for Air Force Needs through Organic-Inorganic Hybrid Materials Brian Korgel, Allen Bard, Ananth Dodabalapur, and David Vanden Bout, *UT Austin*	1	2	3	4
▪ Hybrid Tandem Solar Cells with Carbon Nanotube Interlayers Anvar Zakhidov and John Ferraris, *UT Dallas*	1	2	3	4
▪ Supercapacitors John Ferraris, *UT Dallas*		2	3	4
▪ High-Performance Fibers Containing Single-Walled Carbon Nanotubes (SWNTs) Matteo Pasquali and James Tour, *Rice University*		2		
▪ Enhancing Optical Absorption in Polymer Solar Cells with Plasmonic Nanostructures Julia W. P. Hsu, *UT Dallas*				4
▪ Production and Manufacturing Optimization of Single Wall Nanotubes Wade Adams, Rice University				4
▪ Alignment and Characterization of SWNT-based Armchair Quantum Wire Wade Adams, Rice University				4

2.0 RESULTS and DISCUSSION

The technical reports for the 18 projects active in the last year of the CONTACT program can be found in the appendices.

2.1 Meetings

CONTACT Annual Review Meetings had been held at various CONTACT universities and also at Wright Patterson Air Force Base as represented below in Table 3.

Table 3. CONTACT Annual Review Meetings

CONTACT ANNUAL REVIEW MEETINGS	
Oct 2007	Industry / Air Force Nanoscience Research Focus Meeting Rice University, Houston, Texas
Aug 2008	CONTACT Program Review Meeting Arlington, TX
Sept 2009	CONTACT Annual Review Meeting UT Pan American, Edinburg, Texas
Oct 2010	Lockheed Martin CONTACT Program Joint Technical Symposium & CONTACT Program Annual Review Meeting Rice University, Houston, Texas
Nov 2011	The CONTACT Program 4th Technical and Annual Review Meeting Wright Patterson Air Force Base, Ohio
March 2012	CONTACT Program Follow-up Meeting Wright Patterson Air Force Base, Ohio

2.2 Air Force

CONTACT Principal Investigators had sustained collaborations with Air Force counterparts for projects resulting in stronger connectivity from year to year. Principal investigators made visits to Wright Patterson to engage with their Air Force partners. Meetings such as the last annual review held at Wright Patterson also provided opportunities for interaction. Dr. Karen Martirosyan from UT Brownsville was a two-time recipient of the USAF Summer Faculty Fellow Program in 2010 and 2011 which provided the opportunity to delve into his research in the area of nano energetics at Eglin Air Force Base. These collaborations have resulted in numerous publications and new projects and programs.

2.3 Industrial Advisory Committee

The Industrial Advisory Committee consisted of 35 members as a final count representing several industrial sectors including: aerospace, materials, instrumentation, electronics, photonics, energy, and safety (Table 4). Members had participated in the program in various capacitiies such as attending and presenting at meetings, reviewing white papers, and collaborating in research and commercial endeavors.

Table 4. CONTACT Industrial Advisory Committee Members

CONTACT INDUSTRIAL ADVISORY COMMITTEE

AEROSPACE
- Lockheed Martin
- Boeing
- Spirit Aerosystems
- Honeywell
- Northrop Grumman
- General Dynamics
- Eloret
- Birkeland Current
- InfoSciTex
- Pratt & Whitney

PHOTONICS
- Luna Innovations
- Semerane

MATERIALS
- Goodyear
- AdamCo
- Applied Nanotech
- Scientific Simulation Systems
- Rolls-Royce
- Xerion Advanced Battery
- Designed Nanotubes
- Systems & Materials Research

ENERGY
- Bright Star Global Energy
- Shell
- Quantum Wired
- Weatherford

INSTRUMENTATION
- Applied Nanofluorescence
- Smart Imaging Technologies
- Infrared Cameras
- CytoViva, Inc.
- Brewer Science
- TSI
- Hysitron

ELECTRONICS
- GigaCircuits
- Tyco Electronics
- Unidym

SAFETY
- Nano Risk Assessment

These alliances also lead to other activities. Lockheed Martin's successful partnership with both CONTACT and Rice University in the LANCER (Lockheed Martin Advanced Nanotechnology Center of Excellence at Rice University) had resulted in an interest from Lockheed Martin to pursue further research relationships with other CONTACT universities. The development of another LANCER-like program (LANCE) would result in the achievement of one of the anticipated goals with the CONTACT Industrial Advisory Committee. A new LANCE would open avenues to not only research collaborations, but potential Air Force partnerships, funding opportunities, outreach and internships. Lockheed Martin also partnered with CONTACT to host the joint technical meeting at Rice University in October 2010. Presentations were provided by Lockheed Martin, CONTACT principal investigators, and members of the Industrial Advisory Committee.

Another success story arose from Adamco, another member of the committee. CONTACT was involved in the effort to establish manufacturing sites in both Houston and Dallas to bring its groundbreaking nano-reinforced aluminum technology to the U.S. This technology could make a potential significant impact in the aerospace, defense, energy and transportation industries.

2.4 Student Travel Grant

The Student Travel Grant program concluded with a total of 74 grants awarded to 52 students from various universities across the state of Texas (see Figure 3). This program has provided valuable support for research and access to state-of-the-art facilities resident at the CONTACT universities.

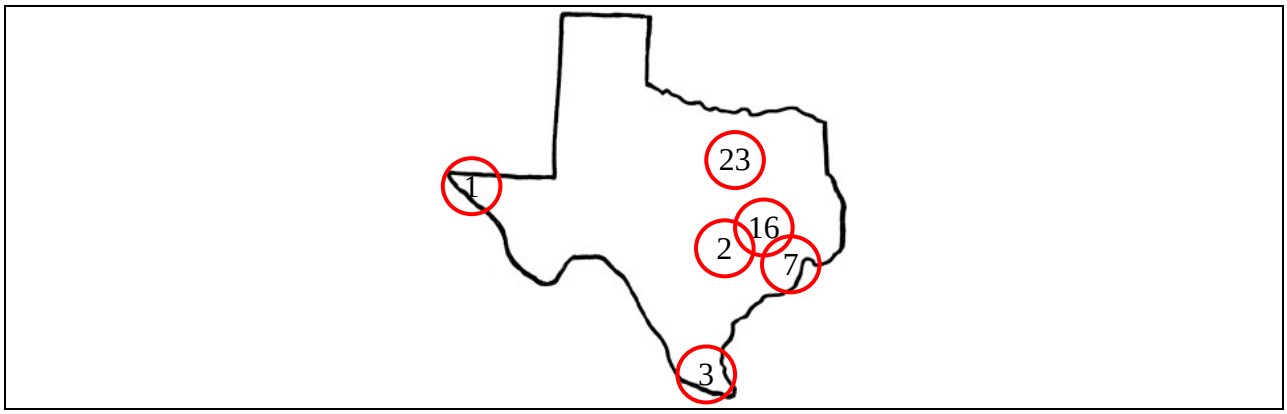

Figure 3. Origin of Student Travel Grant recipients

The CONTACT Program office also administered the NSMMS (National Space Missile Materials Symposium) Student Travel Grant Program sponsored by the Air Force Office of Scientific Research. This program provided funding for student participation in the meeting. CONTACT administered this program for four years, from 2009 to 2012.

2.5 Nano-at-the-Border

CONTACT supported the Nano-at-the-Border, an initiative to help develop the nanotechnology capabilities at both the University of Texas at Pan American (UTPA) and University of Texas at Brownsville (UTB). A CONTACT Annual Review Meeting was held at UTPA to coincide with HESTEC (Hispanic Engineering, Science and Technology Week) which promoted nanotechnology awareness. UTPA, lead by CONTACT PI Karen Lozano, successfully launched FibeRio Technology which has commercialized nanofiber production equipment that was invented from her nanomaterials research laboratory. The expanding company is also contributing to an increasing workforce in the region. CONTACT also supported UT Brownsville in launching a new nano-photonic research initiative which resulted in the school's first experimental physics laboratory. Both schools have effectively procured nano-science related funding from government agencies which have significantly impacted students and faculty members.

2.6 Other Achievements

Several start-up companies (Table 5) have resulted from the CONTACT research leading to new jobs created in Texas and the promotion of nanotechnology in the local regions. The CONTACT Program and its participants reported numerous other accomplishments including: publications, patents, awards, meeting presentations and invited talks, new partnerships, funding grants, and new centers and equipment which are included in the technical reports in the appendices.

Table 5. Start-up companies resulting from CONTACT-funded research

START-UP COMPANIES
Semerane, Inc., Dr. Weidong Zhou, UT Arlington Based on silicon photonics, nanomembranes and electronics.
Pinon Technologies, Inc., Dr. Brian Korgel, UT Austin Commercializes application based on nanowire technology.
Solarno, Inc., Dr. John Ferraris and Anvar Zakhidov, UT Dallas Providing solar cell technology based on nanostructured materials.
FibeRio, Technology, Dr. Karen Lozano, UT Pan American Developing applications for nanofiber technology.

3.0 CONCLUSIONS

The CONTACT Program was successful in providing a valuable framework for cooperative nanotechnology research between Texas universities and the Air Force within the Texas region. A mulititude of achievements resulted ranging from supporting student research, creating new companies and jobs, procuring new funding, developing infrastructure, and promoting collaborative activities between the Air Force, academia, and industry. The impact has been broad with many partnerships that will be sustained and new ventures in the horizon.

APPENDIX A - "Nanocomposites as Structural Materials"
PI: Jun Lou, Rice University

Carbon nanofibers (CNFs) have been widely considered for applications in composite material for decades owing to their unique mechanical, thermal and electrical properties. Consequently, an in-depth understanding of mechanical properties of individual CNFs especially after chemical functionalization would provide important insight into its effective integration into composite materials. Successful fluorination and amination of CNFs were first achieved and systematic chemical characterizations of functionalized CNFs were performed. An in situ tensile testing method, which combines a simple micro-fabricated device with a quantitative nanoindenter inside a scanning electron microscope (SEM) chamber, was subsequently employed to measure mechanical properties of individual pristine, fluorinated and amino-functionalized CNFs. The nominal CNFs strengths follow the Weibull distribution with characteristic strengths between 1.94~3.05 GPa, and the fluorinated CNFs are found to possess higher nominal strength but similar strain compared with the pristine as well as the amino-functionalized CNFs. The relatively small Weibull moduli reflect a broad spectrum of flaws induced during functionalization for fluorinated and amino-treated CNFs. Further, SEM fracture surfaces analysis show that all nanofibers failed in a similar cup-and-cone fashion. High resolution transmission electron microscope (HRTEM) image of fluorinated CNFs reveals an unexpected change of the hollow core before and after fiber fracture, which is attributed to the possible effects of fluorination-induced compression on nanofiber surfaces. The results demonstrate the potential of fluorination on improving both the mechanical properties of CNFs and their successful integration into composites. In another work, we compare nanoscale frictional characteristics of three types of chemically treated graphene nanoribbons (GNRs) via atomic force microscope. Measurements in both ambient and low humidity conditions demonstrate that covalently bonded functional groups have a significant impact on the frictional response of GNRs. The measured tip-sample adhesion forces seem to support the observed friction force dependence on functionalizations, and the friction and adhesion differences could also be attributed to the surface reactivity and hydrophilicity differences induced by different chemical functionalization schemes.

The overall objective of this research is to understand fundamental mechanisms that govern the behaviors at the nano reinforcing agent (carbon nanotubes, nanofibers or graphene)-matrix interface (load transfer, adhesion, de-bonding, friction etc.) for structural nanocomposite applications that is important for the Air Force mission. Additionally, interfacial behaviors of low dimensional nanomaterials with other functional applications are also investigated in this project.

Referred Journal Publications:

1. J. Zhang, W. Lu, J.M. Tour and J. Lou, Nanoscale Frictional Characteristics of Graphene Nanoribbons, Applied Physics Letter, accepted, 2012.

2. J. Zhang, P. Loya, C. Peng, V. Khabashesku and J. Lou, Quantitative In-situ Mechanical Characterization of Effects of Chemical Functionalization on Individual Carbon Nanofibers, Advanced Functional Materials, published online, 2012. DOI: 10.1002/adfm.201200593.

3. P. Dong, C. Pint, M. Hainey, F. Mirri, Y. Zhan, J. Zhang, M. Pasquali, R.H. Hauge, R. Verduzco, M. Jiang, H. Lin and J. Lou, Vertically Aligned Single Wall Carbon Nanotubes as Low-cost and High Electrocatalytic Counter Electrode for Dye-Sensitized Solar Cells, ACS

Applied Materials & Interfaces, Vol. 3 (8), 3157-3161, 2011. DOI: 10.1021/am200659y.

4. Z. Liu, L. Hu, J. Liu, C. Qiu, H. Zhou, D. Hashim, G. Shi, C. Peng, S. Najmaei, L. Sun, J. Lou, and P. M. Ajayan, *Correlation Between Droplet-Induced Strain Actuation and Voltage Generation in Single-Wall Carbon Nanotube Films*, Nano Letters, Vol. 11 (12), 5117-5122, 2011. DOI: 10.1021/nl201910j.

5. Y. Ganesan, C. Peng, Y. Lu, P. Loya, P. Moloney, E. Barrera, J. Tour, B. Yakobson, R. Ballarini and J. Lou, *Interface Toughness of MWNT Reinforced Epoxy Nanocomposites*, ACS Applied Materials and Interfaces, Vol. 3 (2), 129-134, 2011. DOI: 10.1021/am1011047.

6. H. Lu, J. Zhang and J. Lou, *Localized Characterization of Chemical Functionalization Effects on Adhesion Properties of SWNT*, Journal of Nanomaterials, Volume 2011, Article ID 145148, 1-5, 2011. DOI:10.1155/2011/145148.

7. Y. Ganesan, C. Peng, Y. Lu, L. Ci, A. Srivastava, P.M. Ajayan and J. Lou, Effects of Nitrogen Doping on the Mechanical Properties of Carbon Nanotubes , ACS Nano, Vol. 4 (12), 7637-7643, 2010. DOI: 10.1021/nn102372w.

8. Y. Ganesan, Y. Lu, C. Peng, H. Lu, R. Ballarini and J. Lou, Development and Application of a Novel Micro-fabricated device for In Situ Tensile Testing of 1-D Nanomaterials, Journal of Microelectromechanical Systems, Vol. 19 (3), 675-682, 2010.

9. F. Landolsi, H. Lu, Y. Sun, F. Ghorbel and J. Lou, Regular and Reverse Nanoscale Stick-slip Behaviors: Modeling and Experiments, Applied Surface Science, Vol. 256, 2577-2582, 2010.

10. Y. Lu, Y. Ganesan and J. Lou, A Multi-step Method for In Situ Mechanical Characterization of 1-D Nanostructures Using a Novel Micromechanical Device, Experimental Mechanics, Vol. 50, 47-54, 2010.

11. Y. Ganesan and J. Lou, Mechanical Characterization of Carbon Nanotube Reinforced Polymer Matrix Nanocomposites – An Unfolding Story of Interface, JOM, Vol. 61, no. 1, 32-38, 2009.

12. J. Lou, H. Lu, J. Goldman, F. Ding and B.I. Yakobson, Mesoscale Reverse Stick-slip Nanofriction Behavior of Vertically Aligned Multiwalled Carbon Nanotube Superlattices, Applied Physics Letter, Vol. 92, 203115-1-3, 2008. (Published also in the Virtual Journal of Nanoscale Science & Technology, vol. 17, Issue 23, June 9, 2008; http://www.vjnano.org).

13. H. Lu, J. Goldman, F. Ding, Y. Sun, V. Khabashesku, B. Yakobson and J. Lou, Friction and Adhesion Properties of Vertically Aligned Multi-walled Carbon Nanotube Arrays and Fluoro-Nanodiamond Films, Carbon, Vol. 46, 1294-1301, 2008.

Awards and additional funding received from other sources helped by participation in CONTACT:

AFOSR Young Investigator Program Award 2008

NSF CMMI (Awarded) – "Nanomechanical Characterizations of Interfaces in Carbon Nanotube Reinforced Nanocomposites", July 2008 – June 2011, PI (with B. Yakobson and R. Ballarini)

Presentations:

1. Y. Ganesan, C. Peng, L. Ci, V. Khabashesku, P.M. Ajayan and J. Lou, *Effect of Sidewall Fluorination on the Mechanical Properties of Catalytically Grown Multi-Wall Carbon Nanotubes*, Mater. Res. Soc. Symp. Proc. Vol. 1284, 157-162, 2011.

2. Y. Ganesan, Y. Lu, H. Lu and J. Lou, In Situ Mechanical Characterizations of One Dimensional Nanoscale Building Blocks Using Microfabricated Devices, IEEE-NANO Conf. Proc., 8, 783-786, 2008.

3. Y. Ganesan, Y. Lu, J. Ye, A. Minor, R. Ballarini and J. Lou, A Simple In Situ Micro-device to Study Mechanical Properties of One Dimensional Nanoscale Building Blocks, ASME International Mechanical Engineering Congress and Exposition (IMECE08), Boston, MA, 2008.

4. Y. Ganesan, Y. Lu, A. Minor and J. Lou, Design and Fabrication of In Situ Micro-device to Study Mechanical Properties of One Dimensional Nanoscale Building Blocks, TMS Spring Meeting, New Orleans, LA, 2008.

Patents:

J. Lou, Y. Ganesan, Y. Lu and C. Peng, "Novel Micromechanical Devices for *In-situ* Characterizations of One Dimensional Nanomaterials", US patent issued Nov. 2011, # 8058613.

Student achievements (degrees awarded, awards…):

Yogi Ganesan, First Prize in Poster Competition, CONTACT Review Meeting 2009

Yogi Ganesan, Jack C. Pollard Fellowship, Rice 2008

Ph.D. Student graduated: Dr. Yogi Ganesan (2011). Now works at Intel.

Collaborations:

Dr. Roberto Ballarini, University of Minnesota

Dr. Boris Yakobson, Rice University

Dr. Pulickel Ajayan, Rice University

Dr. Enrique Barrera, Rice University

Dr. James Tour, Rice University

Dr. Bob Hauge, Rice University

Dr. Fathi Ghorbel, Rice University

Dr. Valery Khabashesku, University of Houston

Dr. Hong Lin, Tsinghua University

Dr. Benji Maruyama, Air Force Research Lab

Media Coverage:

1. Nano research fit for a king
http://www.media.rice.edu/media/NewsBot.asp?MODE=VIEW&ID=15316
2. http://www.nanowerk.com/news/newsid=19967.php
3. http://www.physorg.com/news/2011-02-nano-king-scientists-strength-composite.html
4. http://nanotechwire.com/news.asp?nid=11531
5. http://nanotechweb.org/cws/article/yournews/45024

APPENDIX B - "Investigation of Hybrid Materials for the Development of Sensors and Actuators"

PIs: Karen Lozano and Mircea Chipara, UT Pan American

This project started in October 2010 and the PIs worked on the (1) development of inorganic-organic hybrid nanofibers by the forcespinning™ method, (2) development of polyvinylidene fluoride (PVDF) nanofibers with enhanced piezoelectric properties, (3) development of polymeric photovoltaics by brush-paint processes, and (4) development of composites based on ferroelectric and piezoelectric polymeric matrix filled with magnetic iron oxides.

(1) In the case of producing 1D nanostructures based on semiconducting conjugate polymer a mixture of poly-3-hexylythiophene (P3HT) and polyethylene oxide (PEO) doped with lead suplphide (PbS) nanoparticles has been used to successfully produce composite nanofibers (Figure 4). A referee-reviewed journal article was submitted to ACS Applied Materials and Interfaces. [Ram Thapa, Joan Ibarra, and Karen Lozano; "Forcespun Nanofibers Prepared from Semiconducting Polymeric Blends" Submitted].

Figure 4. (A) P3HT nanofiber mat and (B) single P3HT nanofiber with PbS nanoparticles individually dispersed and distributed within the nanofiber

(2) PVDF nanofibers with enhanced piezoelectric properties were developed (Figure 5). In PVDF, α phase characteristics are attributed to the peaks at 2θ angles of 18.6 and 20.3 and these are the non polar phases. The β phase crystal in PVDF is associated with the angles of 20.3 and 20.7 and is known as highly polar. As it can be observed in the results, the produced fibers have both α and β phase crystals.

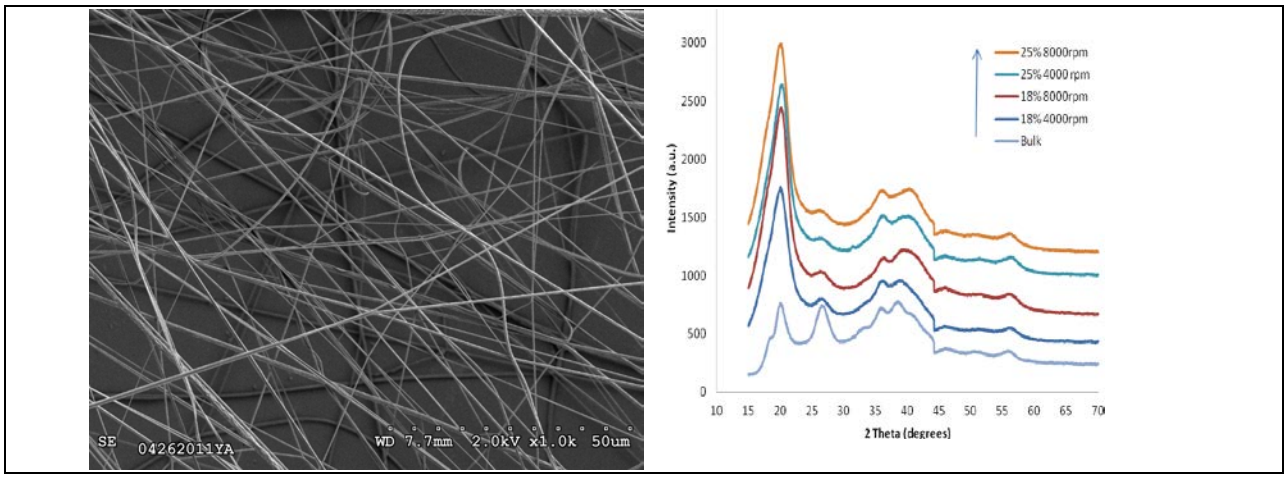

Figure 5. (A) PVDF nanofibers, the average diameter observed to be 290nm and produced at large scales in very short period of time (1-2minutes for several grams) (B) XRD spectra were the enhancement of the beta polar phase

Currently the team is working on the development of electronic devices that will use the piezoelectric properties of the produced PVDF nanofibers. PVDF nanofiber mats were connected to two electrodes made from conductive silver paste on a plastic substrate in order to bend it and cause deformation of the fibers to obtain and measure the piezoelectric response. The signal from the fibers was connected to an instrumentation amplifier and then to an oscilloscope. However, the piezoelectric response has not been as expected and the group is trying to figure out whether or not the poling of the PVDF fibers has been correctly achieved to obtain the expected response.

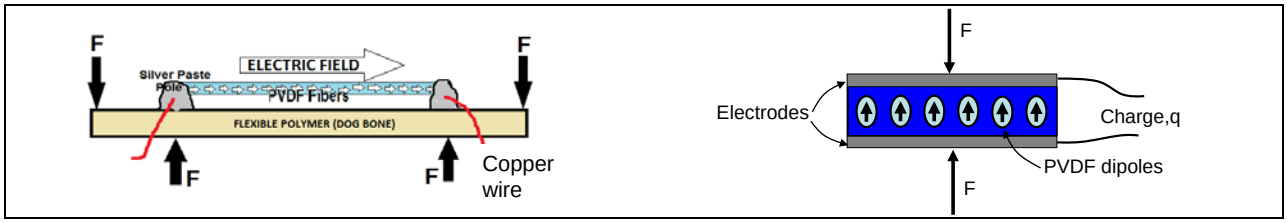

Figure 6. PVDF piezoelectric sensor configurations

The group is also working on constructing other configurations of piezoelectric sensors that might be simpler to mount and test using PVDF layers of fibers between electrodes, such as indium-tin-oxide (ITO) glass, in order to determine their response when dynamically subjected to forces pressing against the electrodes. However, the process to align the dipoles of the PVDF nanofiber films to obtain a satisfactory piezoelectric response is an ongoing task our group needs to complete. The results obtained in this project were presented in November, 2012, at the SHPE (Society of Hispanic Professional Engineers) Conference in Fort Worth, Texas. We are also searching for other opportunities for applications of our PVDF nanofibers such as in fuel cell membranes and supercapacitors.

(3) The development of polymeric photovoltaics by brush-paint processes had shown promising results and more importantly, these were developed at room temperature in air environment (outside of the glove box). Efficiency of the produced cells was verified by two

different methods. A journal publication was submitted to Solar Energy Materials and Solar Cells. [Ram Thapa, Ruben Reyna, and Karen Lozano, “High Efficiency Brush-Painted Photovoltaic Device Fabricated in Air”, Submitted].

It has been reported that power conversion efficiency (PCE) is significantly affected by measurement techniques. New solar cells efficiency records have continuously been reported. Even though several articles on proper measurement techniques of mainly organic solar cells have been published, it seems they are not always followed and controversy about reported values has arisen. The main issues with solar cells measurement techniques are calibration of solar spectrum with reference solar cell and the determination of the active area of the solar cells. Although researchers have started to use reference cell for calibrating the solar spectrum, many are still debating about active area of the solar cell. Many researchers consider crossing area of top and bottom electrodes as the area of the cell. They do not consider the contribution from the illuminated part other than the crossing area for determining the solar cell efficiency. As a result, many groups are reporting solar cell power conversion efficiency illuminating the whole substrate while taking in consideration only the electrode crossing area as the active area of their solar cells. Moreover, some reports lack information on how the cell is iluminated. Following these two methods a significant discrepancy in our results was observed. Using a shadow mask to illuminate only the electrode a PCE of 6.97% was obtained, following the method suggested by NREL, the PCE showed to be 1.67%. The PCE is still considered high considering the fact that it was produced via brush painting outside the glove box without controlling the temperature of the substrate while brush-painting.

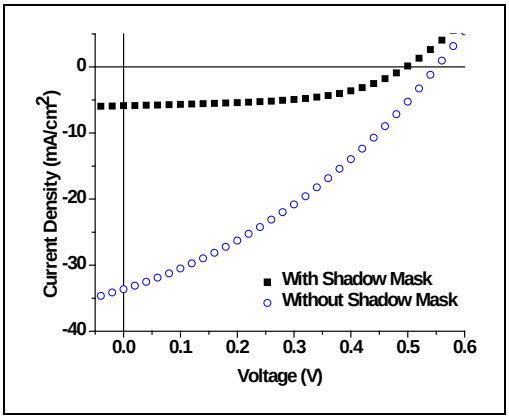

Figure 7. I-V characteristics of the brush-painted solar cells with (solid squares) and without (open circles) aperture (shadow mask) applied

(4) In the case of the development of hybrid structures with multifunctional features such as fluorinated polymers, composites based on PVDF filled with magnetic iron oxides were prepared with concentration ranging from 0-20 wt%. Two series, one doped with Fe_2O_3 and the other with Fe_3O_4 were prepared. The study based on PS-TiO_2 nanocomposites is still ongoing. This year the focus has also been centered on the study of the magnetic properties of nanomaterials and nanocomposites starting with the characterization of iron doped tin (stanium) oxide. Magnetic properties were demonstrated and experiments aiming at the estimation of the blocking temperature are in course. The research involved transmission electron microscopy, electron spin resonance, wide angle X-ray scattering, Raman spectroscopy, and SQUID/VSM measurements.

Preliminary data on the physical properties of these nanocomposites was presented at a conference and subsequently submitted for publication to Journal of Nanoscience and Nanotechnology. The manuscript is under revision. The research is a continuation of a theoretical and experimental effort aiming for a better (experimental and theoretical) understanding of the magnetism of metallic oxides.

In terms of human factors, one postdoctoral researcher participated as well as at least seven undergraduate students and one MS student.

Publications (undergraduate students underlined):

1. Ramos CT, Thapa R, Lozano K, Chipara M, Ferrer D, Gutierrez JJ; "Synthesis and characterization of poly(butylene oxide) grafted carbon nanofibers" J Nanosci Nanotechnol. 2011 May;11(5):3965-9.

2. Ram Thapa, Steven French, Carlos T. Ramos, Jose J. Gutierrez, Mircea Chipara, and Karen Lozano, "Electrorheological Analysis of Colloidal Dispersions of Aluminum Oxide and Silicone" J. Nanosci. Nanotechnol. 11, 6852-6857 (2011).

3. Ram Thapa, Ruben Reyna, and Karen Lozano, "High efficiency brush-painted organic photovoltaic device" (submitted).

4. Ram Thapa, Joan Ibarra, and Karen Lozano, "Development of semiconducting nanofibers for photovoltaic applications" (submitted).

5. X. Wei, R. Georgescu, N. Ali, I. Morjan, T. A. George, F. Dumitrache, R. Birjega, M. Chipara, R. Skomski, D. J. Sellmyer "On the Synthesis and Physical Properties of Iron Doped SnO_2 Nanoparticles" Submitted to J. Nanosc and Nanotechnol.

6. Proton Exchange Membranes for Fuel Cells. Beny Vasquez; Horacio Vasquez; Karen Lozano; Dorina Mihut. Undergraduate Honors Thesis. Honors Program at UTPA. April 2011. (Beny graduated May 2011 and is now an MS student in the Electrical Engr dept at University of Minnesota).

7. X. Wei, R. Georgescu, N. Ali, I. Morjan, T. A. George, F. Dumitrache, R. Birjega, M. Chipara, R. Skomski, and D. J. Sellmyer, "On the Synthesis and Physical Properties of Iron Doped SnO2 Nanoparticles", Journal of Nanoscience and Nanotechnology, Vol. 12, 12, 9299-9301, Dec 2012.

8. M. Chipara, X. Yu, N. Ali, R. Skomski, L. T. Yue, D. J. Sellmyer, "Ferromagnetic Resonance of FePt Nanoclusters in Polyimide" submitted to Applied Surface Science; also presented at Nanosmat-USA, 27^{th}-30^{th} March 2012, Tampa, FL.

Conference Presentations:

1. Joan Ibarra, Ram Thapa, and Karen Lozano, "Conjugated Polymeric Nanofibers Produced by ForceSpinning," poster presentation- Partnership for Research and Education in Materials (PREM), Edinburg, TX, *April*, 2011.

2. Samantha Mendez, Ram Thapa, and Karen Lozano, "Phase Diagram of Conjugated Polymer-Inorganic Nanoparticles Blends" poster presentation- Partnership for Research and Education in Materials (PREM), Edinburg, TX, *April*, 2011.

3. X. Wei, R. Georgescu, N. Ali, I. Morjan, T. A. George, M. Chipara, R. Skomski, D. J. Sellmyer "On the Synthesis and Physical Properties of $Sn_{1-x}Fe_xO_2$ Nanoparticles" Nanosmat

2011, Tampa Florida, March 26-30, 2012.

4. Beny Vasquez; Horacio Vasquez; Karen Lozano, "Preparation of PVDF/PWA Composite Nanofiber Membranes by Forcespinning for Proton Exchange Membranes", HESTEC Poster in 2010. Won 3rd place in the Mechanical Engineering Department. September 2010.

5. Ruben Suarez; Horacio Vasquez; Karen Lozano, "TiO_2 Nanofiber Applications in Solar Cells" HESTEC Poster. September 2010.

6. Jose Luis Duran; Chris Garza; Horacio Vasquez; Karen Lozano; "Preparation of Polyvinylidene Fluoride Nanofiber Membranes by Forcespinning™" HESTEC Poster. September 2011.

APPENDIX C - "Dispersion and Electromechanical Properties of Nano-Laden Systems"
PI: Venkat Ganesan, UT Austin

This project proposes to develop a fundamental understanding of the *microscopic features governing the dispersion structure and properties of nanoparticle dispersions* in simple and polymeric fluids. Our research efforts focus primarily on two broad issues: (1) Electrical and magnetic field effects on dispersion characteristics of nanofillers in polymer matrices; (2) Electrical and magnetorheological properties of nanocomposites; (3) Using simulations to unearth new strategies for controlling nanoparticle dispersions and properties.

We have made substantial progress in the questions listed above.

(1) We have conducted Brownian dynamics simulations which quantify the combined role of shear and AC electric fields upon the dispersion and orientation characteristics of nanotube suspensions. More recently, we have combined these results with a model for the rheology of such suspensions. The evaluation of our model predict that applying an external electric field at an orientation to the shear field results in novel electrorheological properties which may find use in actuators and other electromagnetic devices. This work appeared in the journal *Macromolecules*.

(2) In a recent work, we examined the connections between structure and properties of polymer nanocomposite materials. Explicitly, we focused on the aging behavior and the barrier properties of such materials. Our analysis led to several interesting insights regarding the mechanistic underpinnings of such properties and its connections to the macroscopic structure. Specifically, our studies explained the origins of the noncontinuum behavior noted in the barrier and aging properties of such systems.

(3) Recently, considerable interest has arisen in utilizing particle self-assembly as a bottom-up route to material assembly. It was generally believed that it is difficult for isotropically interacting spherical particles to *self-assemble* into non-spherical superstructures. In a recent experimental collaboration, we have provided striking counterexamples to this line of thought. Explicitly, spherical inorganic nanoparticles isotropically grafted with polymeric brushes were shown to self-assemble into anisotropic structures when they are placed in the corresponding homopolymer. These experiments also demonstrated that such an approach to nanoparticle self-assembly enables considerable control for the creation of polymer nanocomposites with enhanced mechanical properties. This work appeared in the journal *Nature Materials*.

Publications: Publications relating to the above projects have appeared in *Nature Materials*, and the journals *Macromolecules* and *Soft Matter*. Several departmental and conference invited lectures have also been presented on the above topics.

Seminars/Visits to the AFRL: Visited WPAFB in July and presented a seminar on the above topic. Met with other researchers at WPAFB and discussed potential opportunities for collaboration.

Awards and Honors:

1. American Physical Society's John H. Dillon Medal which "recognizes outstanding research accomplishments by young polymer physicists who have demonstrated exceptional research promise early in their careers."
2. Kavli Fellow, US National Academy of Sciences, 2009.
3. Invited Participant in National Academy of Sciences Frontiers of Science Meeting, Kunming, China (2009).
4. Visiting Professorship, Indian Institute of Science, Bangalore, India (Aug– Dec 2008).
5. Faculty Research Award (FRA), The University of Texas at Austin, 2008.
6. Frank Liddell Centennial Fellowship in Engineering (2007- Present).
7. Invited panelist at DOE Office of Science sponsored Workshop on Computational Materials Science and Chemistry for Innovation (July 2010)

Editorial Activities:

1. Editor of the Special Issue of the Journal of Polymer Science. Part B. Polymer Physics Edition, December 2009.
2. Editorial Advisory Board, Macromolecules (2011 – present).

Publications:

1. Venkat Ganesan*, Chris Ellison and Victor Pryamitsyn, "Mean-field models of structure and dispersion of polymer-nanoparticle mixtures," Invited Review, Soft Matter, 6, 4010 - 4025 (August 2010).
2. Victor Pryamitsyn and Venkat Ganesan*, "Structure of Aggregating Rod Suspensions Under Combined Shear and Electric Fields," Macromolecules, 42, 7184 (September 2009).
3. Pinar Akcora, Hongjun Liu, Sanat K. Kumar, Joseph Moll, Yu Li, Brian C. Benicewicz, Linda S. Schadler, Devrim Acehan, Athanassios Z. Panagiotopoulos,Victor Pryamitsyn, Venkat Ganesan, Jan Ilavsky, Pappanan Thiyagarajan, Ralph H.Colby and Jack F. Douglas, "Anisotropic Self-Assembly of Spherical Polymer-Grafted Nanoparticles," Nature Materials, 8, 354 - 359 (April 2009).
4. Venkat Ganesan*, "Some Issues in Polymer Nanocomposites: Theoretical and Modeling Opportunities for Polymer Physics," Invited Viewpoint Article, J. Poly. Sci. Pol. Phys. B., 46, 2666 - 2671 (December 2008).

Invited Talks:

1. Structure and dynamics in polymer nanocomposites, Indo-US Bilateral Workshop on Nanoparticle Assembly, New Delhi, India, December 2011.
2. Coarse-graining techniques for barrier properties of polymer nanoparticle mixtures, Army Research Laboratories, Natick, November 2011.
3. Dispersion and electromechanical properties of nanoladen systems, Lockheed Martin CONTACT Program Joint Technical Symposium, Rice University, October 2010.
4. Structure and dynamics in polymer nanocomposites, Department of Chemical Engineering, Seoul National University, October 2010.
5. (5)Modeling of Polymers for Energy Applications, Department of Chemical Engineering,

Columbia University, October 2010.

6. Modeling of Polymers for Energy Applications, Korean Polymer Society Meeting, Daegu, Korea, October 2010.

7. Modeling of Polymers for Energy Applications, North American Thermal Analysis Society, September 2009.

8. Structure and dynamics in polymer nanocomposites, Department of Chemical Engineering, University of California at Santa Barbara, April 2009.

9. Polymer-Particle Mixtures: Equilibrium and Dynamics, Telluride Workshop on Polymer Physics, Telluride, July 2009.

10. Coarse-graining techniques for polymer nanoparticle mixtures, Army Research Laboratories, Aberdeen, April 2009.

11. Equilibrium and dynamical aspects of multicomponent polymers, American Physical Society, March Meeting, Dillon Medal Symposium, March 2009.

12. Polymer-Particle Mixtures: Equilibrium and Dynamics, Department of Polymer Science and Engineering, University of Massachusetts, Amherst, April 2009.

13. Polymer-Particle Mixtures: Equilibrium and Dynamics, Department of Mechanical Engineering, Indian Institute of Technology, Kanpur, November 2008.

14. Novel dynamical phenomena in Polymer-Particle Mixtures, Department of Physics, Indian Institute of Science, Bangalore, October 2008.

15. Equilibrium aspects of Polymer-Particle Mixtures, Department of Chemistry, Indian Institute of Science, Bangalore, August 2008.

16. Structure and Thermodynamics of Multicomponent Polymers, National Center for Biological Sciences, Bangalore, India, August 2008.

17. Novel Simulation Methods for Polymer-Particle Mixtures, CECAM Workshop on Dissipative Particle Dynamics: Addressing Deficiencies and Establishing New Frontiers, Lausanne, July 2008.

18. Electromagnetic Field Aided Novel Strategies for Dispersion of Nanotubes in Polymer Matrices, Airforce Research Labs, Wright Patterson Air Force Base, June 2008.

19. Polymer-Particle Mixtures: Dynamics, American Physical Society March Meeting 2008.

20. Polymer-Particle Mixtures: Equilibrium and Dynamics, Yale University, Department of Mechanical Engineering, September 2007.

21. Polymer-Particle Mixtures: Equilibrium and Dynamics, University of Florida, Department of Chemical Engineering, October 2007.

PhD students partially supported through CONTACT funds:

1. Manas Shah (2009): Modeling Self-Assembly and Structure-Property Relationships in Block Copolymers, Chemical Engineering, Univ. of Texas at Austin.

2. Landry Khounlavong (2010): Modeling and coarse-grained simulations of structure and properties of polymer nanocomposites, Chemical Engineering, Univ. of Texas at Austin.

3. David Trombly (2011): Modication of Surfaces Using Grafted Polymers: A Self Consistent Field Theory Study, Chemical Engineering, Univ. of Texas at Austin.

APPENDIX D - "Nanoenergetic 'Gas-Generator'"

PIs: Karen Martirosyan, UT Brownsville, and Dan Luss, University of Houston

During this period we developed a rapid oxidation model of spherical aluminum nanoparticles surrounded by oxygen, using Cabrera-Mott oxidation model with self-consistent potential and taking self-heating into account. In this model, aluminum ions are helped to escape aluminum surface (overcoming ionization potential W_i), and to move through oxide layer to its outer part with the help of self-consistent electric field potential (V) created by the imbalance between excess positive aluminum ions and electrons. Excess concentrations of electrons and ions in oxide layer in turn are dependent on electric field potential via appropriate Gibbs factors, leading to a self-consistent version of Poisson equation. In contrast with Coulomb potential, our result shows that for aluminum nanoparticles (less than 100 nm), a double layer potential leads to enhanced oxidation rates throughout the oxidation process.

Our study revealed that Al/Bi_2O_3 and Al/I_2O_5 nanocomposites can generate a transient pressure pulse three-four times larger than that during the explosion of traditional thermite reactive mixtures. The shock wave velocity and rate of energy release increased by up to 3 orders of magnitude when the particle sizes of either aluminum and/or the oxidizer were reduced to a nanosize range. The proposed systems can have higher energy densities (up to 26 kJ/cm^3) than conventional explosives and generate high pressure discharge and shock waves. We developed a rapid oxidation model of spherical aluminum nanoparticles which predicted that for aluminum nanoparticles (less than 100 nm), a double layer potential leads to enhanced oxidation rates throughout the oxidation process.

The impact of aluminum particle size and the thickness of surrounding alumina layer on the dynamic pressure discharge of nanothermite reactions in the Bi_2O_3/Al system were also studied. A pressure discharge from 9 to 13 MPa was generated using as-synthesized Bi_2O_3 nano-particles produced by combustion synthesis and Al nanoparticles with size from 3 μm to 100 nm. The maximum reaction temperature was measured to be ~2700 ºC. The estimated activation energy of the reaction was 45 kJ/mol. A very large (several orders of magnitude) difference existed between the rate of the pressure pulse release by nanothermite reactions and by thermite reactions with large aluminum particles. The maximum observed pressurization rate was 3200 GPa/s. The time needed to reach the peak pressure was 0.01 ms and 100 ms for aluminum particles with diameter of 100 nm and 70 microns, respectively. The discharge pressure was a monotonic decreasing function of the thickness of the surrounding alumina layer. The behavioral features of the Bi_2O_3/Al and I_2O_5/Al-based nanothermite mixtures indicate potential for applications as propulsion, explosives and pyrotechnic components.

The risk of bioterrorism events involving the intentional airborne release of contagious agents has led to development of new approaches for bio agent defeat technologies both indoors and outdoors. The spore-forming bacteria, in particular Bacillus anthracis is one of the biologic agents most likely to be used as a bio-weapon. Nanostructured thermite reaction based on I_2O_5+Al may produce intensive iodine gas phase, which can be used as biocidal agents to destroy harmful bacteria and microorganisms. The other significant advantage to use nanothermites is the time efficiency. If the iodine solutions are effective after 20 minutes, the nano-structured thermite mixture is effective in seconds-after explosion and deposition of iodine on infected surface. The controlling experiments show that by vaporising of iodine in quantities of

milligrams, it is possible to disinfect areas of hundreds of meters. The study has shown that I_2O_5/Al nanosystem is extremely effective in sterilizing potentially harmful biological agents in seconds.

Patent:

1. K.S. Martirosyan and D. Luss, *Carbon combustion synthesis of oxides*, US Patent # 7,897,135, 2011.

Peer-reviewed Publications:

1. M. Zyskin, K.S. Martirosyan, Rapid oxidation and self-heating model of aluminum spherical nanoparticles, Proceedings of Nano Science and Technology Institute, Vol. 2, 649-652, 2012.

2. K.S. Martirosyan, High Density Nanoenergetic Gas Generators, Chapter in book "Handbook of Nanoscience, Engineering, and Technology", Third Edition, Edited by Goddard, Brenner, Lyshevski, and Iafrate, CRC, Elsevier, 2012.

3. M. Hobosyan, A. Kazansky and K.S. Martirosyan, Nanoenergetic composite based on I2O5/Al for biological agent defeat, Proceedings of Nano Science and Technology Institute, Vol. 3, 599-602, 2012.

4. L. Wang, D. Luss and K.S. Martirosyan, The behavior of nanothermite reaction based on Bi_2O_3/Al, J. Appl. Phys. 110, 074311, 2011.

5. K.S. Martirosyan, Nanoenergetic gas generators, Principles and Applications, *J. Mater. Chem.*, 21, 9400-9405, 2011.

6. K.S. Martirosyan, L. Wang and D. Luss, Tuning the Gas Pressure Discharge of Nanoenergetic Materials by Boron and Carbon Nanotubes Additives, proceedings of NSTI, *NanoTech*, Vol.1, 323-326, 2011.

7. K.S. Martirosyan, L Wang, A. Vicent and D. Luss, Synthesis and performance of bismuth trioxide nanoparticles for high energy gas generator use, Nanotechnology, 20, 405609, 2009, [highlighted in http://nanotechweb.org/cws/article/lab/40661].

8. K.S. Martirosyan, L Wang and D. Luss, Novel nanoenergetic system based on iodine pentoxide, Chem. Phys. Lett, 483, 107-110, 2009.

9. K.S. Martirosyan and D. Luss, Fabrication of metal oxides nanoparticles by highly exothermic reactions, Chem. Eng. Technology, 32, 9, 1376-1383, 2009.

10. K.S. Martirosyan, L Wang, A. Vicent and D. Luss, Nanoenergetic gas-generator: design and performance, Propellants, Explosives, Pyrotechnics, 34, 532-538, 2009.

11. K.S. Martirosyan, L Wang, A. Vicent and D. Luss, Fabrication of bismuth trioxide nanoparticles for gas-generators applications, NSTI, NanoTech, Vol. 2, 82-85, 2009.

12. K.S. Martirosyan, L. Wang, and D. Luss, Development of nanoenergetic materials based on Al/I2O5 system, NSTI, NanoTech, Vol.1, 137-140, 2010.

13. K.S. Martirosyan and D. Luss, Nanoenergetic fabrication of dense ceramics for lunar exploration program, Lunar and Planetary Science, paper # 1689, 2008.

14. K.S. Martirosyan, L. Wang and D. Luss, Nanoenergetic gas-generator, IEEE Explore Database- IEEE Nanotechnology-2008, p. 817-818, 2008.

Conference Presentations:

1. M. Hobosyan, Kh.G. Kirakosyan, S.L. Kharatyan, and K.S. Martirosyan, Study of Dynamic Features of Highly Energetic Reactions by DSC and High-speed Temperature Scanner (HSTS), Annual Meeting Materials Research Society, November 25-30, Boston, USA, 2012.

2. Z.Ramazanova, M.Zyskin, K.S.Martirosyan, Modeling of oxidation of aluminum nanoparticles by using Cabrera Mott Model, Bulletin of the American Physical Society, Joint Fall 2012 Meeting of the Texas Sections of the APS, Lubbock, TX, USA, v. 57, 10, 2012.

3. M. Hobosyan, Tyler, K.S. Martirosyan, Self-Assembled Nano-energetic Gas Generators based on Bi2O3, Bulletin of the American Physical Society, Joint Fall 2012 Meeting of the Texas Sections of the APS, Lubbock, TX, USA, v. 57, 10, 2012.

4. R. Singh, N. Badi, M. Hobosyan and K. Martirosyan, Reactivity Enhancement of Nanoenergetic Materials Through Functionalized $Al/Bi_2O_3/I_2O_5$ Core-Shell Architecture, TechConnect World, June 18-21, 2012, Santa Clara, California.

5. M. Zyskin, K.S. Martirosyan, Rapid oxidation and self-heating model of aluminum spherical, TechConnect World, June 18-21, 2012, Santa Clara, California.

6. M. Hobosyan, A. Kazansky and K.S. Martirosyan, Nanoenergetic composite based on I2O5/Al for biological agent defeat, TechConnect World, June 18-21, 2012, Santa Clara, California.

7. K.S. Martirosyan Advanced nanostructured systems for energy, environmental and biomedical applications, OIHE MSI Symposium UTPA, February 20-22, 2012.

8. M. Hobosyan, A. Kazansky, and K.S. Martirosyan, Nanoenergetic gas generators for biological agent defeat, Chemical and Biological Defense Science and Technology (CBD S&T) Conference, 14-18 November 2011, Las Vegas, Nevada.

9. M. Hobosyan, A. Kazansky, KS Martirosyan, Nanostructured thermites based on iodine pentoxide for bio agent defeat systems, American Physical Society, Joint Fall 2011 Meeting of the Texas Sections of the APS, AAPT, October 6-8, 2011.

10. K.S. Martirosyan Carbon combustion synthesis of nanostructured complex oxides: fundamentals and applications, International Conference Nonisothermal Phenomena & Processes: from Thermal Explosion Theory to Structural Macrokinetics, Moscow, November 27-30, 2011 (invited).

11. K.S. Martirosyan, High Density Nanoenergetic Gas Generators: Fundamentals and Perspectives, SHS-2011, XI International Symposium on Self-Propagating High Temperature Synthesis, September 5-9, 2011, Anavyssos, Attica, Greece, (invited keynote lecture).

12. K.S. Martirosyan and D. Luss Nanoenergetic Gas Generators for Emerging Military and Space Applications, National Space and Missile Materials Symposium, June 27-July 1, Madison, Wisconsin, USA, 2011.

13. K.S. Martirosyan, L. Wang and D. Luss, Tuning the Gas Pressure Discharge of Nanoenergetic Materials by Boron and Carbon Nanotubes Additives, proceedings of NSTI, NanoTech - 2011, June 13-16, 2011, Boston.

14. K.S. Martirosyan, Nanostructured Oxygen Generators for Aerospace Life Supporting System, at Joint Fall 2010 Meeting of the Texas Sections of the APS, San Antonio, Oct 22, 2010.

15. K.S. Martirosyan, L. Wang, and D. Luss, Development of nanoenergetic materials based on Al/I2O5 system, NanoTech - 2010, 21-25 June, 2010, Anaheim, CA, USA.

16. K.S. Martirosyan, Nanoenergetic gas generators: Fundamentals and applications, Gordon Research Conference on Energetic Materials, June 12-18, Tilton, NH, USA, 2010, (invited key lecture).

17. J. Agee, A. Chow, K.S. Martirosyan, D. Luss, F. Chen, and C. W. Chu, Nanoenergetic Materials and Sensors Research for Space, National Space and Missile Materials Symposium, June 28- July 2, 2010, Scottsdale, AZ, USA.

18. K.S. Martirosyan and D. Luss Nanoenergetic Gas Generators: shock wave velocity and pressure discharge, National Space and Missile Materials Symposium, June 28- July 2, 2010, Scottsdale, AZ, USA.

19. K.S. Martirosyan, Nanoenergetic materials for terrestrial and space environments use, First International Symposium on Nanotechnology, Energy, and Space, October 25-28, 2009, NASA, Houston, TX.

20. K.S. Martirosyan, Development of advanced nanostructured systems for energy, environmental and biomedical applications, Annual meeting AIChE, November 8-13, 2009, Nashville, TN.

21. K.S. Martirosyan, L Wang, A. Vicent, and D. Luss, Development of high-efficient nanoenergetic gas-generators, AIChE Annual Meeting, 16-21 November, Philadelphia, 2008.

22. K.S. Martirosyan, Development of reactive nanostructured systems for energy, environmental and biomedical applications, AIChE Annual Meeting, 16-21 November, Philadelphia, 2008.

23. K.S. Martirosyan, L. Wang, and D. Luss, Nanoenergetic gas-generator, The 8th IEEE International Conference on Nanotechnology, 18-21 August, Arlington, TX, 2008, (invited key lecture).

Invited lectures:

1. High Density Energetic Materials: Theory and Experiment, June 12, 2012, AF Base, Eglin, Florida.

2. Review of Reactive Nanostructured Systems for Energy, Environmental and Biomedical Applications, University of Texas San Antonio, March 30, 2012.

3. Nanoenergetic Gas Generators, fundamentals and applications, Eglin Air Force Base, Florida, Dec 6, 2011.

4. High Energy Density Nanoscale Materials for Emerging Applications, University of Texas Pan American, April 1, 2011.

5. Reactive Nanostructured Patterns, University of Houston, May 16, 2011.

6. Tuning the Properties of Nanoenergetic Materials, University of Florida, REEF, July 20, 2011.

7. High Density Nanostructured Energetic Materials: Military and Space Applications, University of Texas at Brownsville, Sept 20, 2011.

8. Nanoenergetic Gas Generators, Wright Patterson Air Force Base, Materials and Manufacturing Directorate, Ohio, Nov 8, 2011.

9. Emerging Nanotechnologies, Fundamentals and Applications, March 2, 2010, Texas State University, San Marcos.

10. Reactive nanostructured materials, May 13, 2010, City College of New York, NY.

11. Nanoenergetic gas generators: fundamentals and applications, Gordon Research Conference on Energetic Materials, June 17, 2010, Tilton, NH, USA.

12. Nano Engineered Energetic Materials, July 12, 2010, AFRL, Eglin, Florida.

13. Nanoenergetic Materials: Current Stage and Future Developments, University of Florida, REEF, July 15, 2010.

14. The Magic of Nanoscience, Monday Night Physics Lecture, University of Texas at Brownsville, September 27, 2010.

15. Nanoenergetic Gas Generators, Lockheed Martin CONTACT Program Joint Technical Symposium & CONTACT Program Annual Review Meeting, Oct 13, 2010.

16. Digital Images Capture and Processing, University of Texas at Brownsville, Nov. 30, 2010.

17. Reactive nano systems: fundamental and applications, Nov, 12, 2009, University of Texas at Brownsville, TX.

18. Design and development of multifunctional nano-textured structures: synthesis and properties, Houston IEEE chapter, Houston, Jan. 25, 2008.

19. Novel multifunctional nanostructured systems, Lamar University, March 12, 2008.

Awards and additional funding received from other sources aided by participation in CONTACT:

2010; 2011; and 2012 US Air Force Summer Research Fellowship: One of the PI - Karen Martirosyan was awarded 2010, 2011, and 2012 US Air Force Summer Research Fellowship Program and spent 10 weeks (each summer) at Eglin Air Force Base conducting research on nanoenergetic materials.

Awarded Projects:

1. National Science Foundation, $437,970, 09/2011-08/2013

MRI- Consortium: Acquisition of Cryogen-free Cryocooler-based Physical Property Measurement System to Support Transformative Device and Materials Research in the Rio Grande Valley, PI- K S Martirosyan

Collaborative with UTD (A. Zakhidov), UTPA (M. Chipara), and UH (D. Litvinov)

2. National Science Foundation, $200,000, 10/2011-08/2013

NUE- NUE: Development of the Nanoscale Engineering Concentration (NEC) at the University of Texas at Brownsville, PI- K S Martirosyan

3. US Air Force Research Lab, $65,000, 09/2011-10/2012

Tailoring of Pressure Discharge and Shock Wave Velocity in High Energy Density Nanoenergetic Gas Generators, PI-K S Martirosyan

Student achievements:

PhD Thesis:

Graduate student Leizheng Wang successfully completed his PhD thesis titled “Nanoenergetic Gas Generators” in Chemical and Biomolecular Engineering at the UH.

MS Thesis:
Graduate student Mkhitar Hobosyan working on his MS thesis in Physics titled Novel Energetic Materials for Space and Terrestrial Applications" at the UTB.

MS Thesis:
Graduate student Zamart Ramazanova working on her MS thesis in Physics titled "Simulation of pressure discharge and shock wave by nanoenergetic systems" at the UTB.

Students award:
Mkhitar Hobosyan's presentation was recognized the Best Work presented at the Meeting and was granted the TSAPS Fall 2012 Graduate Student Presentation Award at 2012 Meeting of the Texas Sections of the APS, Lubbock, Texas.

Collaborations:
Strong collaborative effort was established with University of Texas at Dallas (Dr. A. Zakhidov), University of Texas Pan American (M. Chipara), and University of Houston (D. Litvinov) for Acquisition of Cryogen-free Cryocooler-based Physical Property Measurement System to Support Transformative Device and Materials Research in the Rio Grande Valley and Development of the Nanoscale Engineering Concentration (NEC) at the University of Texas at Brownsville. Both efforts supported by NSF.

APPENDIX E - "Spectrally-Selective Photonic Infrared Sensors for Gas Sensing"
PI: Weidong Zhou, UT Arlington

Over the last few months of the project, we have completed the proposed tasks with the demonstration of spectrally-selective infrared photodetectors based on InGaAs nanomembranes stacked on top of Si Fano resonance photonic crystal filters. We completed device characterization with the measurements of spectral dependent photocurrents. A manuscript has been submitted for review.

Over the entire period of the CONTACT project, we have completed all the tasks proposed in the project, with the focus on a new type of spectrally selective photodetectors based on epitaxial and colloidal quantum dots (QDs) in various photonic crystal cavities. We have made the following major technical contributions:

(1) Demonstrated spectral selective infrared absorption enhancement at midwave MWIR (~10μm wavelength). Both optical and electrical measurements were carried out, with higher operation temperatures and larger photocurrent and signal to noise ratio.

(2) Developed a dip-coating based self-assembly process for the formation of one-dimensional photonic crystals for colloidal QDs based near IR photodetectors.

(3) Demonstrated a new type of spectrally selective photodetectors, based on the Fano resonances in periodic structures and stacked nanomembranes on glass and flexible substrates.

(4) Detailed investigation of absorption enhancement in Fano filters on flexible substrate with the incorporation of colloidal QDs.

(5) Demonstrated a new type of flexible Fano filters based on transferred nanomembranes on flexible substrates. The angular and polarization properties of Fano filter transmission has also been investigated theoretically and experimentally.

(6) Demonstration of absorption enhancement in ultra-thin InGaAs nanomembranes stacked on top of Si Fano resonance photonic crystal filters.

(7) Demonstration of spectrally-selective infrared photodetectors in InGaAs nanomembranes stacked on top of Si Fano resonance photonic crystal filters.

Presentations:

As a result of the AFRL CONTACT support, we have a total of over 30 publications and conference presentations, including 7 journal papers (1 pending) and 11 invited conference talks. One of the papers we published was selected as one of five highlights (significant advances) in a recent special issue on silicon photonics published in the journal of *Electronics Letters*.

Published Journal papers:

1. A. Chadha, S. Chuwongin, G. J. Brown, Z. Ma, and W. Zhou, "Fano Resonance enhanced photonic crystal Infrared Photodetectors based on transfer-printed InGaAs/Si nanomembranes", *IEEE Photon. Tech. Lett.* (under review).

2. L. Chen, H. Yang, Z. Qiang, H. Pang, L. Sun, Z. Ma, R. Pate, A. Stiff-Roberts, S. Gao, J. Xu, G. J. Brown, and W. Zhou, "Colloidal quantum dot absorption enhancement in flexible Fano filters," *Appl. Phys. Lett.* 96, 083111 (2010).

3. W.D. Zhou, Z. Ma, H. Yang, Z. Qiang, G. Qin, H. Pang, L. Chen, W. Yang, S. Chuwongin, and D. Zhao, "Flexible photonic-crystal Fano filters based on transferred semiconductor

nanomembranes (review)", *J. Phys. D.* 42, 234007 (2009).

4. L. Chen, Z. Qiang, H. Yang, H. Pang, Z. Ma, and W. D. Zhou, "Polarization and angular dependent transmissions on transferred nanomembranes Fano filters", *Opt. Express*, vol 17, 8396-8406, (2009).

5. Z. Qiang, H. Yang, L. Chen, H. Pang, Z. Ma, and W. D. Zhou, "Fano filter modal analysis based on transferred silicon nanomembranes on flexible substrates", *Appl. Phys. Lett.* Vol.93, 061106, 2008. Also selected at *Virtual Journal of Nanoscale Science & Technology*, Aug. 25, 2008.

6. H. Yang, Z. Qiang, H. Pang, Z. Ma, and W. D. Zhou, "Surface-Normal Fano Filters Based on Transferred Silicon Nanomembranes on Glass Substrates", *Electron. Lett.*, vol. 44 (14), 858-9, 2008.

7. W. D. Zhou, L. Chen, Z. Qiang, G. J. Brown, "Spectrally selective infrared absorption in a single-defect photonic crystal slab", *J. Nanophotonics*, vol.1, 013515, 2007.

Invited Conference Presentations:

1. W. D. Zhou and Z. Ma, "Nanomembrane Photonics for Si Photonic Integration and Flexible Optoelectronics (Invited)", *APS March Meeting*, Feb. 27-Mar. 2, 2012, Boston, MA.

2. W. D. Zhou and Z. Ma, "Nanomembrane Heterogeneous Integration for Si Photonics and Flexible Optoelectronics (Invited)", *1st International Congress on Nano Science and Technology*, Oct. 23-26, 2011, Dalian, China.

3. W. D. Zhou, Z. Ma, W. Yang, S. Chuwongin, Y. Shuai, J. Seo, D. Zhao, H. Yang, and R. Soref "Stacked crystalline semiconductor nanomembranes for 3D Si photonics (Invited)", *International Topical Meeting on Information Photonics*, May 18-20, 2011, Ottawa, Canada.

4. W. D. Zhou and Z. Ma, "Semiconductor nanomembranes for stacked and flexible photonics (Invited)", *Photonics West* 2010, San Jose, CA.

5. W. D. Zhou and Z. Ma, "Nanophotonic devices based on Fano resonances on stacked nanomembranes (Invited)", *216th ECS Meeting, Oct. 4-9, 2009, Vienna, Austria.*

6. W. D. Zhou and Z. Ma, "Nanophotonic devices based on Fano resonances on stacked nanomembranes (Invited)", *The International Conference on Nanophotonics 2009, Harbin, China, May 11-14, 2009.*

7. W. D. Zhou, " Photonic Crytal Infrared Photodetectors (Invited)", *NASA TSGC Fall Meeging, Grand Prairie, TX*, Nov. 4-5, 2008,

8. W. D. Zhou, H. Yang, Z. Qiang, L. Chen, and G. J. Brown, "Spectrally Selective Infrared Absorption Enhancement in Photonic Crystal Cavities (Invited)", *SPIE Annual Meeting*, Aug. 10-14, 2008, San Diego, CA.

9. W. D. Zhou, "Heterogenous Material Integration with Photonic Crystal Platforms for Nanophotonic Devices on Silicon (Invited)", *ICALEO 2008*, Oct. 20 – 23, 2008, Pechanga Resort, Temecula, CA.

10. Z. Ma, W. D. Zhou, "Semiconductor nanomembranes and applications in electronics and photonics (Invited)", *IEEE Nano 2008*, Aug. 18-21, 2008, Arlington, TX, USA.

11. W. D. Zhou, "Photonic Crystal Slabs for Infrared Detectors and Filters (Invited)", *JSPS – UNT Winterschool on Nanophotonics*, Denton, TX, Feb. 14-15,2008.

Contributed Conference Presentations:

1. M. Rakhmanov, T. D. Miler, A. Gribovskiy, S. Chuwongin, D. Zhao, and W.D. Zhou, "Sub-wavelength Diffraction Losses in a Silicon Nano-Patterned Membrane Reflector", IEEE Photonics Conference (IPC2012), Sept. 23-27, San Francisco, CA. (accepted).

2. A. Chadha, W. Yang, W.D. Zhou, Z. Ma, and G. J. Brown, "Spectral selective absorption enhancement from stacked ultra-thin InGaAs/Si Fano resonance membranes", *Photonics West* 2012, San Jose, CA, Jan. 2012.

3. F. J. Agee and W. D. Zhou, "CONTACT – Sensors for Aerospace and Fano Resonance Photonic Crystal Cavities", *SPIE Defense, Security, and Sensing*, April 5 - 9 2010, Orlando, FL, USA. [DSS10-DS224-4]

4. T. Miller, S. Cantu, V. Quetschke, M. Rakhmanov, Y. Shuai, D. Zhao, and W. Zhou, "Optical losses and wave-front distortions in the reflection of light from a photonic-crystal mirror," *Bulletin of the American Physical Society*, vol. 55, 2010.

5. L. Chen, H. Yang, Z. Qiang, L. Sun, Z. Ma, R.Pate, A. Stiff-Roberts, J. Xu, G. J. Brown, and W. D. Zhou, "Direct measurement of spectrally selective absorption enhancement in Fano resonance photonic crystal cavities on plastic substrates", *Photonics West 2010, Jan. 23-28, 2010, San Francisco, CA.*

6. W. Yang, H. Yang, G. Qin, G. Pang, J. Berggren, M. Hammar, R. Soref, Z. Ma, and W. D. Zhou, "Crystalline Silicon Nanomembrane Stacking for Large-Area Flexible Photodetectors", *IEEE 6th 6th International Conference on Group IV Photonics*, September 9-11, 2009, San Francisco, CA.

7. L. Chen, H. Yang, Z. Qiang, H. Pang, Z. Ma, J. Xu, G. J. Brown, and W. D. Zhou, "Angle and Polarization Dependent Characteristics of Colloidal Quantum Dot Absorption in Fano Filters on Flexible Substrates", *Photonics West, Jan.24-29, 2009, San Jose, CA.*

8. L. Chen, H. Yang, Z. Qiang, H. Pang, Z. Ma, J. Xu, G. J. Brown, and W. D. Zhou, "Angle and Polarization Dependent Characteristics of Colloidal Quantum Dot Absorption in Fano Filters on Flexible Substrates", *Proc. SPIE*, vol.7222, 72220V, 2009.

9. W. D. Zhou, H. Yang, Z. Qiang, L. Chen, and G. J. Brown, "Spectrally Selective Infrared Absorption Enhancement in Photonic Crystal Cavities (Invited)", *Proc. SPIE*, vol.7095, 709507, 2008.

10. Z. Qiang, L. Chen, H. Yang, H. Pang, Z. Ma, and W. D. Zhou, "Fano filter modal analysis based on transferred silicon nanomembranes on flexible substrates", *Proc. SPIE*, vol. 7031, 703109, 2008.

11. Z. Qiang, W. D. Zhou, M. Lu, and G. J. Brown, "Fano Resonance Enhanced Infrared Absorption for Infrared Photodetectors", Proc. SPIE, vol. 6901, 69010F, 2008.

12. Z. Qiang, W. D. Zhou, M. Lu, and G. J. Brown, "Fano Resonance Enhanced Infrared Absorption for Infrared Photodetectors", *Photonics West*, Jan.21-24, 2008, San Jose, CA.

13. Z. Qiang, H. Yang, L. Chen, H. Pang, Z. Ma, W. D. Zhou, and G. J. Brown, "Characteristics of Surface-Normal Fano Filters on Plastic Substrates", *IEEE Nano 2008*, Aug. 18-21, 2008, Arlington, TX.

14. H. Yang, Z. Qiang, H. Pang, Z. Ma, W. D. Zhou, M. Lu, and R. A. Soref, "Surface-Normal Fano Filters Based on Transferred Silicon Nanomembranes on Glass Substrates", *CLEO'08*, May 4-7, 2008, San Jose, CA.

15. Z. Qiang, L. Chen, H. Yang, H. Pang, Z. Ma, and W. D. Zhou, "Fano filter modal analysis based on transferred silicon nanomembranes on flexible substrates", *SPIE Annual Meeting*, Aug. 10-14, 2008, San Diego, CA.

16. H. Yang, L. Chen, Z. Qiang, W. D. Zhou, W. Zhang, A. D. Stiff-Roberts, S. Krishna, G. J. Brown, "Characteristics of photonic crystal cavity based infrared photodetectors", *IEEE LEOS Annual Meeting*, Oct. 17-21, 2007, Orlando, FL.

Awards and additional funding received from other sources aided by participation in CONTACT:

DoD MURI Project: 06/01/2008 -05/30/2013
Title: MURI: Adaptive Intelligent Photonic/Electronic Systems Based on Silicon Nanomembranes
Leading PI: U. Wisconsin Max Lagally total: $5.8million)
UTA subcontract: $750,000 for five years

Start-up companies and jobs generated:

Semerane, Inc. in Arlington, Texas, was co-founded by Dr. Weidong Zhou at UT Arlington through an AFOSR STTR Phase I grant to investigate "Nanomembrane Integrated Lasers on Silicon". Two new STTR awards have been received: an AFOSR STTR Phase II award on "Nanomembrane Integrated Lasers on Si" and another STTR Phase I award on multi-color imaging focal plane arrays. One more NSF SBIR Phase I project was awarded on flexible RF electronics. The company has created 2 jobs in Texas.

Student achievements:

The CONTACT program provided partial support for three PhD students (Hongjun Yang graduated with a PhD degree in 2010, Li Chen graduated with a PhD degree in 2010, and Arvinder Chadha is a 4^{th} year PhD student). Hongjun was a best paper finalist in one of the international conferences.

Collaborations:

We also have close collaborations with AFRL, especially Dr. Gail Brown and her team at WPAFB (over 10 jointed publications so far). Recently, through CONTACT office, we have also started collaborations with Prof. Malik Rakhmanov and his group at University of Texas at Brownsville. We are excited about the joint research opportunities between UTA and UTB. As a result of the collaborations between UTA and UTB, two conferenced papers have been generated.

With support of student travel grant, my PhD students Hongjun Yang, Yichen Shuai, and Santhad Chuwongin can travel to Austin to fabricate nanophotonic devices, at UT Austin MRC facility site.

APPENDIX F - "Terahertz Spatial Light Modulators for High Speed Imaging"
PI: Dan Mittleman, Rice University

The goal of this research program has been to develop new tools for terahertz imaging and sensing. One key aspect has been to design, develop, and demonstrate a practical, fast and inexpensive method for acquiring images with terahertz (THz) radiation. The idea of forming such images (using frequencies from a few hundred GHz up to a few THz) dates back at least 30 years. The potential impact and value of video-rate THz cameras has been recognized for almost as long, and the list of possible applications is massive. This would undoubtedly be a disruptive technology, if it were available. Yet, despite several decades of research, THz imaging is still not in widespread use.

In the last few years, some important progress has been made, eliciting a great deal of excitement. Video-rate imaging systems operating at lower frequencies (e.g., 94 GHz) have become available through several commercial vendors [1]. Also, laboratory systems operating in the THz range have been demonstrated, albeit with the use of expensive and scarce high-power sources [2]. But a cheap, practical fast imaging system remains out of reach.

We propose to solve this problem by exploiting a newly emerging concept in image acquisition. This approach relies on compressive sensing, a dimensionality-reduction-based sensing procedure that removes the need for a multi-element parallel detection array. With a need for only a single-pixel detector, we can move away from the standard paradigm in THz science, which has been directed towards the idea of building the equivalent of a multi-pixel digital camera for THz radiation. Instead, we can rely on a multi-pixel *spatial light modulator*, or SLM, which is (at least in principle) much easier to develop.

Our initial efforts were directed towards the demonstration of a 16-pixel spatial light modulator based on metamaterial concepts, and were very successful [3]. However, scale-up to 1024 pixels has proved to be a challenge. While we continue to pursue this avenue of research, in collaboration with our colleagues at Los Alamos National Laboratory, we have recently begun a parallel thrust which could provide an alternate solution. This idea has been inspired by the discovery of extraordinary transmission through subwavelength apertures due to plasmonic effects [4]. We envision a SLM where the modulation is based, not on the switching of a resonant metamaterial structure, but on the control of plasmonic transmission. In the THz regime, subwavelength apertures are straightforward to fabricate, by deposition of a metal layer (with a slit or opening) onto a dielectric substrate. Moreover, the substrate can be a lightly doped epilayer of silicon on an intrinsic Si wafer. In this case, the charge carrier density within the gap of the small aperture can be controlled by an applied DC bias. Since the THz absorption is highly sensitive to the carrier density within the gap, the transmission can be controlled over a wide range. An array of such structures is therefore an excellent candidate for a multi-pixel modulator.

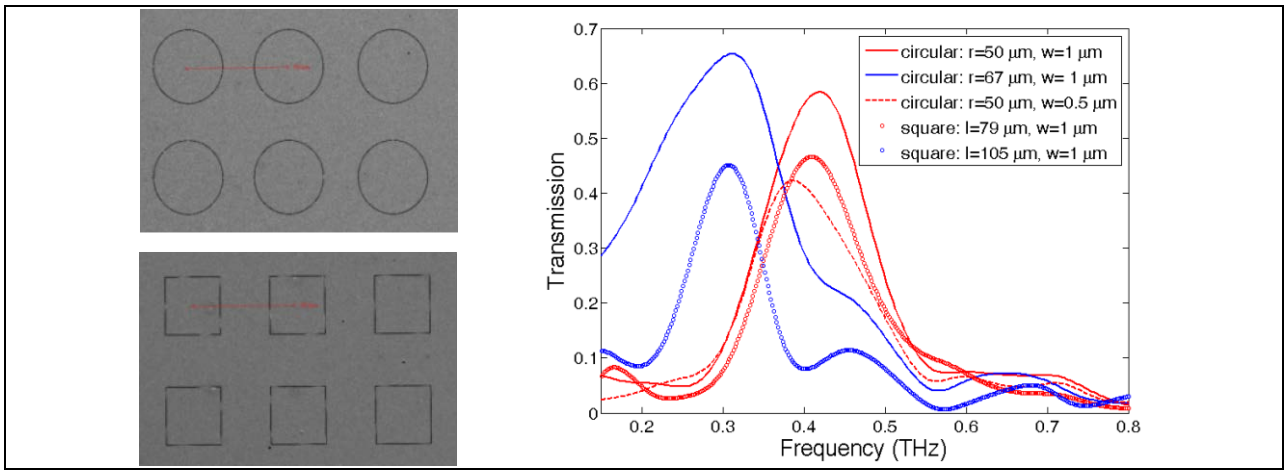

Figure 8. (left) SEM image of fabricated apertures, consisting of slits forming the edges of a square or the edge of a circle. (right) transmission spectra of a variety of samples with varying slit geometries

Our first results are very promising, demonstrating high transmission through subwavelength slits fabricated of gold deposited on intrinsic silicon, and much lower (~18 dB) transmission when the substrate included a doped epilayer (see Figure 9). We are now in the process of fabricating similar structures with optimized p-i-n structures, so that they can be electrically switched between the low and high transmissive states. A paper describing these first results has been published [5].

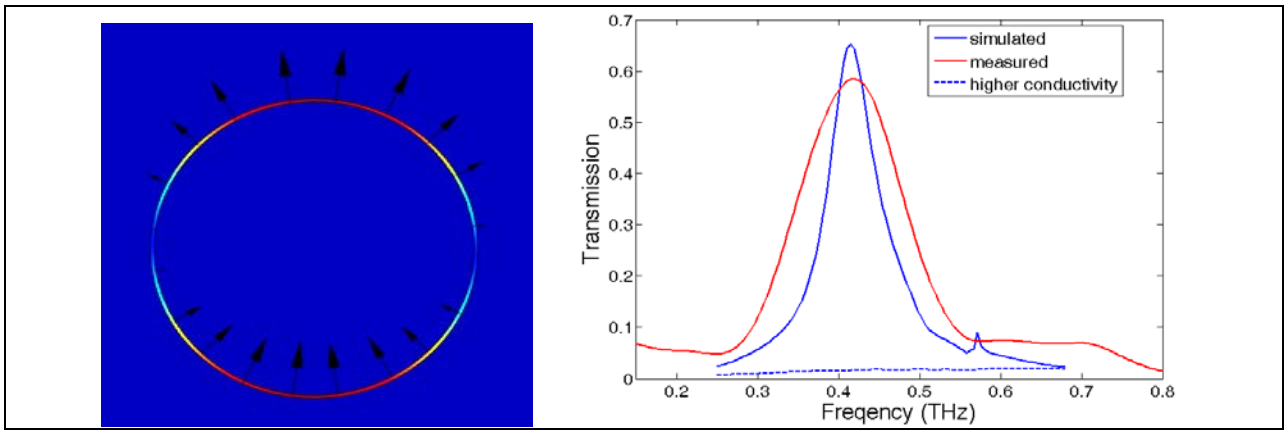

Figure 9. (left) Computed E-field distribution of the TE_{11} mode in the ring aperture, assuming a radius of 50 μm and a width of 1 μm. (right) Measured (red) and simulated (blue) power transmission spectra of circular ring aperture with r = 50 μm in a gold film on an intrinsic silicon substrate . With a carrier density of 3×10^{17} cm^{-3} in the substrate, the transmission is reduced by ~18 dB (dashed).

Finally, we have also begun working on another aspect of terahertz sensing, based on the idea of building a resonant cavity within a terahertz waveguide. This geometry can produce very narrow resonances, and can therefore be a valuable tool for sensing. It is especially well suited for microfluidic applications, as the resonator channel is accessible along the direction perpendicular to the terahertz beam propagation direction. Building on our earlier work in this area [6], we

have recently shown that this sensing geometry can be parallelized, so that multiple independent microfluidic streams can simultaneously and independently be monitored [7].

References:

[1] R. Appleby, P. Coward, and J. N. Sanders-Reed, *Proc. SPIE* **7309**, 73090A1 (2009).

[2] A. W. M. Lee, Q. Qin, S. Kumar, B. S. Williams, Q. Hu, and J. L. Reno, *Appl. Phys. Lett.* **89**, 141125 (2006).

[3] W. L. Chan, K. Charan, D. Takhar, K. F. Kelly, R. G. Baraniuk, and D. M. Mittleman, *Appl. Phys. Lett.* **93**, 121105 (2008).

[4] T. W. Ebbesen, H. J. Lezec, H. F. Ghaemi, T. Thio, and P. A. Wolff, *Nature*, **391**, 667 (1998).

[5] Jie Shu, Ciyuan Qiu, Victoria Astley, Daniel Nickel, Daniel M. Mittleman and Qianfan Xu, *Opt. Express*, **19**, 26666-26671 (2011).

[6] R. Mendis, V. Astley, J. Liu, and D. M. Mittleman, *Appl. Phys. Lett.*, **95**, 171113 (2009).

[7] V. Astley, K. Reichel, J. Jones, R. Mendis, and D. M. Mittleman, *Appl. Phys. Lett.*, **100**, 231108 (2012).

Publications:

1. "Terahertz microfluidic sensing using a parallel-plate waveguide sensor," Victoria Astley, Kimberly Reichel, Rajind Mendis, and Daniel M. Mittleman, *Journal of Visualized Experiments*, 66, e4304, (2012).

2. "Terahertz multichannel microfluidic sensor based on parallel-plate waveguide resonant cavities," Victoria Astley, Kimberly Reichel, Jonathan Jones, Rajind Mendis, and Daniel M. Mittleman, *Applied Physics Letters*, 100, 231108 (2012).

3. "A tunable universal THz filter using artificial dielectrics," Rajind Mendis, Abhishek Nag, Frank Chen, and Daniel M. Mittleman, *Applied Physics Letters*, 97, 131106 (2010).

4. "Whispering gallery-mode THz pulse propagation on a curved metallic plate," Rajind Mendis and Daniel M. Mittleman, *Applied Physics Letters*, 97, 031106 (2010).
"Bending and coupling losses in terahertz wire waveguides," Victoria Astley, Julianna Scheiman, Rajind Mendis, and Daniel M. Mittleman, *Optics Letters*, 35, 553-555 (2010).

5. "Comparison of the lowest-order transverse-electric (TE_1) and transverse-magnetic (TEM) modes of the parallel-plate waveguide for terahertz pulse applications," Rajind Mendis and Daniel M. Mittleman, *Optics Express*, 17, 14839–14850 (2009).

6. "A spatial light modulator for terahertz beams," Wai Lam Chan, Hou-Tong Chen, Antoinette J. Taylor, Igal Brener, Michael J. Cich, and Daniel M. Mittleman, *Applied Physics Letters*, 94, 213511 (2009).

APPENDIX G - "Design and Control of the Electromagnetic Casimir Force in Nanomechanical Systems"
PI: Andreas Hanke, UT Brownsville

Introduction

The research objective of this proposal is to gain sufficient understanding of the dependence of the electromagnetic Casimir force on geometry and material to permit its use as an actuating force in nanomechanical systems. The Casimir force between metallic or dielectric surfaces, generated by quantum fluctuations of the electromagnetic field, has been predominantly studied for simple geometries, such as two parallel plates, and perfectly conducting metals. However, the Casimir force has a strong – and often unpredictable – dependence on both the geometry and the optical properties of the interacting bodies. The goal of the proposed research is to understand and explain this dependence in terms of fundamental physical principles. Besides its intellectual merit, the proposed research will open the possibility to engineer Casimir forces in nanomechanical systems by tailoring their geometry and materials. If successful, this research will enable us to make active use of the Casimir force as actuating force in nanomechanical systems, and thereby transform the entire field of nanomechanics. It will impact the Air Force by providing new technology for nanoscale sensors and actuators.

The PI will establish a computational nanoscience laboratory at the University of Texas at Brownsville (UTB) to calculate the electromagnetic Casimir force in nanomechanical systems by using advanced computational tools (solving for Green's functions in imaginary frequency on a high-performance Linux cluster) and innovative theoretical methods (adapted coordinates). The project will train students in solving problems in computational electromagnetism and handling a sophisticated computer environment. Computational electromagnetism is an important ingredient in the development of emitters and sensors of electromagnetic waves. *This project will therefore impact the Air Force by providing new technology for telecommunication devices and electromagnetic sensors.*

The PI will collaborate with the experimental group of Dr. Ho Bun Chan (University of Florida), a leader in the field, to verify the predictions obtained in the computational lab for the following prototypes of nanomechanical systems:

System (1): Casimir force between a sphere and a silicon surface with nanoscale trench arrays; experimental data for this system are available by Dr. Chan's group (Chan, Bao et al. 2008).

System (2): Lateral Casimir force generated by a modulation step of a nanostructured surface.

Background and Significance

Nanomechanics is a rapidly developing research frontier where basic science and modern technology converge. The increasing miniaturization of nanomechanical systems requires an understanding of fundamental forces acting on the nanoscale. When the distance between metallic or dielectric surfaces is reduced to the submicron range, forces of pure quantum electrodynamical origin emerge. This force was first predicted 1948 by H. B. G. Casimir for two infinitely extended, perfectly conducting, electrically neutral plates in vacuum, for which he found the attractive force $F(z)$ per unit area A (Casimir 1948)

$$\frac{F(z)}{A} = -\frac{\pi^2 \hbar c}{240}\frac{1}{z^4} \qquad (1)$$

where c is the speed of light, $\hbar$ is Planck's constant divided by 2π, and z is the separation between the plates. This remarkable prediction of quantum electrodynamics can be understood as resulting from the modification of the quantum fluctuations of the electromagnetic field by the presence of boundaries; hence, the energy, $E(z)$, of the system depends on the separation z between the plates, resulting in a force $F(z) = -\frac{d}{dz}E(z)$. If the separation is reduced to $z = 100$ nm the Casimir force is already about $10\,\mathrm{N/m^2}$, corresponding to 10^{-4} atm, and at $z = 10$ nm it is as large as one atmosphere. Hence, on the submicron scale the Casimir force becomes the dominant interaction.

The initial attempts at observing the Casimir force were not conclusive, partly because of the difficulty of keeping two flat plates sufficiently parallel (Sparnaay 1958). The first clear evidence of the Casimir effect was achieved by measuring the Casimir force between a sphere and a plate which avoided this problem (Blokland and Overbeek 1978). High precision measurements of the Casimir force have become available only a decade ago using a torsion pendulum (Lamoreaux 1997) and an atomic force microscope (Mohideen and Roy 1998). This was followed by a large body of experimental studies which confirm the theory to a few percent accuracy; see, e.g., (Capasso, Munday et al. 2007; Chen, Klimchitskaya et al. 2007), and references cited therein. Most of the experiments measure the Casimir force between a sphere and a plate to avoid alignment problems for the interacting surfaces. A notable exception is the experiment by Bressi et al. who directly verified equation (1) by measuring the Casimir force between two flat plates (Bressi, Carugno et al. 2002).

In 2001, Ho Bun Chan and collaborators at Bell Labs pioneered experiments that demonstrated the possibility of using the Casimir force as an actuation force of micromechanical components; motion of a micromechanical torsional plate was induced solely by the Casimir force (Chan, Aksyuk et al. 2001); and the Casimir force was found to have a profound influence on the oscillatory behavior of the device (Chan, Aksyuk et al. 2001) (Figure 10). Other groups have demonstrated the feasibility of tuning the Casimir force by illuminating a semiconductor to change its optical properties (Chen, Klimchitskaya et al. 2007). This opens the intriguing opportunity of *dynamically controlling* the Casimir force in a nanomechanical system during operation. These experiments establish the importance of quantum electrodynamical effects in micro- and nanomechanical systems (MEMS and NEMS), hence the convergence of fundamental physics and real world technological applications (Capasso, Munday et al. 2007).

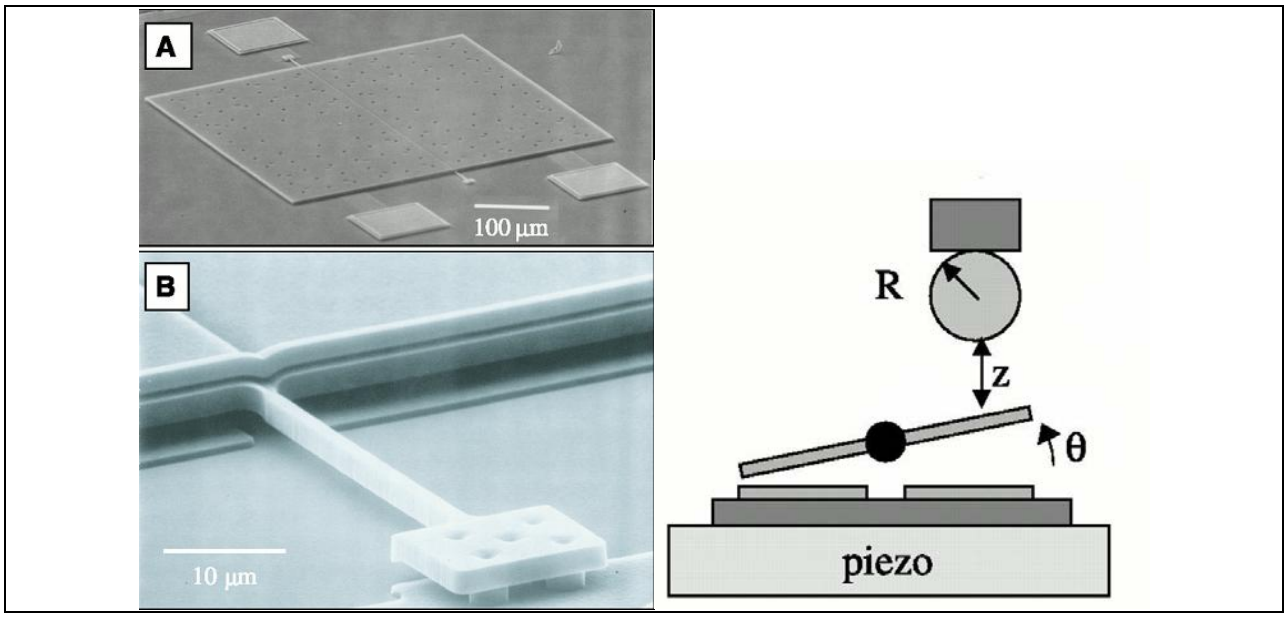

Figure 10. Left: (A) Scanning electron micrograph of the micromachined torsional device to measure the Casimir force between a silicon plate and a spherical metallic surface. (B) Close-up of one of the torsional rods anchored to the substrate (Chan, Aksyuk et al. 2001). Top: Schematic depiction of the experimental set-up.

The Casimir force has a strong, and often unpredictable, dependence on both the geometry and the optical properties of the interacting bodies. The strong boundary shape dependence of the Casimir force results from the *topological nature of the Casimir force as a fluctuation-induced force*; probing the global shape of the boundary that confines the vacuum fluctuations (Emig, Hanke et al. 2001). This applies, in particular, to nanomechanical systems actuated by the Casimir force which exhibit movable elements and therefore will in general deviate from the simple plate-plate or sphere-plate geometry. Recently, our collaborator Dr. Ho Bun Chan measured the Casimir force on a silicon surface with nanoscale trench arrays (Chan, Bao et al. 2008) (Figure 11). This experiment unambiguously demonstrates the strong boundary shape dependence of the Casimir force.

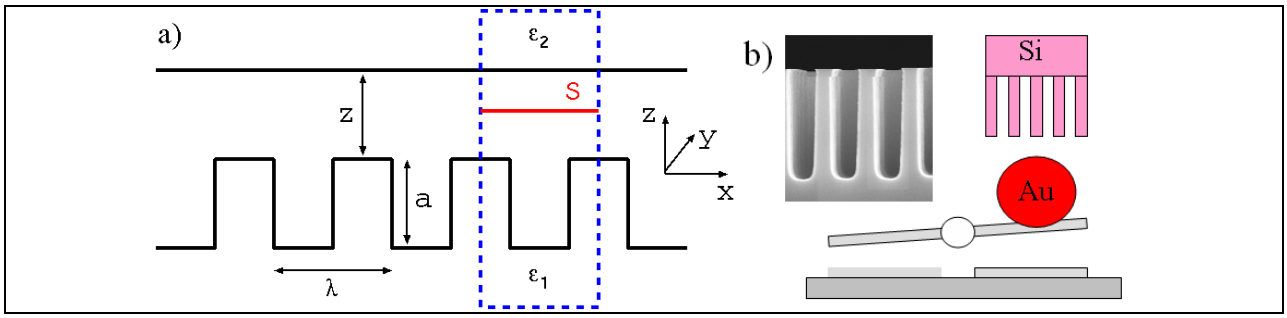

Figure 11. a) 3D rectangular grating with period λ in x-direction of System (1). The structure is translation invariant in y- direction. The 2D computational cell (blue) is used to calculate the Casimir force by integrating the electromagnetic stress tensor component $\langle T_{zz} \rangle$ along a surface between the two plates (red); cf. equation (2). b) Schematic depiction of the experimental set-up of the measurement of the Casimir force between a gold surface and a nanostructured surface with rectangular trench arrays (Chan, Bao et al. 2008). Inset: Electron micrograph showing a cross-section of rectangular trenches in silicon with λ = 400 nm and a = 980 nm. (Courtesy Ho Bun Chan)

Proposed Research

Numerical Method: Computation of the Casimir Force using Imaginary Frequency

Green's Functions and the Stress Tensor

The Casimir force $\mathbf{F} = (F_1, F_2, F_3)$ on a body is given by $F_j = \int_0^\infty d\zeta \iint_S \sum_{k=1}^3 \langle T_{jk}(\mathbf{r}, i\zeta) \rangle dS_k$ where $\langle T_{jk} \rangle$ is the mean stress tensor evaluated at imaginary frequency $\omega = i\zeta$ (Lifshitz and Pitaevskii 1980). Here, the zero-temperature limit $T = 0$ is assumed for simplicity, converting the sum over Matsubara frequencies ζ_n to an integral over ζ. The surface integral runs over any closed surface S surrounding the body. For nonmagnetic materials the stress tensor is given by (Lifshitz and Pitaevskii 1980)

$$\begin{aligned} \langle T_{jk}(\mathbf{r}, i\zeta) \rangle = {} & \varepsilon(\mathbf{r}, i\zeta) \left[\langle E_j(\mathbf{r}) E_k(\mathbf{r}) \rangle_\zeta - \frac{1}{2} \delta_{jk} \sum_{l=1}^3 \langle E_l(\mathbf{r}) E_l(\mathbf{r}) \rangle_\zeta \right] \\ & + \left[\langle H_j(\mathbf{r}) H_k(\mathbf{r}) \rangle_\zeta - \frac{1}{2} \delta_{jk} \sum_{l=1}^3 \langle H_l(\mathbf{r}) H_l(\mathbf{r}) \rangle_\zeta \right] \end{aligned} \qquad (2)$$

The correlation functions of the electromagnetic fields at imaginary frequency $\omega = i\zeta$ are related, via the fluctuation-dissipation theorem, to imaginary-frequency Green's functions G_{jk}: $\langle E_j(\mathbf{r}) E_k(\mathbf{r}') \rangle_\zeta = \frac{\hbar}{\pi} \zeta^2 G_{jk}(\mathbf{r}, \mathbf{r}'; \zeta)$ and $\langle H_j(\mathbf{r}) H_k(\mathbf{r}') \rangle_\zeta = -\frac{\hbar}{\pi} (\nabla\times)_{jm} (\nabla'\times)_{kn} G_{mn}(\mathbf{r}, \mathbf{r}'; \zeta)$ where $(\nabla\times)_{jm} a_m = (\nabla \times \mathbf{a})_j$ and summation over repeated indices is understood. The Green's function $G_{jk}(\mathbf{r}, \mathbf{r}'; \zeta)$ is determined as solution of the equation

$$\left[(\nabla\times\nabla\times)_{jm} + \delta_{jm} \frac{\zeta^2}{c^2} \varepsilon(\mathbf{r}, i\zeta) \right] G_{mk}(\mathbf{r}, \mathbf{r}'; \zeta) = \delta_{jk} \delta(\mathbf{r} - \mathbf{r}') \qquad (3)$$

with boundary conditions at the dielectric interfaces corresponding to the electric field in classical electromagnetism (Lifshitz and Pitaevskii 1980). Numerical computation of G_{mk} via equation (3) amounts to the inversion of the linear operator $\hat{D}_{jm}(\mathbf{r}) = \left[(\nabla \times \nabla \times)_{jm} + \delta_{jm} \frac{\zeta^2}{c^2} \varepsilon(\mathbf{r}, i\zeta) \right]$ with $(\nabla \times \nabla \times)_{jm} = \frac{\partial^2}{\partial x_j \partial x_m} - \delta_{jm} \nabla^2$. Since $\varepsilon(\mathbf{r}, i\zeta)$ is always real due to causality (Milonni 1993; Jackson 1998), the operator $\hat{D}$ is symmetric and, for $\zeta \neq 0$, positive definite. Furthermore, the resulting Green's function is exponentially decaying and non-oscillatory as a function of ζ, which facilitates the final numerical integration over ζ (or summation over discrete Matsubara frequencies ζ_n) to obtain the force.

In this project, equation (3) will be solved for G_{mk} on a high-performance Linux cluster using advanced tools of computational electromagnetism (Chew, Jin et al. 2001). The Linux cluster will consist of 20 2.5 GHz Intel Xeon Quad Core processors assembled in 5 units with 4 processors each, and a motherboard with Intel Xeon Quad Core processor (Microway). The obtained predictions for the Casimir force will be verified for the following experimental systems.

Casimir force between a sphere and a silicon surface with nanoscale trench arrays
This system will allow us to implement the numerical method and to test the results on available experimental data for a nontrivial geometry (Chan, Bao et al. 2008). Experimentally, periodic surface gratings can be readily produced by lithographic patterning methods. Figure 11a shows a rectangular grating with periodicity λ as used in the experiment; Figure 11b shows the experimental setup for measuring the Casimir force between a gold sphere and a silicon surface with nanoscale trench arrays (inset) using a micromechanical torsional balance (Chan, Bao et al. 2008).

The grating has periodicity λ in x - direction and is translation invariant in y - direction. Choosing a flat surface S for the stress tensor integral we obtain the force per unit area at $T = 0$ between the plates $\frac{F_z}{A} = \int_0^\infty d\zeta \frac{1}{\lambda} \int_0^\lambda dx \left\langle T_{zz}(\mathbf{r}; i\zeta) \right\rangle$ where $\mathbf{r} = (x, y, z)$ runs over the portion of S for which x is restricted to one period $[0, \lambda]$ with y, z fixed. This portion of S is shown as the red line in Figure 11a. As shown above, the mean stress tensor $\left\langle T_{zz}(\mathbf{r}; i\zeta) \right\rangle$ is expressed via the Green's function in terms of contributions $G_{jl}(\mathbf{r}, \mathbf{r}; \zeta)$. By Fourier transforming the y - direction and using Bloch's theorem in x - direction (Ashcroft and Mermin 1976) we find
$\int_0^\infty d\zeta \frac{1}{\lambda} \int_0^\lambda dx\, G_{jl}(\mathbf{r}, \mathbf{r}; \zeta) = \int_0^\infty d\zeta \frac{1}{\lambda} \int_0^\lambda dx \int_{-\pi/\lambda}^{\pi/\lambda} \frac{dk_x}{2\pi} \int_{-\infty}^{\infty} \frac{dk_y}{2\pi} U_{jl}(x, x; z, z; k_x, k_y)$.

The kernel U_{jl} is determined as solution of the equation

$$\hat{D}'_{jm} U_{ml}(x, x; z, z; k_x, k_y) = \delta_{jl} \delta_\lambda (x - x') \delta(z - z') \qquad (4)$$

in the domain $-\infty < z < \infty$, $x \in [0, \lambda]$, with periodic boundary conditions in x - direction and with boundary conditions corresponding to the electric field at the dielectric interfaces. The operator $\hat{D}'$ is obtained from $\hat{D}$ by replacing $\partial/\partial y$ with ik_y and $\partial/\partial x$ with $\partial/\partial x + ik_x$. $\delta_\lambda(x) = \sum_{n=-\infty}^{\infty} \exp(i2\pi nx/\lambda)$ is the delta-function restricted to the space of λ - periodic functions. The wave vector components $k_x \in [-\pi/\lambda, \pi/\lambda]$ and $-\infty < k_y < \infty$ appear as fixed parameters. Numerical computation of U_{jl} via equation (4) amounts to the inversion of the operator $\hat{D}'$. This standard problem can be solved by a variety of techniques (Chew, Jin et al. 2001).

We propose to calculate the Casimir force between a flat surface and a surface endowed with a rectangular grating by implementing the above computational method on a high-performance Linux cluster. We will verify the results with the available data from the experiment (Chan, Bao et al. 2008). This will provide groundwork for the design of nanomechanical systems actuated by the Casimir force, as shown below.

Lateral Casimir force generated by a modulation step of a nanostructured surface. Actuation in a nanomechanical system typically requires the existence of a *lateral force* on a surface in close proximity to a second surface. Such a force can only exist if the translation invariance in lateral direction is broken, either through the change of the patterning of a nanostructured surface across a modulation step or through the change of material across a chemical step. We here study the prototype of a modulation step as shown in Figure 12.

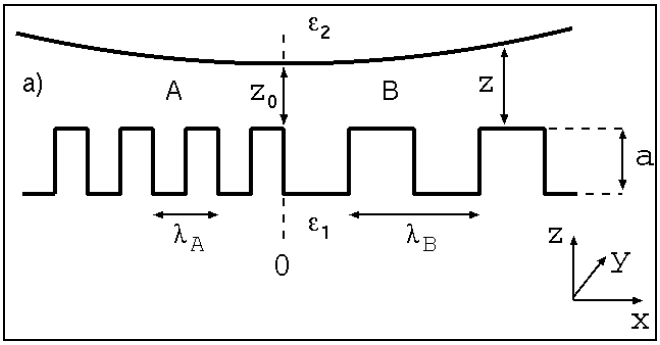

Figure 12. Spherical surface above a nanostructured, on average flat surface. The lower surface is modulated with different periodicities λ in regions A ($x < 0$) and B ($x > 0$), forming a modulation step at $x = 0$.

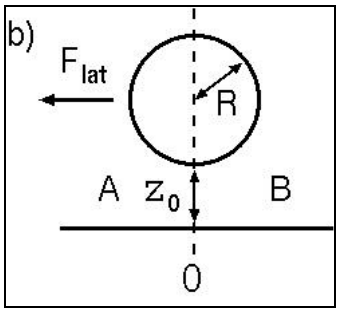

Figure 13. Same as a) shown on a larger scale. The modulation of the lower surface is not shown. The difference in Casimir energy density in regions A and B generates a lateral force on the sphere as indicated.

The PI and graduate student Marco Milan have generated a FORTRAN program to implement the numerical method of computing the Casimir force between bodies of given material and shape. The method is based on solving for Green's functions in imaginary frequency by using tools from computational electromagnetism, and was originally developed by the group of Dr. Stephen Johnson and collaborators at MIT. We have verified the method for the Casimir force between a sphere and a silicon surface with nanoscale trench arrays, for which experimental data are available by Dr. Chan's group. Dr. Chan's group was able to obtain more accurate data than reported in their original publication on this system [H. B. Chan, Y. Bao *et al,* Phys. Rev. Lett. 101, 030401 (2008)]. A publication for the comparison of the experimental data with our calculations is in preparation.

We have also started a new project to study the possibility of non-equilibrium, *repulsive* Casimir forces between macroscopic objects when they are kept at different temperatures. It is known that non-equilibrium repulsive forces between molecules can be generated by suitable detuning of the resonance frequencies. This suggests that for macroscopic objects held at different temperatures similar repulsive effects should exist close to material resonances in the thermal region. The creation of repulsive Casimir forces between extended objects is of primary interest in applications to overcome the problem of stiction between movable elements in MEMS. A publication related to non-equilibrium Casimir forces in a dissipative medium confined by vibrating plates is currently under review with PLoS ONE.

Recent papers and invited talks at meetings:
KITP Program: The Theory and Practice of Fluctuation-Induced Interaction
August 18 - November 21, 2008
University of California at Santa Barbara
Invited participation September 29 – October 31, 2008
Oral presentation: Non-equilibrium Casimir force between moving plates

Conference:
New Frontiers in Casimir Force Control
September 27 – 29, 2009
Santa Fe, New Mexico
Invited participation

A. Hanke, Non-equilibrium thermal Casimir force between vibrating plates.
Under review with PLoS ONE.

References:

Ashcroft, N. W. and N. D. Mermin (1976). Solid State Physics. Philadelphia, Saunders College Publishing.

Blokland, P. H. G. M. v. and J. T. G. Overbeek (1978). J. Chem. Soc., Faraday Trans. 74: 2637.

Bressi, G., G. Carugno, et al. (2002). "Measurement of the Casimir force between parallel metallic surfaces." Phys. Rev. Lett. 88: 041804.

Capasso, F., J. N. Munday, et al. (2007). "Casimir forces and quantum electrodynamical torques: Physics and Nanomechanics." IEEE J. Sel. Top. Quant. Electr. 13: 400.

Casimir, H. B. G. (1948). Proc. K. Ned. Akad. Wet. 51: 793.

Chan, H. B., V. A. Aksyuk, et al. (2001). "Nonlinear Micromechanical Casimir Oscillator." Phys. Rev. Lett. 87: 211801.

Chan, H. B., V. A. Aksyuk, et al. (2001). "Quantum Mechanical Actuation of Microelectromechanical Systems by the Casimir Force." Science 291: 1941.

Chan, H. B., Y. Bao, et al. (2008). "Measurement of the Casimir force between a gold sphere and a silicon surface with nanoscale trench arrays." Phys. Rev. Lett. 101: 030401.

Chen, F., G. L. Klimchitskaya, et al. (2007). "Control of the Casimir force by the modification of dielectric properties with light." Phys. Rev. B 76: 035338.

Chew, W. C., J.-M. Jin, et al. (2001). Fast and Efficient Algorithms in Computational Electromagnetics. Boston, Artech House.

Emig, T., A. Hanke, et al. (2001). "Probing the strong boundary shape dependence of the Casimir force." Phys. Rev. Lett. 87: 260402.

Jackson, J. D. (1998). Classical Electrodynamics. New York, Wiley.

Lamoreaux, S. K. (1997). "Demonstration of the Casimir Force in the 0.6 to 6 micrometer Range." Phys. Rev. Lett. 78: 5.

Lifshitz, E. M. and L. P. Pitaevskii (1980). Statistical Physics: Part 2. Oxford, Pergamon.

Milonni, P. W. (1993). The Quantum Vacuum: An Introduction to Quantum Electrodynamics. San Diego, Academic.

Mohideen, U. and A. Roy (1998). "Precision Measurement of the Casimir Force from 0.1 to 0.9 micrometers." Phys. Rev. Lett. 81: 4549.

Sparnaay, M. J. (1958). Physica (Utrecht) 24: 751.

APPENDIX H - "Photothermal/Photopyro/Photoacoustic Effects in Nanowires"
PI: Paul Chu, University of Houston

During the period of August 2008 - February 2013, our work has been kindly supported in part by CONTACT. Compounds of interest, both new and old, have been successfully synthesized and studied, with novel phenomena observed, models proposed to account for the observations, and records in magnetoelectric effect and T_c in 122 Fe-based superconductors observed and explained. New techniques have been developed for large charge-induction, storage, and negative capacity determination. While room temperature superconductivity as envisioned for the project has not been realized, exciting results in different but related areas have been achieved, and are listed by topic below:

Photothermal/Photopyro/Photoacoustic Effects in Nanowires

1. We have found that the photoacoustic effect in single wall carbon nano wires (SWCNW) is stronger than in Si-nanowires (Si-NW), tentatively attributed to the catalyst nano particles present in the latter.

2. We have shown that the induced sound appears to depend on both the light intensity and the pulse duration with apparent thresholds: the sound amplitude on single-wall carbon nanotubes under a fixed pulse-width of 1/64 sec, for example, increases with the light intensity only after a threshold of ~0.03 J/cm^2. The sound intensity on the same samples under light intensities of 0.07 J/cm^2 and 0.2 J/cm^2 also continuously increases with the pulse width up to 1 sec. The data therefore suggest that the heating process is a rather slow one.

3. We have demonstrated that the photoacoustic effect increases with flashlight pulse width, suggesting a much slower thermal response under conventional model (e.g., very low "thermal conductivity" along the radius direction) or a new mechanism. The observation calls for a new model to account for the nonlinear response of sound amplitude vs. light intensity.

4. We have developed a self-alignment and dielectriophoresis technique to align SWCNW and Si-NW for possible devices based on the photoacoustic and photopyro effects.

5. We have estimated the temperature to be 1200 °C, suggesting an enhanced EM absorption and great potential for application.

Study of Negative Electric Capacity in Nano-Aggregates at Low Frequency

1. We have developed experimental techniques for precision capacitance and resistance measurements at very low frequency down to 10^{-5} per sec. and demonstrated it not to be associated with superconductivity in spite of its tantalizing implication.

2. We have established and confirmed the effect in several material systems and demonstrated the important role of moisture in the effect.

3. We have developed a universal model in terms of a lossy component of the material systems and demonstrated its universal success in applications to various examples from nano-inorganic aggregates through semiconductor superlattices, to chemical cells and bio-membranes.

Field-Induced Change in the Electronic Properties of Solids

1. We have succeeded to generate and store very high surface electron density for both nano field-effect transistors (and more) and nano energy suppliers.

2. We have developed a technique to control the experimental environment. Using techniques

developed by us and electron double-layer (EDL) charging, we have achieved an estimated surface charge density of 4 x 10^{15} electrons/cm^2, which is translated to ~ 3 x 10^{23} electrons/cc and should turn anything to a metal without introducing any undesirable defects. Preliminary data show that EDL charging on graphene film (reduced graphene oxide) showed an increase of electric conductivity of ~20%. We are now in the process to acquire samples of improved quality to amplify the charging effect.

3. We have also detected near 50 Hz a negative resonance capacitance in the electrolyte liquid used. The cause is yet to be determined.

Search for Superconductivity with Higher T_c via Nano-Route

1. We have discovered an unusual non-bulk superconducting transition in the electron-doped single-crystalline (Ca,R)Fe_2As_2, where R = La, Ce, Pr, Nd, with a T_c up to 49 K, more than 30 K higher than that of the known compounds of Ca-R-Fe-As, accompanying another 22 K bulk superconducting transition.

2. We have demonstrated that the 49 K superconducting transition has an unusually large magnetic anisotropy of greater than 30, in comparison with a geometric anisotropy of 3-4 expected of the sample examined, while the 22 K transition shows only 3-4, similar to that observed in other bulk FeAs122 compounds.

3. We have shown that the 49 K transition is of the Josephson-coupling type that survives only in a weak magnetic field less than 300 Oe, whereas the 22 K transition remains at above 5 T.

4. We have suggested that the 49 K superconductivity may be attributed to the novel interfacial superconductivity, based on the above observations, although more definitive studies are warranted.

The Search for High T_c in Novel Superconductors

1. We synthesized and studied the 32 K superconducting and non-superconducting $Rb_xFe_2Se_2$ single crystals at ambient and high pressure and found that superconductivity depends critically on the chemical stoichiometry, the defect density, and the synthesis conditions.

2. We have investigated the ARPES of AFe_2Se_2 and observed possible unusual spectra and excitations.

3. We have synthesized and characterized the 3.8 K superconducting $Cu_xBi_2Se_3$. We found that both x and synthesis conditions affect the T_c sensitively and the reported bulk nature of superconductivity in these compounds is yet to be settled. We have also found the absence of the zero-biased conduction peak, raising the intriguing question of whether the compound is indeed a topological superconductor.

4. We have obtained dibenzopentacene and started doping it with alkaline elements—superconductivity in the 20s K is not yet achieved.

5. We have synthesized two new Cu-based As compound systems, $Sr_{1-}K_xCu_4As_2$ (142), but unfortunately without sign of superconductivity yet.

6. We have observed a pressure-induced superconducting – semiconducting transition at 24 GPa in the two-layer YBCO and proposed possible higher T_c to above the current record of 165 K under pressure in three-layer HBCCO if one can avoid electronic instability detected in the two-layer compound.

7. We have studied the pressure effect on thin films of strained $FeSe_{0.5}Te_{0.5}$ superconductors

and shown that the anion height in FeSe/Te has an effect on the superconducting T_c; however, it is not the only parameter controlling T_c and other parameters have to be considered.

8. We have shown that the pressure-induced shift of T_c in the hole-doped systems, SmFeAs(O,F) and $K_xSr_xFe_2As_2$, strongly depends on the doping state and predicted the existence of a possible ceiling of T_c in iron pnictide superconductors.

9. We discovered, synthesized, and extensively studied the new superconductor LiFeAs through magnetic, transport, thermodynamic, and high-pressure methods and have proven that LiFeAs is the only stoichiometric, self-doped iron pnictide superconductor with relatively high T_c up to 18 K.

10. We have shown the existence of quantum critical scaling above the superconducting dome of $K_xSr_{1-x}Fe_2As_2$, suggesting the important role of spin fluctuations in the normal state and superconductivity of iron pnictide superconductor.

11. We have shown that NaFeAs is a bulk superconductor only if the stoichiometry deviates from the 1:1:1 composition, in contrast to the related compound LiFeAs.

12. We have synthesized the metastable compound $NaFe_2As_2$ and shown the existence of superconductivity up to 25 K.

13. We discovered a new pnictide oxide superconducting layered system, $Ba_{1-x}Na_xTi_2Sb_2O$. The compound class is of high interest since superconductivity apparently resides in Ti_2O planes (antiphase to the TiO_2 planes of the lower T_c reduced $SrTiO_3$). We have studied the physical properties and the pressure effect on the normal and superconducting states.

14. We have discovered a series of intermetallic superconductors, such as Zr-doped Nb_5Ge_3 and V_5Ge_3 that were synthesized and made superconducting with a T_c up to 11 K.

15. We have investigated the doping effect on several layered compounds and found doping through intercalation can be detrimental to superconductivity.

Search for High T_c in Compound Systems via Optimization of Various Interactions Starting in the Multiferroics

1. We have synthesized high-quality single crystals of substituted $Mn_{1-x}T_xWO_4$ (T=Fe, Co, Cu, Zn) for magnetic, dielectric, pyroelectric, thermodynamic, and neutron scattering studies. Large single crystals showing a single structural domain have been prepared and investigated by neutron scattering.

2. We have studied the multiferroic phase diagram of $Mn_{1-x}Fe_xWO_4$ and discovered a reentrant multiferroic/ferroelectric phase in external magnetic fields.

3. We have identified the various commensurate, incommensurate, collinear, and non-collinear magnetic orders in the complex phase diagram of $Mn_{1-x}Fe_xWO_4$ through elastic neutron scattering experiments and revealed the important role of magnetic frustration and competing interactions.

4. We have measured spin wave excitation spectrum and extracted the detailed magnetic exchange interactions in $MnWO_4$ through inelastic neutron scattering experiments. We found that the magnetic exchange interactions in this compound are long-ranged and extend up to 11 nearest neighbors.

5. We have discovered a robust multiferroic/ferroelectric state in the spin-diluted system $Mn_{1-x}Zn_xWO_4$ that survives a 50% removal of Mn spins.

6. We have completely resolved the multiferroic phase diagram of $Mn_{1-x}Co_xWO_4$ showing that the ferroelectric polarization changes direction twice with increasing Co content. This resolves a contradiction between different publications with results reported by research groups in the United States, Korea/Japan, and Spain.

7. We have identified the magnetic orders and the multiferroic phases in $Mn_{1-x}Co_xWO_4$ through elastic neutron scattering experiments.

8. We have studied the effects of magnetic fields on the multioferroic states in $Mn_{1-x}Co_xWO_4$ and discovered the reversal of the ferroelectric polarization in $Mn_{0.85}Co_{0.15}WO_4$ at a critical temperature in magnetic fields.

9. We have identified and revealed the magneto-elastic coupling in frustrated $Co_3V_2O_8$ through optical measurements in high magnetic fields.

10. We have discovered a sizable magnetoelectric effect and a spontaneous polarization in $HoFe_3(BO_3)_4$ and the solid solution $Ho_{1-x}Nd_xFe_3(BO_3)_4$.

11. We have found a large bilinear magnetoelectric effect and strong magnetoelastic coupling in $TmAl_3(BO_3)_4$. This discovery proves that the rare earth moments are the driving force for the magnetoelectricity in the borate class of compounds and that the spins of the transition metals are not an essential ingredient.

12. We have found a correlation between the magnetic anisotropy and the magnitude of the magnetoelectric effect in the system $RAl_3(BO_3)_4$ (R = Tb, Er, Tm, Ho), which has led to the optimization of the chemistry of the compounds.

13. We have discovered a record magnetoelectric polarization in $HoAl_3(BO_3)_4$ at high magnetic field. The magnitude of the field-induced electrical polarization does exceed all reported values for magnetoelectric and multiferroic compounds.

14. We have discovered ferromagnetic order in $AAg_2M[VO_4]_2$ (A=Ba, Sr; M=Co, Ni), a system with super-super exchange interactions and frustration.

15. We have found an unusual coexistence of ferromagnetic and antiferromagnetic spin chains and antiferromagnetic long-range order in $BaAg_2Cu[VO_4]_2$, giving rise to unconventional properties of the magnetization and heat capacity. The experimental results could be confirmed and are supported by first principle band structure calculations.

16. We have discovered weak ferromagnetism, internal magnetoelectric coupling, and an external magnetoelectric effect in the polar crystal $LiFeP_2O_7$.

Publications (*CONTACT acknowledgement)

1. "Pressure-Induced Shift of T_c in the System $K_xSr_{1-x}Fe_2As_2$ (x=0.2, 0.4, 0.7): Analogy to the High-T_c Cuprate Superconductors," M. Gooch, B. Lv, B. Lorenz, A. M. Guloy and C. W. Chu, Phys. Rev. B "Rapid Communications" 78, 180508 (2008).

2. "Magnetic Switching and Phase Competition in the Multiferroic Antiferromagnet $Mn_{1-x}Fe_xWO_4$," F. Ye, Y. Ren, J. A. Fernandez-Baca, H. A. Mook, J. W. Lynn, R. P. Chaudhury, Y. Q. Wang, B. Lorenz and C. W. Chu, Phys. Rev. B 78, 193101 (2008).

3. "Pressure Shift of the Superconducting T_c of LiFeAs," M. Gooch, B. Lv, J. H. Tapp, Z. Tang, B. Lorenz, A. M. Guloy and C. W. Chu, Europhysics Letters 85, 27005 (2009).

4. "Evidence of Quantum Criticality in the Phase Diagram of $K_xSr_{1-x}Fe_2As_2$ from Measurements of Transport and Thermoelectricity," M. Gooch, B. Lv, B. Lorenz, A. M. Guloy

and C. W. Chu, Physical Review B 79, 104504 (2009).

5. "The Superconductor $K_xSr_{1-x}Fe_2As_2$: Normal State and Superconducting Properties," B. Lv, M. Gooch, B. Lorenz, F. Chen, A. M. Guloy and C. W. Chu, New Journal of Physics 11, 025013 (2009).

6. "The Synthesis and Characterization of LiFeAs and NaFeAs," C. W. Chu, F. Chen, M. Gooch, A. M. Guloy, B. Lorenz, B. Lv, K. Sasmal, Z. J. Tang, J. H. Tapp and Y. Y. Xue, Physica C 469, 326 (2009).

7. "High Pressure Studies on Fe-Pnictide Superconductors," C. W. Chu and B. Lorenz, Physica C 469, 385 (2009).

8. "Re-entrant Spiral Magnetic Order and Ferroelectricity in $Mn_{1-x}Fe_xWO_4$," R. P. Chaudhury, B. Lorenz, Y. Q. Wang, Y. Y. Sun, C. W. Chu, F. Ye, J. Fernandez-Baca, H. Mook and J. Lynn, Journal of Applied Physics 105, 07D913 (2009).

9. "Unusual Doping Dependency of Superconductivity in Na_xFeAs," K. Sasmal, B. Lv, Z. J. Tang, F. Chen, Y. Y. Xue, B. Lorenz, A. M. Guloy and C. W. Chu, Phys. Rev. B 79, 184516 (2009).

10. "Interfacial Resistive Oxide Switch by Reversible Modification of Defect Structures," S. Tsui, Y. Y. Xue, N. Das, Y. Q. Wang and C. W. Chu, Phys. Rev. B 80, 165415 (2009).

11. "Re-entrant Ferroelectricity and the Multiferroic Phase Diagram of $Mn_{1-x}Fe_xWO_4$," R. P. Chaudhury, B. Lorenz, Y. Q. Wang, Y. Y. Sun and C. W. Chu, New Journal of Physics 11, 033036 (2009).

12. "General Mechanism for Negative Capacitance Phenomena," J. Shulman, Y. Y. Xue, S. Tsui, F. Chen and C. W. Chu, Phys. Rev. B 80, 134202 (2009).

13. "Magnetoelectric Effect and Spontaneous Polarization in $HoFe_3(BO_3)_4$ and $Ho_{0.5}Nd_{0.5}Fe_3(BO_3)_4$," R. P. Chaudhury, F. Yen, B. Lorenz, Y. Y. Sun, L. N. Bezmaternykh, V. L. Temerov and C. W. Chu, Phys. Rev. B 80, 104424 (2009).

14. "High-Temperature Superconductivity: Alive and Kicking," C. W. Chu, Nature Physics 5, 787 (2009).

15. "Kinetics and Relaxation of Electroresistance in Transition Metal Oxides: Model for Resistive Switching," N. Das, S. Tsui, Y. Y. Xue, Y. Q. Wang and C. W. Chu, Phys. Rev. B 80, 115411 (2009).

16. "Electrical Characterization of Resistive Memory in Metal-$Pr_{0.7}Ca_{0.3}MnO_3$ Interface: A Future Non-Volatile Memory Device," N. Das, Y. Y. Xue, Y. Q. Wang and C. W. Chu, Proceedings of the 10th Annual Non-Volatile Memory Technology Symposium (NVMTS), October 25-28, 2009 (IEEE, 2009), pp. 28-47.

17. "Lower Critical Field, Anisotropy, and Two-Gap Features of LiFeAs," K. Sasmal, B. Lv, Z. Tang, F. Y. Wei, Y. Y. Xue, A. M. Guloy and C. W. Chu, Phys. Rev. B 81, 144512 (2010).

18. "Evidence for Multiple Gaps in Specific Heat of LiFeAs Crystals," F. Wei, F. Chen, K. Sasmal, B. Lv, Z. J. Tang, Y. Y. Xue, A. M. Guloy and C. W. Chu, Phys. Rev. B 81, 134527 (2010).

19. "Superconductivity in Ternary Iron Pnictides: AFe_2As_2 (A = Alkali Metal) and LiFeAs," M. Gooch, B. Lv, K. Sasmal, J. H. Tapp, Z. J. Tang, A. M. Guloy, B. Lorenz and C. W. Chu, Physica C 470, S276 (2010).

20. "Magnetic Phase Diagram and Magnetoelectric Properties of $Ho_{0.25}Nd_{0.75}Fe_3(BO_3)_4$," R. P.

Chaudhury, B. Lorenz, Y. Y. Sun, L. N. Bezmaternykh, V. L. Temerov, and C. W. Chu, Journal of Applied Physics 107, 09D913 (2010).

21. "Critical Scaling of Transport Properties in the Phase Diagram of Iron Pnictide Superconductors $K_xSr_{1-x}Fe_2As_2$ and $K_xBa_{1-x}Fe_2As_2$," M. Gooch, B. Lv, B. Lorenz, A. M. Guloy, and C. W. Chu, Journal of Applied Physics 107, 09E145 (2010).

22. "Magnetoelectricity and Magnetostriction due to the Rare Earth Moment in $TmAl_3(BO_3)_4$," R. P. Chaudhury, B. Lorenz, Y. Y. Sun, L. N. Bezmaternykh, V. L. Temerov and C. W. Chu, Phys. Rev. B 81, 220402(R) (2010).

23. "Magnetic and Multiferroic Phases of Single-Crystalline $Mn_{0.85}Co_{0.15}WO_4$," R. P. Chaudhury, F. Ye, J. A. Fernandez-Baca, Y. Q. Wang, Y. Y. Sun, B. Lorenz, H. A. Mook and C. W. Chu, Phys. Rev. B 82, 184422 (2010).

24. "The Evolution of HTS: T_c-Experiment Perspectives," C. W. Chu, Ch. 16 in *50 Years of Bardeen, Cooper and Schrieffer*, ed. by L. N. Cooper and D. Feldman (Singapore: World Scientific, 2010), p. 391.

25. "Magneto-elastic Coupling in Magnetically Frustrated $Co_3V_2O_8$," J. L. Musfeldt, L. I. Vergara, J. Cao, L. C. Tung, Y. J. Wang, F. Yen, Y. Q. Wang, B. Lorenz, N. Rogado and R. J. Cava, Mag Lab Reports 18(2), 12 (2011).

26. "Carrier Contribution to the Specific Heat Coefficient of $Sr_{1-x}K_xFe_2As_2$," F. Y. Wei, B. Lv, F. Chen, Y. Y. Xue, and C. W. Chu, Phys. Rev. B 83, 024503 (2011).

27. "Incommensurate Spin-Density Wave and a Multiband Superconductivity Phase in Na_xFeAs Revealed by Nuclear Magnetic Resonance," M. Klanjšek, P. Jeglič, B. Lv, A. M. Guloy, C. W. Chu and D. Arčon, Phys. Rev. B 84, 054528 (2011).*

28. "Doping Dependence of Phase-Separation Morphology in $(Sr,K)Fe_2As_2$," F. Y. Wei, B. Lv, F. Chen, K. Sasmal, J. Shulman, Y. Y. Xue, and C. W. Chu, Phys. Rev. B 83, 094517 (2011).

29. "Robust Ferroelectric State in Multiferroic $Mn_{1-x}Zn_xWO_4$," R. P. Chaudhury, F. Ye, J. A. Fernandez-Baca, B. Lorenz, Y. Q. Wang, Y. Y. Sun, H. A. Mook and C. W. Chu, Phys. Rev. B 83, 014401 (2011).

30. "Generation of Negative Capacitance in a Nanocolloid," J. Shulman, Y. Y. Xue, S. Tsui, F. Chen and C. W. Chu, J. Appl. Phys. 109, 034304 (2011).*

31. "A Possible Pressure-Induced Superconducting-Semiconducting Transition in Nearly Optimally Doped Single Crystalline $YBa_2Cu_3O_{7-\square}$," T. Muramatsu, D. Pham and C. W. Chu, Appl. Phys. Lett. 99, 052508 (2011).*

32. "Long-Range Magnetic Interactions in the Multiferroic Antiferromagnetic $MnWO_4$," F. Ye, R. S. Fishman, J. A. Fernandez-Baca, A. A. Podlesnyak, G. Ehlers, H. A. Mook, Y. Q. Wang, B. Lorenz and C. W. Chu, Phys. Rev. B, "Rapid Communications" 83, 140401 (2011).

33. "Two-Gap Features in the Specific Heat of $(M,K)Fe_2As_2$ with M = Ba, Sr," F. Y. Wei, B. Lv, Y. Y. Xue and C. W. Chu, Phys. Rev. B 84, 064508 (2011).*

34. "Giant Magnetoelectric Effect in $HoAl_3(BO_3)_4$," K.-C. Liang, R. P. Chaudhury, B. Lorenz, Y. Y. Sun, L. N. Bezmaternykh, V. L. Temerov and C. W. Chu, Phys. Rev. B "Rapid Communications" 83, 180417 (2011).

35. "High-Pressure Study of Superconducting and Nonsuperconducting Single Crystals of the Same Nominal Composition $Rb_{0.8}Fe_2Se_2$," M. Gooch, B. Lv, L. Z. Deng, T. Muramatsu, J. Meen, Y. Y. Xue, B. Lorenz and C. W. Chu, Phys. Rev. B 84, 184517 (2011).*

36. "The Unusual Superconducting State at 49 K in Electron-Doped $CaFe_2As_2$ at Ambient," B. Lv, L. Z. Deng, M. Gooch, F. Y. Wei, Y. Y. Sun, J. Meen, Y. Y. Xue, B. Lorenz and C. W. Chu, Proceedings of the National Academy of Sciences USA 108, 15705 (2011).*

37. "Multiferroic Phase Control in $MnWO_4$ Doped with Fe, Co, and Zn: A Comparative Study," K.-C. Liang, R. P. Chaudhury, B. Lorenz, Y. Q. Wang, Y. Y. Sun and C. W. Chu, Integrated Ferroelectrics 131, 47 (2011).

38. "Raman Scattering Study of Electron-Doped $Pr_xCa_{1-x}Fe_2As_2$ Superconductors," A. P. Litvinchuk, B. Lv and C. W. Chu, Phys. Rev. B 84, 092504 (2011).

39. "Electronic Band Structure of $SrCu_4As_2$ and KCu_4As_2: Metals with Diversely Doped CuAs Layers," V. G. Hadjiev, B. Lv and C. W. Chu, Phys. Rev. B "Brief Reports" 84, 073105 (2011).

40. "Control of Improper Ferroelectricity by Chemical Substitution and Magnetic Fields in Multiferroic $Mn_{1-x}Cu_xWO_4$," K.-C. Liang, Y. Q. Wang, Y. Y. Sun, B. Lorenz and C. W. Chu, submitted to Ferroelectrics (November 16, 2011).

41. "Magnetoelectricity in the System $RAl_3(BO_3)_4$ (R = Tb, Ho, Er, Tm)," K.-C. Liang, R. P. Chaudhury, B. Lorenz, Y. Y. Sun, L. N. Bezmaternykh, I. A. Gudim, V. L. Temerov and C. W. Chu, Journal of Physics: Conference Series 400, 032046 (2012).

42. "Cuprates—Superconductors with a T_c up to 164 K," C. W. Chu, Section 4.4 of Chapter 4, "Materials," in *100 Years of Superconductivity*, ed. by H. Rogalla and P. H. Kes (Boca Raton FL: Taylor & Francis/CRC, 2012), p. 244.

43. "Materials," C. W. Chu, Section 4.1 of Chapter 4, "Materials," in *100 Years of Superconductivity*, ed. by H. Rogalla and P. H. Kes (Boca Raton FL: Taylor & Francis/CRC, 2012), p. 233.

44. "Pressure Effects on Strained $FeSe_{0.5}Te_{0.5}$ Thin Films," M. Gooch, B. Lorenz, S. X. Huang, C. L. Chien and C. W. Chu, J. Appl. Phys. 111, 112610 (2012).

45. "Field-Induced Continuous Rotation of the Polarization in Multiferroic $Mn_{0.95}Co_{0.05}WO_4$," K.-C. Liang, R. P. Chaudhury, Y. Q. Wang, Y. Y. Sun, B. Lorenz, and C. W. Chu, Journal of Applied Physics 111, 07D903 (2012).

46. "A Possible Approach from BCS through HTS to RTS with Three Examples," C. W. Chu, Physica C 482, 33 (2012).*

47. "Spin Dynamics in the Multiferroic Materials," F. Ye, R. S. Fishman, J. Haraldsen, B. Lorenz, C. W. Chu and T. Kimura, J. Appl. Phys. 111, 07E137 (2012).

48. "The Complex Multiferroic Phase Diagram of $Mn_{1-x}Co_xWO_4$," K.-C. Liang, Y.-Q. Wang, Y. Y. Sun, B. Lorenz, F. Ye, J. A. Fernandez-Baca, H. A. Mook and C. W. Chu, New Journal of Physics 14, 073028 (2012).

49. "Thermodynamic Evidence for Pressure-Induced Bulk Superconductivity in the Fe-As Pnictide Superconductor $CaFe_2As_2$," Y. Zheng, Y. Wang, B. Lv, C. W. Chu and R. Lortz, New Journal of Physics 14, 053034 (2012).

50. "Weak Ferromagnetism and Internal Magnetoelectric Effect in Multiferroic $LiFeP_2O_7$," K.-C. Liang, W. Zhang, B. Lorenz, Y. Y. Sun, P. S. Halasyamani and C. W. Chu, Phys. Rev. B 86, 094414 (2012).

51. "$AAg_2M[VO_4]_2$ (A = Ba, Sr; M = Co, Ni): A Series of Ferromagnetic Insulators," A. Möller, N. E. Amuneke, P. Daniel, B. Lorenz, C. R. dela Cruz, M. Gooch and C. W. Chu, Phys. Rev. B 85, 214422 (2012).

52. "$Ba_{1-x}Na_xTi_2Sb_2O$ ($0.0 \leq x \leq 0.33$): A Layered Titanium-based Pnictide Oxide Superconductor," P. Doan, M. Gooch, Z. J. Tang, B. Lorenz, A. Möller, J. Tapp, C. W. Chu and A. M. Guloy, Journal of the American Chemical Society 134, 16520 (2012).

53. "Magnetic order and spin-flop transitions in the cobalt-doped multiferroic $Mn_{1-x}Co_xWO_4$," F. Ye, S. X. Chi, J. A. Fernandez-Baca, H. B. Cao, K.-C. Liang, Y. Q. Wang, B. Lorenz and C. W. Chu, Phys. Rev. B 86, 094429 (2012).

54. "Superposition of Ferromagnetic and Antiferromagnetic Spin Chains in the Quantum Magnet $BaAg_2Cu[VO_4]_2$," A. A. Tsirlin, A. Möller, B. Lorenz, Y. Skourski and H. Rosner, Phys. Rev. B 85, 014401 (2012).

55. "Disorder-induced bulk superconductivity in $ZrTe_3$ single crystals via growth control," X. Y. Zhu, B. Lv, F. Y. Wei, Y. Y. Xue, B. Lorenz, L. Z. Deng, Y. Y. Sun, and C. W. Chu, Phys. Rev. B 87, 024508 (2013).*

56. "Experimental Investigation of the Electronic Structure of $Ca_{0.83}La_{0.17}Fe_2As_2$," Y. B. Huang, P. Richard, J. H. Wang, X. P. Wang, X. Shi, N. Xu, Z. Wu, A. Li, J. X. Yin, T. Qian, B. Lv, C. W. Chu, S. H. Pan, M. Shi and H. Ding, Chinese Physics Letters 30, 017402 (2013).*

57. "Anomalous hysteresis as evidence for a magnetic-field-induced chiral superconducting state in LiFeAs," G. Li, R. R. Urbano, P. Goswami, C. Tarantini, B. Lv, P. Kuhns, A. P. Reyes, C. W. Chu and L. Balicas, Phys. Rev. B 87, 024512 (2013).

58. "Observation of Temperature-Induced Crossover to an Orbital-Selective Mott Transition in $A_xFe_{2-y}Se_2$ (A=K, Rb) Superconductors," M. Yi, D. H. Lu, R. Yu, S. C. Riggs, J. H. Chu, B. Lv, Z. Liu, M. Lu, Y. T. Cui, M. Hashimoto, S. K. Mo, Z. Hussain, C. W. Chu, I. R. Fisher, Q. Si and Z. X. Shen, accepted for publication in Phys. Rev. Lett. (January 8, 2013).

59. "The Rise of T_c: A Promising Paradigm via Interfacial Mechanism," C. W. Chu, B. Lv, L. Z. Deng, B. Lorenz, B. Jawdat, M. Gooch, K. Shrestha, K. Zhao, X. Y. Xue, and F. Y. Wei, submitted to Proceedings of the Materials & Mechanisms of Superconductivity (M^2S 2012) Conference, Washington DC, July 29 - August 3, 2012, to be published in Journal of Physics: Conference Series (January 10, 2013).

Presentations

080806 - 080813 Amsterdam, The Netherlands, 25th International Conference on Low Temperature Physics, "Pressure-Induced Reversal of the Low-Temperature Ferroelectric Polarization in Multiferroic YMn_2O_5," R. P. Chaudhury, B. Lorenz, C. R. dela Cruz, Y. Y. Sun, C. W. Chu, S. Park and S. W. Cheong

080806 - 080813 Amsterdam, The Netherlands, 25th International Conference on Low Temperature Physics, "Superconductivity in $(K_{1-x}Sr_x)Fe_2As_2$: The Phase Diagram and Pressure Effects," B. Lorenz et al.

080806 - 080813 Amsterdam, The Netherlands, 25th International Conference on Low Temperature Physics, "Lattice Strain and Heat Capacity Anomalies at the Spin Re-Orientation Phase Transitions of ErFeO3 Orthoferrite," R. P. Chaudhury, B. Lorenz, C. W. Chu, Ya. B. Bazaliy and L. T. Tsymbal

080820 Chicago, Illinois, invited talk, 2008 Applied Superconductivity Conference, "The Unusual Observations in AFe_2As_2 with R = Rare-Earth and A = Alkaline and Ce(O/F)FeAs," C. W. Chu

080826 Santa Fe, New Mexico, invited talk, Symposium on Correlated Electron Physics, in

honor of Jim Smith's 65th birthday, "The Promises and Challenges of the Newly Discovered FeAs-Superconductors," C. W. Chu

080829 Shanghai, China, invited talk, Shanghai Education Commission Conference, C. W. Chu

081001 Nafplion, Greece, invited talk, Second CoMePhS Workshop in Controlling Phase Separations in Electronic Systems, "What Have We Learned from High Pressure Study on the Fe-Pnictides Superconductors?", C. W. Chu

081005 - 081007 Kyoto, Japan, invited talk, Science and Technology in Society (STS) Forum, "New Materials: What Can They Do for Sustainable Society," C. W. Chu

081007 Pittsburgh, Pennsylvania, Materials Science & Technology Conference, "Control of Ferroelectric and Magnetic Phases in Multiferroic Compounds Through External Pressure and Substitutions," B. Lorenz

081008 Honolulu, Hawaii, invited talk, Asia-Pacific Homeland Security Summit, C. W. Chu

081110 Houston, Texas, Condensed Matter Seminar, Rice University, "Fe-As Based Superconductors: A New Class of High-T_c Superconducting Compounds," B. Lorenz

081110 - 081114 Austin, Texas, 53rd Conference on Magnetism and Magnetic Materials, "Reentrant Spiral Magnetic Order and Ferroelectricity in Multiferroic $Mn_{1-x}Fe_xWO_4$ (x = 0.035)," R. P. Chaudhury, B. Lorenz, Y. Q. Wang, Y. Y. Sun, C. W. Chu, F. Ye, J. Fernandez-Baca, H. Mook and J. Lynn

081011 Taipei, Taiwan, The Allure of Physics, public dialogue between C. W. Chu and C. N. Yang

081116 - 081117 College Park, Maryland, invited talk, International Workshop on Fe-Pnictide Superconductors, "One Layer FeAs Pnictides," C. W. Chu

081203 Upton, New York, Basic Energy Sciences Distinguished Lecture, Brookhaven National Laboratory, "Brief History of the New Era of Superconductivity: From BCS to HTS and Possibly RTS," C. W. Chu

081204 Houston, Texas, opening plenary talk, International Workshop on Coated Conductors for Applications (CCA 08), "Practical HTS Coated Conductors: Maximization and Optimization," C. W. Chu

081219 Houston, Texas, 36th Semiannual TCSUH Student Symposium, "Doping Dependency of Superconductivity in Na_xFeAs and $(Sr,K)Fe_2As_2$," K. Sasmal

090105 - 090106 Hong Kong, invited talk, Inaugural Symposium: Mapping Frontiers of Science, Institute for Advanced Study, Hong Kong University of Science and Technology, "Superconductivity and Global Sustainable Economic Development," C. W. Chu

090113 - 090114 Kuala Lampur, Malaysia, invited plenary talk, Third International Meeting on Frontiers of Research, "High Temperature Superconductivity and Global Sustainable Economic Development," C. W. Chu

090316 - 090320 Pittsburgh, Pennsylvania, 2009 American Physical Society March Meeting, "Thermoelectric Power of $RO_{1-x-y}F_xFeAs$," F. Chen, K. Sasmal, M. Gooch, F. Y. Wei, B. Lorenz, Y. Y. Xue, C. W. Chu, B. Lv, Z. Tang and A. M. Guloy

090316 - 090320 Pittsburgh, Pennsylvania, 2009 American Physical Society March Meeting, "Evidence for Two Gaps From Specific Heat in LiFeAs Single Crystals," F. Y. Wei, B. Lv, F. Chen, Y. Y. Xue, A. M. Guloy and C. W. Chu

090316 - 090320 Pittsburgh, Pennsylvania, 2009 American Physical Society March Meeting, "Pressure-Induced Shift of T_c in $K_xSr_{1-x}Fe_2As_2$ (x = 0.2, 0.4, 0.7): Analogy to the High-T_c Cuprate Superconductors," M. Gooch, B. Lv, B. Lorenz, A. M. Guloy and C. W. Chu

090316 - 090320 Pittsburgh, Pennsylvania, 2009 American Physical Society March Meeting, "Magnetic Switching and Phase Competition in the Multiferroic Antiferromagnet $Mn_{1-x}Fe_xWO_4$," F. Ye, Y. Ren, J. A. Fernandez-Baca, H. A. Mook, J. W. Lynn, R. P. Chaudhury, Y. Q. Wang, B. Lorenz and C. W. Chu

090316 - 090320 Pittsburgh, Pennsylvania, 2009 American Physical Society March Meeting, "Evolution of Magnetic Exchange Interactions in the Multiferroic $Mn_{1-x}Fe_xWO_4$," J. A. Fernandez-Baca, F. Ye, R. Fishman, H. A. Mook, Y. Qiu, R. P. Chaudhury, Y. Q. Wang, B. Lorenz and C. W. Chu

090316 - 090320 Pittsburgh, Pennsylvania, 2009 American Physical Society March Meeting, "Reentrant Ferroelectricity and the Multiferroic Phase Diagram of $Mn_{1-x}Fe_xWO_4$," R. P. Chaudhury, B. Lorenz, Y. Q. Wang, Y. Y. Sun and C. W. Chu

090316 - 090320 Pittsburgh, Pennsylvania, 2009 American Physical Society March Meeting, "Superconducting Fe-Based Compounds $(A_{1-x}Sr_x)Fe_2As_2$ with A = K and Cs with Transition Temperatures up to 37 K," K. Sasmal, B. Lv, B. Lorenz, A. M. Guloy, F. Chen, Y. Y. Xue and C. W. Chu

090316 - 090320 Pittsburgh, Pennsylvania, 2009 American Physical Society March Meeting, "Quantum Critical Regime in the Phase Diagram of $K_xSr_{1-x}Fe_2As_2$," B. Lorenz, M. Gooch, B. Lv, A. M. Guloy and C. W. Chu

090316 - 090320 Pittsburgh, Pennsylvania, 2009 American Physical Society March Meeting, "Electric Field Induced Sub-Microsecond Resistive Switching," N. Das, S. Tsui, Y. Q. Wang, Y. Y. Xue and C. W. Chu

090323 - 090325 Ithaca, New York, Hans Bethe Distinguished Lectures, Cornell University, Hans Bethe Physics Colloquium: "From BCS Through HTS to RTS?"; Solid State Physics Seminar: "High Pressure Studies on Fe-Pnictide Superconductors;" Hans Bethe Public Lecture: "An Odyssey of Discovery: From Searching for HTSs in Houston to Developing HKUST in Hong Kong," C. W. Chu

090404 Houston, Texas, TCSUH Seminar, "Fe-As Based High-Temperature Superconductors: The Breakthrough of the Year (2008)," B. Lorenz

090423 East Lansing, Michigan, Colloquium, Department of Physics and Astronomy, Michigan State University, "From BCS Through HTS to RTS?", C. W. Chu

090427 Houston, Texas, University Presidents' Panel Discussion, Workshop on Science Collaborations Across Borders, James A. Baker III Institute for Public Policy, Rice University, C. W. Chu, D. W. Leebron, G. N. Su, and M. C. Lai

090505 Houston, Texas, 37th Semiannual TCSUH Student Symposium, "Evidence for Quantum Criticality in the Phase Diagram of $K_xSr_{1-x}Fe_2As_2$," M. Gooch [selected 1st Place]

090506 Wuhan, China, Luo Jia Rostrum, Wuhan University, "An Odyssey of Discovery: From Searching for HTSs in Houston to Developing HKUST in Hong Kong," C. W. Chu

090511 Los Alamos, New Mexico, Lujan Colloquium, Los Alamos National Laboratory, "Tuning Magnetism and Ferroelectricity in Multiferroics: The Effects of Pressure, Magnetic Fields, and Substitutions," B. Lorenz

090512 - 090516 Hayama, Japan, invited talk, International Workshop on the Search for New Superconductors: Frontier and Future, "A Holistic Multidisciplinary Empirical Approach in the Search for Novel Superconductors of Higher T_c and J_c," C. W. Chu

090527 Arlington, Virginia, U.S. Air Force Office of Scientific Research Joint Electronics Program Review, Plenary Talk, "A Holistic Multidisciplinary Enlightened Empirical Approach in the Search for Novel Superconductors with Higher T_c," C. W. Chu and B. Lorenz

090608 Hong Kong, invited talk, 2009 Gordon Research Conference on Superconductivity, "High Pressure Study on Fe-Pnictide Superconductors," C. W. Chu

090624 - 090626 University Park, Pennsylvania, 51st Electronic Materials Conference, "Electro-Resistive Memory in Transition Metal Oxides: A 'Model' for Future Non-Volatile Memory Device," N. Das, S. Tsui, Y. Y. Xue, Y. Q. Wang and C. W. Chu

090720 Singapore, invited distinguished public lecture, Conference on Concepts of Condensed Matter Physics, Inauguration of the School of Physical and Mathematical Sciences (SPMS), Nanyang Technological University, "Physics, Mathematics and Chemistry: Divergence and Convergence," C. W. Chu

090721 Singapore, invited talk, Conference on Concepts of Condensed Matter Physics, Inauguration of the School of Physical and Mathematical Sciences (SPMS), Nanyang Technological University, "A Multidisciplinary Enlightened Empirical Approach in the Search for Novel Superconductors of Higher T_c," C. W. Chu

090726 - 090731 Karlsruhe, Germany, International Conference on Magnetism (ICM 2009), "Control of Magnetic and Ferroelectric Phases in Multiferroic $MnWO_4$ Through Substitutions of Magnetic (Fe) and Nonmagnetic (Zn) Ions," B. Lorenz, R. P. Chaudhury, Y. Q. Wang, Y. Y. Sun and C. W. Chu

090802 - 090815 Santa Barbara, California, International Center for Materials Research Summer School on Novel Superconductors, "Quantum criticality in the phase diagram of $K_xSr_{1-x}Fe_2As_2$," M. Gooch, B. Lv, B. Lorenz, A. Guloy, C. W. Chu

090807 Santa Barbara, California, invited talk, International Center for Materials Research Summer School on Novel Superconductors, "The Excitements and Agonies in the Long Search for Novel Superconductors with Higher T_c's," C. W. Chu

090906 - 090913 Tokyo, Japan, invited summary talk on Materials presentations, 9th International Conference on Materials and Mechanisms of Superconductivity (M^2S-HTSC-IX), C. W. Chu

090906 - 090913 Tokyo, Japan, invited talk, 9th International Conference on Materials and Mechanisms of Superconductivity (M^2S-HTSC-IX), "Superconductivity in the iron pnictides $(A,A')Fe_2As_2$ and AFeAs (A=alkali metal, A'=alkaline earth)," B. Lorenz and C. W. Chu

090906 - 090913 Tokyo, Japan, 9th International Conference on Materials and Mechanisms of Superconductivity (M^2S-HTSC-IX), "Superconductivity and quantum criticality in the iron pnictide system $K_xSr_{1-x}Fe_2As_2$," B. Lorenz, M. Gooch, B. Lv, A. Guloy, C. W. Chu

090928 - 091002 Fort Lauderdale, Florida, Nanoelectronic Devices for Defense & Security Conference, "Electric Field Induced Resistive Switch in Transition Metal Oxides: A 'Model' for Future Non-Volatile Memory Devices," N. Das, S. Tsui, Y. Y. Xue, Y. Q. Wang and C. W. Chu

090929 Naples, Italy, invited talk, International Meeting on "Future Perspectives in Superconductivity and Josephson Effect" held in honor of Prof. Antonio Barone's 70th birthday, "A Novel Approach Towards Novel Superconductors with Higher T_c," C. W. Chu

091001 Edinburg, Texas, CONTACT Annual Review Meeting, “Photoacoustic Effects in Nanotubes,” F. Chen, Y. Y. Xue, V. Hadjiev, C. W. Chu and N. Wang

091012 College Park, Maryland, Condensed Matter Colloquium, University of Maryland, “A Possible Path from BCS through HTS to RTS,” C. W. Chu

091013 College Park, Maryland, W. J. Carr Lecture, University of Maryland, “An Odyssey of Discovery: Between Science and Administration, from Houston to Hong Kong,” C. W. Chu

091020 Vancouver, British Columbia, Canada, Colloquium, Department of Physics, University of British Columbia, “A Possible Path from BCS through HTS to RTS,” C. W. Chu

091025 - 091028 Portland OR, 2009 10th Non-Volatile Memory Technology Symposium, “Electric Field Induced Resistive Switch in Transition Metal Oxides: A ‘Model’ for Future Non-Volatile Memory Devices,” N. Das, S. Tsui, Y. Y. Xue, Y. Q. Wang and C. W. Chu

091105 Taipei, Taiwan, invited distinguished keynote lecture, Seventh Annual Global Chinese Business Leaders Forum, “How to Integrate Talents from the U.S., China, and Taiwan to Build a Better World,” C. W. Chu

091110 Taipei, Taiwan, invited K. T. Li Professor Chair Award lecture, National Cheng Kung University, C. W. Chu

091119 Houston, Texas, invited keynote, Chinese Community Center 30th Anniversary Gala, C. W. Chu

091208 Taipei, Taiwan, invited talk, Mini-Workshop on Superconductivity and Applications, National Tsinghua University, “A Possible Approach Toward Room Temperature Superconductivity,” C. W. Chu

091212 Taipei, Taiwan, invited joint public speech on “Crossing Borders: Science and Humanities,” Y. T. Lung and C. W. Chu

100118 - 100122 Washington DC, 11th Joint MMM-Intermag Conference, “Magnetoelectric Properties of $Ho_{0.25}Nd_{0.75}Fe_3(BO_3)_4$, R. P. Chaudhury, B. Lorenz, Y. Y. Sun, L. Bezmaternykh, V. Temerov and C. W. Chu

100118 - 100122 Washington DC, 11th Joint MMM-Intermag Conference, “Magnetic Quantum Critical Point and Scaling in the Iron Pnictide Superconductor $K_xSr_{1-x}Fe_2As_2$,” M. Gooch, B. Lv, B. Lorenz, A. M. Guloy and C. W. Chu

100218 San Marcos, California, “Frontiers in Science” Seminar Series, California State University, “Probing an Electrorheological Colloid: Development of a General Mechanism for Negative Capacitance Phenomena,” J. Shulman

100223 Houston, Texas, Colloquium, University of Houston Department of Physics, “The Iron Age of Superconductivity: Fe-Pnictide and -Chalcogenide Superconductors,” B. Lorenz

100315 - 100319 Portland, Oregon, invited talk, 2010 American Physical Society March Meeting, “A Possible Path from BCS Through HTS to VHTS,” C. W. Chu

100315 - 100319 Portland, Oregon, GMAG Student Award Talk, 2010 American Physical Society March Meeting, “Effects of High Pressure, Magnetic Fields and Substitutions on Multiferroic Systems,” R. P. Chaudhury

100315 - 100319 Portland, Oregon, 2010 American Physical Society March Meeting, “Magnetic Order, Spontaneous Polarization, and Magnetoelectric Effect in Rare Earth Iron Borates: $Ho_{1-x}Nd_xFe_3(BO_3)_4$, B. Lorenz, R. P. Chaudhury, Y. Y. Sun, C. R. dela Cruz, L. Bezmaternykh, V. Temerov and C. W. Chu

100315 - 100319 Portland, Oregon, 2010 American Physical Society March Meeting, "Evidence for Dynamic Spin Fluctuation in Specific Heat of $Sr_{1-x}K_xFe_2As_2$ Crystals," F. Wei, B. Lv, F. Chen, Y. Y. Xue, A. M. Guloy, and C. W. Chu

100315 - 100319 Portland, Oregon, 2010 American Physical Society March Meeting, "Synthesis and Properties of CaCuAs and $CaCu_2As_2$," F. Chen, B. Lv, Y. Y. Xue, and C. W. Chu

100315 - 100319 Portland, Oregon, 2010 American Physical Society March Meeting, "A Possible New Phase in Ba-Fe-As System," B. Lv, F. Chen, Y. Y. Xue, and C. W. Chu

100315 - 100319 Portland, Oregon, 2010 American Physical Society March Meeting, "Electric Field Induced Resistive Switch in Transition Metal Oxides: A 'Model' for Future Non-Volatile Memory Devices," N. Das, Y. Y. Xue, Y. Q. Wang and C. W. Chu

100315 - 100319 Portland, Oregon, 2010 American Physical Society March Meeting, "Ternary Iron Pnictides AFe_2As_2 (A = Alkali Metal) and LiFeAs: A Systematic Study of Magnetic Properties and Transport Measurements," M. Gooch, B. Lv, K. Sasmal, B. Lorenz, J. Tapp, Z. Tang, A. M. Guloy and C. W. Chu

100315 - 100319 Portland, Oregon, 2010 American Physical Society March Meeting, "Phonon Probe of Structural Variations in $FeSe_{1-x}Te_x$," K. Sasmal, V Hadjiev, M. Iliev and C. W. Chu

100315 - 100319 Portland, Oregon, 2010 American Physical Society March Meeting, "A General Mechanism for Negative Capacitance Phenomena," J. Shulman, Y. Y. Xue, S. Tsui, F. Chen and C. W. Chu

100406 San Francisco, California, invited talk, MRS Spring Meeting, "The driving force for superconductivity in iron arsenides – Charge doping versus suppression of magnetic order," B. Lorenz and C. W. Chu

100409 Tokyo, Japan, invited G-COE Seminar, Global Center of Excellence for Physical Sciences Frontier, University of Tokyo, "A Perspective of Room Temperature Superconductors," C. W. Chu

100504 Houston, Texas, 39th Semiannual TCSUH Student Symposium, "Effects of Different Ionic Substitutions on Multiferroic Systems," R. P. Chaudhury [selected 2nd Place]

100628 - 100702 Scottsdale, Arizona, 2010 National Space and Missile Defense Symposium, "Evidence for critical scaling in $K_xSr_{1-x}Fe_2As_2$ and $K_xBa_{1-x}Fe_2As_2$ from transport measurements," M. Gooch, B. Lv, B. Lorenz, A. Guloy, and C. W. Chu

100705 Taipei, Taiwan, invited talk, Academia Sinica 29th Convocation of Academicians "From Bench Physics to Higher Education," C. W. Chu

100721 - 100722 F. Chen, "A novel physical doping technique," AFOSR Mini-Workshop on the Search for Novel Superconductors with Higher T_c, Texas Center for Superconductivity at the University of Houston, Houston TX

100721 - 100722 R. P. Chaudhury, "Tuning of multiferroics," AFOSR Mini-Workshop on the Search for Novel Superconductors with Higher T_c, Texas Center for Superconductivity at the University of Houston, Houston TX

100721 - 100722 B. Lv, "Novel isomorphs of Fe-pnictides," AFOSR Mini-Workshop on the Search for Novel Superconductors with Higher T_c, Texas Center for Superconductivity at the University of Houston, Houston TX

100721 - 100722 T. Muramatsu, "A possible HTS-insulator transition in YBCO," AFOSR Mini-Workshop on the Search for Novel Superconductors with Higher T_c, Texas Center for

Superconductivity at the University of Houston, Houston TX

100721 - 100722 C. W. Chu, "Nature of the pressure induced superconductivity in Ca122," AFOSR Mini-Workshop on the Search for Novel Superconductors with Higher T_c, Texas Center for Superconductivity at the University of Houston, Houston TX

100721 - 100722 M. Gooch, "Quantum criticality in K-doped Sr- and Ba122," AFOSR Mini-Workshop on the Search for Novel Superconductors with Higher T_c, Texas Center for Superconductivity at the University of Houston, Houston TX

100721 - 100722 F. Y. Wei, "Two superconducting gaps in Li111," AFOSR Mini-Workshop on the Search for Novel Superconductors with Higher T_c, Texas Center for Superconductivity at the University of Houston, Houston TX

100721 - 100722 Y. Y. Xue, "SDW and SC in Fe-pnictides," AFOSR Mini-Workshop on the Search for Novel Superconductors with Higher T_c, Texas Center for Superconductivity at the University of Houston, Houston TX

100807 C. W. Chu, "Search for Novel Superconductors via Novel Doping in Unconventional Materials," U.S. Air Force Office of Scientific Research Superconductivity Program Review, Washington DC

100807 B. Lorenz, R. P. Chaudhury, Y. Y. Sun, Y. Q. Wang, and C. W. Chu, "Chemical and Physical Tuning of Multiferroics," U.S. Air Force Office of Scientific Research Superconductivity Program Review, Washington DC

100807 B. Lv, F. Chen, and C. W. Chu, "New Compounds of the Fe-pnictide and Related Types," U.S. Air Force Office of Scientific Research Superconductivity Program Review, Washington DC

100823 C. W. Chu, "Superconductivity under high pressure," Kick-off Conference on Pressure Effects on Materials, ICMR, UC Santa Barbara, Santa Barbara CA

100927 T. Muramatsu, D. Pham, and C. W. Chu, "A Possible Pressure-Induced Superconducting-Semiconducting Transition in Cuprate HTS," brief presentation, China/US Workshop on Novel Superconductors, Beijing, China

101013 - 101014 C. W. Chu, F. Chen, and Y. Y. Xue, "Field-Induced Change in the Electronic Properties of Solids," Lockheed Martin CONTACT Program Joint Technical Symposium & CONTACT Program Annual Review Meeting, Houston TX

101015 - 101020 B. Lorenz, "Multiferroic phase control in $MnWO_4$ through substitution of magnetic and nonmagnetic ions," International Symposium on Multifunctionality of Ferroics and Multiferroics, University of Texas - San Antonio, San Antonio TX

101017 - 101021 C. W. Chu, T. Muramatsu, and D. Pham, "A Possible Pressure-Induced High-Temperature-Superconducting - Semiconducting Transition in $YBa_2Cu_3O_{7-x}$," Materials Science & Technology 2010 Conference & Exhibition, Houston TX

101017 - 101021 B. Lorenz, R. P. Chaudhury, Y. Q. Wang, Y. Y. Sun, C. W. Chu, F. Ye, J. A. Fernandez-Baca, H. A. Mook, and J. Lynn, "Multiferroic phases in substituted $MnWO_4$: Effects of magnetic and nonmagnetic ions," Materials Science & Technology 2010 Conference & Exhibition, Houston TX

101129 - 101202 C. W. Chu, participant, panel discussion on "Fostering a Creative Culture in Taiwan," Board Meeting of Science and Technology Advisory Board (STAG) of ROC Executive Yuan, Taipei, Taiwan ROC

101206 M. Gooch, "LiFeAs: The Puzzling Superconductor," 40th Semiannual TCSUH Student Symposium, Houston TX

110303 - 110305 C. W. Chu, "Present Status of High Temperature Superconductors," luncheon keynote, First International Workshop on Lunar Superconductor Applications (LSA 2011), Houston TX

110321 - 110325 C. W. Chu, "The arrival of high temperature superconductors," 2011 American Physical Society March Meeting, Dallas TX

110321 - 110325 B. Lorenz, R. P. Chaudhury, Y. Q. Wang, Y. Y. Sun, C. W. Chu, F. Ye, H. A. Mook, and J. A. Fernandez-Baca, "Remarkably robust ferroelectric state in multiferroic $Mn_{1-x}Zn_xWO_4$," 2011 American Physical Society March Meeting, Dallas TX

110321 - 110325 F. Chen, B. Lv, Y. Y. Xue, C. W. Chu, and H. Wang, "Electric Double Layer Charging on Graphene," 2011 American Physical Society March Meeting, Dallas TX

110321 - 110325 J. A. Fernandez-Baca, F. Ye, R. S. Fishman, A. Podlesnyak, G. Ehlers, H. A. Mook, Y. Q. Wang, B. Lorenz, and C. W. Chu, "Spin Waves and Magnetic Interaction in the Multiferroic Antiferromagnet $MnWO_4$," 2011 American Physical Society March Meeting, Dallas TX

110321 - 110325 K. C. Liang, R. P. Chaudhury, Y. Q. Wang, Y. Y. Sun, B. Lorenz, F. Ye, J. A. Fernandez-Baca, H. A. Mook, and C. W. Chu, "Magnetic and multiferroic phases of single-crystalline $Mn_{1-x}Co_xWO_4$," 2011 American Physical Society March Meeting, Dallas TX

110321 - 110325 R. P. Chaudhury, B. Lorenz, Y. Y. Sun, C. W. Chu, L. N. Bezmaternykh, and V. L. Temerov, "Magnetoelectricity and magnetostriction due to the rare-earth moment in $TmAl_3(BO_3)_4$," 2011 American Physical Society March Meeting, Dallas TX

110321 - 110325 L. Z. Deng, B. Lv, Y. Y. Xue, and C. W. Chu, "Synthesis and Characterization of ACu_4Pn_2, with A = alkaline and Pn = As and Sb," 2011 American Physical Society March Meeting, Dallas TX

110321 - 110325 K. Sasmal, G. Mu, H. H. Wen, B. Lorenz, and C. W. Chu, "Pressure shift of the superconducting T_c of $(Pr_{1-x}Sr_x)FeAsO$ and $Sm(O_{1-x}F_x)FeAs$," 2011 American Physical Society March Meeting, Dallas TX

110321 - 110325 B. Lv, B. Lorenz, M. Gooch, F. Chen, L. Z. Deng, and C. W. Chu, "Phase Transitions in CuAs-based $K_xSr_{1-x}Cu_4As_2$ System," 2011 American Physical Society March Meeting, Dallas TX

110321 - 110325 M. Gooch, B. Lorenz, S. X. Huang, C. L. Chien, and C. W. Chu, "Pressure effects on strained $FeSe_{0.5}Te_{0.5}$ thin films," 2011 American Physical Society March Meeting, Dallas TX

110321 - 110325 F. Y. Wei, B. Lv, F. Chen, Y. Y. Xue, and C. W. Chu, "Two-Gap Pairing of the Optimal Doped $(M,K)Fe_2As_2$ with M = Ba, Sr," 2011 American Physical Society March Meeting, Dallas TX

110321 - 110325 T. Muramatsu, "Electrical resistance measurement of optimal doped YBCO under pressure," 2011 American Physical Society March Meeting, Dallas TX

110327 - 110402 B. Lorenz, "Pressure effects on the ferroelectricity in multiferroics," Sixth Meeting of the Study of Matter at Extreme Conditions (SMEC 2011), Miami FL

110327 - 110402 M. Gooch, B. Lorenz, S. X. Huang, C. L. Chien, and C. W. Chu, "Pressure effects on strained $FeSe_{0.5}Te_{0.5}$ thin films," Sixth Meeting of the Study of Matter at Extreme

Conditions (SMEC 2011), Miami FL

110410 C. W. Chu, participant, Harvard China Forum panel on "Higher Education Reform in China," Harvard University, Cambridge MA

110420 C. W. Chu, "Superconductivity—from 4 K to 164 K and beyond," colloquium, Boston College, Boston MA

110425 - 110429 C. W. Chu, "The Promise and Limitation of High Pressure to Novel Superconductors," 2011 Materials Research Society Spring Meeting, San Francisco CA

110503 K. C. Liang, "Giant Magnetoelectric Effect in $HoAl_3(BO_3)_4$," 41st Semiannual TCSUH Student Symposium, Houston TX

110523 - 110526 C. W. Chu and B. Lv, "Search for and Study of Novel Superconductors," AFOSR Joint Electronics Program Review, Arlington VA

110618 C. W. Chu, "The Evolution of High Temperature Superconductivity," "Frontiers of Theoretical Physics" Workshop, Nankai University, Tianjing, China

110618 C. W. Chu, short talk on opening of memorial stone for Prof. S. S. Chern, "Frontiers of Theoretical Physics" Workshop, Nankai University, Tianjing, China

110710 - 110714 C. W. Chu, "The unusual superconductivity up to 49 K in single crystalline R-doped $CaFe_2As_2$ (Ca122) at ambient with R = rare earth," 2011 Eurasia-Pacific Conference on Correlated Electrons, Turunc-Marmaris, Turkey

110801 - 110805 C. W. Chu, "The arrival of high temperature superconductivity, present and future," plenary, Seventh Joint Meeting of Chinese Physicists Worldwide (OCPA7): International Conference on Physics Education and Frontier Physics, Kaohsiung, Taiwan ROC

110801 - 110806 C. W. Chu, "An Exciting Odyssey of a Physicist: Between Science and Administration; and Between Houston and Hong Kong," keynote, opening ceremony, 14th Chien-Shiung Wu Science Camp, Chitou, Taiwan ROC

110801 - 110806 C. W. Chu, "The Wonderful World of Nothingness," lecture, 14th Chien-Shiung Wu Science Camp, Chitou, Taiwan ROC

110804 - 110809 C. W. Chu, "The Unusual 122-Phase of the FeAs- and FeSe-Superconductors," International Symposium on Centennial Discovery of Superconductivity - in Memory of B. T. Matthias, Conference on Novel Superconductivity (NSc-2011), Tainan, Taiwan ROC

110810 - 110817 C. W. Chu, "A possible unusual superconductiving state up to 49 K in single crystalline R-doped $CaFe_2As_2$ (Ca122) at ambient with R = rare earth," 26th International Conference on Low Temperature Physics (LT26), Beijing, China

110810 - 110817 B. Lorenz, K.-C. Liang, R. P. Chaudhury, Y. Y. Sun, L. N. Bezmaternykh, V. L. Temerov, I. A. Gudim, C. W. Chu, "Giant Magnetoelectric Effect in $RAl_3(BO_3)_4$ (R = Tb, Ho, Er, Tm)," 26th International Conference on Low Temperature Physics (LT26), Beijing, China

110916 C. W. Chu, "HTS Materials: Past, Present and Future," Low Temperature Symposium, University of Twente, Enschede, Netherlands

110918 - 110923 C. W. Chu, "A Possible New Superconducting State in Doped $CaFe_2As_2$ at Ambient and High Pressure," Superconductivity Centennial Conference, Den Haag, Netherlands

111010 - 111013 C. W. Chu, "A Holistic Approach from BCS through HTS to RTS," Seventh International Conference on Magnetic and Superconducting Materials (MSM11), Port Dickson,

Negeri Sembilan, Malaysia

111013 C. W. Chu, invited talk, Universiti Putra Malaysia (UPM), Serdang, Malaysia

111030 - 111103 F. Ye, R. S. Fishman, J. Haraldsen, B. Lorenz, C. W. Chu, T. Kimura, "Spin Dynamics in the Multiferroic Materials," 56th Annual Conference on Magnetism and Magnetic Materials (MMM 2011), Scottsdale AZ

111030 - 111103 K.-C. Liang, R. P. Chaudhury, Y. Q. Wang, Y. Y. Sun, B. Lorenz, F. Ye, J. A. Fernandez-Baca, H. A. Mook, C. W. Chu, "Chemical Doping and Magnetic Fields Effects on the Multiferroic Phases of Single-Crystalline $Co_xMn_{1-x}WO_4$," 56th Annual Conference on Magnetism and Magnetic Materials (MMM 2011), Scottsdale AZ

111108 - 111110 C. W. Chu, "A Possible Novel Mechanism to Higher T_c via Nano-Crystallographic Structure," CONTACT (Consortium for Nanomaterials for Aerospace Commerce and Technology) Technical & Annual Review Final Meeting, Wright-Patterson Air Force Base, Dayton OH

111111 C. W. Chu, Research Overview to 1st and 2nd Year Graduate Students, Department of Physics, University of Houston, Houston TX

111128 - 111130 C. W. Chu, Invited talk on recruiting, educating, and retaining talents for the 21st Century, Meeting of the Advisory Committee of Chinese Overseas Experts of the Overseas Chinese Affairs Office, State Council, People's Republic of China, Hangzhou, China

111203 M. Gooch, "Superconductivity and You," Science Fair, Harmony Endeavor School, Houston Independent School District, Houston TX

111206 L. Z. Deng, "Unusual Superconducting State in Pr-Doped $CaFe_2As_2$," 42nd Semiannual TCSUH Student Symposium, Houston TX

111209 M. Gooch, "Superconductivity and You," Harmony Science Academy NW, Houston Independent School District, Houston TX

111212 - 111216 C. W. Chu, B. Lv, "Mini-MURI Summary: A Possible Novel Mechanism for the Enhanced T_c of Non-Bulk Superconductivity in Doped and Undoped Ae122 with Ae = Ca, Sr and Ba and Other Material Systems," U.S. Air Force Office of Scientific Research Superconductivity Program Review and USAF China Workshop, Santa Barbara CA

111212 - 111216 B. Lorenz, K.-C. Liang, Y. Q. Wang, Y. Y. Sun, C. W. Chu, "New Magnetoelectric Compounds with Record Polarizations," U.S. Air Force Office of Scientific Research Superconductivity Program Review and USAF China Workshop, Santa Barbara CA

111212 - 111216 L. Z. Deng, B. Lv, M. Gooch, F. Y. Wei, Y. Y. Sun, J. K. Meen, Y. Y. Xue, B. Lorenz, C. W. Chu, "Unusual superconducting state in Pr-doped $CaFe_2As_2$," U.S. Air Force Office of Scientific Research Superconductivity Program Review and USAF China Workshop, Santa Barbara CA

111212 - 111216 M. Gooch, B. Lv, L. Z. Deng, T. Muramatsu, J. K. Meen, Y. Y. Xue, B. Lorenz, C. W. Chu, "$RbxFe_2Se_2$: A study of superconductivity under high pressure," U.S. Air Force Office of Scientific Research Superconductivity Program Review and USAF China Workshop, Santa Barbara CA

111212 - 111216 F. Y. Wei, B. Lv, L. Z. Deng, Y. Y. Sun, Y. Y. Xue, C. W. Chu, "Defect-Associated Superconductivity in $(Pr,Ca)Fe_2As_2$," U.S. Air Force Office of Scientific Research Superconductivity Program Review and USAF China Workshop, Santa Barbara CA

111212 - 111216 B. Lv, F. Y. Wei, L. Z. Deng, M. Gooch, X. Y. Zhu, G. Wu, B. Lorenz, Y. Y.

Xue, C. W. Chu, "Search for and Study of Novel Superconductors," U.S. Air Force Office of Scientific Research Superconductivity Program Review and USAF China Workshop, Santa Barbara CA

111212 - 111216 A. Howard, N. Cornell, M. Salamon, A. Zakhidov, B. Lv, F. Y. Wei, C. W. Chu, "Unconventional Low Field Microwave Absorption in Electron-Doped $Pr_xCa_{1-x}Fe_2As_2$: Signature of Interfacial Superconductivity with an Onset T_c ~ 49K," U.S. Air Force Office of Scientific Research Superconductivity Program Review and USAF China Workshop, Santa Barbara CA

120117 - 120119 C. W. Chu, "A Possible Approach from BCS through HTS to RTS-three examples," invited plenary talk, 2012 Annual Meeting of the Physical Society of Republic of China (PSROC), National Chung Cheng University, Chia-Yi, Taiwan ROC

120129 M. Gooch, "Superconductivity and You," Mars Rover Celebration, University of Houston, Houston TX

120203 - 120204 C. W. Chu, "Early days of high T_c-superconductivity," Mini-symposium celebrating the 70th birthday ("Koki") of Prof. Koichi Kitazawa, University of Tokyo, Tokyo, Japan

120225 C. W. Chu, "Superconductivity: 25 Years of Progress and More," Quarknet Saturday Physics Seminar, University of Houston, Houston TX

120227 - 120302 B. Lv, F. Y. Wei, L. Z. Deng, Y. Y. Sun, Y. Y. Xue, M. Gooch, J. K. Meen, C. W. Chu, "Microstructure and the non-bulk superconductivity up to 49K in electron-doped Rare-earth (Ca, R)Fe_2As_2 (R=La, Ce, Pr and Nd) Single Crystals," 2012 American Physical Society March Meeting, Boston MA

120227 - 120302 L. Z. Deng, B. Lv, M. Gooch, F. Y. Wei, Y. Y. Sun, J. K. Meen, Y. Y. Xue, B. Lorenz, C. W. Chu, "Unusual superconducting state in Pr-doped $CaFe_2As_2$," 2012 American Physical Society March Meeting, Boston MA

120227 - 120302 M. Gooch, B. Lv, L. Z. Deng, T. Muramatsu, J. K. Meen, Y. Y. Xue, B. Lorenz, C. W. Chu, "RbxFe$_2$Se$_2$: A study of superconductivity under high pressure," 2012 American Physical Society March Meeting, Boston MA

120227 - 120302 M. Yi, D. H. Lu, Z. K. Liu, S. Riggs, J.-H. Chu, B. Lv, S.-K. Mo, M. Hashimoto, R. G. Moore, Z. Hussain, I. R. Fisher, C. W. Chu, Z.-X. Shen, "ARPES studies of the AFe_2Se_2 (A=K, Rb, Cs) iron-based superconductors," 2012 American Physical Society March Meeting, Boston MA

120227 - 120302 F. Y. Wei, B. Lv, L. Z. Deng, Y. Y. Sun, Y. Y. Xue, C. W. Chu, "Defect-Associated Superconductivity in (Pr,Ca)Fe_2As_2," 2012 American Physical Society March Meeting, Boston MA

120227 - 120302 K. Sasmal, B. Lv, Z. Tang, F. Y. Wei, Y. Y. Xue, A. M. Guloy, C. W. Chu, "Lower critical field, anisotropy, and two-gap features of LiFeAs," 2012 American Physical Society March Meeting, Boston MA

120227 - 120302 K.-C. Liang, R. P. Chaudhury, B. Lorenz, L. N. Bezmaternykh, V. L. Temerov, C. W. Chu, "The magnetoelectric effect in the $RAl_3(BO_3)_4$ (R=Tb, Ho, Er, and Tm)," 2012 American Physical Society March Meeting, Boston MA

120227 - 120302 B. Lorenz, K.-C. Liang, Y. Q. Wang, Y. Y. Sun, F. Ye, J. A. Fernandez-Baca, H. A. Mook, C. W. Chu, "The complex multiferroic phase diagram of $Mn_{1-x}Co_xWO_4$," 2012 American Physical Society March Meeting, Boston MA

120227 - 120302 F. Ye, S. X. Chi, H. B. Cao, J. A. Fernandez-Baca, B. Lorenz, Y. Q. Wang, C. W. Chu, "Spin flop transition in the multiferroic $Mn_{1-x}Co_xWO_4$ studied by neutron diffraction," 2012 American Physical Society March Meeting, Boston MA

120227 - 120302 X. Y. Zhu, B. Lv, L. Z. Deng, F. Y. Wei, Y. Y. Sun, Y. Y. Xue, C. W. Chu, "Synthesis, Structure, Physical Properties of several Zirconium Chalcogenides," 2012 American Physical Society March Meeting, Boston MA

120227 - 120302 A. Sushkov, D. Drew, C. Kant, A. Shuvaev, A. Pimenov, S. Zvyagin, B. Lorenz, S. W. Cheong, "Colossal magnetodielectric effect in $DyMn_2O_5$: Electromagnons or rare earth?" 2012 American Physical Society March Meeting, Boston MA

120328 C. W. Chu, "Asia and America: Paradigm Shift in Higher Education in the New Century," featured conversationalist facilitating table discussion, University of Houston Honors College Great Conversation, Houston TX

120329 B. Lorenz, "Weak ferromagnetism and strong internal magnetoelectric effect in multiferroic $LiFeP_2O_7$," TCSUH Principal Investigators Meeting, Houston TX

120412 B. Lv, F. Y. Wei, L. Z. Deng, M. Gooch, Y. Y. Sun, Y. Y. Xue, J. K. Meen, B. Lorenz, C. W. Chu, "Unusual superconductivity up to 49K and possible interfacial superconductivity mechanism in e(Ca, RE)Fe_2As_2 (RE=La, Ce, Pr and Nd) system," invited talk, Symposium on "25 Years After YBCO, What Has It Done for Science and Society?" celebrating discovery of YBCO and Professor Paul C. W. Chu's 70th birthday, National Dong Hwa University, Hualien, Taiwan ROC

120412 C. W. Chu, invited talk, Symposium on "25 Years After YBCO, What Has It Done for Science and Society?" celebrating discovery of YBCO and Professor Paul C. W. Chu's 70th birthday, National Dong Hwa University, Hualien, Taiwan ROC

120416 - 120420 I. Zeljkovic, C. L. Song, D. Huang, B. Lv, C. W. Chu, J. Hoffman, "Scanning Tunneling Microscopy Studies of $Ca_{1-x}Pr_xFe_2As_2$," 2012 Villa Conference on Iron-based Superconductors, Orlando FL

120426 C. W. Chu, "100 Years of Superconductivity: Impacts on Science, Technology and Global Development," invited talk, Physics Department, Hong Kong University, Hong Kong

120428 C. W. Chu, Invited public lecture on higher education and economic development, Dongguan Institute of Technology 20th anniversary celebration, Dongguan, Guangdong, People's Republic of China

120430 M. Gooch, "Superconductivity and You," Key Middle School Science Night, Houston Independent School District, Houston TX

120501 K.-C. Liang, "The Complex Phase Diagram of Spiral Magnet $Co_xMn_{1-x}WO_4$," 43rd Semiannual TCSUH Student Symposium, Houston TX

120502 C. W. Chu, "Interfacial Superconductivity - A Possible New Paradigm to Higher T_c," invited talk, 3rd Annual Texas-Korea Nanotech Workshop, Dallas TX

120517 C. W. Chu, "High Temperature Superconductivity: Past, Present, Future," invited Technical Forum presentation, Samsung Austin Semiconductor, Austin TX

120614 C. W. Chu, Participant, Panel Discussion, Release event for the National Research Council's Committee on Research Universities report, *Research Universities and the Future of America: Ten Breakthrough Actions Vital to Our Nation's Prosperity and Security*, Washington DC

120711 - 120718 Erice, Sicily, Superstripes 2012: Quantum Phenomena in Complex Matter, Ettore Majorana Foundation and Centre for Scientific Culture, "HTS: Past, Present and a Promising Future with Evidence," C. W. Chu

120726 Jeddah, Saudi Arabia, invited presentation, Department of Physics, King Abdulaziz University, C. W. Chu

120729 - 120803 Washington DC, International Conference on Materials and Mechanisms of Superconductivity (M^2S 2012), "Investigation of the phase diagram for a pnictide oxide compound with hole doped titanium-oxygen layers: normal and superconducting states," B. Lorenz, P. Doan, Z. Tang, A. M. Guloy, C. W. Chu, and M. Gooch

120729 - 120803 Washington DC, International Conference on Materials and Mechanisms of Superconductivity (M^2S 2012), ICAM / I2CAM Sponsored Session: The Foundations of High-Temperature Superconductivity: Twenty-five Years Young, "High Temperature Superconductivity: Past, Present, and a Promising Future with Evidence," C. W. Chu

120729 - 120803 Washington DC, International Conference on Materials and Mechanisms of Superconductivity (M^2S 2012), "Superconductivity induced by hole doping into the titanium-oxygen layer of a pnictide oxide compound," B. Lorenz, P. Doan, M. Gooch, Z. Tang, A. M. Guloy, and C. W. Chu

120729 - 120803 Washington DC, International Conference on Materials and Mechanisms of Superconductivity (M^2S 2012), "Evidence for Interface-Induced T_c-Enhancement in Fe-Pnictide and -Chalcogenide Superconductors and Others," C. W. Chu, B. Lv, F. Y. Wei, M. Gooch, L. Z. Deng, J. K. Meen, Y. Y. Xue, and B. Lorenz

120729 - 120803 Washington DC, International Conference on Materials and Mechanisms of Superconductivity (M^2S 2012), "Observation of temperature-induced orbital-selective Mott transition in iron selenide superconductors," M. Yi, D. H. Lu, S.-K. Mo, M. Hashimoto, Y. T. Cui, J.-H. Chu, B. Lv, Z. K. Liu, M. H. Lu, S. Riggs, R. Yu, Z.-X. Shen, Q. M. Si, I. R. Fisher, C. W. Chu, and Z. Hussain

120818 Missouri City TX, invited keynote talk, Education Workshop hosted by Southern News Group, Fort Bend Community Church, "Que Sera Sera," C. W. Chu

120926 Shanghai, China, invited talk, meeting of the Advisory Committee of Chinese Overseas Experts, Overseas Chinese Affairs Office, State Council, China, "Research Universities and the Sustainable Economic Development in the 21st Century," C. W. Chu

121015 - 121019 Tashkent, Uzbekistan, invited talk, NATO Advanced Research Workshop on physical properties and applications of low-dimensional functional materials, "Superconductivity with Higher T_c via Nano-2D Structures," C. W. Chu

121017 - 121018 San Jose CA, invited talk, Almaden Institute 2012 meeting on "Superconductivity at 297K: Synthetic Highways to Room Temperature Superconductivity," IBM Almaden Research Center, "The Holistic Multidisciplinary Empirical Approach to Higher T_c with Possible Evidence for Interfacial Mechanism," C. W. Chu

121107 - 121109 Jeju Island, Korea, invited plenary talk, 2012 Dasan Conference on Superconductivity, "The Holistic Multidisciplinary Empirical Approach to Higher T_c via Possible 2D-Nanostructures," C. W. Chu

121130 C. W. Chu, Research Overview to 1st and 2nd Year Graduate Students, Department of Physics, University of Houston, Houston TX

121203 - 121205 Tokyo, Japan, invited Special Plenary Lecture, 25th International

Symposium on Superconductivity (ISS2012), "Possible Evidence for Interface-Enhanced T_c in Fe-Pnictides and -Chalcogenides," C. W. Chu

121208 Taipei, Taiwan, keynote address, National Manufacturing and Innovation Conference

130114 - 130118 Chicago IL, 12th Joint MMM/Intermag Conference, "The complex multiferroic phase diagram of single-crystalline $Co_xMn_{1-x}WO_4$," K.-C. Liang, Y.-Q. Wang, Y. Y. Sun, B. Lorenz, F. Ye, J. A. Fernandez-Baca, H. Mook, and C. W. Chu

130124 - 130126 Hong Kong, invited talk, Third US-China Workshop on Novel Superconductors, "The Search and Study of HTS at TCSUH," C. W. Chu, L. Z. Deng, M. Gooch, A. Guloy, B. Lorenz, B. Lv, Y. Y. Xue and X. Y. Zhu

130124 - 130126 Hong Kong, invited talk, Third US-China Workshop on Novel Superconductors, "The unusual magnetic interactions in $LiFeP_2O_7$ and their possible implications for superconductivity," B. Lorenz et al.

130124 - 130126 Hong Kong, Third US-China Workshop on Novel Superconductors, "Investigation of the normal and superconducting states of $Ba_xNa_{1-x}Ti_2Sb_2O$ ($0 \geq x \geq 0.33$): a pnictide oxide compound with hole doped titanium-oxygen layers," M. Gooch, P. Doan, Z. Tang, B. Lorenz, A. Möller, J. Tapp, D. Pratt, J. Lynn, A. M. Guloy and C. W. Chu

130125 Hong Kong, public lecture, "Six Decades of Learning: Taiwan, America, Hong Kong and Mainland," C. W. Chu

Awards

1. C. W. Chu, selected to present the 2008 Basic Energy Sciences Distinguished Lecture, Brookhaven National Laboratory, Upton, New York, December 2008

2. C. W. Chu, recipient, Prize Ettore Majorana - Erice - Science for Peace 2007, Ettore Majorana Foundation and Centre for Scientific Culture, awarded December 2008

3. C. W. Chu, selected to present the 2009 Hans Bethe Distinguished Lectures, Cornell University, Ithaca, New York, March 2009

4. M. Gooch, First Place Winner, 37th Semiannual TCSUH Student Symposium, May 2009

5. C. W. Chu, selected to present the Luo Jia Rostrum (most distinguished forum at Wuhan University), Wuhan University, Wuhan, China, May 2009

6. N. Das, selected to give student presentation at the 51st Electronic Materials Conference, University Park, Pennsylvania, June 2009

7. C. W. Chu, Distinguished Visiting Chair Professorship, National Cheng Kung University, Tainan, Taiwan, 2009

8. C. W. Chu, One of 100 Influential Alumni, University of California, San Diego, Alumni Association, 2009

9. C. W. Chu, K. T. Li Professor Chair Award, National Cheng Kung University, Tainan, Taiwan, November 2009

10. C. W. Chu, Honorary Professorship, National Tsinghua University, December 2009

11. M. Gooch, High-Pressure Low-Temperature Group, TCSUH Student Travel Award, January 2010

12. R. P. Chaudhury, High-Pressure Low-Temperature Group, Student Travel Award, 11th MMM-Intermag Conference, January 2010

13. R. P. Chaudhury, High-Pressure Low-Temperature Group, APS-GMAG Dissertation Award, March 2010

14. C. W. Chu, Member, Honor Society of Phi Kappa Phi, March 2010

15. R. P. Chaudhury, High-Pressure Low-Temperature Group, Second Prize Winner, TCSUH Student Competition, May 2010

16. M. Gooch, High-Pressure Low-Temperature Group, CONTACT Travel Award, 2010 National Space and Missile Defense Symposium. June 2010

17. M. Gooch, First Prize Winner, 40th Semiannual TCSUH Student Symposium, December 6, 2010

18. C. W. Chu, recipient, Hong Kong Institution of Engineers Hall of Fame Award, December 2, 2010

19. K.-C. Liang, TCSUH Student Travel Award, 2011

20. C. W. Chu, named Fellow of the Hong Kong Institution of Science, October 2011

21. L. Z. Deng, 1st prize winner, TCSUH Student Symposium, December 2011

22. L. Z. Deng, TCSUH Student Travel Award, 2012

23. K.-C. Liang, 2nd prize winner, TCSUH Student Symposium, May 2012

24. K. Shrestha, TCSUH Student Travel Award, 2013

25. Five papers with C. W. Chu group authors published in Phys. Rev. B and Phys. Rev. Lett. were selected as Editor's Suggestions [K. Sasmal et al., PRL 101, 107007 (2008); M. Gooch et al., PRB 78, 180508(R) (2008); R. P. Chaudhury et al., PRB 81, 220402(R) (2010); R. P. Chaudhury et al., PRB 83, 014401 (2011); and F. Ye, PRB 83, 140401(R) (2011)]; one paper with C. W. Chu group co-authors was selected as a Mag Lab research highlight [one of 40 out of 417 submitted; L. I. Vergara et al., PRB 81, 012403 (2010)]

APPENDIX I - "Nonuniform Resonator Sensors for Enhanced Sensitivity"
PIs: Dumitru Caruntu and Horacio Vasquez, UT Pan American

This project started in October 2010. The PI has worked on investigating electrostatically actuated MEMS/NEMS cantilever resonators for sensing applications (Figure 14). This research dealt with nonlinear parametric resonances of cantilever M/NEMS beams due to soft AC electrostatic excitation (nonlinear parametric force) and fringe effect, for mass sensing applications. The methods used in this research are the Method of Multiple Scales (MMS) and the Reduced Order Method (ROM). Electrostatic actuation is produced by a DC voltage and/or AC voltage between a flexible M/NEMS structure, such as a cantilever, and a rigid ground plate. This actuation creates a variety of nonlinear parametric resonances depending on system parameters, excitation frequency, and excitation voltage. These resonances can be used to design mass sensors, microscopy probes, filters, and resonators. Numerical simulations conducted in this research show a softening effect in all nonlinear parametric resonances.

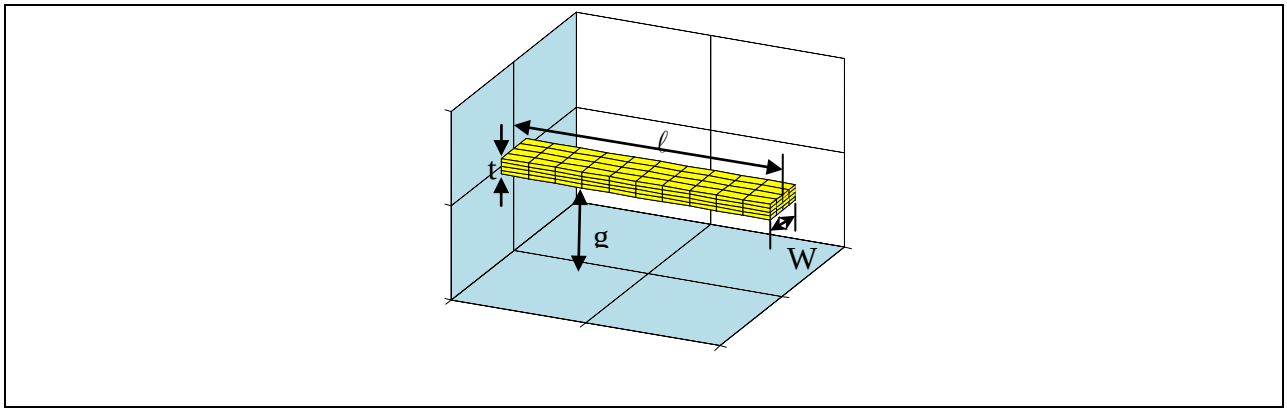

Figure 14. MEMS/NEMS cantilever resonator under electrostatic actuation

From this research, 3 journal papers are sent or to be sent for publication, 5 conference papers are published or to be published, 3 HESTEC conference posters were presented, and 7 national and international invited seminars were given.

In terms of human factors, 2 undergradate students and 3 master's degree students were involved in this research. The two undergraduate students graduated with a Mechanical Engineering bachelor degree. Two graduate students graduated with an MS in Mechanical Engineering degree, and the third graduate student graduated in December 2012 with an MS in Electrical Engineering degree.

1. The investigation of the resonance near natural frequency of a MEMS cantilever resonator under soft AC electrostatic actuation for sensing applications predicted that a) the resonator goes into a pull-in phenomenon (contact with the ground plate) from an amplitude of 0.8 (Figure 15) and b) the bifurcation point B where the system looses stability as the frequency is swept up is less than predicted by the MMS (which is limited in predicting accurately the bifurcation points).

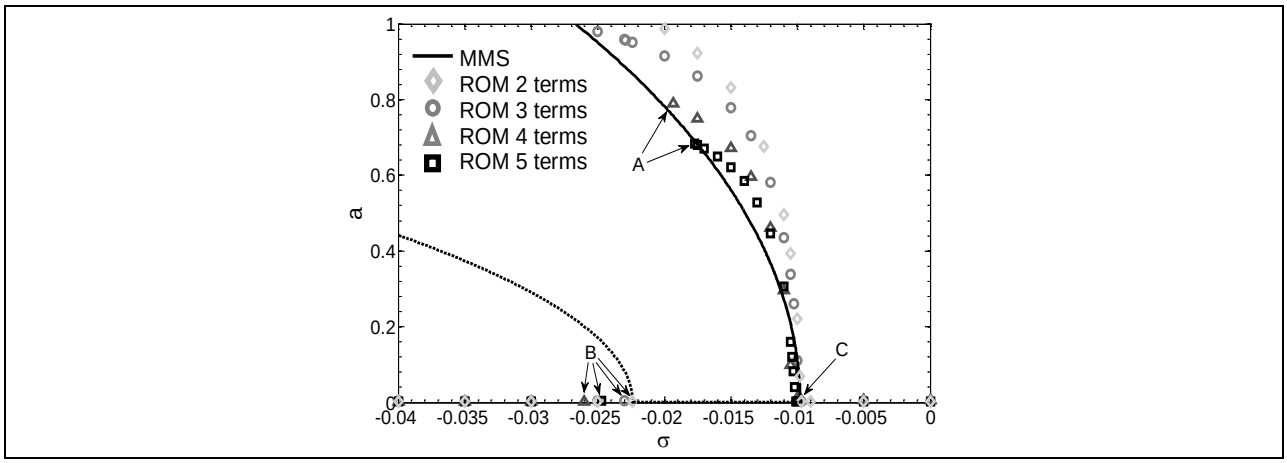

Figure 15. Frequency response of MEMS resonator. Solid and dashed lines are MMS stable and unstable solutions, respectively. A and B are where pull-in is predicted using the 4 and 5 term ROM. C is where the stable branch of solutions begins.

$$\alpha = 0,\ \delta_{0A} = 0.1,\ f = 0.26, \text{ AND } c^* = 0.01 \tag{5}$$

2. The investigation of the soft DC voltage influence on the resonance near natural frequency of AC-DC electrostatically actuated MEMS cantilever resonators predicted a significant change of the behavior of the resonator. As there is no DC voltage two pitchfork bifurcations are predicted. Any DC voltage changes the behavior of the system. Zero amplitudes fail to be steady-states for the resonator, and a saddle-node bifurcation replaces the subcritical pitchfork bifurcation (Figure 16).

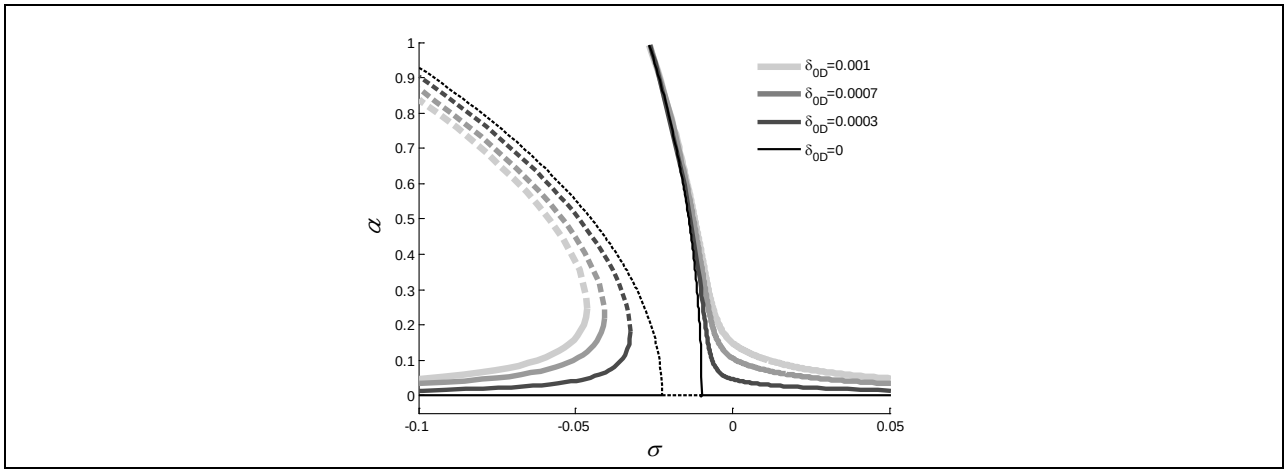

Figure 16. ACDC.m Frequency vs. Amplitude with near natural frequency AC/DC excitation for a single beam with varying δ_{0D}. The solid and dotted lines represent stable and unstable solutions respectively. α = 0, δ_{0A} =0.1, f = 0.26, and c = 0.01

3. Reduced Order Model (ROM) method showed that the behavior of the system cannot be accurately predicted by the MMS (Figure 17). This investigation shows that the points where the resonator looses stability as we sweep the frequency are underestimated by MMS. The point where the stability is lost as the frequency is swept down is showed to be of 0.9 of the gap

between the resonator and the ground plate. Also, the bifurcation frequency when frequency is swept up is higher than predicted by MMS, and for an amplitude of 0.5 of the gap.

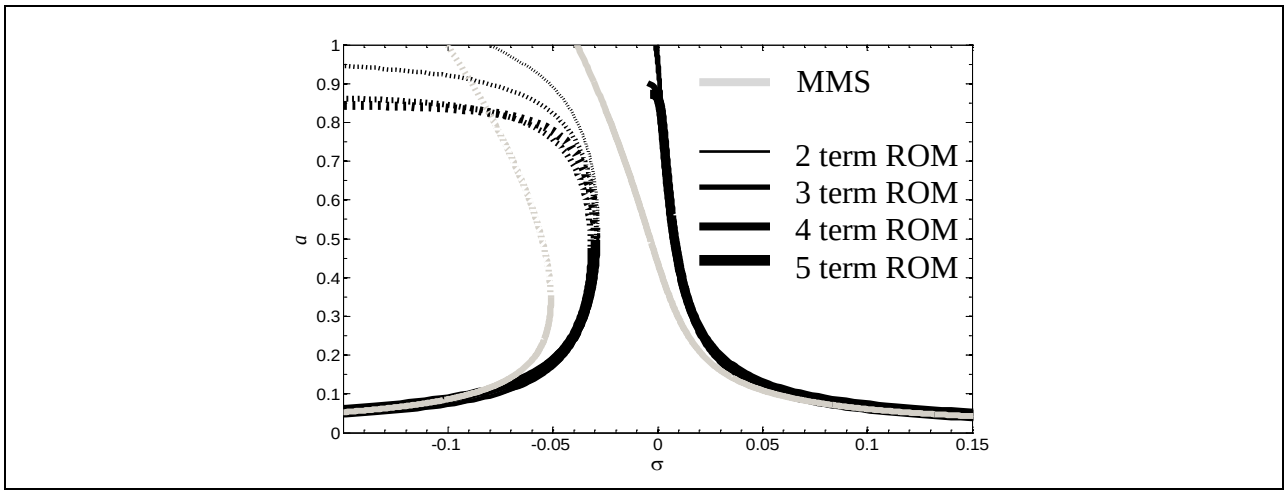

Figure 17. Amplitude-frequency response near half natural frequency using the MMS [16] and a two, three, four and five term ROM for dimensionless parameter values b*=0.01, δ=0.1 and f=0.26

Peer Reviewed Journal Publications:

1. Caruntu, D., Taylor, K., DC influence on the frequency response of MEMS cantilever resonators under soft electrostatic AC actuation, *International Journal of Mechanical Sciences* (to be sent).

2. Caruntu, D., Knecht, M., 2012, MEMS cantilever resonators under soft AC voltage of frequency near natural frequency, *Journal of Dynamic Systems, Measurement and Control* (under review).

3. Caruntu, D., Martinez, I., Taylor, K.N., Voltage-amplitude response of MEMS resonators under soft AC voltage of frequency near half natural frequency. Reduced Order Model versus Method of Multiple Scales, *Mechanics Research Communications* (accepted).

4. Caruntu, D., Martinez, I., Knecht, M.W., Reduced Order Model analysis of frequency response of alternating current near near half natural frequency electrostatically actuated MEMS cantilevers, *Journal of Computational and Nonlinear Dynamics* (in press).

Peer Reviewed Conference Publications:

1. Caruntu, D., Taylor, K., 2012, DETC2012-71535 Nonlinear dynamics of electrostatically actuated coupled MEMS parallel cantilever resonators, *ASME 2012 Proceedings of International Design Engineering Technical Conferences & Computers and Information in Engineering Conference, DETC2012, 24th Conference on Mechanical Vibration and Noise (VIB),* August 12-15, 2012, Chicago, IL, © The American Society of Mechanical Engineers (ASME).

2. Caruntu, D., Martinez, I., Knecht, M.W., 2012, DETC2012-70326 Reduced Order Model of electrostatically actuated MEMS resonators near half natural frequency, *ASME 2012 Proceedings of International Design Engineering Technical Conferences & Computers and Information in Engineering Conference 24th Conference on Mechanical Vibration and Noise (VIB),* August 12-15, 2012, Chicago, IL, © ASME.

3. Caruntu, D., Taylor, K., 2012, IMECE2012-85966 Reduced Order Model of electrostatically actuated coupled MEMS parallel cantilever resonators, *Proc. of International Mechanical Engineering Congress and Exposition 2012*, November 9-15, Houston, TX, © ASME.

4. Caruntu, D., Zapata, R.J., Knecht, M.W., 2011, DETC2011-48367 Reduced Order Model of Nanoelectromechanical Systems to Include Casimir Effect, *ASME 2011 Proceedings of International Design Engineering Technical Conferences & Computers and Information in Engineering Conference, DETC2011, 23rd Biennial Conference on Mechanical Vibration and Noise (VIB)*, August 28-31, 2011, Washington, DC, © ASME.

5. Caruntu, D., Knecht, M.W., Zapata, R.J., 2011, DSCC2011-5966 Casimir influence on NEMS cantilever resonators, *Proceedings of ASME 2011 Dynamic Systems and Control Conference*, Oct 31- Nov 2, 2011, Arlington, VA, © ASME.

Conference Presentations:

1. Solis, J.C., Caruntu, D., 2011, Reduced Order Model of electrostatically actuated MEMS/NEMS resonator sensors, HESTEC Poster, September 2011.

2. Taylor, K.N., Caruntu, D., 2011, Coupled MEMS resonators for sensing applications, HESTEC Poster, September 2011.

3. Zapata, R., Caruntu, D., Casimir effect on NEMS resonator sensors using reduced Order Model method, HESTEC Poster, September 2011, *Won 3rd place in the Mechanical Engineering Department*.

Invited Seminars:

1. CONTACT (Consortium for Nanomaterials for Aerospace Commerce and Technology) Annual Review, Electrostatically Actuated M/NEMS for Sensing Applications, AFRL Wright-Patterson, 11/8-9/2011.

2. ARL Sensors: Nonlinear dynamics of electrostatically actuated MEMS/NEMS, 09/02/11.

3. ARL Weapons and Materials: Nonlinear dynamics of electrostatically actuated MEMS/NEMS, 07/29/2011.

4. SUPMECA (Institute Superieur de Mecanique de Paris): Nonlinear dynamics of MEMS/NEMS, 05/19/2011.

5. SUPMECA (Institute Superieur de Mecanique de Paris): Nonlinear dynamics of MEMS/NEMS, 05/16/2011.

6. SUPMECA (Institute Superieur de Mecanique de Paris): Nonlinear dynamics of MEMS/NEMS, 05/13/2011.

7. CONTACT Annual Review, Nonuniform Resonator Sensors for Enhanced Sensitivity, Rice, 10/13-14/2010.

APPENDIX J - "Light Storage and Amplification in Photonic Crystal Nanocavities"
PI: Malik Rakhmanov, UT Brownsville

Optical Properties of FCC Opals

We conducted experimental investigations of the optical properties of the silica opals using both their direct and inverted forms. The opal samples were provided to us by Dr. Anvar Zakhidov at UT Dallas. We also conducted theoretical investigations of the opals using the Finite-Difference Time-Domain (FDTD) model and completed calculations of the photonic bands in opals using Plane-Wave Expansion (PWE) method on the parallel computer cluster. We began with negative refraction in opals. Modeling with FDTD showed that for some angles of incidence, the opals indeed show NIM behavior. However, this effect was difficult to prove experimentally due to random orientations of crystalline domains in the opals. The opal samples were produced by self assembly and always consisted of a large number of small crystalline domains randomly oriented with respect to each other. We continued studies of the optical properties of opals shifting the emphasis on their spatial diffraction. We conducted experiments with three lasers (405, 630, and 1550 nm) and a broadband white-light source and analyzed their diffraction patterns as a function of the angles of the reflected beam. The orientation of the crystallographic planes in a particular domain can be determined from these diffraction patterns. This research was conducted in collaboration with Dr. Zakhidov at UT Dallas.

Photonic-Crystal Membrane Reflector

We conducted experimental and theoretical investigation of the reflectivity of the silicon membrane reflector (Si-MR) which is a 2-dimensional photonic-crystal slab (Figure 18, left). Si-MR devices promise many applications in photonic integrated circuits and can be used as ultra-compact mirrors with controlled spectral response. Built entirely from dielectric materials, such membrane reflectors can have very low losses and therefore can deliver near-100% reflectivity both in narrow and wide-band configurations (Figure 18, right).

To conduct optical characterization of the Si-MR mirrors, we used two devices with the reflectivity peaked at 1550 nm designed and fabricated by Dr. Weidong Zhou at UT Arlington. We measured the parameters of the reflected beam and investigated the fine structure of the light reflected by the Si-MR mirror as a function of the polarization angle. To study the modal properties of the Si-MR mirror, we built a cavity which stores and amplifies the EM modes generated by this mirror. We have successfully resonated a laser beam (wavelength: 1550 nm) in this cavity and obtained optical fields in which the Hermite-Gauss modes are combined with the diffraction modes produced by the photonic crystal. These experiments proved to be difficult to conduct in air. We therefore designed a vacuum chamber with optical viewports and electric feed-through flanges to contain the entire experiment. The vacuum chamber is being manufactured at A&N.

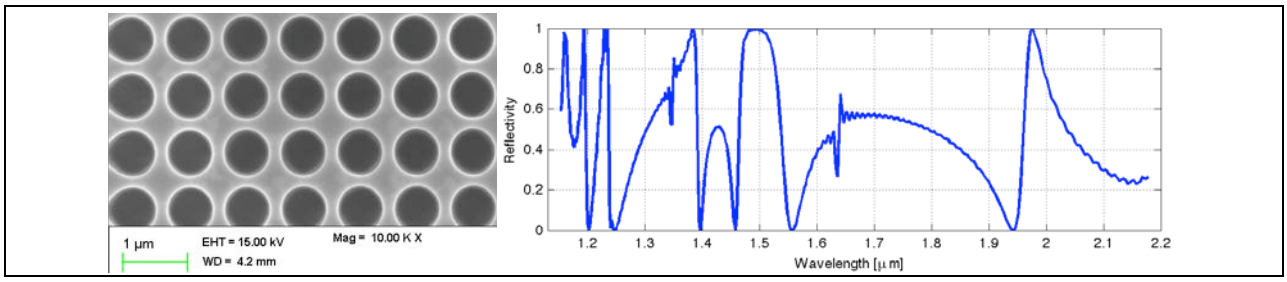

Figure 18. Left: SEM image (from Dr. Zhou, UTA) of the Si-MR (the lattice spacing is a = 850 nm); Right: The reflectivity of the Si-MR as a function of the wavelength of the incident light calculated with the FDTD algorithm. Notice several high-reflectivity areas (near 100%) and a broad-band peak at 1.5 µm.

During these experiments, we found that the main beam reflected by the Si-MR is accompanied by a wide-angle diffraction field originating from the lattice structure of the sub-wavelength scale on the Si-MR reflector. The sub-wavelength diffraction pattern possessed a number of unique properties, e.g. its intensity modulation is linked to the polarization of the beam incident on the reflector. Analysis of this diffraction field leads to understanding of the fundamental limitations of the reflectivity of the Si-MR devices. This research was conducted in collaboration with Dr. Zhou at UT Arlington.

Photonic-Crystal Nanocavities

The collaborations with UT Arlington and UT Dallas facilitated our transition to research focused on control of photonic-crystal nanocavities. We planned to study mechanisms for achieving light confinement in photonic-crystal nanocavities with the goal of developing various ways to control the cavity and its light storing property. Our approach was to utilize the techniques and ideas currently used in locking of conventional cavities of the Fabry-Perot design. In particular, one of the most powerful methods for controlling Fabry-Perot cavities is based on the Pound-Drever-Hall (PDH) locking. We thus focused on developing a method which is similar to the PDH locking technique but applicable to photonic-crystal nanocavities.

We conducted FDTD modeling of a 2-dimensional photonic crystal nanocavity formed by a single defect. Figure 19 (left) shows an integrated photonic circuit which consists of a nanocavity and two parallel waveguides: the left waveguide couples light to the cavity and the right waveguide is needed to produce the error signal. By tuning the wavelength of light in the first waveguide, one can achieve significant coupling of light into the cavity where it is amplified and stored. This process is followed by the leakage of light from the cavity into the second waveguide. By recombining the light exiting from the two waveguides, we obtain superposition of the pump light with the phase-shifted leakage light, in a manner similar to that of the PDH scheme. The superposition of light fields will lead to the intensity beats which have both in-phase and quadrature components with respect to the pump light. We have found that the intensity beats of the quadrature component contain the desired error signal (Figure 19, right).

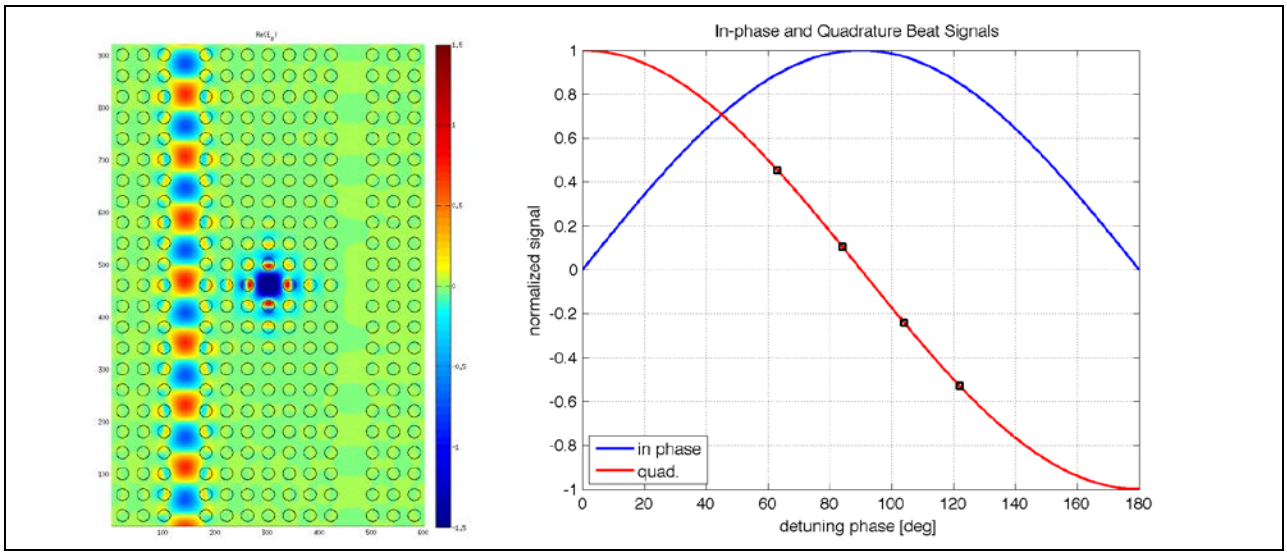

Figure 19. Left: Dual waveguide design to control photonic crystal nanocavity. The left waveguide couples light to the cavity, the right waveguide serves to extract leakage field. Right: The error signal obtained from the intensity beat of the light in two waveguides. Note the zero-crossing of the error signal (red trace) at the detuning phase corresponding to the center of the resonance in the cavity.

We have shown that a unique error signal can be obtained this way and this signal can then be used to adjust the wavelength of light coupled to the photonic-crystal nanocavity. In other words, by feeding back this error signal to the laser one can control the nanocavity. We plan to continue this research beyond this funding cycle. The next step is to design such an integrated circuit with the controlled nanocavity and fabricate it for future experiments.

M. Rakhmanov continues the experiments with the silicon nano-patterned membrane and has recently initiated in-vacuum cavity measurements, which will increase the sensitivity of the measurements hundred-fold.

Peer–reviewed publications:

"Sub-wavelength Diffraction Losses in a Silicon Nano-Patterned Membrane Reflector," M. Rakhmanov, W. Zhou, et al., abstract accepted for "IEEE Photonics Conference 2012", Burlingame, CA, September 23-27, 2012

Invited Lectures:

1. *"Dynamics of light in resonant cavities, waveguides, and photonic crystals,"* M. Rakhmanov, a talk given for the NSF REU Program, Department of Physics, University of Texas at Brownsville, June 27, 2012.
2. *"Hadamard's ill-posed problems in physics and engineering,"* a seminar for the Rutherford Lecture Series at the Department of Physics, University of Texas, Austin, TX, July 16, 2010.
3. *"Optical Cavities: new and unusual roles,"* Colloquium at the Department of Physics, University of Texas, Austin, TX, April 9, 2010.
4. *"How university research can change regional economy,"* an invited talk at Lockheed Martin WBT Showcase 2010, University of Texas, Arlington, TX, March 16, 2010.

Conference Presentations:

1. *"Sub-wavelength Diffraction Losses in a Silicon Nano-Patterned Membrane Reflector,"* M. Rakhmanov and A. Bogdanovskiy, at the IEEE Photonics Conference 2012, Burlingame, CA, September 23-27, 2012. (This work was done in collaboration with Dr. Zhou at UT Arlington.)

2. *"Development of experimental optics and nanophotonics at UTB,"* M. Rakhmanov, a talk given at the "Renewable Energy and Nano-Science" Symposium, University of Texas, Brownsville, April 11, 2012.

3. *"Light storage and amplification in photonic crystal nanocavities,"* M. Rakhmanov, a talk given at the Annual Review Meeting of CONTACT, Wright Patterson Air Force Base, Materials and Manufacturing Directorate, March 22, 2012 .

4. *"Modeling of optical resonators using Gaussian Beams and Ray Tracing techniques,"* L. Ruiz, S. Cantu, V. Quetschke, and M. Rakhmanov, a talk given at the Annual Meeting of the Texas Section of the American Physical Society, Commerce, TX, October 6, 2011.

5. *"Optical losses and wave-front distortions in the reflection of light from a photonic-crystal mirror,"* T. Miller, B. Frost, V. Quetschke, M. Rakhmanov, Y.-C. Shuai, D. Zhao, and W. Zhou, a poster presentation at the Joint Fall 2010 Meeting of the Texas Sections of the APS, University of Texas at San Antonio, TX, October 21, 2010.

6. *"Experimental investigation of the possibility for negative refraction in silica opals,"* L. Ruiz-Diaz, V. Quetschke, and M. Rakhmanov, a poster presentation at the Joint Fall 2010 Meeting of the Texas Sections of the APS, University of Texas at San Antonio, TX, October 21, 2010.

7. "Light storage and amplification in photoic crystal nanocavities (The 1st year of optics and nanophotonics program at UT Brownsville)," M. Rakhmanov, a talk given at the Annual Review Meeting for CONTACT, Rice University, Houston, TX, October 13, 2010.

8. *"3-Dimensional analysis of optical properties of opal photonic crystals,"* T. Miller, A. Farrell, L. Ruiz-Diaz, M. Rakhmanov, R. Moussa and A. Zakhidov, a poster presentation at the National Space & Missile Materials Symposium at Scottsdale, Arizona, June 27, 2010.

9. *"Numerical analysis of negative refraction in 3-dimensional structures for both direct and inverse forms,"* A. Farrell, R. Moussa, M. Rakhmanov, and A. Zakhidov, a poster presentation at Tri-Service 6.1 Metamaterial Review, Virginia Beach, VA, May 24, 2010.

10. "Optical Cavities: from km size to nano scale. (The launch of Optics and Nanophotonics program at UT Brownsville)," a talk given at the Annual Review Meeting for CONTACT, Edinburg, TX, September 29, 2009.

Awards and additional funding received from other sources helped by participation in CONTACT:

1. National Science Foundation (NSF)

   Award amount: $100k, period: 2009 – 2010, title: "Optics for LIGO" awarded under the CREST Program (Principal Investigators: M. Diaz and M. Rakhmanov)

2. NASA

   Award amount: $5M, period: 2009 – 2014, title: "Center for Gravitational Wave Astronomy," awarded under NASA URC program (Principal Investigators: M. Diaz, M. Rakhmanov, et al.)

University Research Infrastructure Development:
This research initiated experimental studies of photonic crystals and nanocavities at the University of Texas at Brownsville (UTB) and led to the development of a new laboratory at UTB dedicated to optics and nanophotonics. The lab renovation began in 2009 and was completed in 2011. Today, the Optics and Nanophotonics laboratory at UTB conducts research in laser resonators, photonic crystals, and optical interferometry, and accommodates more than ten students at both graduate and undergraduate levels.

Student achievements:
MS Theses

Graduate student Alan Farrell completed his MS degree in Physics at UTB in 2010. His work was focused on opals (3-d photonic crystals) in both direct and inverted forms and their FDTD modeling with RSoft. He is now pursuing his PhD at EE Dept., UCLA.

Graduate student Liliana Ruiz-Diaz is working on her MS thesis "Experimental Investi-gation of Optical Properties of Direct and Inverted Opals (3-d photonic crystals)." Expected graduation date is May 2013.

Travis Miller defended his MS thesis "Experimental Investigation of the Photonic Crystal Cavity" in December 2012. He is now studying in the US Naval Academy. The work he has done under CONTACT was crucial for securing him a position with the Navy. (This is the second MS thesis that was under with Dr. Rakhmanov under CONTACT.)

Collaborations:
We established collaborations with the NanoFab Lab at the University of Texas at Arlington and the MacDiarmid NanoTech Institute at the University of Texas at Dallas. At the NanoFab Lab, we interact with Dr. Zhou and his group focusing our research on the silicon nano-patterned membrane reflectors. At MacDiarmid Institute, we collaborate with Dr. Zakhidov and Dr. Aliev on optical properties of direct and inverted opal photonic crystals. We also collaborated with Dr. Touhami at UTB to obtain high-resolution scans of the opal samples and nano-patterned membrane reflectors with Atomic Force Microscopy.

APPENDIX K - "Spectroscopy of InAs/GaSB Superlattices for the Development of High Operating Temperature Infrared Detectors"
PI: Junichiro Kono, Rice University

Short-period superlattices (SLs) based on alternating layers of InAs and GaSb are expected to be a promising material for infrared (IR) detectors. Due to the type-II band alignment of these SLs, the band gap can be tuned to the mid-IR range by an appropriate choice of SL period. Also, it is expected that the band structure of these SLs can be tailored to reduce Auger recombination and tunneling currents to make room temperature operation possible. However, growth and fabrication of high-quality detectors using these SLs still remains challenging, and basic materials properties, especially dynamic properties, are not well understood.

In the last reporting period, from April 2012 to the present, we have continued to investigate the carrier lifetime via differential reflectivity measurements using a non-standard pump-probe technique where our pump laser beam is pulsed however our probe beam is a continous wave beam. Using this technique, we have measured the carrier lifetime of more samples that have a different design. The basic change in design replaces the GaSb layers with the alloy, GaInSb, in order to create an effective bandgap that corresponds to longer wavelengths than the original series of samples that were provided in this collaboration. Some of our results are included in a manuscript that was recently prepared and will be submitted to Applied Physics Letters.

During the course of the entire project, we were able to set up a pump-probe experiment to measure the full relaxation as a function of time via differential reflectivity measurements by developing a non-standard pump-probe technique to cover very long delays. Early in the project, we investigated the coherent phonon dynamics of these superlattice structures using standard pump-probe techniques, and our results were published. In total, using both of the techniques, our differential reflectivity measurements reveal the carrier and phonon dynamics continuously covering time scales from ~150 fs (the pulse duration of our laser beam) to 1 ms (the time separation between laser pulses). This covers almost 10 orders of magnitude in time delay. We have investigated a variety of samples based on the type-II band alignment of InAs/GaSb superlattices in order to help the sample grower identify the growth conditions appropriate for producing high quality samples to be eventually used as mid-infrared detectors.

Publication:

G.T. Noe, H.J. Haugan, G.J. Brown, G.D. Sanders, C.J. Stanton, J. Kono, Coherent Phonon Dynamics in Short-Period InAs/GaSb Superlattices, Superlattices and Microstructures (2012), doi:http://dx.doi.org/10.1016/j.spmi.2012.08.010

Presentations:

August 2011 NGS 15, Blacksburg, VA. Poster Presentation – "Coherent Phonon Dynamics in Short-Period InAs/GaSb Superlattices"

Oct. 2010 CONTACT Program – Annual Review Meeting, Houston, TX. Poster Presentation – "Spectroscopy of InAs/GaSb Superlattices for the Development of High-Operating Temperature Infrared Detectors"

Student Achievement:
June 2011 M.S. Degree – “Ultrafast and Magneto-Optical Spectroscopy of Semiconductor Heterostructures” by Gary Timothy Noe II

APPENDIX L - "Integrated Flexible Sensors (Smart Skin) for Structural Health Monitoring"

PIs: Zeynep Celik-Butler and Donald Butler, UT Arlington

The objective is to develop integrated MEMS sensors on flexible substrates for structural health monitoring of aircraft (Figure 20). The sensors include accelerometers, pressure sensors, temperature sensors, and acoustic sensors. These MEMS (microelectromechanical)-based embedded structural sensor strips will support the realization of a reliable system, capable of sensing material changes that may affect aircraft structural integrity.

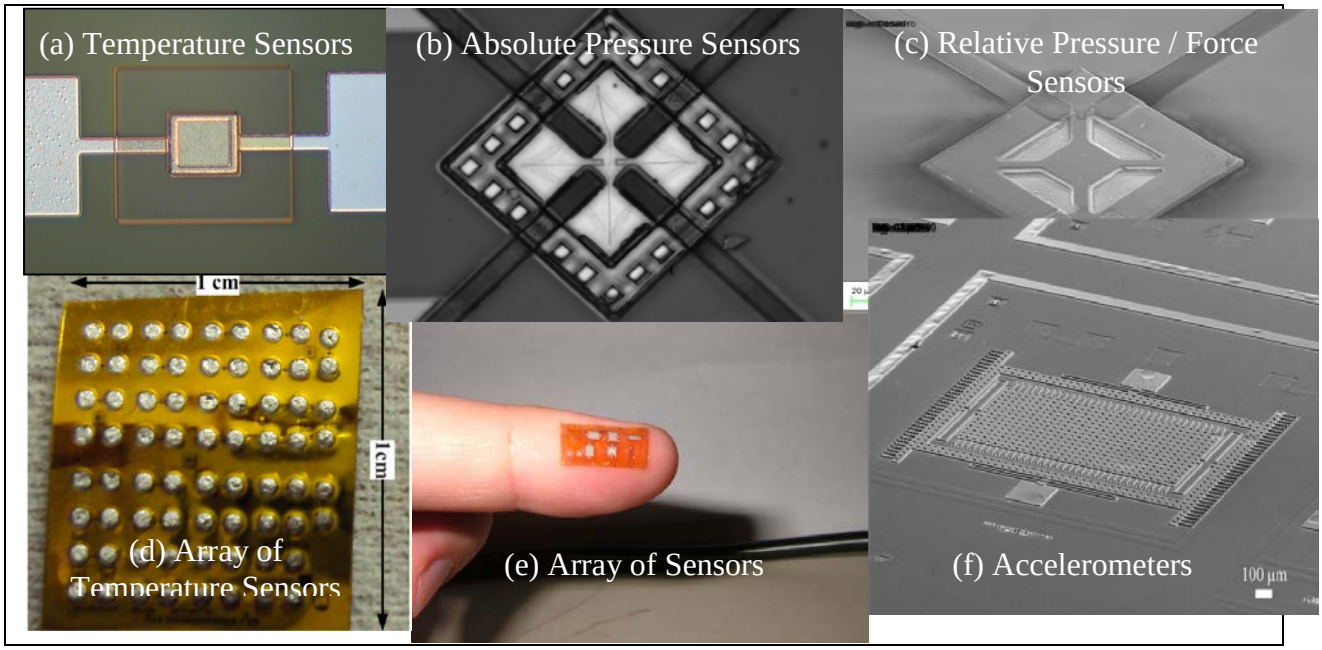

Figure 20. Different kinds of sensors on flexible substrates developed by our group

During this last reporting period, we have been working on the development of acoustic emission sensors for crack detection. In this case, the acoustic emission sensor detects the acoustic energy produced by crack formation and propagation. Capacitive acoustic emission sensors, optimized for the frequencies of acoustic energy reported for metal crack formation and propagation, have been designed and numerically analyzed using finite element method with the aid of Coventorware and Comsol.

During the CONTACT funding period, a variety of MEMS sensors on flexible substrates were designed, fabricated, and characterized. This work has demonstrated that a variety of MEMS-based sensors can be fabricated on flexible polymer substrates without the loss of performance, towards the development of a smart skin. These flexible sensors include amorphous silicon-based temperature sensors, nichrome based piezoresistive, absolute pressure sensors, tactile sensors and force sensors, and capacitive accelerometers. The sensors are sandwiched between a polyimide substrate and superstrate, placing them at a low stress plane, and were thus packaged at the device-level. The flexible sensor package is grown during the device fabrication process. This allows the sensors to be integrated directly with flexible circuit boards while maintaining overall flexibility. Some notable features are the incorporation of a sealed vacuum cavity for the absolute pressure sensors and the formation of a hermetically sealed cavity to contain the

accelerometers in a constant atmosphere. This work was motivated by the need to monitor temperature, force and pressure and acceleration on non-planar surfaces for structural health monitoring, biomedical, aerospace, automation and automotive industries. Furthermore, these pressure/force/tactile sensors on flexible substrates hold great promise for potential applications such as smart tags, sensitive electronic skin, and electronics fabric [1].The use of a flexible substrate in conjunction with a flexible superstrate allowed these sensor arrays to conform to non-planar surfaces, moving towards the integration of self-packaged and self-powered 'smart skin' [2].

References:

[1] K. Gilleo, *Handbook of Flexible Circuits*, Van Nostrand Reinhold, New York, NY, 1992.

[2] Z. Celik-Butler, D. P. Butler, *J. of. Nanoelec. & Optoelec.*, vol. 1, pp. 194-202, 2006.

Publications:

1. Suraj K. Patil, Zeynep Celik-Butler, and Donald P. Butler, "Characterization of MEMS Piezoresistive Pressure Sensors using AFM," Ultramicroscopy **110**, pp. 1154-1160 (2010).

2. M. Shahriar Rahman, Murali Chitteboyina, Donald P. Butler, Zeynep Celik-Butler, Sergio Pacheco, and Ronald McBean, "Device-level vacuum packaged MEMS resonator," IEEE/ASME Journal of Microelectromechanical Systems **19**, pp. 911-917 (2010).

3. Suraj K. Patil, Zeynep Celik-Butler, and Donald P. Butler, "Nanocrystalline Piezoresistive Polysilicon Film by Aluminum Induced Crystallization for Pressure Sensing Applications," IEEE Transactions on Nanotechnology 9, pp. 640-646 (2010).

4. Suraj K. Patil, Zeynep Celik-Butler, and Donald P. Butler, "Piezoresistive Polysilicon Film Obtained by Low-Temperature Aluminum Induced Crystallization," Thin Solid Films **519**, pp. 479-486 (2010).

5. İsmail Erkin Gönenli, Zeynep Çelik-Butler, and Donald P. Butler, "Surface Micromachined MEMS Accelerometers on Flexible Polyimide Substrate," IEEE Sensors Journal **11**, pp. 2318-2326 (2011).

6. Moinuddin Ahmed, Murali M. Chitteboyina, Donald P. Butler, and Zeynep Celik-Butler, "Temperature Sensor in a Flexible Substrate," IEEE Sensors Journal **12**, pp. 864-869 (2012).

7. Gaviraj S. Nadvi, Donald P. Butler, Zeynep Celik-Butler and İsmail Erkin Gönenli, "Micromachined Force Sensors using Thin Film Nickel Chromium Piezoresistors," Journal of Micromechanics and Microengineering **22**, pp. 065002 (10pages) (2012).

Conference Papers:

1. M. Shahriar Rahman, Murali Chitteboyina, Donald P. Butler, Zeynep Celik-Butler, Sergio Pacheco, and Ronald McBean, "Self-Packaged MEMS Device," Presented at the IMAPS 6th International Conference and Exhibition on Device Packaging, Scottsdale, Arizona, USA, March 8 – 11, 2010. Also published in Special Feature in Electronic Parts & Components Magazine, Korea, pp. 42-46, November, 2010.

2. İsmail Erkin Gönenli, Zeynep Çelik-Butler, and Donald Butler, "MEMS Accelerometers on Polyimides for Failure Assessment in Aerospace Systems," Presented at the 2010 IEEE Sensors Conference, Waikoloa, Hawaii, November 1-4, 2010. Conference Proceedings.

3. Moinuddin Ahmed, Donald P. Butler, Zeynep Celik-Butler, "The flicker noise in amorphous

silicon based temperature sensors in flexible substrates," Presented at the 2011 International Conference on Noise and Fluctuations, June 12-16, 2011, Toronto, Canada. Conference Proceedings.

4. Moinuddin Ahmed, Donald P. Butler, and Zeynep Celik-Butler, "MEMS relative pressure sensor on flexible substrate," Presented at the 2011 IEEE Sensors Conference, Limerick, Ireland, 28-31 October 2011. Conference Proceedings. pp. 460-463.

5. Moinuddin Ahmed, Donald P. Butler, and Zeynep Celik-Butler, "MEMS absolute pressure sensor on a flexible substrate," Presented at the 2012 IEEE MEMS Conference, Paris, France, 29 January-2 February 2012. Conference Proceedings. pp. 575-578.

6. Moinuddin Ahmed, Donald P. Butler, Mukti M. Rana, and Nouriddine Melikechi "Pyroelectric Modified Lead Titanate Thin Films for Uncooled Infrared Detection," Presented at the IEEE Optical MEMS and Nanophotonics Conference, 6-9 August 2012, Banff, Alberta, Canada. Conference Proceedings.

Awards and additional funding:

1. Lockheed Martin, "Integrated Flexible Sensors (Smart Skin) for Structural Health Monitoring," $40,000, 10/6/2010-10/5/2012.

Presentations:

1. Zeynep Çelik-Butler, and Donald P. Butler, "MEMS-Based Conformal Sensors for Real-Time Structural Health Monitoring," *Proc. Of ONR Naval Science and Technology Partnership Conference,* Nov. 8 – 10, 2010, Washington DC.

2. Zeynep Çelik-Butler and Donald P. Butler, "Integrated Flexible Sensors (Smart Skin) for Structural Health Monitoring," CONTACT (Consortium for Nanomaterials for Aerospace Commerce and Technology) Annual Review Meeting, Houston, TX, October 13-14, 2010.

Student achievements:

Temperature Sensor in a Flexible Substrate, IEEE Sensors Journal, Vol. 12, No. 5, May 2012, (paper was one of the 25 most downloaded Sensors Journal papers in the month of April, 2012).

Collaborations:

Lockheed-Martin Company

APPENDIX M - "Electronic Devices for Air Force Needs through Organic-Inorganic Hybrid Materials and Processing Development"

PIs: Brian Korgel, Allen Bard, Ananth Dodabalapur, and David Vanden Bout, UT Austin

We have made progress in two areas:

(1) Synthesis processing, and performance of new photovoltaic "inks" based on inorganic nanocrystals.

The research has focused on the development of semiconductor nanocrystal inks for low-cost processing of photovoltaic devices. The research has involved two aspects: (i) demonstrate high efficiency is possible using nanocrystal layers and (ii) demonstrate functional PV devices on flexible low-cost and lightweight substrates. We have made progress in both of these directions. With respect to high efficiency devices, we have been using $CuInSe_2$ (CIS) nanocrystals to deposit device layers on CdTe devices to create tandem, or multijunction, solar cells. The CIS layer absorbs light in a different wavelength range than CdTe and can enhance device performance. Even a 2-3% enhancement in CdTe solar cell efficiency would have a significant impact on lowering the current cost of PV electricity. Ultimately, multijunction cells with three semiconductor layers are desired. The challenge is integrating several different materials that cannot be processed using high temperature. The nanocrystal inks may solve this problem.

With respect to low temperature deposition of PV device layers on flexible and lightweight substrates, we have made significant progress in this direction, and have demonstrated functioning PV devices on various substrates, including polyethylene and other carbon-based substrates. Device efficiencies were in the range of 2-3%, so the current research effort is focused on developing methods to achieve higher device efficiency.

(2) Semiconductor Nanowires as the Basis for new Advanced Textiles and Composites.

Silicon and germanium nanowires are being synthesized and tested as the basis for new functional textiles and composites. The nanowire optical, mechanical, electrochemical and electrical properties of the nanowire fabrics are being tested. Si and Ge nanowires have been found to be very good lithium storage materials for lithium ion batteries and we recently demonstrated that a Si nanowire fabric can serve as a self-supporting standalone anode. Both Si and Ge nanowire fabric is extremely optically opaque due to light-scattering within the material. No visible light passes through a 50 micrometer film of the material. Ongoing research is focused on understanding the electronic properties of the materials and its potential use as advanced multifunctional coatings.

Publications resulting from the funded research:

1. C. M. Hessel, et al., "Synthesis of Ligand-Stabilized Silicon Nanocrystals With Size-Dependent Photoluminescence Spanning Visible to Near Infrared Wavelengths," *Chem. Mater.*, 24 (2012) 393-401.

2. A. M. Chockla, J. T. Harris, V. A. Akhavan, T. D. Bogart, V. C. Holmberg, C. Steinhagen, C. B. Mullins, K. J. Stevenson, B. A. Korgel, "Silicon Nanowire Fabric as a Lithium Ion Battery Electrode," *J. Am. Chem. Soc.* (2011) ASAP contents.

3. V. A. Akhavan, B. W. Goodfellow, M. G. Panthani, C. Steinhagen, T. Harvey, C. J. Stolle, B. A. Korgel, "Colloidal CIGS and CZTS Nanocrystals: A Precursor Route to Printed Photovoltaics," *J. Solid State Chem.* (2011) in press.

4. V. C. Holmberg, K. A. Collier, B. A. Korgel, "Real-Time Observation of Impurity Diffusion

in Silicon Nanowires," *Nano Lett.* 11 (2011) 3803-3808.

5. V. C. Holmberg, R. N. Patel, B. A. Korgel, "Electrostatic Charging and Manipulation of Semiconductor Nanowires," *J. Mater. Res.* 26 (2011) 2305-2310.

6. A. T. Heitsch, V. A. Akhavan, B. A. Korgel, "Rapid SFLS Synthesis of Si Nanowires Using Trisilane with In Situ Alkyl-Amine Passivation," *Chem.Mater.* 23 (2011) 2697-2699.

7. H. Ye, H. S. Park, V. A. Akhavan, B. W. Goodfellow, M. G. Panthani, B. A. Korgel, A. J. Bard, "Photoelectrochemical Characterization of $CuInSe_2$ and $Cu(In_xGa_{1-x})Se_2$ Thin Films for Solar Cells," *J. Phys. Chem. C* 115 (2011) 234-240.

8. D. P. Ostrowski, M. S. Glaz, B. W. Goodfellow, V. A. Akhavan, M. G. Panthani, B. A. Korgel, D. A. Vanden Bout, "Mapping Spatial Heterogeneity in $Cu(In_{1-x}Ga_x)Se_2$ (CIGS) Nanocrystal-Based Photovoltaics with Scanning Photocurrent and Fluorescence Microscopy," *Small* 6 (2010) 2832-2836.

9. B. W. Goodfellow, R. N. Patel, M. G. Panthani, D.-M. Smilgies, B. A. Korgel, "Melting and Sintering of a Body-Centered Cubic Superlattice of PbSe Nanocrystals Followed by Small Angle X-ray Scattering," *J. Phys. Chem. C* 115 (2011) 6397-6404.

10. V. A. Akhavan, M. G. Panthani, B. W. Goodfellow, D. K. Reid, B. A. Korgel, "Thickness-Limited Performance of $CuInSe_2$ Nanocrystal Photovoltaic Devices," *Optics Express* 18 (2010) A411-A420.

11. V. A. Akhavan, B. W. Goodfellow, M. G. Panthani, D. K. Reid, D. J. Hellebusch, T. Adachi, B. A. Korgel, "Spray-Deposited $CuInSe_2$ (CIS) Nanocrystal Photovoltaics," *Energy & Environmental Science* 3 (2010) 1600-1610.

12. V. A. Akhavan, B. W. Goodfellow, M. G. Panthani, B. A. Korgel, "Towards a Next Generation of Ultralow Cost Photovoltaics Using Nanocrystal Inks," *Modern Energy Reviews* 2 (2010) 25-27.

13. Dunn, L.; Dodabalapur, A; "Temperature Dependent Transient Velocity and Mobility Studies in an Organic Fild-Effect Transistor; *Journal of Applied Phys*ics 107 (2010) 113714.

14. V. C. Holmberg, M. R. Rasch, B. A. Korgel, "PEGylation of Carboxylic Acid Functionalized Germanium Nanowires," *Langmuir* 26 (2010) 14241-14246.

15. V. C. Holmberg, B. A. Korgel, "Corrosion Resistance of Thiol- and Alkene-Passivated Germanium Nanowires," *Chemistry of Materials* 22 (2010) 3698-3703.

16. D. A. Smith, V. C. Holmberg, B. A. Korgel, "Flexible Germanium Nanowires: Ideal Strength, Room Temperature Plasticity and Bendable Semiconductor Fabric," *ACS Nano* 4 (2010) 2356-2362.

17. C. K. Chan, R. N. Patel, M. J. O'Connell, B. A. Korgel, Y. Cui, "Solution-Grown Silicon Nanowires for Lithium-Ion Battery Anodes," *ACS Nano* 4 (2010) 1443-1450.

18. C. M. Hessel, A. T. Heitsch, B. A. Korgel, "Gold Seed Removal from the Tips of Silicon Nanorods," *Nano Letters* 10 (2010) 176-180.

19. V. C. Holmberg, M. G. Panthani, B. A. Korgel, "Phase Transitions, Melting Dynamics and Solid-State Diffusion in a Nano Test Tube," *Science* 326 (2009) 405-407.

20. B. Koo, R. N. Patel, B. A. Korgel, "Wurtzite-Chalcopyrite Polytypism in $CuInS_2$ Nanodisks," Chem. Mater. 21 (2009) 1962-1966.

21. D. K. Smith, B. Goodfellow, D. M. Smilgies, B. A. Korgel, "Self-Assembled Simple Hexagonal AB_2 Binary Nanocrystal Superlattices: SEM, GISAXS and Defects," *J. Am. Chem.*

Soc. 131 (2009) 3281-3290.

22. B. Koo, R. N. Patel, B. A. Korgel, "$CuInSe_2$ Nanocrystals: Synthesis, Trigonal Pyramidal Shape, and Self-Assembly into Triangular Lattices," *J. Am. Chem. Soc.* 131 (2009) 3134-3135.

23. C. Steinhagen, M. G. Panthani, V. Akhavan, B. Goodfellow, B. Koo, B. A. Korgel, "Synthesis of Cu_2ZnSnS_4 (CZTS) Nanocrystals for Use in Low-Cost Photovoltaics," *J. Am. Chem. Soc.* 131 (2009) 12554-12555.

24. A. T. Heitsch, C. M. Hessel, V. A. Akhavan, B. A. Korgel, "Colloidal Silicon Nanorod Synthesis," *Nano Lett.* 9 (2009) 3042-3047.

25. Bolinger, J. C.; Fradkin, L.; Lee, K.-J.; Palacios, R. E.; Barbara, P. F., "Light-Assisted Deep-Trapping of Holes in Conjugated Polymers," *Proc. Nat. Acad. Sci.* 106 (2009) 1342-1346.

26. Fradkin, L.; Palacios, R. E.; Bolinger, J. C.; Lee, K.-J.; Lackowski, W. M.; Barbara, P. F., "Factors Controlling Hole Injection in Single Conjugated Polymer Molecules," *J. Phys. Chem. A* 113 (2009) 4739-4745.

27. Bolinger, J.; Lee, K.-J.; Palacios, R. E.; Barbara, P. F., "Detailed Investigation of Light Induced Charge Injection into a Single Conjugated Polymer Chain," *J. Phys. Chem. C* 112 (2008) 18606-18615.

28. Palacios, R. E.; Lee, K.-J.; Rival, A.; Adachi, T.; Bolinger, J. C.; Fradkin, L.; Barbara, P. F., "Single Conjugated Polymer Nanoparticle Capacitors," *J. Chem. Phys.* 357 (2009) 21-27.

29. Matthew G. Panthani, Vahid Akhavan, Brian Goodfellow, Johanna P. Schmidtke, Lawrence Dunn, Ananth Dodabalapur, Paul Barbara, and Brian A. Korgel, "Synthesis of $CuInS_2$, $CuInSe_2$ and $Cu(In_xGa_{1-x})Se_2$ (CIGS) Nanocrystal "Inks" for Printable Photovoltaics, Journal of the American Chemical Society, submitted, 2008.

30. Josh Bolinger, Leonid Fradkin, Kwang-Jik Lee, Rodrigo E. Palacios, Paul F. Barbara*, "Are the Electronic Properties of Conjugated Polymers Deformable?", Science, invited submission, 2008.

31. Koo B (Koo, Bonil), Korgel BA (Korgel, Brian A.), Coalescence and interface diffusion in linear CdTe/CdSe/CdTe heterojunction nanorods, NANO LETTERS, Volume: 8, Issue: 8, Pages: 2490-2496, Published: AUG 2008.

APPENDIX N - "Tandem Solar Cells with Carbon Nanotube Interlayers: Parallel OPV/DSC True Hybrids"

PIs: Anvar Zakhidov and John Ferraris, UT Dallas

UTD/SOLARNO team has been developing a novel design for "Hybrid Parallel solar cell tandems" of both polymeric and small molecule types, based on transparent carbon nanotube charge collecting common electrodes, and comparing with traditional in-series design of tandems. We have proven both theoretically and experimentally that parallel connection is always better (as compared to usual in-series tandem) for OPV device sub-cells with similar V_{oc} and largely different short circuit currents (I_{sc}). We have prepared two patents on this concept and have shown those results at CONTACT meetings.

To achieve highest efficiency we needed to fabricate high efficiency sub-cells: front cell and back cells (one of which must be inverted), that can be achieved by using newly developed polymers and dopants. We most recently achieved 5.6 % efficiency in single OPV with PTB7/PCBM and 4.9% efficiency in inverted polymeric OPV on same PTB7 /PCBM system, (and with current better polymers this should give > 7 % efficiency), and if properly combined with a low gap polymer OPV, this should give expected efficiency 9-10 %. We have invented a new concept of truly hybrid tandem of solar cell with a supercapacitor, connected via common carbon nanotube (CNT) electrode, which will be patented.

CNT Forest Growth by Induction-CVD Synthesis

Spinnable carbon nanotube forests provide a novel way to draw conductive transparent sheets for various applications. These tubes are typically grown in atmospheric CVD systems on silicon substrate materials. Heating of the substrate is normally achieved by resistive element heating in tube furnaces. An innovative way is to use inductive heating to quickly heat the substrate to growth temperatures. Samples can be heated to growth temperatures over 700 ºC in less than 2 minutes. This quick heating and control over the heat rate aid in particle formation and minimizes Ostwald Ripening. This produces nanotube forests with very good spinnability and uniformity. Gas heating via a standard tube furnace is used to heat the incoming gasses separately from the substrate. This gives fine control over the substrate and gas temperatures independently.

In the standard method of growing carbon nanotubes, a CVD furnace is used to heat the samples in a resistively heated furnace. This method proves to have many disadvantages:

- Slow to heat up and cool down
- Difficult to view/study *in-situ* growth
- Need to cool furnace between runs
- Cannot control gas and substrate temperature independently

Growth in Induction Coil on the other hand occurs within an induction heating coil. The fast heat up creates very uniform forests that are extremely spinnable. Samples sit on a graphite susceptor for heat transfer. Gasses are preheated in a standard furnace to allow proper dissociation of the reaction gas. This method provides many advantages:

- Fast heat up and cool down

- Can visibly see growth, allows for *in–situ* monitoring
- Can leave pre-heat furnace on between sample runs, no need to cool down between runs
- Independent control over the gas and substrate temperatures

Figures 21 and 22 illustrate the induction systems mentioned.

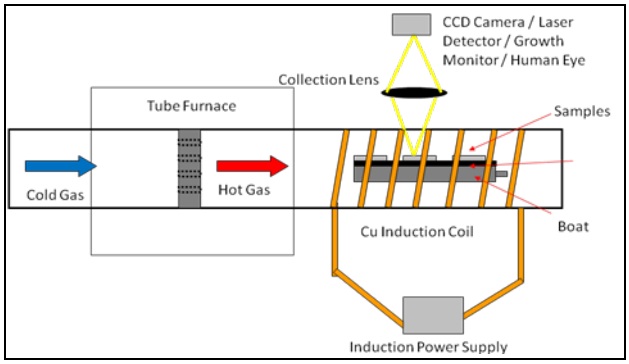

Figure 21. Schematic showing the versatility of the induction system

Figure 22. Induction System in Operation and susceptor at Production Temperature of 750ºC.

A Key objective of project is producing carbon nanotube sheets with low sheet resistance. CNT forests are grown with a CVD process on silicon substrates using an iron catalyst. The application of self assembled monolayers (SAMs) on CNT sheets may also increase the conductivity of CNT sheets. Our results have shown that the resistivity of CNT sheets decreased to approximately 100-150 ohm/sq by higher temperature synthesis in RF induction system, while transparency stays at the level of 80-85 %. In addition, we can still produce CNT with transparency of 90 %, but higher R_{sheet} of 600 Ohm/sq.

Finally, we will utilize the CNT forest properties to produce CNT sheets at low cost and high volume. Figure 23 shows the drawing process of CNT sheets from CNT forests and transfer to devices. Each step of the process is illustrated (Figure 23a to c). Actual devices are shown in Figure 23d. In addition, a motor can be used to draw the CNT sheets from the forest for large volume applications (Figure 23e).

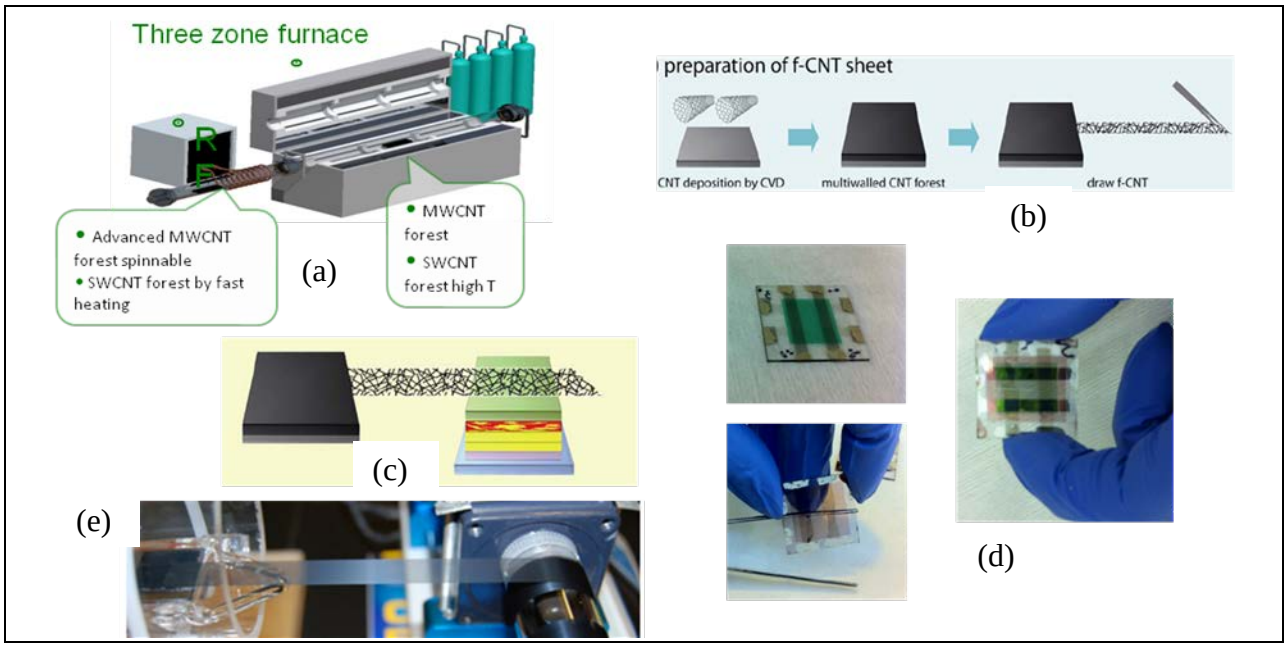

Figure 23. (a-c) CNT draws process and lamination to devices, (d) device photographs, (e) motorized draw of CNT sheets.

Parallel vs Series Tandem organic cells: Conceptual differences

Tandem organic solar cells (OSC) consist of two or more vertically stacked cells connected in a series or parallel configuration. In series connected tandem cells in a tandem, the holes are coming from the bottom cell, while electrons are arriving from the top cell (Figure 24a) so the transfer of the charge at the interface in a monolithic tandem requires that the holes recombine with the electrons. The voltages of top and bottom cells add, while the lowest current can pass through in-series tandem, and current balancing is required. In contrast, for a parallel tandem the photocurrents add ($I = I_{bot} + I_{top}$) in a charge collecting layer (CCL), while the average voltage is generated (Figure 24b). The parallel tandem cell is able to provide higher overall power conversion efficiency than the conventional series tandem cell. In series connection, the front cell has to be thin in order to avoid the current loss by the back cell with weak light absorption; however, in parallel connection, by choosing materials with close V_{oc}, overall current is contributed by the sum of photocurrent from two cells. Thus, a thicker active layer in the parallel tandem cell can be fabricated which allows the rise of our 3-dimensional CNT charge collector leading to higher current without big voltage loss and an increase in the overall power conversion efficiency to reach 10%. Moreover, improving CNT sheet's conductivity is another approach to enhance the cell performance.

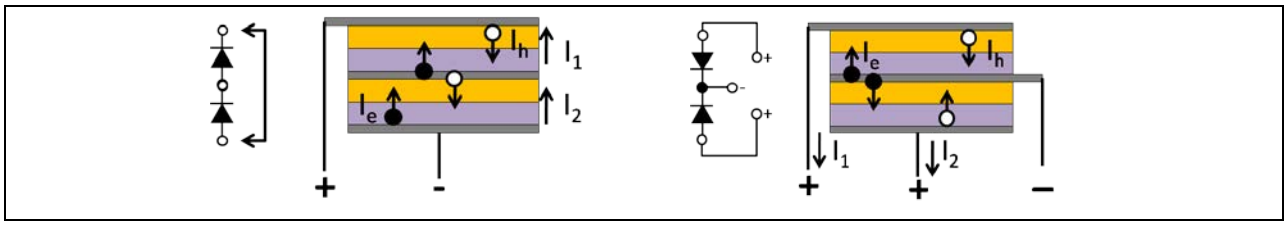

Figure 24 . Tandem cell connection types: a) In-Series Tandem: conventional for inorganic PV, b) Parallel Tandem developed in our project

Advantages of parallel versus in-series connection for OPV and Hybrid solar cell Tandems: Comparison with Model

Tandems of solar cells can provide additional boost to the solar cells' efficiency by absorbing larger portions of the solar spectrum. Hybrid tandems made of sub-cells of different nature (inorganic and organic or dye sensitized photovoltaic cells) may have very different parameters: largely non-balanced photocurrents, voltages and filling factors. Therefore, to maximize tandem's efficiency certain conditions arising from the electric circuit analysis of each sub-cell should be fulfilled. Using the single-diode model, we have shown that parallel connection of dis-similar solar cells is more beneficial in parallel tandems, as compared to conventional in-series connections. We demonstrate several experimental examples of tandems of two polymeric OPVs, tandem of small molecule organic and polymeric OPV/PPV, and tandem of OPV with DSC with largely differing parameters and compare with predictions of model. We prove that indeed the equilibration of the open circuit voltages of the individual cells is important in parallel hybrid tandems, while both short circuit current and fill factor should be matched in in-series tandems. We also prove that parallel connection is preferable when a tandem consists of two current unbalanced solar cells.

Single-diode model

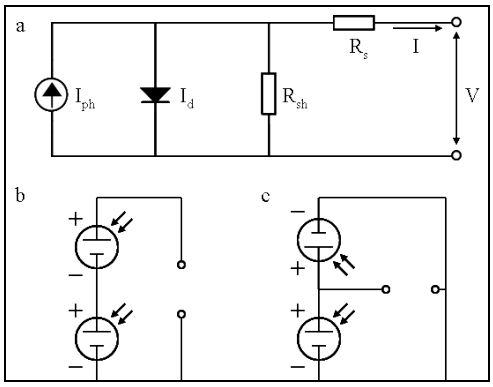

Figure 25. An equivalent circuit of one solar cell (a) series (b) parallel (c) tandem.

A solar cell may be modeled using an electrically equivalent circuit shown in Figure 25a, which consists of a current source, a diode, a shunt resistance, and a series resistance. The current produced by the solar cell is given by:

$$I = I_{ph} - I_0\left\{\exp\left[\frac{e(V + I \cdot R_S)}{nkT}\right] - 1\right\} - \frac{V + I \cdot R_S}{R_{SH}}, \qquad (6)$$

where V is the applied voltage, I_{ph} is the photogenerated current, R_{sh} and R_s are the shunt and series resistances respectively, I_0 is the reverse saturation current of the diode, and n is the diode ideality factor.

The analysis of the equivalent circuit shows that a high-performance solar cell should have high shunt resistance R_{sh} to minimize leakage current going through it. Shunt resistance is usually associated with the losses of generated charge carriers because of the electron-hole recombination at the donor/acceptor interface. On the other hand, series resistance R_s should be low to decrease the voltage drop on it. The series resistance reflects the resistance of charge

transport materials and contacts. Current leakage across the p-n junction under reverse bias worsens the diode behavior of a solar cell by increasing both the reverse saturation current I_0 and the ideality factor n.

The solution of equation 6 can be found using Lambert W-function as

$$I = \frac{R_{SH}\left(I_{ph} + I_0\right) - V}{\left(R_S + R_{SH}\right)} - \frac{n\alpha}{R_S} \cdot W\left\{\frac{R_S R_{SH} I_0}{n\alpha\left(R_S + R_{SH}\right)} \exp\left[\frac{R_{SH}\left(R_S I_{ph} + R_S I_0 + V\right)}{n\alpha\left(R_S + R_{SH}\right)}\right]\right\}, \qquad (7)$$

Where kT/e = 0.259 V at the room temperature. Using the equation 2, we can show that the short-circuit current I_{sc} (current at $V = 0$) and the open-circuit voltage V_{oc} (voltage at $I = 0$) are given by:

$$I_{SC} = \frac{R_{SH}\left(I_{ph} + I_0\right)}{\left(R_S + R_{SH}\right)} - \frac{n\alpha}{R_S} \cdot W\left\{\frac{R_S R_{SH} I_0}{n\alpha\left(R_S + R_{SH}\right)} \exp\left[\frac{R_S R_{SH}\left(I_{ph} + I_0\right)}{n\alpha\left(R_S + R_{SH}\right)}\right]\right\}, \qquad (8)$$

$$V_{OC} = R_{SH}\left(I_{ph} + I_0\right) - n\alpha \cdot W\left\{\frac{R_{SH} I_0}{n\alpha} \exp\left[\frac{R_{SH}\left(I_{ph} + I_0\right)}{n\alpha}\right]\right\}. \qquad (9)$$

Fill factor FF, defined as the ratio of the maximum obtainable power to the product of V_{oc} and I_{sc}, was calculated by maximizing the total power $P = I \cdot V$ on the interval $0 < V < V_{oc}$.

The behavior of two solar cells connected in a tandem can be described by the system of two transcendental equations similar to eq. (6). In a parallel tandem, the total current equals to the sum of currents through individual cells, each written in the form of eq. (7). To find the solution for a series tandem, we need to express voltage V as a function of current I. Then the total voltage equals to the sum of voltages on each cell. Thus, the exact analytical solutions (not shown here to save space) can be found for both series and parallel tandems. This approach can be generalized for tandems made of three and more solar cells.

Tandems of solar cells: Model analysis of parallel versus in-series connections

The efficiency of two identical solar cells connected in a tandem will be twice larger than the efficiency of one solar cell. However, in the case of two different solar cells connected together, certain conditions should be fulfilled to maximize the efficiency. Obviously, the tandem efficiency is limited by the sum of individual cells' efficiencies. In the present work we analyze the parameters of individual solar cells required for maximizing the tandem efficiency.

Parallel and series connections of three different solar cells with the following parameters were investigated. Cell 1 had I_{ph} = 7 mA; $I_0 = 1*10^{-11}$ mA; R_s = 10; R_{sh} = 1000; n = 1. Cell 2 had reverse saturation current $I_0 = 1*10^{-5}$ mA, which decreased the open circuit voltage twice as compared to cell 1. Cell 3 had higher series resistance R_s = 200 which decreased the short circuit current twice as compared to cell 1 (Table 6). The I-V curves of solar cells 1, 2, and 3 are shown in Figure 26a. Figures 26b-d show the I-V curves of the individual cells (black lines) as well as the series (green) and parallel (red) connections of the corresponding cells.

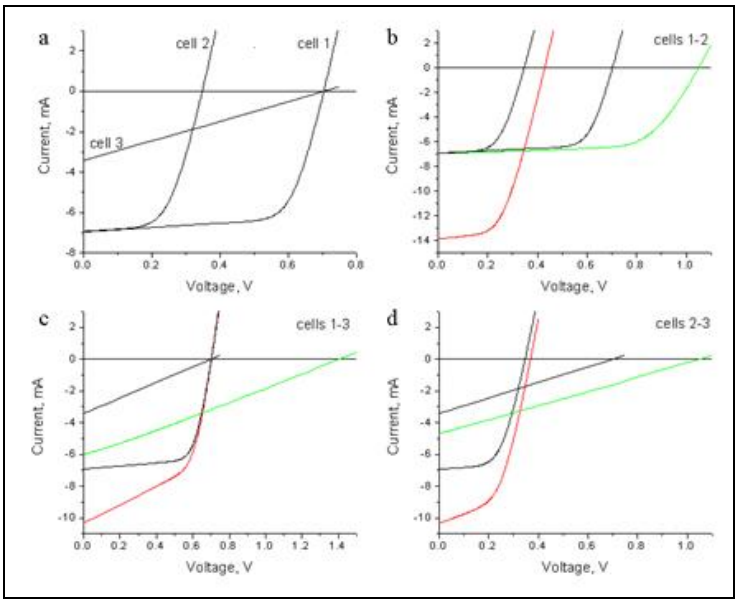

Figure 26. I-V characteristic of the individual (black) solar cells (a), the series (green) and the parallel (red) tandems made of cells 1-2 (b), 1-3 (c), and 2-3 (d)

Table 6. Open circuit voltage (V_{oc}), short circuit current (I_{sc}), fill factor (FF), and efficiency (η) of the individual solar cells and the series and parallel tandems.

cell type	V_{oc}, V	I_{sc}, mA	FF	η, %
cell 1	0.703	6.93	0.70	3.42
cell 2	0.347	6.93	0.57	1.38
cell 3	0.703	3.41	0.25	0.60
series 1-2	1.049	6.93	0.66	4.79
series 1-3	1.405	6.00	0.26	2.23
series 2-3	1.049	4.68	0.25	1.25
parallel 1-2	0.429	13.86	0.51	3.05
parallel 1-3	0.703	10.34	0.53	3.82
parallel 2-3	0.369	10.34	0.50	1.92

If two identical cells are connected in series, the V_{oc} is doubled, while I_{sc} remains the same as for one cell. When individual solar cells are different, V_{oc} of a tandem equals to the sum of open circuit voltages for each cell (see Table 6). The losses in efficiency of a series tandem arise from the reduction of the short circuit current. When the tandem is shorted, the cell with the lower I_{sc} partially consumes the current from the cell with the higher I_{sc} in order to equilibrate the system. Also, if the short circuit currents of the individual cells are not equilibrated, the tandem's fill factor is reduced to almost that of the low-performing cell. Thus, in order to maximize the efficiency of a series tandem it is important to have similar short circuit currents and fill factors of individual cells.

In the case of a parallel connection of two solar cells, the tandem's I_{sc} equals to the sum of the short circuit currents in each cell (see Table 6). The open circuit voltage of a parallel tandem is greatly reduced if it is not balanced in the individual cells. This happens because the voltage

from the cell with higher V_{oc} partially drops on the other cell. Thus, in order to maximize the parallel tandem's efficiency it is important to equilibrate open circuit voltages of individual cells.

In addition, rigorous analysis of the parallel tandem's characteristic equation shows that for $R_s<R_{sh}$, the reduction in the parallel tandem's fill factor is much smaller than that in a series tandem. That is why the parallel tandem performs better than the series one, when both the I_{sc} and V_{oc} of the individual cells are substantially different (Figure 26d).

Conclusions on parallel versus in-series connections modeling

Series and parallel connections of solar cells were analyzed using the single-diode model. We demonstrated that to maximize the efficiency of series tandems it is important not only to match the short circuit currents but also the fill factors of the individual cells. In parallel tandems, the open circuit voltages should be equilibrated. In general, if two solar cells are not balanced, then the parallel connection is preferable due to smaller losses in the fill factor. We also showed that the direct connection of two unbalanced solar cells can result in overall lower efficiency when one of the cells is much less efficient than the other.

Tandems of solar cells: comparison of model with experiments with different PVs

The efficiency of two identical solar cells connected in a tandem will be twice as large as the efficiency of one solar cell. However, in the case of two different solar cells connected together, certain conditions should be fulfilled to maximize the efficiency. Obviously, the tandem efficiency is limited by the sum of individual cells' efficiencies. In the present work we analyze the parameters of individual solar cells required for maximizing the tandem efficiency. We have analyzed the results of several different experimental tandems made of imbalanced dissimilar sub-cells: 1. PPV-CNT-OPV (non inverted, low efficiency), 2. PPV-CNT-OPV with inverted PPV by inorganic selective ZnO inversion layers, 3. Non-monolithic DSC-OPV with in-series and parallel connections, 4. Small molecule OPV-CNT-OPV tandems.

To improve the performance of parallel tandems, one should keep in mind that one of subcells should be inverted. It means that ITO on a transparent top cell parallel tandem should play a role of a cathode (not a usual anode). For this it can be inverted by ZnO nanoparticles layer, and the result of such tandems are shown below in Section of Inverted cells. Dye synthesized solar cells are also excitonic PVs like OPV, but due to electrolyte involvement cannot be connected monolithically into tandems. We demonstrate here the non-monolithic connection results, showing that high efficiency can be achieved in correspondence with our model of parallel tandems.

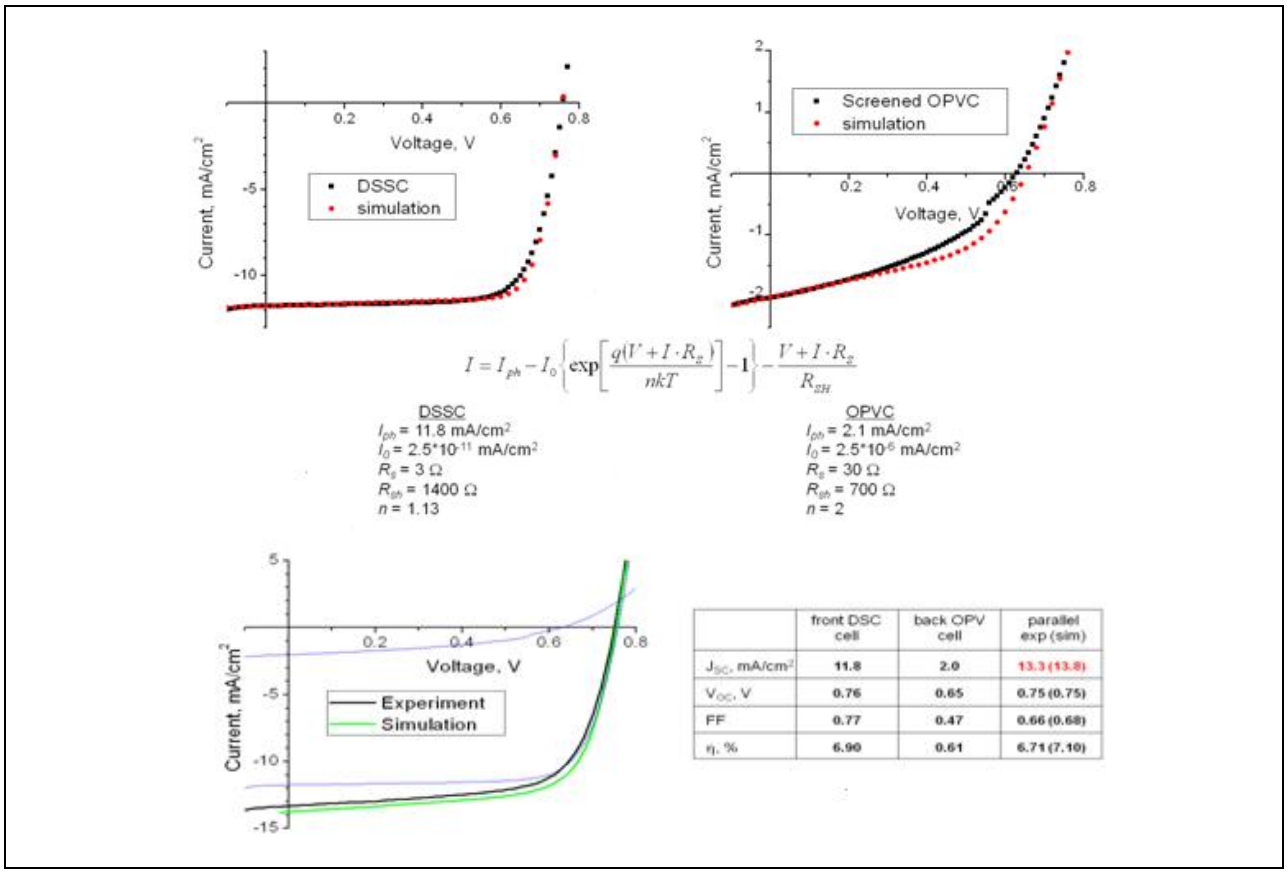

Figure 27. Comparison of model with experiments with different PVs for non-monolithic DSC-OPV tandem the overall efficiency of 6.71 % was demonstrated, which is higher than efficiency of each sub-cell

Figure 27 shows good fitting of experimental results on DSSC-OPV parallel tandem in which the bad-good situation is observed, regarding the low FF in OPV and much better FF in DSSC, so the resulting Voc is not losing much value, while current is increased.

Summary of the possible situations for Voc for parallel tandems made of different types of sub-cells have been here proven from experimental observations in correspondence with predictions of theoretical model. The voltage shift in the parallel tandem (blue line), depending on the unbalanced voltages and FF quality (bad: linear or good: box type) in subcells. If the sub-cell with lower Voc has a bad FF, but the cell with higher Voc has a good FF, then it doesn't decrease the resulting Voc, (second line bellow). On the contrary if the FF of a lower Voc sub cell is good, then Voc drops more (last line below).

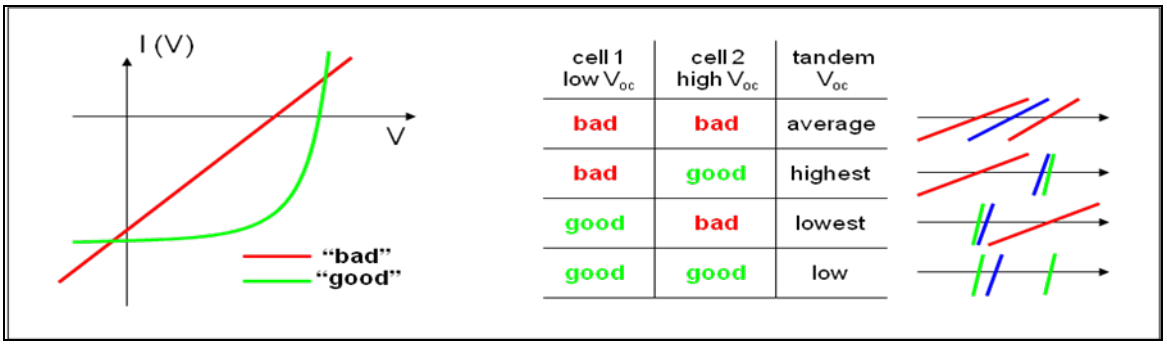

Figure 28. Summary of the possible situations for Voc for parallel tandems

Doping of Carbon Nanotubes Common electrode

To have high performance of any parallel tandem the common electrode interlayer should have low sheet resistance and properly adjusted work function: low w.f. for common cathode, and high w.f. for a common anode, which can be achieved by doping CNTs.

We require high conductivity and transparency from our nanotubes to achieve the objective of high efficiency OPV. Post-fabrication doping of the carbon nanotubes (CNT) provides the best method to improve the conductivity of carbon nanotubes without decreasing transparency. Doping also improves the electrical contact with the active area of the solar cell through improved electrode work function and doped hole transport layers. There are four methods of note: doping with an acid, doping by formation of an ionic double layer, doping by a self-assembled monolayer and doping by a strong electron acceptor or donor. Our work has focused on the latter two.

Double layer charging shows a strong, tunable modulation of work function and conductivity. It is possible to increase or decrease the work function of nanotubes. If large ions are used, the process is fairly stable. However as this is a wet process, there are limitations on usage in a center electrode or top electrode configurations.

Doping with a Self Assembled Monolayer

Doping via growth of a self assembled monolayer of dipolar molecules allows for strong doping in a dry (vapor-based) process. We have found that fluoro-alkyl-trichlorosilanes (FTS) produce a strong doping effect in single walls with an improvement in conductivity of up to four times and a smaller, but notable improvement in multiwalled carbon nanotubes of about 50% (Figure 29a).

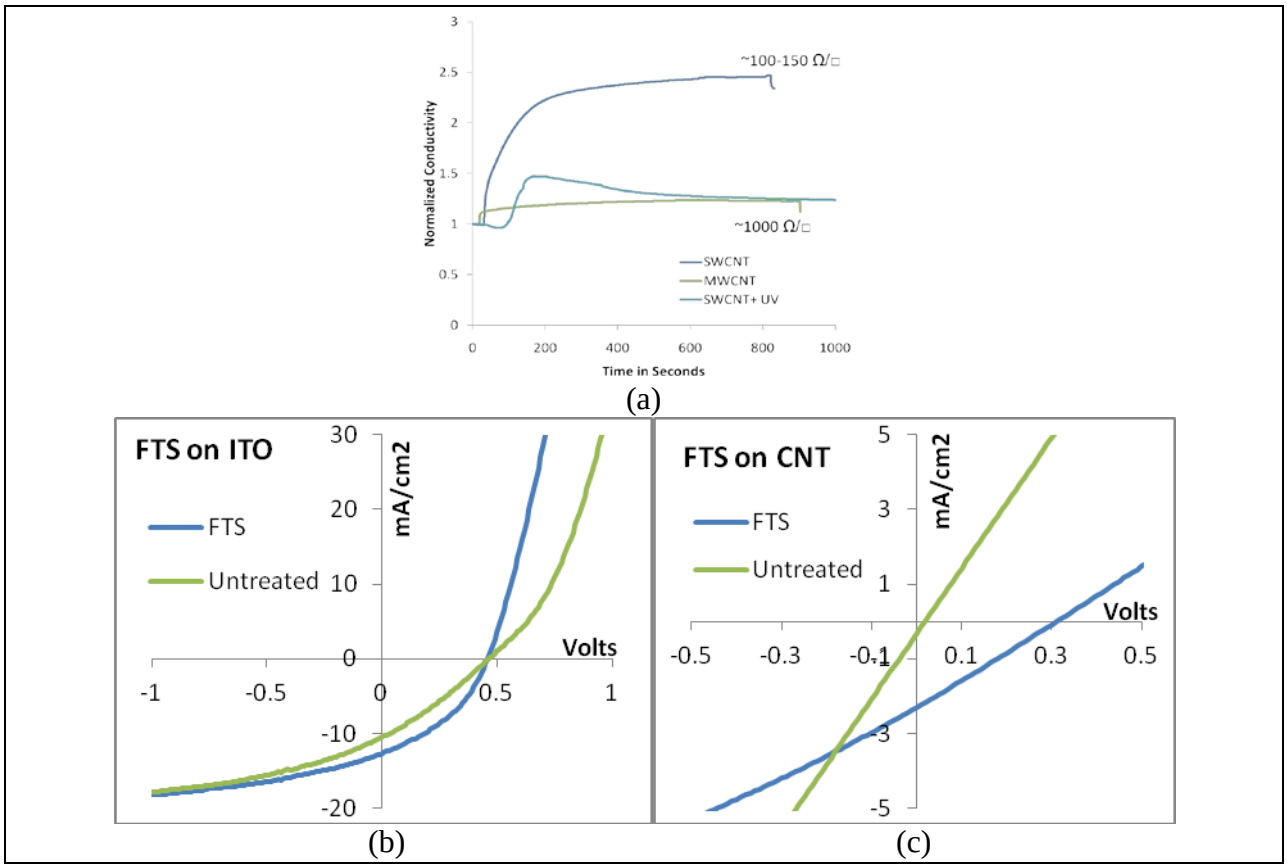

Figure 29. a) Displays the change in conductivity of carbon nanotubes exposed to a vapor of FTS, b) CuPC: C60 devices with ITO anodes exposed to FTS vapor prior to deposition of the active area, c) CuPC: C60 devices with CNT anodes exposed to FTS vapor prior to deposition of the active area.

Table 7. Device Parameters from Figures 29b and 29c

Solar Cells with FTS doped CNT		**Uoc (V)**	**Isc** $\left(\frac{mA}{cm^2}\right)$	**FF**	**Eff (%)**
ITO	FTS	0.46	12.64	0.39	2.24
	Untreated	0.46	10.50	0.29	1.42
CNT	FTS	0.31	2.30	0.25	0.18
	Untreated	0.02	0.32	0.24	0.00

Solar cells with CNT electrodes doped with this method also appears to improve the hole extraction properties. Notably we have observed that this method dramatically improves the filling factor of small molecular solar cells with either ITO or CNT anodes. (Figure 29b and c) We have also demonstrated inverted structure OPV with carbon nanotubes top Anodes doped with FTS. These solar cells show an improvement in filling factor due to the increased conductivity of the CNT.

P-type Doping with a Strong Acceptor Molecule

The final method uses a strong electron acceptor or donor to dope carbon nanotubes. This method has the particular benefit of being able to dope hole transport layers or electron transport layers with the same dopant material. We have focused our work on the small organic acceptor molecule, F4-TCNQ (Tetrafluoro-tetracyanoquinodimethane). When deposited from vacuum or by solution processing, this material dopes carbon nanotubes to increase the conductivity up to four times, (Figure 30, Table 8) and also dopes hole transport materials such as MeO-TPD. We have found that the doping process is the strongest in the case of solution processing and is improved further with proper pre-processing and post processing annealing. We have also noted that that this P-Type dopant shows a large degree of air-stability.

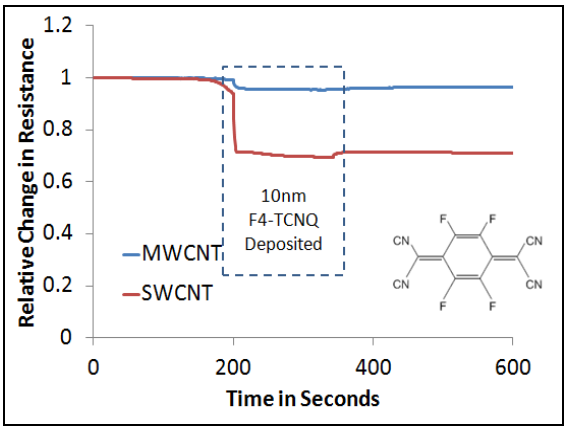

Figure 30. CNT doped with F4-TCNQ by a vacuum deposition method

Table 8. Change in resistance of a very thin layer of SWNT doped with F4-TCNQ dissolved in chloroform

Solution Processed Doping of SWNT		
	Normalized Resistance	**Sheet Resistance (KΩ/ϒ)**
Initial	1	8.95
Doped	0.35	3.16
Annealed	0.25	2.22

This dopant method could also be used on electron transport materials such as CNT Bphen or BCP with an electron donating n-type dopant such as acridene orange base or an alkali metal. We do not yet have an N-dopant material of the same quality as F4-TCNQ.

In solar cells, we have observed that F4-TCNQ improves the electrical contact between the anode and the active area of the solar cell. This is observed in the form of improved filling factors in ITO and CNT based devices. F4-TCNQ doping of the active area of polymeric solar cells has also been reported to improve the hole transport and reduce exciton recombination in literature [Felix Deschler, et al. PRL 107, 127402 (2011)].

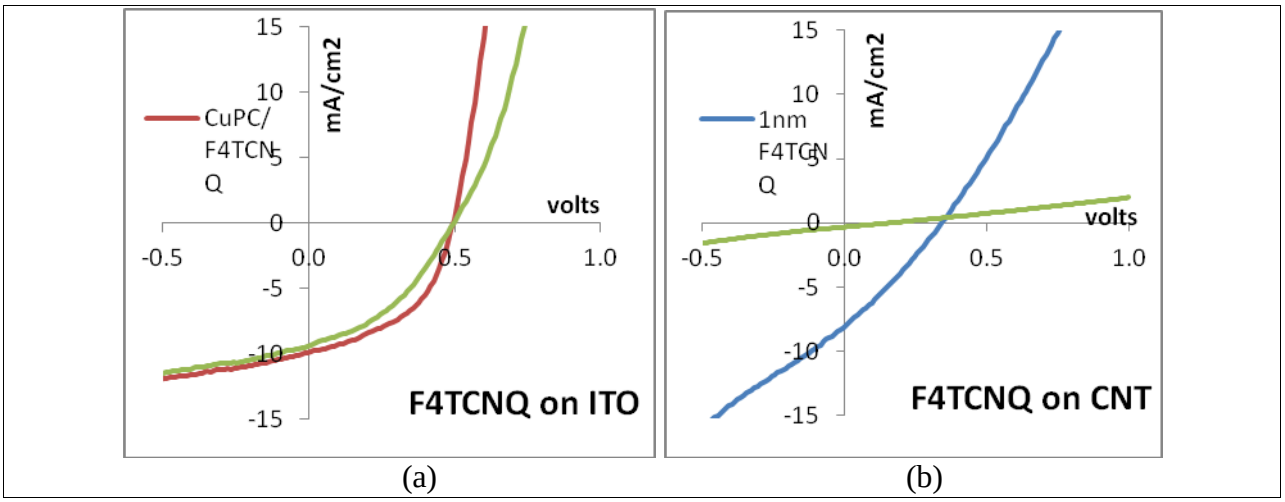

(a) (b)

Figure 31. a) CuPC: C60 devices with a thin layer of F4-TCNQ codeposited with CuPC onto the ITO anode prior to deposition of the active area, b) CuPC: C60 devices with a thin layer of F4-TCNQ deposited onto the CNT anode prior to deposition of the active area.

Table 9. Device parameters for devices depicted in Figures 25 and 26.

Solar Cells with FTS doped CNT		Uoc (V)	Isc $\left(\frac{mA}{cm^2}\right)$	FF	Eff (%)
ITO	FTS	0.5	9.82	0.48	2.33
	Untreated	0.5	9.36	0.39	1.82
CNT	FTS	0.35	7.96	0.28	0.77
	Untreated	0.16	0.31	0.26	0.01

These results still show considerable room for improvement. Introduction of a hole transport layer would improve the Voc and filling factor of these solar cells. Doping of carbon nanotube interlayers and hole transport layers in a parallel tandem organic solar cell has also been demonstrated. These devices are described later in the document.

High Performance Single OPVs for Back Cells of Tandem

Our work focused on testing new high efficiency materials in single cells. Typical OPV cells with an ITO (15 Ω/sq) cathode were fabricated. An appropriate pattern ITO was fabricated using photolithography and HCl etching. Substrates were cleaned by sonication in several organic solutions. For a photoactive layer, we used a bulk heterojunction structure with typical poly(3-hexylthiophene) (P3HT) and [6,6]-phenyl-C61 butyric acid methyl ester (PCBM). We also investigated other commercially available low band gap polymers in single bulk heterojunction cells with acceptor PCBM and PC71BM. In case of P3HT:PCBM cells a weight ratio of 1:1 (chlorobenzene solution, 3 wt% for P3HT) was spin coated (700 rpm, 40 s) on the substrates. The thickness of the P3HT:PCBM layer was approximately 150–200 nm. Before the photoactive layer, a poly(3,4-ethylenedioxythiophene):poly(4-styrenesulfonate) (PEDOT:PSS) layer was spin coated at 3000 rpm. The PEDOT:PSS layer plays two roles for this OPV cell. It acts as an electron blocking layer and improves the lateral conductivity in the case of the MWCNT sheet anode. Annealing processes were then performed on the cell in a glove box under

N_2 atmosphere. This annealing process crystallizes the P3HT:PCBM layer and removes water from the PEDOT:PSS layers. The current-density–voltage (*J–V*) characteristics of the samples were measured in the glove box using a source measure unit (Keithley 236). For the photo *J–V* characteristics, a solar simulator (Model 91160, Newport-Oriel Instruments) was used as a light source. The light parameter used was 100 mW, AM 1.5 (AM: air mass) solar illumination.

Commercially available low band gap polymers such as poly((4,8-bis(octyloxy)benzo(1,2-b:4,5-b')dithiophene-2,6-diyl)(2-((dodecyloxy)carbonyl)thieno(3,4-b)thiophenediyl)) (PTB1)and dithiene [3,2- b:2′,3′-d]silole)-2,6-diyl-alt-(4,7-bis(2-thienyl)-2,1,3-benzothiadiazole)-5,5′-diyl] (Si-PCPDTBT) were purchased and single bulk heterojunction cells with acceptor PCBM or PC71BM were fabricated. The typical corresponding efficiencies the cells were 3.7%. In addition, in collaboration with Prof. Ferraris group at UT Dallas tested a new donor-acceptor copolymer PBDTDTBT-EH with efficiency as high as 4%.

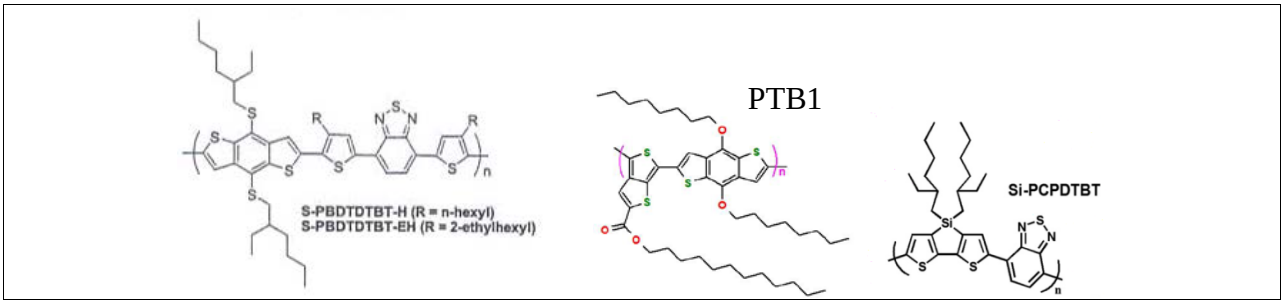

Figure 32. Small band gap material structures

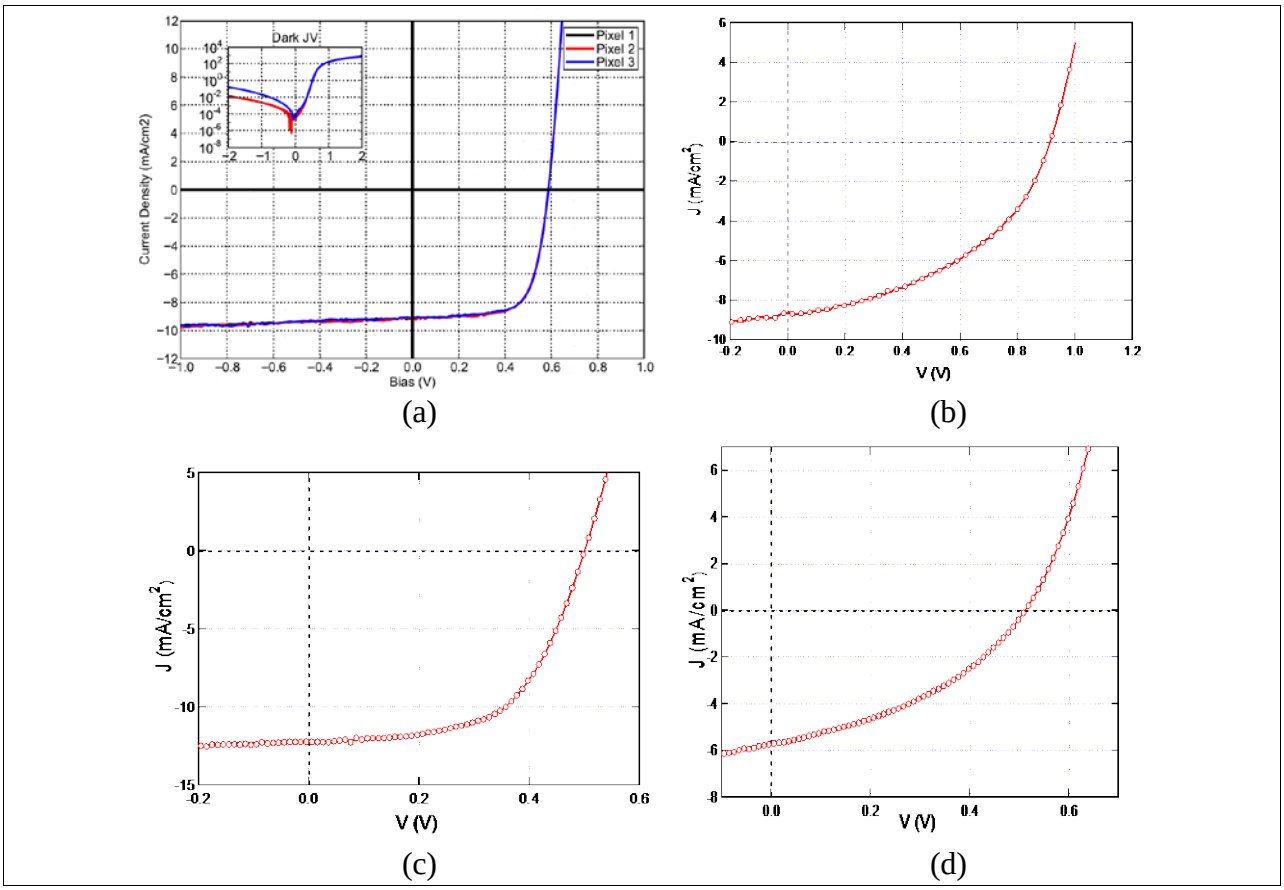

Figure 33. a) P3HT:PCBM device characteristics, b) PBDTDTBT-EH:PCBM device characteristics, c) PTB1:P71CBM device characteristics, d) Si-PCPDTBT:PCBM device characteristics.

Table 10. Summary of polymeric devices performance

Active layer	Voc	Isc	FF	Efficiency
	(V)	(mA/cm^2)		(%)
P3HT:PCBM	0.59	9.18	0.7	3.72
PBDTDTBT-EH :PCBM	0.91	8.64	0.49	3.86
PTB1:P71CBM	0.5	12.3	0.57	3.56
Si-PCPDTBT:PCBM	0.51	5.77	0.38	1.14

Furthermore, small molecule materials were also tested in single cells but produced lower efficiencies compared to polymeric cells. We fabricated small molecule organic solar cell (OSC) devices. Preliminary devices are built with copper phthalocyanine (CuPc) fullerene (C60) active layer on ITO with efficiency higher than 2%. We are currently investigating additional materials for OSC cells. We recently reported devices fabricated by co-deposition of 2-((7-(5-(dip-tolylamino)thiophen-2-yl)benzo[c][1,2,5]thiadiazol-4-yl)methylene) malononitrile (DTDCTB) or 2-((Z)-2-((E)-2-(1,1-dimethyl-5,6-dihydro-1Hpyrrolo[3,2,1-ij]quinolin-2(4H)-ylidene)ethylidene)-3-ox (HB194) with C60. Figure 34 shows the device characteristics of small molecule device with HB194. We observed efficiency of 2.52% and open circuit voltage of Voc=0.81V (Isc = 7.92mA/cm^2 and FF = 0.39). The lower efficiency is attributed to low quality

of material commercially available. We are in the process of purifying the materials for increased performance.

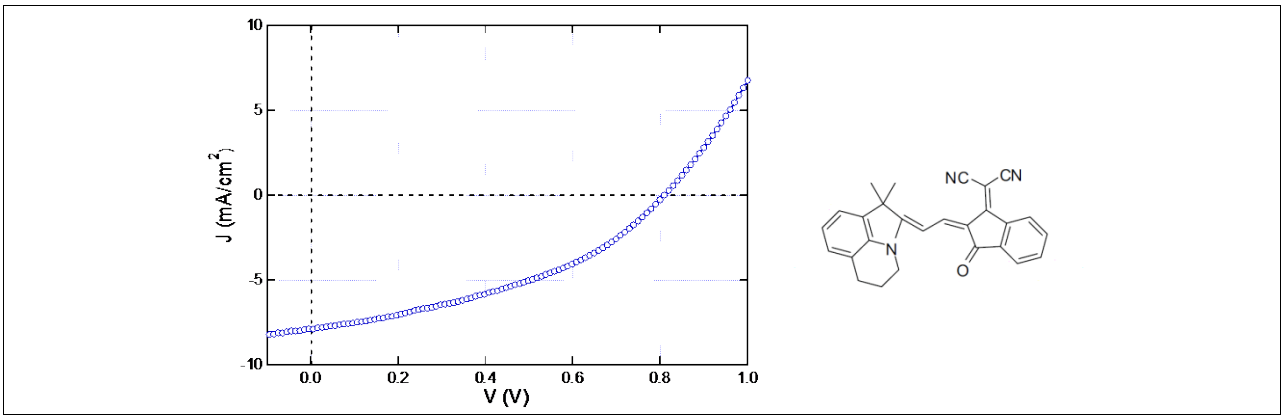

Figure 34. HB194:C60 device characteristics

Application of additives in P3HT:PCBM bulk heterojunction cells

Many low band-gap polymers are sensitive and degrade with active layer annealing. This can cause problems when P3HT:PCBM is used as the complimentary active layer. In order to address this problem, the P3HT:PCBM must be fabricated in such a way that high performance can be achieved with minimal to no heating. One such method is the 'slow growth' or 'vapor annealing' methods, where a high boiling point (low vapor pressure) solvent is used and the films are allowed to dry over a long (>30 minutes) period while exposed to the vapors of this solvent. This method results in high performance devices (>3%) but has several pitfalls. During this extended drying period the solvent can bleed through the previous layers and destroy the front cell's active layer. Additionally, the slow growth method is difficult to reproduce and small defects in the films can lead to large scale aggregations, causing failed devices. As an alternative to these techniques, small volumes of special solvents can be blended together and used as the solvent for casting active layers resulting in near optimal morphologies without any annealing. The additive solvent must have a high boiling temperature, low vapor pressure, and be able to selectively dissolve the fullerene molecule while being miscible in the host solvent. One such solvent combination tested with success is 1-Chloronapthalene (CN) and Chlorobenzene (CB) as additive and host solvents respectively. Several volume fractions were tested with P3HT:PCBM ranging from 0.5 vol% to 5 vol% CN in CB.

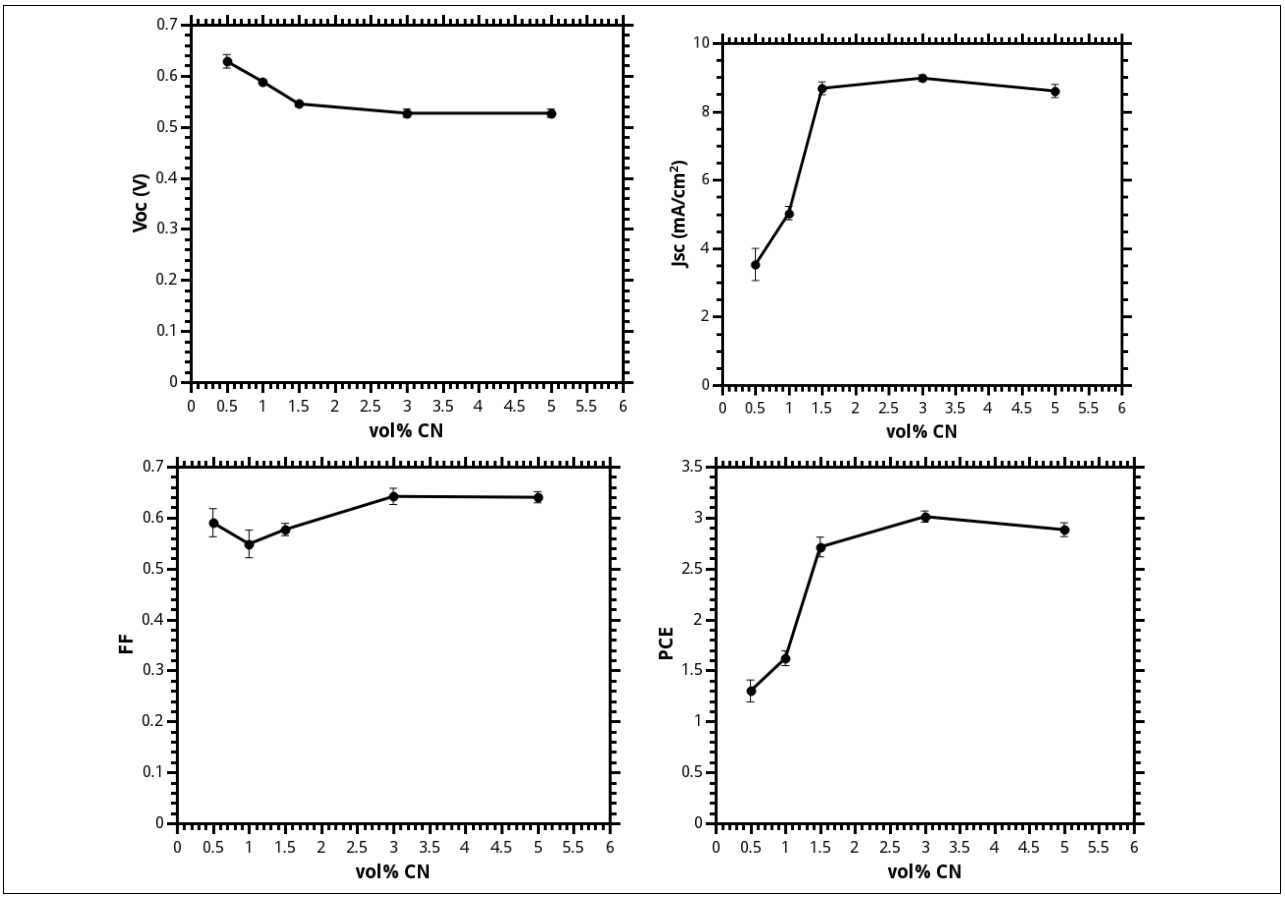

Figure 35. Device performance characteristics based on volume fraction of CN in CB.

Each device was fabricated on glass substrates with patterned ITO (15-20 Ohm/sq) which was cleaned sequentially in Detergent, DIW, Methanol, Hexane, Acetone, and Isopropyl Alcohol and exposed to UV-Ozone immediately before fabrication. A 30 nm thick layer of PEDOT:PSS was spin coated and annealed at 180C for 5 minutes. The active layer was spincoated from a 45mg/ml total concentration solution of 1:1 wt% P3HT:PCBM with varying volume fractions of 1-chloronapthalene in chlorobenzene. Following the active layer deposition, 10nm of calcium and 100nm of aluminum were deposited through a shadow mask and then measured.

After 1% vol% CN the open circuit voltage stabilizes to 0.52V, the decrease in Voc can be attributed to an improvement in morphology, this phenomenon is also observed in P3HT:PCBM during thermal annealing. As short circuit current improves over the 0.5-1.5% vol% CN range the the open circuit voltage drops just as is commonly observed with thermal annealing. A peak in filling factor as well as short circuit current when 3% vol% CN is used the device achieves the a power conversion efficiency of over 3%.

All these devices were fabricated with no thermal annealing of the active layer and were able to achieve high power conversion efficiencies. Furthermore, these devices were fabricated using a fast drying solvent that will have a reduced chance of bleeding through the previous layers when used in a tandem structure. This can allow P3HT:PCBM to be used as a back cell where the front cell cannot be thermally annealed.

Inverted OPVs for back unit of tandem cells

Our work focused on optimization of the inverted front P3HT cell fabrication process. This included studies on blends of zinc oxide nanoparticles, active layer annealing and composition as well as various hole transport layers. Through careful fabrication steps and optimizations, a highly efficient P3HT based inverted cell was fabricated. A layer of highly transparent and trap-free zinc oxide nanoparticles dispersed in butanol was spincoated on patterned ITO coated glass. Rather than using PCBM as the acceptor molecule bisPCBM was used instead. With an additional side-group the LUMO level is shifted from -3.9eV (PCBM LUMO level) to -3.7eV. The open circuit voltage for an OPV is given by eVoc = HOMO(Donor) – LUMO(Acceptor) – Δ , where Δ represent the energy losses due to exciton separation and higher order processes. From this relation between HOMO(Donor) and LUMO(Acceptor) a shift in LUMO(Acceptor) of 0.2eV from PCBM to bisPCBM should result in a 0.2V increase in a devices open circuit voltage.

One challenge faced as a result of this change was a decrease in filling factor and current generation. A drop in filling factor can be attributed to poor morphology, as the molecule is larger and less mobile within the donor:acceptor matrix. Current generation was also affected through the inclusion of bisPCBM because the additional side chain can hinder exciton separation at the donor/acceptor interface. By using the inverted structure and zinc oxide nanoparticles as the electron transport layer the active layer could be thermally annealed at much higher temperatures and for longer durations than possible for other charge transport layers. In order to address the poor morphology due to slow movement of the fullerene we needed to heat the device stack at 190C for 30minutes. This appears to be higher than the glass transition temperature for our P3HT because the layer forms a gel and can even cause the top metallic electrode to crumple and delaminate. However, when the polymer is heated to such a high temperature and becomes soft the fullerene molecules become free to rearrange into a more favorable morphology, this results in improved currents and fill factors. Due to fluid nature of the active layer at this temperature it is critical to anneal the device after active layer deposition and prior to hole transport layer deposition and allow ample time for the layer to cool. After annealing at 190C for 30minutes and allowing the ITO/ZnO-NP/P3HT:bisPCBM layer to cool a 20nm layer of MoO3 hole transport material was blanket deposited followed by deposition of aluminum through a shadow mask. The resulting device shows an improved Voc of 0.76V as is predicted by the shift in the acceptors LUMO level, a short circuit current of 10.22mA/cm2, a fill factor of 0.53 resulting in a power conversion efficiency of 4.10%. The current is over 10mA/cm2 due to proper morphology as a result of optimal annealing and because the ZnO-NP layer is much more transparent than the optimal PEDOT:PSS layer in regular structured device configurations over P3HT's absorption range.

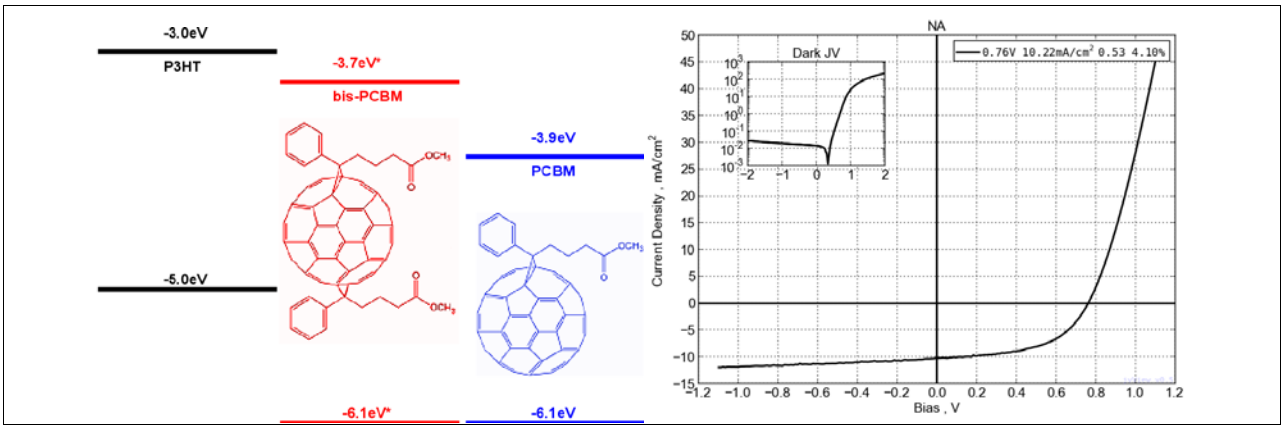

Figure 36. a) Comparison of energy levels of bis-PCBm and PCBM, b) devices characteristics of invertedP3HT cell 4.1%

An additional polymer that was investigated in inverted configuration was the PBDTDTBT-EH. The device structures was ITO/Cs_2CO_3/PBDTDTBT-EH:PCBM/MoO_3/Ag . The resulting device shows an Voc of 0.9V, a short circuit current of 6.32mA/cm2, a fill factor of 0.43 resulting in a power conversion efficiency of 2.45%. Figure 41 illustrate a typical JV characteristic.

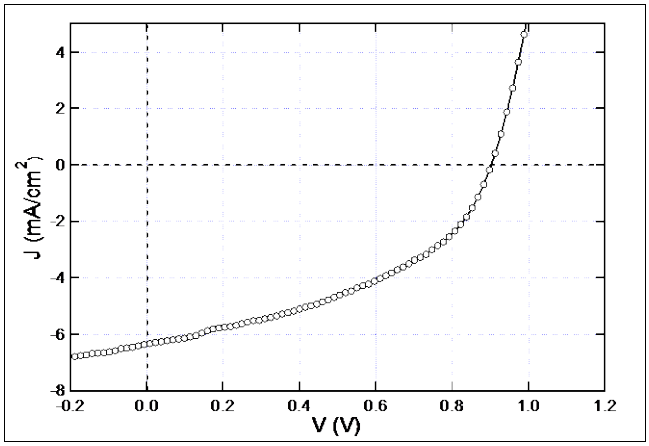

Figure 37. Inverted PBDTDTBT-EH:PCBM OPV cell

Inverted cells with CNT sheets

Nanotubes may also be laminated onto the top of a solar cell, which allows us to create semi-transparent solar cells. An inverted P3HT:PCBM solar cell was fabricated in the same manner as the previous section. A freestanding MWCNT or SWNT sheet is placed onto the P3HT:PCBM layer. Compared to a sheet of ITO, the MWCNT sheet typically show higher sheet resistance and a slightly higher work function (~5.2 eV). The MWCNT sheet was then densified using surface-tension effects, ethanol is applied to the sheet on top of the solar cell. The rapid evaporation of the ethanol causes compression of the MWCNT sheet by surface-tension forces leading to its densification. After densification, the MWCNT sheet was approximately 50–100 nm thick. In this configuration, less transparent but more conductive nanotubes can be used which allows us to directly observe the effect of nanotube resistance on device performance. In Table 11 the label 'x min' refers to the length of time the nanotubes were gathered from the CVD process and is inversely proportional to the conductivity of the tubes.

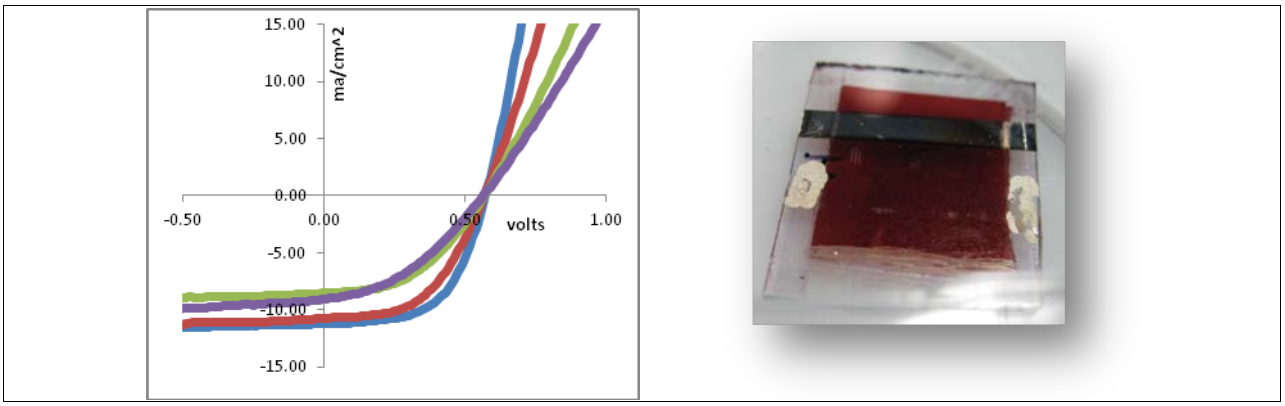

Figure 38. Inverted cell characteristics with CNT anodes and photograph of actual device

Table 11. Device performance of inverted cells with various types of CNTs

Device	V_{oc} (V)	J_{sc} (mA/cm^2)	FF	PCE (%)
Al	0.57	11.25	0.57	3.68
18 min	0.57	10.76	0.51	3.12
12 min	0.57	8.53	0.45	2.20
8 min	0.57	9.10	0.38	1.99

We successfully fabricated semitransparent organic solar cell devices by combining two materials that have high optical transparency and electrical conductivity, such as ITO and carbon nanotube (CNT) sheets. In the past these two materials could not be used as anode/cathode paired materials because they have nearly the same work functions (~ -4.8eV), however in this new architecture this is possible as well as maintaining high performance. The device performance can be further improved by enhancing CNT sheet performance.

Series small molecule tandem OPV

In addition to the parallel tandem solar cells, we are investigating tandem cells in series configuration. The in-series tandem OSCs were fabricated with combinations of units with active layers consisted of copper phthalocyanine (CuPc): fullerene (C60) and zinc phthalocyanine (CuPc): fullerene (C60). A patterned ITO layer was used as the anode, while a thin layer of Ag was the interlayer between top and botton cells. Typical device characteristics are shown in Figure 39 bellow. Typical high open circuit voltage was observed (V_{oc}=0.79V) but low short circuit current of just I_{sc} = 4.45mA/cm^2 due to shadowing of the back cell and low photocurrent generation that limited the tandem cell operation to efficiency of 1.43%.

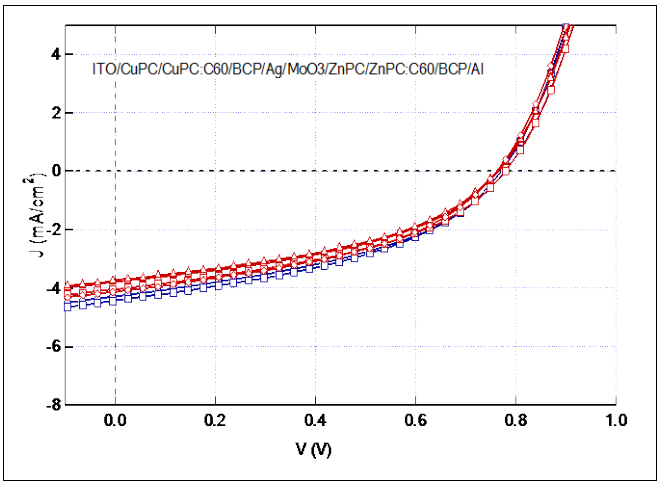

Figure 39. In series tandem OSC with CuPc:C60 sub cells

Parallel small molecule tandem OPV

Copper phthalocyanine (CuPc): fullerene (C60) cells were also used to fabricate a parallel tandem cell. The device structure was the following :ITO/CuPC/CuPc:C60/C60/BCP/Ag/BCP/C60/C60:CuPc/CuPc/ MoO_3/Ag .IV characteristics and performance of these cell is shown in Figure 40 and Table 12. The interlayer of the parallel tandem described here is also consisted by a thin layer of Ag. The interlayer is a active electrode and can be addressed to measure each individual cell. Initial results show that the stacking of cells with same absorption layers is not recommended for high performance cell. The photocurrent of the back cell is decreased due to screening and overall performance may be slightly above a single cell. Additional screening of back cell is caused from semi-transparent interlayer. Improved performance cells require sub cells with complimentary absorption spectra.

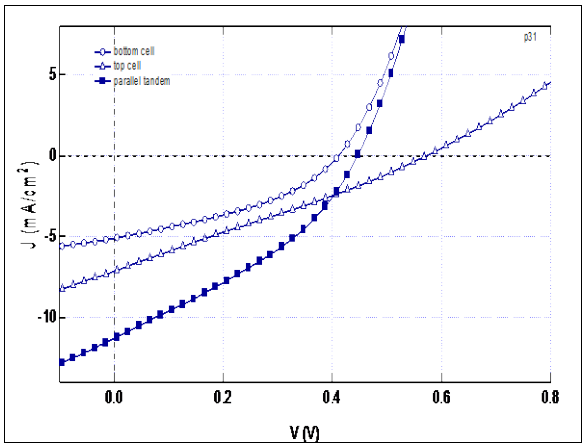

Figure 40. In parallel tandem OSC with CuPc:C60 sub cells.

Table 12. Performance of two CuPc:C60 subcells and of parallel tandem

	Uoc (V)	Isc (mA/cm2)	FF	Efficiency (%)
back cell	0.41	5.11	0.38	0.81
front cell	0.58	7.19	0.26	1.09
parallel tandem	0.45	11.35	0.34	1.75

Parallel Polymeric Tandem cells with inverted Ag Interlayers

Furthermore, we fabricated OSCs with polymer based cells. A typical device structure is the following:
ITO/ZnO/P3HT:PCBM/PEDOT:PSS/Ag/PEDOT:PSS/PBDTDTBT-EH:PCBM/LiF/Al. The front cell of the tandem had P3HT:PCBM active layer, the back cell at the same time had PBDTDBT-EH:PCBM low band gap polymer. The complimentary absorption of the two cell is can be an advantage for high performance. The tandem cell efficiency (Table 13) of approximately 2% is due to the screening of the Ag middle electrode. The Ag layer of about 12nm has low transparency and therefore the application on CNT sheets as interlayer is crucial for improved cells.

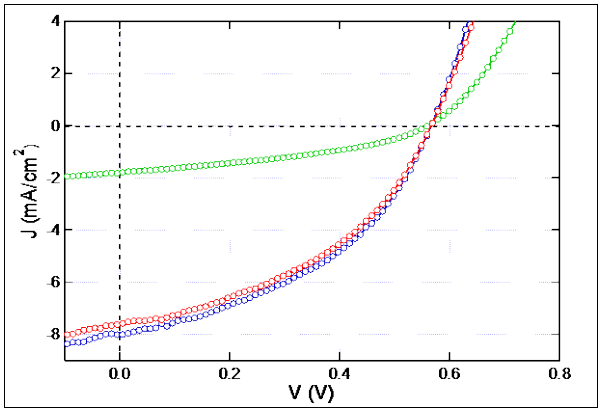

Figure 41. JV characteristics parallel tandem cell and individual sub cells.

Table 13. Device performance of parallel tandem cell and individual sub cells.

	Uoc (V)	**Isc (mA/cm^2)**	**FF**	**Eff (%)**
P3HT:PCBM front cell	0.56	7.71	0.42	1.83
PBDTDTBT-EH:PCBM back cell	0.55	1.82	0.37	0.38
Parallel Tandem cell	0.57	8.02	0.43	1.94

Non monolithic parallel tandem

The reported above efficiency is notably lower than expected due unoptimized structure, low conductivity of interlayer and shadowing of the back cell. To investigate and address the issue we fabricated non-monolithic cells. Such devices can be fabricated and electrically connected in different ways. The screening effect of each sub cell and of the interlayer can also be investigated. Results of P3HT and PTB1 cells used in parallel configuration are shown in Figure 42 and Table 14. The individual cell showed efficiency of 2.61% and 3.35% respectively when tested individually. The efficiency of the parallel tandem was as high as 5.9% and in the case of screening the back cell with the front (as would occur in monolithic structures) the efficiency was 4.92%.

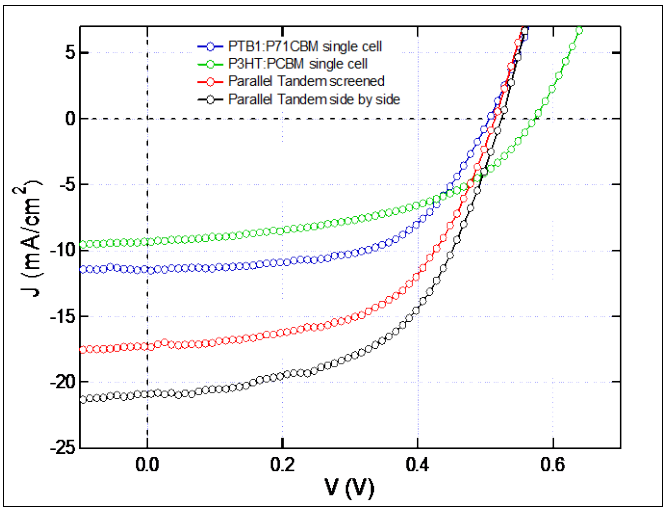

Figure 42. High efficiency polymeric parallel tandem cell

Table 14. Device performance of polymeric parallel tandem cell

	Uoc (V)	Isc (mA/cm^2)	FF	Efficiency (%)
PTB1:P71CBM cell	0.51	11.26	0.59	3.35
P3HT:PCBM cell	0.57	9.26	0.49	2.61
Parallel Tandem screened	0.51	17.24	0.56	4.92
Parallel Tandem side by side	0.52	21.10	0.54	5.92

Non monolithic Hybrid parallel tandem

Results of parallel tandem cells with a combination of polymer and a small molecule materials are reported here. The OPVs of P3HT and DTDCTB small molecule cell used in parallel configuration are shown in Figure 39 and Table 14. The individual cell showed efficiency of 2.61% and 1.49% respectively when tested individually. The efficiency of the parallel tandem was as high as 3.95% and in the case of screening the back cell with the front (as would occur in monolithic structures) the efficiency was 3.35%.

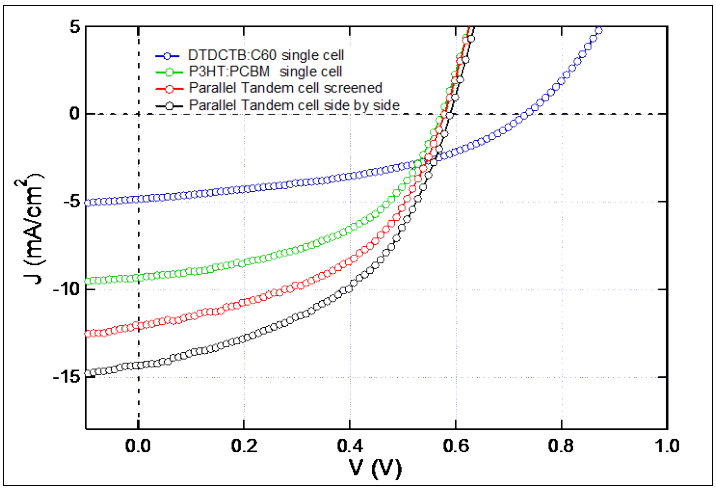

Figure 43. High efficiency hybrid parallel tandem cell.

Table 15. Device performance of hybrid parallel tandem cell.

	Uoc (V)	Isc (mA/cm^2)	FF	Efficiency (%)
DTDCTB:C60 single cell	0.73	4.87	0.42	1.49
P3HT:PCBM single cell	0.57	9.26	0.49	2.61
Parallel Tandem screened	0.58	11.88	0.49	3.35
Parallel Tandem side by side	0.59	14.25	0.47	3.95

Parallel Tandem Cells with undoped CNT interlayer

We have demonstrated parallel tandem OPV devices with CNT interlayer. The active layers of top and bottom sub-cells of the tandem is consisted of small molecule CuPc:C60 and P3HT:PCBM blend respectively. The demonstrated parallel tandems have unoptimized efficiency of 2.25%. But importantly, a photocurrent enhancement is demonstrated in the tandem device. Further tandem device optimization is needed for high efficiency cells.

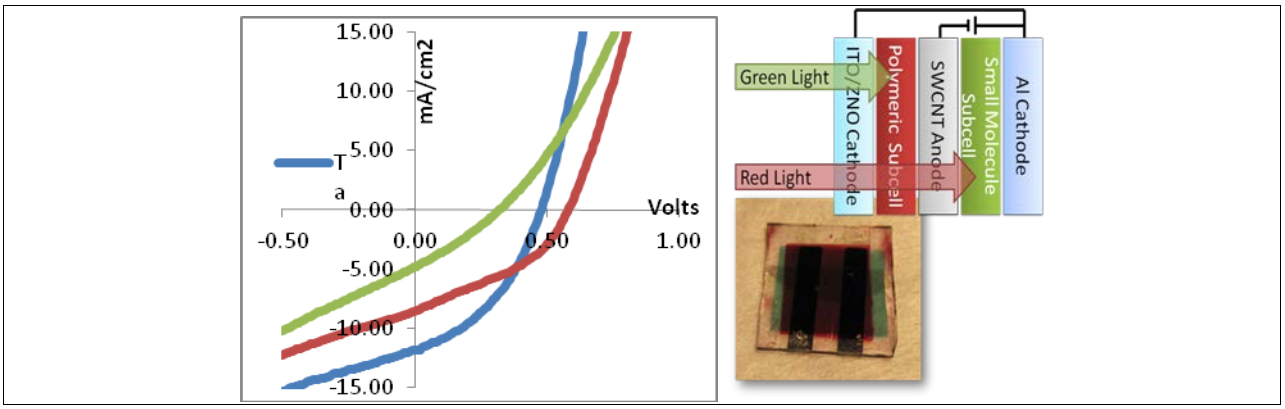

Figure 44. Parallel tandem cell with CNT interlayer

Table 16. Device performance of parallel tandem cell with CNT interlayer

Device	V_{oc} (V)	J_{sc} (mA/cm^2)	FF	PCE (%)
Tandem	0.48	11.83	0.4	2.26
P3HT Subcell	0.59	9.01	0.38	1.89
CuPC Subcell	0.32	4.86	0.29	0.45

Additional effort to increase the performance of tandem OPVs showed that doping of donor and acceptor layers in the tandem further increased the efficiency significantly. We are in progress of purchasing high performance n-type dopants for Novaled, Germany. P-type dopants as F4TCNQ can be used for doping of HTL layer. We have already reported above p-type F4TCNQ doping of CNT sheets. The n and p type dopants will be used in p-i-n type OPVs that have been reported to show significantly improved performance.

Kim et al. has demonstrated inverted small molecule cells with laminated CNT sheets as top cathode [Y.H. Kim, C. Sachsea, A.A. Zakhidov, J. Meiss, A.A. Zakhidov, L. Müller-Meskampa, K. Leo, Organic Electronics Volume 13, Issue 11, November 2012, Pages 2422–2428 (2012)]. Figure 41 illustrates the reported p-i-n layer stack of inverted stack. N-type dopants were introduced in electron transport layer (C60) during the deposition by co-evaporation. The use of dopants enhances the performance of OPV cells and in addition enables CNT sheet application as anodes in single or tandem structures.

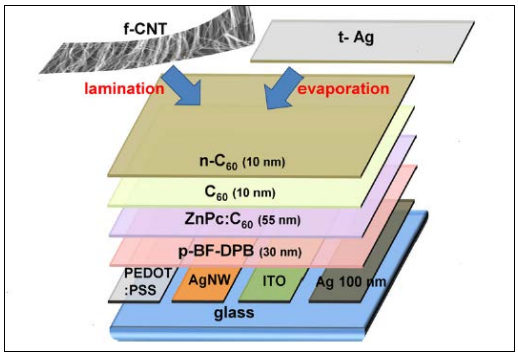

Figure 45. Example of p-i-n stack of OPV cell with various electrodes, including CNT sheet as top electrode [Kim et. al, Org. Elec. 13, 11, 2422 (2012)]

Quantum Efficiency / IPCE Measurement System

Light is composed of photons—or packets of energy—that range in wavelength. When light strikes the surface of a solar cell, some photons are reflected and do not enter the cell. Other photons pass through the active layer. Of these, some are absorbed, but only have enough energy to generate heat, and some have enough energy to separate electrons from their atomic bonds to produce charge carriers—negative electrons and positive holes. Quantum efficiency (QE) is the ratio of the number of charge carriers collected by a photovoltaic (PV) cell to the number of photons—or packets of light—of a given energy shining on the solar cell. Quantum efficiency therefore relates to the response of a solar cell to the various wavelengths in the spectrum of light shining on the cell.

Two types of quantum efficiency of a solar cell are often considered. External QE includes the effect of optical losses such as transmission through the cell and reflection of light away for the cell. It gives detailed data on how efficiently a solar cell converts light into current at various wavelengths. Internal QE refers to the efficiency with which light not transmitted through or reflected away from the cell can generate charge carriers—specifically electrons and holes—that can generate current. By measuring the transmission and reflection of a solar device, the external QE curve can be corrected to obtain the internal QE curve.

The detailed performance information provided by a QE measurement is commonly used by researchers to document and answer questions about:

- Device performance
- Material purity
- Material selection
- Device design
- Process steps

Multi-junction devices, such as tandem solar cells (SCs), enable harvesting of wider regions of the solar radiation spectrum thereby leading to increased overall efficiencies. A general advantage of the tandem structure is its multi-absorption ranges. The wavelength distribution of the solar spectrum has a wide range, covering the UV to IR. Although there are many kinds of inorganic and organic materials that are used as photoactive layers of PV cells, the individual materials have specific and narrow absorption ranges. As an example, Figure 46 illustrates the absorption ranges of three individual materials. Hence, only a part of the solar spectrum is effective in generating the photo carriers in a single junction PV cell. By using materials with a different absorption range for each PV cell of the tandem or multijunction structure, the total absorption range of the tandem OPV cell can approach the superposition of the each PV material.

Our work focused on testing new, high efficiency materials as single cells and tandem cells. Commercially available low band gap polymers were purchased and combined with conventional and inverted P3HT:PCBM cells in parallel tandem configurations. Hybrid cells consisting of polymeric P3HT and small molecule cells were also tested. Higher efficiencies can be obtained by selecting the materials to be used as active layers in tandem configurations. Figure 46 illustrates the absorption different bands of sunlight through each individual cell of an inorganic tandem.

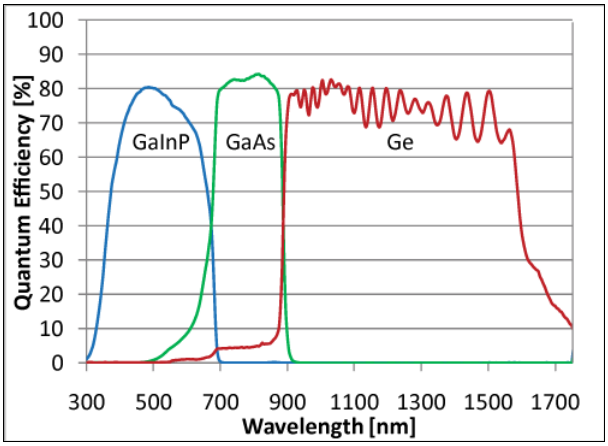

Figure 46. Example of inorganic material with complimentary absorption range

Figure 47 also shows absorption spectra of common organic materials used. The quantum efficiency measurements are particularly important for triple tandem cells. We are expecting delivery of a new Quantum Efficiency Measurement System by PV Measurements.

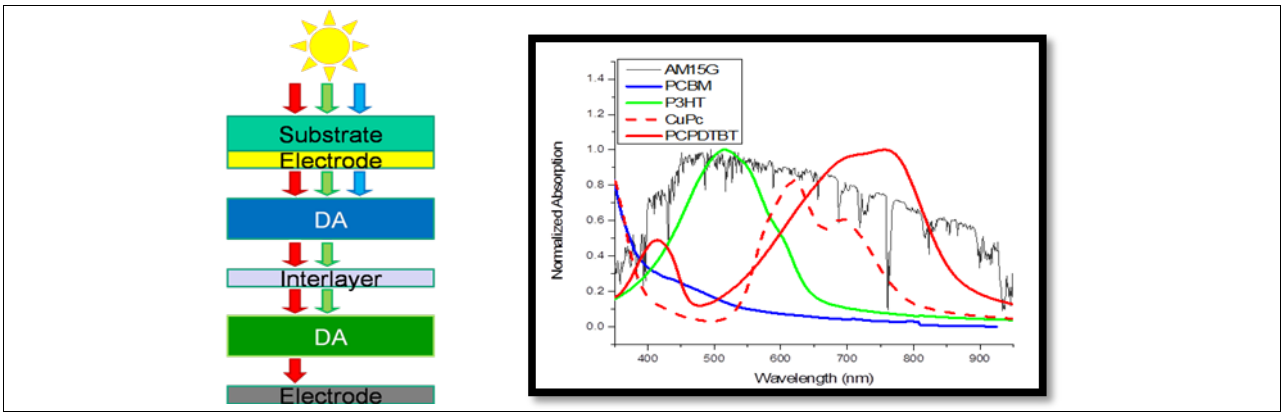

Figure 47. Absorption mechanism in tandem OPVs and absorption spectra of common organic materials

PV Measurements, Inc. located in Boulder, Colorado, is the process of delivering a QEX10 Quantum Efficiency / Spectral Response (SR)/ Incident Photon to Current Conversion Efficiency (IPCE) Measurement System (Figure 48). It uses a xenon arc lamp source, monochromator, filters and reflective optics to provide stable monochromatic light to a photovoltaic test device. A broadband bias light also illuminates the test device to simulate end-use conditions. The system uses a detection circuit designed to maximize measurement speed and accuracy in solar cell research.

Figure 48. QEX10 Quantum Efficiency / Spectral Response (SR)/ Incident Photon to Current Conversion Efficiency (IPCE) Measurement System

The QEX10 includes a broad spectrum white bias light that can be used to bias most devices and provide almost any desired bias spectrum with the correct filtering. Using two or three bias lights, it is easier to get the correct bias light level for each junction. The correct bias lighting, along with the correct voltage bias can make accurate measurements of each of the individual junctions in a multi-junction measurements. Figure 49 illustrates triple junction tandem cells in parallel configurations materials with complimentary absorption spectra.

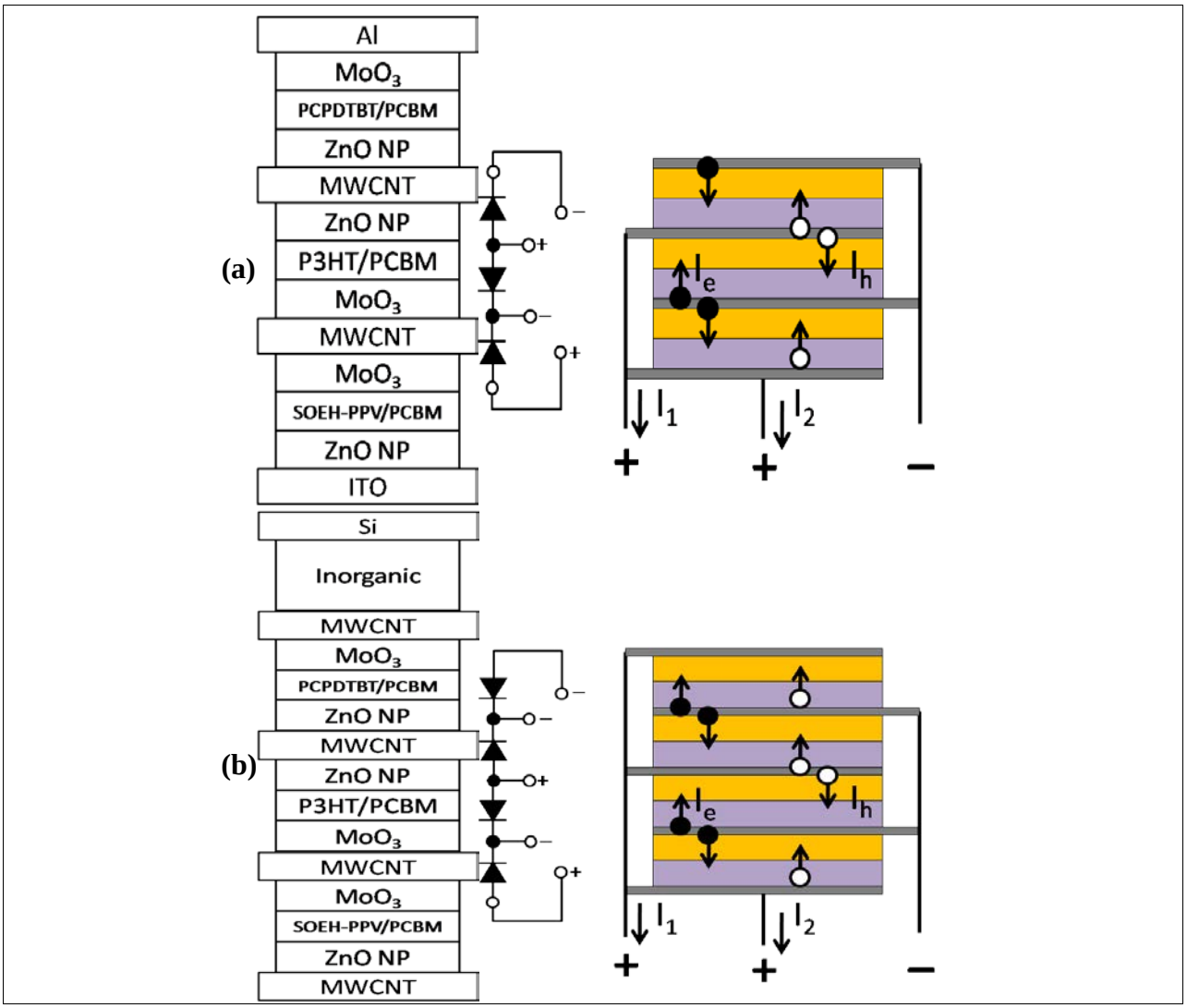

Figure 49. a) triple junction tandem cells in parallel configuration, b) concept of multi-parallel tandem with top inorganic cell

Nanoimprinted Polymer Solar Cell for tandem and triple junction OPV

Among the various organic photovoltaic devices, the conjugated polymer/fullerene approach has drawn the most research interest. The performance of these types of solar cells is greatly determined by the nanoscale morphology of the two components (donor/acceptor) and the molecular orientation/crystallinity in the photoactive layer. A vertically bicontinuous and interdigitized heterojunction between donor and acceptor has been regarded as one of the ideal structures to enable both efficient charge separation and transport. Control of polymer orientation in the nanostructured heterojunction is also critical to improve the performance of polymer solar cells. Nanoimprint lithography has emerged as a new approach to simultaneously control both the heterojunction morphology and polymer chains in organic photovoltaics. Currently, in the area of nanoimprinted polymer solar cells, much progress has been achieved in the fabrication of nanostructured morphology, control of molecular orientation/crystallinity, deposition of acceptor materials, patterned electrodes, understanding of structure property correlations, and device performance.

Hybrid tandems of nanoimprinted P3HT/PCBM cell with one or multiple stacked cells (Figure 50) can be created by lamination of a CNT interlayer sheet coated with selective layer. Initial work has already been demonstrated by Yang et al. at the University of Texas at Dallas [Yi Yang, Kamil Mielczarek, Mukti Aryal, Anvar Zakhidov and Walter Hu, "Nanoimprinted Polymer Solar Cell" ACS Nano 6, 2877 (2012)] .

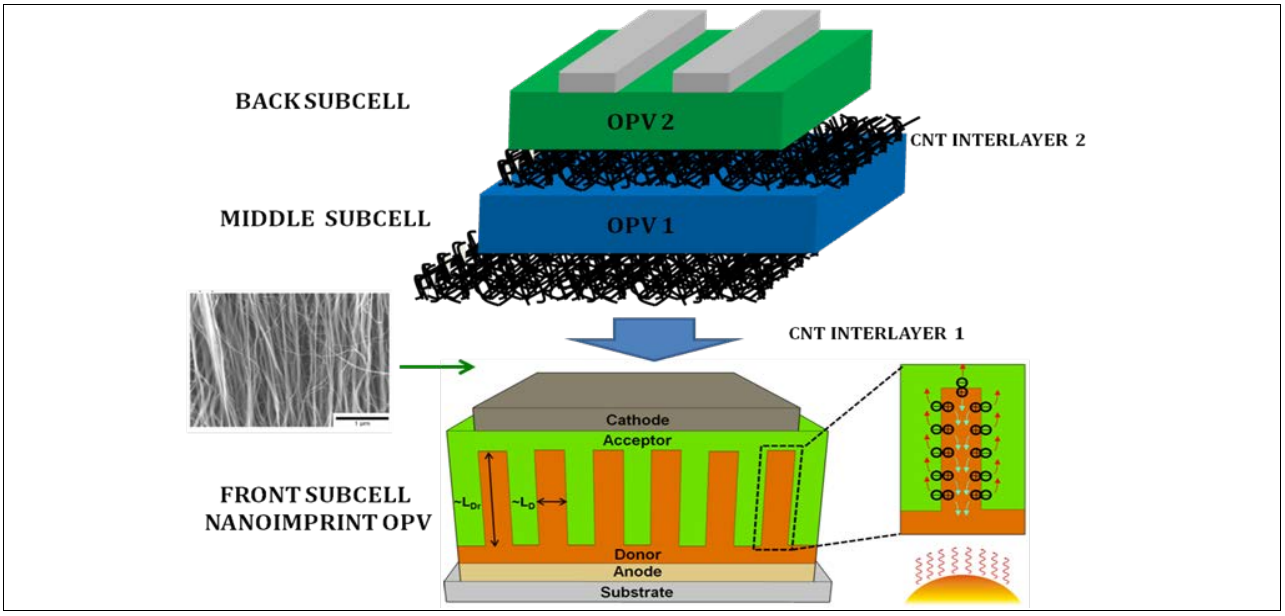

Figure 50. Schematic of the ideal bicontinuous and interdigitated donor-acceptor bulk heterojunction polymer solar cell and advanced concept of tandem cell with three sub cells

Ionic liquid Doping in OPV and New Concept of Parallel Connected OPV-supercapacitor tandem

Initial design and method of preparation are now under development for a parallel connected Organic PV and super-capacitor with the goal of higher efficiency and advanced performance. This new invention is in the field of organic electronics, and uses the advantage of nanoscaled materials and ionic liquids in combination with conventional organic electronics.

The major idea of this novel device structure is to use the transparent nanoscale network of conductive carbon nanotubes or a transparent graphene layer as a common electrode for the OPV cell and super-capacitor, which are thus in parallel connection. Applying voltage to the super-capacitor will dope electrochemically by double layer charging the electrode and carrier transport layer of the OPV. When disconnected the OPV, doping charge persists and the OPV operates with better performance as compared to the un-doped case. Moreover, the operation of the OPV sustains the charged state of OPV super-capacitor tandem. In the special case of properly adjusted energy levels of electrodes, the photocharging of the super-capacitor is also possible, without external source of charging.

This configuration allows application of voltage to the super-capacitor part in such a way that double layer charging of CNTs results in p-type or n-type doping of CNT. This electrochemical doping effect can be the extended (by voltage adjustment) to the conducting polymer electrode of OPV.

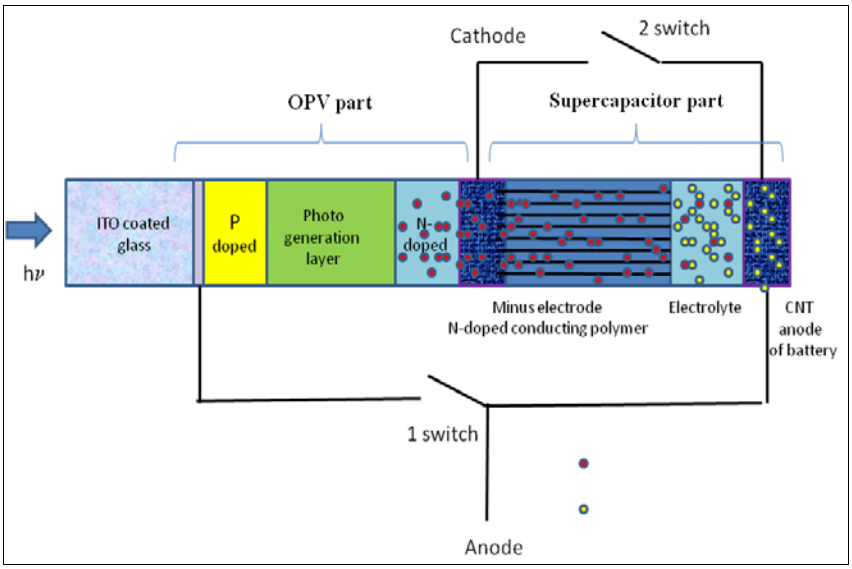

Figure 51. Proprietary design of a new tandem of OPV-Ionic Supercapacitor

Conclusions

We have demonstrated several types of Hybrid organic/polymeric photovoltaic (OPV) cell tandems connected in a parallel electrical configuration, utilizing organic materials with complementary absorption spectra, and transparent single wall carbon nanotubes (SWNT) as an interlayer common electrode. Tandem cells are of importance because they can append to the limited spectral coverage of available organic semiconducting materials. Furthermore tandems configured in a parallel circuit are of interest because there is no need to achieve current balancing as is the case with serial configurations. In contrast to our previous work in which a common anode made up of transparent multiwall carbon nanotubes was used to couple polymeric and molecular photovoltaic cells in a parallel tandem, the present works demonstrates an improvement of the previous work by utilizing proper inversion layers and an improved efficiency is reported. An efficiency of 5 % for each subcell is achieved. The inversion is performed using both charge selective metal oxide layers (ZnO and MoO_3) and n-type doped organic materials. Each cell was characterized independently and the short circuit current of the tandem device is shown to be larger than that of each sub cell. An overall increase in efficiency is observed and attributed to enhanced spectral coverage due to active layers with complementary absorption spectra and the effective use of transparent SWNTs.

To achieve the goal of overall efficiency of 8-10 % the clear strategy is outlined by using photoactive layers of higher performance, that have become available commercially, such as PTB1, PTB7 and similar. Additionally, the transport layers should be doped electronically by n-dopants developed by NOVALED. Our newest discovery of ionic liquid doping of the CNT interlayer will allow us to further increase the overall efficiency in triple junctions over 10 %.

References

1. S. Tanaka, K. Mielczarek, R. Ovalle-Robles, B. Wang, D. Hsu, and A. A. Zakhidov, Appl.Phys. Lett., 94, 113506, 2009

2. A. Zakhidov, A. Papadimitratos, K. Mielczarek, “Multijunction Monolithic Solar Cells with Transparent Interlayers for Inverted Parallel-Connection”, Provisional Patent, June, 2010,

application number 61/352,154

3. William Holmes, "Method and apparatus for substrate and gas heating during CVD nanotube synthesis"

US61/333,327, Provisional Patent May, 2010,

4. "Advantages of Parallel versus in-series connection for Hybrid solar cells Tandems: Comparisson of Experiments with Model", Kamil Mielczarek, Alexander Kuznetsov, Alexios Papadimitratos, Vladimir Pozdin and Anvar Zakhidov, in preparation.

5. Yi Yang, Kamil Mielczarek, Mukti Aryal, Anvar Zakhidov and Walter Hu, "Nanoimprinted Polymer Solar Cell" ACS Nano 6, 2877 (2012).

6. K.Mielczarek, A.Zakhidov, S.Tanaka, et.al. Organic Photovoltaics with Carbon Nanotube Charge Collectors: Inverted Structures for Parallel Tandems, Jap.J. Electronic Mater. (2012).

7. Y. Kim, A. A. Zakhidov, J. Bikova, A. Cook, et.al, and Karl Leo, Solar Energy Materials & Solar cells 96 (2012).

8. Y.H. Kim, C. Sachsea, A.A. Zakhidov, J. Meiss, A.A. Zakhidov, L. Müller-Meskampa, K. Leo, Organic Electronics Volume 13, Issue 11, November 2012, Pages 2422–2428 (2012).

Publications – Conference Presentations and papers in preparation:

1. "Inverted Polymeric Photovoltaic Cells and Parallel Tandems with Transparent Single Wall Carbon nanotubes Interlayer", K. Mielczarek, A. Cook, A. Zakhidov, A. Kaskela, A. Nasibulin, E. Kauppinen, A. Zakhidov, APS March Meeting 2011.

2. "Inverted Parallel Tandem Organic Photovoltaic Cells with Transparent Single Wall Nanotube Common Cathode", Kamil Mielczarek, Alexander Cook, Prakash Sista, Yun-Ju Lee, Antti Kaskela, Albert Nasibulin, Esko Kauppinen, Mihaela C. Stefan, Julia W. Hsu, Anvar Zakhidov, MRS Fall meeting 2011.

3. "Better Hybrid Solar Cell Tandems: Comparisons between Parallel versus In-Series Designs", K. Mielczarek, A. Cook, A. Papadimitratos , V. Pozdin , A. Kuznetsov , J. Velten , Anvar Zakhidov, APS March Meeting 2012.

4. "The Effect of a Self Assembled Monolayer in Small Molecule Organic Solar Cells", A. Cook, K. Mielczarek, A. Zakhidov, APS March Meeting 2012.

5. "Inverted Parallel Tandem Organic Photovoltaic Cells with Transparent Single Wall Nanotube Common Cathode", K. Mielczarek, A. Cook, A. Kaskela, A. Nasibulin, E. Kauppinen, J. Hsu, M. Stefan, Anvar Zakhidov, US-KOREA JSNT 2012.

6. "Organic Photovoltaics with Carbon Nanotube Charge Collectors: Inverted Structures for Parallel Tandems" K.Mielczarek, A. Cook, A.Zakhidov, S.Tanaka, I. Hiromitsu and K. Yoshino, Jap. J. Electronic Mater. (2012).

7. "Semi-Transparent Organic Solar Cells with Laminated Free-Standing Carbon Nanotube Top Electrodes", Y. Kim, A. A. Zakhidov, J. Bikova, A. Cook, et.al, and Karl Leo, Solar Energy Materials& Solar cells 96 (2012).

8. Yi Yang,K.Mielczarek, Walter Hu, A. Zakhidov, et al., "Nanoimprinted OPV," ACS Nano 6, 2877 (2012)

9. "Advantages of Parallel versus in-series connection for Hybrid solar cells Tandems: Comparisson of Experiments with Model", Kamil Mielczarek, Alexander Kuznetsov, Alexios Papadimitratos, Vladimir Pozdin and Anvar Zakhidov, in preparation.

10. B. Lee, Y. Chen, A. Cook, A. Zakhidov, V. Podzorov. Stable doping of carbon nanotubes with fluoroalkyl silane self-assembled molecules, in preparation.

11. A. Cook, K. Mielczarek, A. Zakhidov. Integration of doped carbon nanotube anodes into Organic Solar Cells, in preparation.

12. A. Cook, K. Mielczarek, A. Zakhidov. Inverted Organic solar cells with carbon nanotube top anodes, in preparation.

13. A. Cook, H. Kajii, Y. Ohmori, A. Zakhidov. Organic Light Emitting Transistors with laminated carbon nanotube gate electrodes, in preparation.

Patent Applications:

1. "Multijunction hybrid solar cell with parallel connection and nanomaterial charge collecting interlayers(PCT/US2011/039518)"

2. "Monolithic Parallel Multijunction OLED with Independent Tunable Color Emission(PCT/US11/37481)".

New patent (in preparation):

'Ionic liquid electrochemical doping of Carbon nanotube electrodes in-situ in OPV and OPV tandems"

APPENDIX O - "High Energy Density Supercapacitors Utilizing on Novel Carbons: Nanofibers and Vertically Aligned Carbon Nanotubes"
PI: John Ferraris, UT Dallas
Polyimide-Derived Carbon Nanofibers for Supercapacitor Applications

Carbon nanofibers provide high surface area and porosity, which makes it applicable for supercapacitor electrodes. An aromatic polyimide, composed of 4,4′-hexafluoroisopropylidene diphthalic anhydride (6FDA), 2,4,6-trimethyl-1,3-phenylenediamine (DAM) and 3,5-diaminobenzoic acid (DABA), 6FDA-DAM:DABA, is chosen as carbon nanofiber precursor owing to its electrospinnability and thermal stability. In addition, it has high free volume, caused by the bulkiness of hexafluoroisopropylidene-bridging moieties in 6FDA which can be translated to highly porous carbon material upon thermal treatments. The carboxylic acid moiety in DABA allows the polymer chains to be cross-linked, affecting the mechanical stability of the resultant carbon structure.

6FDA-DAM:DABA was synthesized by stirring 6FDA, DAM and DABA with 1-methyl-2-pyrrolidinone (NMP) in 5:3:2 molar ratios at room temperature. Thermal imidization was used for the ring closure, and then the mixture was precipitated in methanol and dried in a vacuum oven. A 25% 6FDA-DAM:DABA was dissolved in dimethylacetamide (DMAc) and the polymer solution was electrospun under an applied voltage of 15-20 kV. As-spun nanofibers were stabilized in air, and then carbonized under nitrogen. The surface morphology and microstructures of carbon nanofibers were investigated through scanning electron microscopy (SEM) and Raman spectroscopy, respectively. Carbonized nanofibers were activated using steam to improve their surface area and porosity. Undesired functionality induced by steam activation was removed by annealing under nitrogen. For electrochemical testing, coin cells were assembled using ionic liquid electrolyte to assess the supercapacitor performance of the freestanding carbon electrodes. Carbon electrodes derived from 6FDA-DAM:DABA exhibited rectangular cyclic voltammograms that were free of faradic peaks and had a specific capacitance of 126 F/g. Ragone plots, correlating energy density with power density, were obtained from galvanostatic charge-discharge curves. Highest energy and power densities of 6FDA-DAM:DABA-derived carbon electrodes are 70.0 Wh/kg and 9.4 kW/kg, respectively.

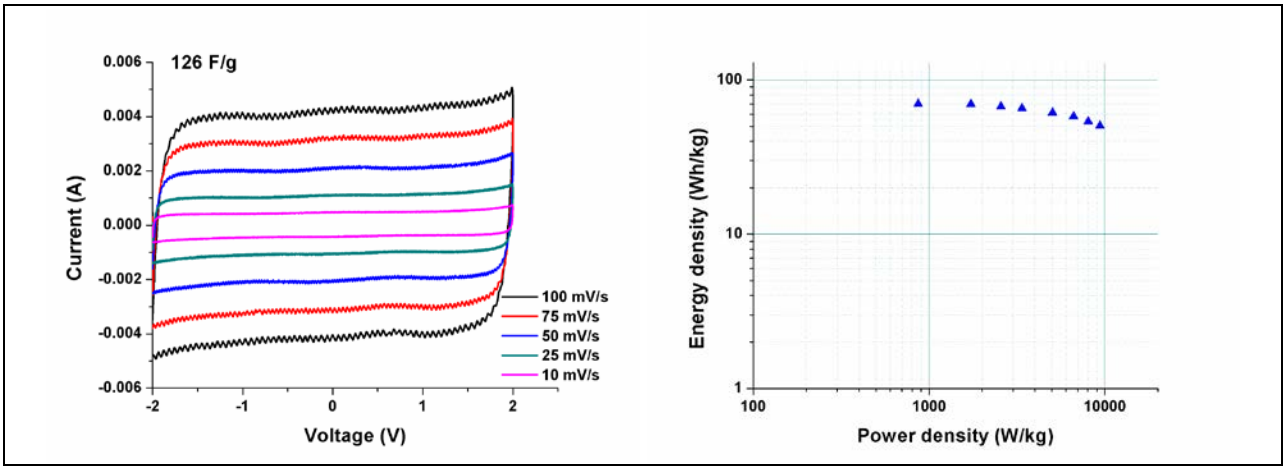

Figure 52. Cyclic voltammogram (left) and Ragone plot (right) of symmetric supercapacitor device from 6FDA-DAM-DABA-derived carbon nanofibers

Journal Articles and Meeting Presentations

1. Jung K-H; Ferraris J.P., Preparation and electrochemical properties of carbon nanofibers derived from polybenzimidazole/polyimide precursor blends. Carbon, 2012, 50(14), 5309-5315

2. dela Cruz, M. E.; Ferraris, J. P., Supercapacitor Electrode Material Comprising Carbon Fibers Incorporating Ammonium Acetate as a Pore-forming Agent, Polymer, submitted

3. dela Cruz, M. E.; Wu, Q.; Nijem, N.; Roodenko, K.; Perez, E. V.; Chou, V.; Yves J. Chabal, Y. J; Ferraris, J. P. Incorporation of templated carbon into electrospun carbon fibers as freestanding supercapacitor electrode material, J. Mater. Chem. submitted

Enhanced and Tunable Open-Circuit Voltage using Dialkylthio Benzo[1,2-b:4,5-b′]dithiophene in Polymer Solar Cells

A common feature of many of today's efficient low band gap donor-acceptor type conjugated polymers in Polymer Solar Cells (PSCs) is the employment of the benzo [1,2-b: 4,5-b'] dithiophene (BDT) unit. This family of polymers based on BDT, specifically dialkoxy substituted moieties, attracted our interest because of their exceptional performance as a common unit in PSCs that can achieve PCEs up to ~8%, which represents one of the highest efficiencies reported for polymer solar cells. Nevertheless, even though some dialkoxy-substituted BDT based polymers exhibit PCEs up to 7.7%, the majority of them have relatively high HOMO levels (in the range of -4.90 to -5.22 eV), leading to open-circuit voltage (V_{oc}) values ranging from 0.56 V to 0.76 V.

In this project, the synthesis of a novel dithioalkoxy-substituted benzo [1,2-b:4,5-b′]dithiophene (BDT) based homopolymer has been introduced, which would operate as an electron donor unit in BHSCs. The polymer (S-PBDT) was successfully synthesized via Pd-catalyzed Stille coupling reaction and fully characterized suggesting promising preliminary photovoltaic performance. The Polymer is readily soluble in common organic solvents, such as THF, chloroform and toluene with excellent thermal stabilities greater than 320^0C. PCE of up to 4 % was achieved using the polymer and PCBM blend. The most encouraging result from the previous work was that V_{oc} of the devices reached up to 0.99 V, resulting from the deeper HOMO level of the polymer with J_{sc} of 7.66 mA/cm^2 and FF of 0.53. The replacement of the alkoxy (-OR) groups with thioalkoxy (-SR) groups helped lower the HOMO energy level of the conjugated polymers and consequently enhance V_{oc}, while still preserving the excellent properties offered by the BDT-based polymers. This PCE is one of the highest efficiencies reported from a homopolymer-based PSC without thermal/solvent annealing or incorporated additives.

Currently, we are working on the synthesis of the low band-gap donor-acceptor copolymers by employing dithioalkoxy-substituted benzo [1,2-b:4,5-b′]dithiophene (BDT) unit which would lead to a strong and broad absorption to better match the solar spectrum. This would improve harvesting more sunlight leading to higher J_{sc} while still maintaining high V_{oc} due to low-lying HOMO energy level of the polymers.

Journal Articles and Meeting Presentations

1. Lee, Doyun; Stone, Shane W.; Ferraris, John P., "A novel dialkylthio benzo[1,2-b:4,5-b']dithiophene derivative for high open-circuit voltage in polymer solar cells", Chemical Communications 47(39), (2011), 10987-10989.

2. Lee, Doyun; Hubijar, Emir.; Kalaw, Grace.; Ferraris, John P., “Enhanced and Tunable Open Circuit Voltage using Dialkylthio Benzo[1,2-b:4,5-b′]dithiophene in Polymer Solar Cells”, Chem. Mater. 2012, 24, 2534−2540.

3. Lee, Doyun; Cook, Alexander; Zakhidov, Anvar; Ferraris, John P., “Novel poly dialkylthio benzo[1,2-b:4,5-b']dithiophene derivative for enhanced open-circuit voltage in PSCs application” Full Text, Abstracts of Papers, 242nd ACS National Meeting & Exposition, Denver, CO, United States, August 28-September 1, 2011 (2011), POLY-218.

4. Zhou, M.; Wang, B.; Jiang, X.; Zakhidov, A. A.; Ferraris, J. P.; Azunskis, D.; Hanley, L. “Synthesis of PbS nanocrystal/functionalized conducting polymers for plastic solar cells”, International Journal of Nanoscience (2011), 10(3), 521-532.

5. Lee, Doyun; Ferraris, John P., “Synthesis of fullerene tethered double-cable diblock copolymers based P3HT and its application in polymer soar cells”, Preprints of Symposia - American Chemical Society, Division of Fuel Chemistry (2010), 55(2), 22-23.

Students receiving Ph. D. in Chemistry from The University of Texas at Dallas that were supported by CONTACT (John P. Ferraris, advisor):

Marilou de la Cruz - Development of Carbon Nanofibers for Supercapacitor Electrode Applications - May 2012

Doyun Lee - Novel π-Conjugated Polymers for Polymer Solar Cells - April 2012

APPENDIX P - "Enhancing Optical Absorption in Polymer Solar Cells with Plasmonic Nanostructures"

PI: Julia Hsu, UT Dallas

Progress since April 2012

Experimentally we focused on finishing up device characterization for the manuscript based on this project. To understand the experimental data better, we started a collaboration with Prof. Weidong Zhou at University of Texas at Arlington, another CONTACT PI, to model the plasmonic effect on solar cells. These simulation results help elucidate our understanding of the experimental results greatly. We have now finished the manuscript on the project based on the past two years of work. The manuscript is ready for submission to Journal of Physical Chemistry.

Research achievement from October 2010 to September 2012

Thin-film solar cells offer great promise for applications valuing light-weight and large area form-factors, such as deployment of un-manned field sensors, power for RPAs, and ensuring operation of communication equipment in remote locations. Most thin-film solar cells will benefit from mechanisms that can lead to enhanced absorption. In this CONTACT project, we explore plasmonic effects from metal nanoparticles to enhance solar absorption in polythiophene polymer based solar cells. Because the active layers of these solar cells are thin (100-200 nm), small-diameter (15 nm in our case) Au nanoparticles are used so that shorting between the top and bottom electrodes is minimized. For 5-20 nm metal nanoparticles, near field enhancement rather than scattering is the primary plasmonic effect. Published work using metal nanoparticles in this regime are often fabricated through dewetting and cluster formation of ultrathin evaporated metal films, but such an approach generates a wide distribution of nanoparticle size, and thus the plasma resonance wavelength and intensity are difficult to control. We focus on having controlled nanoparticle density and studying the competition between energy quenching and near-field enhancement by depositing a ZnO overlayer with controlled thickness to vary the distance between the nanoparticles and the active layer. Au nanoparticles were synthesized by the AFRL researchers. At UT Dallas, the CONTACT project supports a PhD student, Jian Wang, full time as a part of his PhD thesis. Through the optimization of Au nanoparticle deposition conditions and polymer solar cell fabrication parameters, we achieve enhanced performance for the devices that include Au nanoparticles over reference devices. However, the increase in the short circuit photocurrent, which is expected from higher light absorption in the active layer due to the enhanced near-field electromagnetic fields of the plasmonic effect, is insignificant. Instead, the enhancement arises predominantly from higher fill factor of the diode. With recent collaboration with Prof. Zhou's group to model the experimental results by performing finite-difference-time-domain simulation, we found that while there exists enhanced optical field intensity within 15 nm of the Au nanoparticles, the absorption by the Au nanoparticles cause the absorption over the entire active layer to decrease. The fill factor enhancement is likely to due to improved electron transport.

Publications:

"Effect of Plasmonic Au Nanoparticles on Inverted Organic Solar Cell Performance"**,** Jian Wang, Yun-Ju Lee, Arvinder S. Chadha, Juan Yi, Michael L. Jespersen, John J. Kelley, Hue M. Nguyen, Michael Nimmo, Anton V. Malko, Richard A. Vaia, Weidong Zhou, and Julia W. P. Hsu, The Journal of Physical Chemistry C2013117 (1), 85-91.

Awards:
Julia W. P. Hsu was elected to Materials Research Society Fellow in 2011.

Presentations:

1. J. W. P. Hsu, "Enhanced Optical Absorption In Polymer Solar Cells With Plasmonic Nanostructures," 3rd annual CONTACT Review, Houston, TX, October 2010

2. J. W. P. Hsu, "Enhanced Optical Absorption In Polymer Solar Cells With Plasmonic Nanostructures," 4th annual CONTACT Review, Dayton, OH, November 2011

3. J. Wang, Y.-J. Lee, H. M. Nguyen, M. Nimmo, A. V. Mlko, J. W. P. Hsu, M. L. Jespersen, J. J. Kelley, R. A. Vaia, "Enhancement in P3HT:ZnO Solar Cells with Plasmonic Gold Nanostructures," Materials Research Society Fall 2011 Meeting, Boston, MA, November, 2011

4. F. J. Agee, J. W. P. Hsu, A. Chow, "CONTACT – Enhancing Optical Absorption in Polymer Solar Cells with Plasmonic Nanostructures," National Space Missile Materials Symposium, Tampa, FL, June, 2012

Student achievements:
Jian Wang passed the PhD qualifying exam in June 2011.

Collaborations:
The Au nanoparticles were synthesized and the appropriate ligands were exchanged in Dr. Rich Vaia's laboratory at AFRL. Prof. Hsu visited AFRL in January and November 2011 to discuss this project and other possible collaborations with AFRL researchers. The time-resolved photoluminescence was performed in Prof. Anton Malko's laboratory at UT Dallas. In 2012, we started a collaboration with Prof. Weidong Zhou at UT Arlington on simulating the plasmonic effects on the polymer solar cell performance. Prof. Hsu met Prof. Zhou at CONTACT review in 2010. Hence, the fruitful collaboration would not have happened without the CONTACT program.

APPENDIX Q - "Armchair Quantum Wire"
PI: Wade Adams, Rice University
Q.1. Introduction
Development and Manufacturing of the Armchair Quantum Wire (AQW)
The main purpose of the AQW project was to produce a strong, light and highly-conductive material that performs better than similar-sized copper or aluminum wires in conductivity and current-carrying capacity. The applications for this technology are numerous, and some of the more important examples are:

- Vastly improving electrical transmission, thereby conserving energy and enabling new sources of electricity generation to deliver their electricity to market – sources based on emerging, green technologies. This application goes beyond the civilian world and becomes critically relevant to Defense, as all Services strive to improve their power infrastructure for bases and other DOD installations.
- Reducing weight and improving performance in everything electrical – from electric motors and generators to power and signal/communications cables for aircraft – have enormous significance in Aerospace and Defense. Not only does Quantum Wire promise to improve existing technologies by making them lighter, stronger and more powerful, it will also enable defense technologies not yet imagined.

Rice continues to lead the world in the effort to make an effective Single-Wall Carbon Nanotube (SWNT)-based conducting fiber, and the contributing research teams have made significant progress in all of the areas where there are special technical challenges. These challenges are still, however, not completely conquered. Significant research efforts are still needed to reach that goal, beyond the scope of this project within CONTACT.

The challenges are:

- Production Volume: Producing a large enough volume of SWNTs of high quality, length and purity to make a credible fiber.
- Concentration of Metallic SWNTs: Concentrating – whether by post-growth manipulation or by selective growth – the metallic-behaving SWNTs in sufficient purity and volume to make micro- and macro-scaled conductive fibers.
- Alignment: Aligning SWNTs into a coherent, durable and conductive structure.
- Characterization: Measuring the behavior of SWNTs in various structures, to inform theory and help perfect the above pursuits.

The work in this project was performed by ten individual research groups with approximately ten graduate students in the School of Natural Sciences and the School of Engineering. Also contributing were fractional portions of one Senior Faculty Fellow, one laboratory research scientist, a laboratory technician and two administrators.

This work was divided into two main research objectives:

Research Objective 1: Production and Manufacturing Optimization of SWNT
This subtask carried out a program of modifications to the HiPco process and parameter studies by Dr. Robert Hauge with a view to defining the optimum program for increasing the output of

the HiPco process for producing carbon nanotubes.

Research Objective 2: Alignment and Characterization of SNWT-based Armchair Quantum Wire

Work was also performed in moving toward scalability of SWNT production via improvements in catalysis, vertical array growth (also known as "carpet growth") and separation of metallic and semiconducting species, as well as alignment and characterization resulting materials.

Program Goals

The ultimate goal of the AQW program is to manufacture a continuous, highly conductive cable of carbon nanotubes. The cable will consist of fiber comprising well-aligned, well-packed, single-type armchair SWNTs in good electrical contact. It is expected, but not proven, that such fiber will greatly surpass copper and other state-of-the-art conductors for power transmission over long distances as well as in Air Force applications. The expected properties are based on measurements on individual SWNTs; the literature shows that, when viewed as conducting wires, individual SWNTs may greatly outperform copper and other conductors. However, the collective conductivity of SWNT bundles is not yet established in macroscopic samples where the constituent SWNTs are much shorter than the distance between electrodes. Assessing conductivity over macroscopic scales is also an important program goal. If measurements on all-armchair macroscopic specimens show inadequate conductivity, the program will be re-examined, perhaps with additional external experts, or redirected. If macro-scale conductivity is proven, additional funding will be sought from mission-directed agencies or companies.

Defense Motivation

Optimized SWNT materials may further support a broad range of Defense technology interests, including:

- Light, strong power / signal harnesses
- Supercapacitors
- Regenerable CO_2 scrubbers
- Photovoltaics / thermophotovoltaics
- Chemical and optical sensors
- Light, high power density motors and generators
- Fuel cells
- Thermal management / heat pipes
- Multi-functional structures and composites
- Nano-scale electronic and computing systems

SWNT, or 'Buckytubes', are the strongest and the best thermal materials known to man – with a density about one sixth that of copper. These are carbon polymers of a unique class – they conduct electricity. Of the dozens of known Buckytube types, roughly one third are metallic; the rest are direct band-gap semiconductors. The metals, especially the 'armchair' tubes, have been shown to conduct electricity at least as well as copper, and perhaps some ten times better.

SWNT could represent the ultimate in engineering versatility. However, most SWNT applications require, or will be optimized by, using exactly the right kind of Buckytube. Current production technology yields mixed SWNT of all kinds. To unlock their ultimate potential and enable many break-through technologies for Defense, we must develop robust means to produce very pure type-selected SWNT at low cost.

Methods- Approach

Proof of concept includes small scale separation, forming very small arrays (mini-fibrils and films), and characterization of electrical conductivity and morphology, to prove scalability of conductivity in larger arrays of nanotubes. Production includes separation, catalyst design, and amplification, leading to scalable growth processes. Arraying and characterization include dry and wet alignment into fibers and film, and full characterization of larger scale arrays. Modeling is included in all three areas.

Making the AQW

Making the AQW entails one of the first two items below, plus the third, all of which represent significant scientific and engineering advancements:

1) Scalable growth of single-type SWNTs; or
2) Scalable separation of single-type SWNTs; and
3) Scalable arraying of SWNTs into continuous fibers with optimal orientation and packing.

Only one of the first two (scalable growth or separation) needs to be achieved; irrespective of the growth or separation method, scalable arraying must be achieved to realize the AQW. In fact, the AQW could be realized by (1) scalable growth of mixed SWNTs and subsequent scalable separation of armchair SWNTs, followed by arraying; (2) small-scale separation of armchair SWNTs and subsequent scalable amplification (originally called cloning) and arraying; (3) scalable, direct catalytic growth of armchair SWNTs and subsequent arraying.

Although the original AQW concept specifies that the constituent SWNTs should be all armchair and need not have a specific length, it is possible that high conductivity:

1) May require SWNTs longer than a critical length;
2) May be achieved in macroscopic samples comprising more than one SWNT type (e.g., all armchair of mixed type, or mixed armchair and small-bandgap semiconductors, or doped SWNTs).

Specification of the minimum requirements of composition, orientation, SWNT length, and packing density are needed. Validated, physics-based scaling laws describing fiber conductivity vs. manufacturing parameters (composition, orientation, etc) are preferable to simple experimental correlations.

Proving the AQW

Although the conductivity of individual armchair SWNTs has been established experimentally, little is known of the collective conductivity of aligned, ordered assemblies of same-type SWNTs. Conduction over long length scales (much longer than the individual SWNT length) depends both on intrinsic conductivity and effectiveness of inter-tube electron transport. The

nature of this transport, and how it depends on controllable parameters (degree of alignment, length of overlap, applied bias, type of the two SWNTs, distance between the two SWNTs, temperature, and presence of deliberate or environmental dopants) are not understood. Therefore, in lieu of meter-scale AQW engineering samples, it is important to establish whether conductive macroscopic SWNT specimens of minimum testable size can be produced and, if so, what are the minimum requirements on the controllable parameters to attain desired performance. Moreover, having the AQW "existence proof" will help justify and attract further funding to the manufacturing tasks (scalable, growth, separations, and arraying). For proof-of-concept, some requirements can be relaxed: scalable production method and continuous specimen. Establishing conductivity at the millimeter length scale (~1000 times the length of constituent SWNTs) will satisfy the proof-of-concept. Conductivity should be measured on samples (called mini-fibrils or films) with controllable structure, diameter or thickness above one micrometer (1000x SWNT diameter) and length above 100 micrometers (1000x HiPco SWNT length). Of course, the effect of fibril diameter and length should be assessed to verify that macroscopic scaling laws have been attained at the prescribed size (e.g., by placing multiple electrodes on the specimen and measuring conductivity vs. electrode spacing).

Q.2. Results

Q.2.1. Research Objective 1: Production and Manufacturing Optimization of SNWT: modifications to and parameter studies on HiPco process – Hauge Group

The goal of the project will be to move toward an improved manufacturing system for producing SWNTs by multiplying the effectiveness of the proven HiPco process. Included in this program will be:

- Catalyst enhancement with addition of nucleating agents to enhance the rate of iron nanoparticle production
- Multiple slipstream sample collector modules for small-scale midstream sampling. This will permit rapid sample collection after a parameter change in the operation of the HiPco reactor without shutting down the reactor.
- Modeling the HiPco injection nozzle mixing and temperature gradients with Solid Works fluid dynamic software. This facilitates the iterative validation and improvement of the nozzle design and control. Computational fluid dynamic software will also allow the modeling of particle flow in the stream which will provide a better understanding of mixing and nucleation.

Improve the production efficiency of SWNT production through the HiPco process

This effort includes changing the shape and size of the reaction chamber, the nozzles, and the way that the catalyst mixes in the chamber and reducing the size of the reaction zone to about one-seventh of its current size, without reducing its output, currently at one gram per hour. Based on the indications of our preliminary studies and the analysis of Computational Fluid Dynamics (CFD), we anticipate proving that the actual effective reaction zone of conventional HiPco is very small and can be reproduced in a small space.

Once this is established with one zone, the concept is proven, and a follow-on project can bring the additional six zones of the seven-chamber reaction complex online: hence our description of this as the 7x effort. The HiPco process operates as follows (Figure 53): High pressure CO at ~1300 ^{o}C is mixed with room temperature gas containing iron pentacarbonyl. Standard operating conditions are iron carbonyl at 52 mtorr in the reactor with an overall reactor pressure of 30

atmospheres, with a CO recirculating flow rate of 550 slm. Iron clusters form and catalyze the Boudouard reaction 2 CO ➔ CO2 (g) + C (s). Nucleation and growth of SWNT occurs in microseconds near the point of mixing. The SWNTs are then filtered out downstream, CO2 is removed, and CO is recycled to create a continuous process.

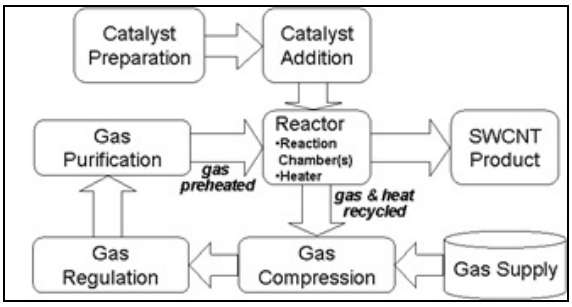

Figure 53. Basic HiPco Process

The HiPco process relies on the following fundamental process components:

- The ability of the catalyst particle to form to the correct size while remaining active.
- The right temperature in the reacting gas flows, which allows the catalyst particle to form and heat to its optimum reaction temperature.

The Boudouard reaction can take place as long as a catalytic surface is available and the kinetic energy of the gas is high enough to maintain the reaction. If the gas temperature is approximately 900C and the catalyst particle is on the order of 1nm in size, a SWNT will form. Any dramatic increase or decrease in temperature will cause the tube growth to stop.

As the cross-sectional area (diameter) of a hot gas flow increases, maintaining thermal homogeneity becomes very difficult. The HiPco process depends on rapid mixing of a cool gas (containing catalyst) and a hot gas (CO) to generate the requisite conditions for reaction. The reaction zone simply consists of two gas streams that are mixed at high velocity. The boundary layer between the two gas flows is believed to be the actual reaction zone/catalyst nucleation zone, and it is at this interface between the two gas phases that the optimal reaction conditions occur. The remaining CO in the flow is not utilized in the reaction, and passes unused through the continuous flow loop of the system. Limiting the diameter of the hot gas inlet or generating a shallow rectangular flow will, theoretically, create an optimum thermal cross-section for reaction. Reaction will occur without wasting the available flow of hot gas. The primary goal of this research is to explore the extent to which production can be scaled higher by altering the mixing of hot and cold gas flows in the reactor. See Figure 54 for current reaction zone.

Result: 1/7th chamber fabricated and ready to test.

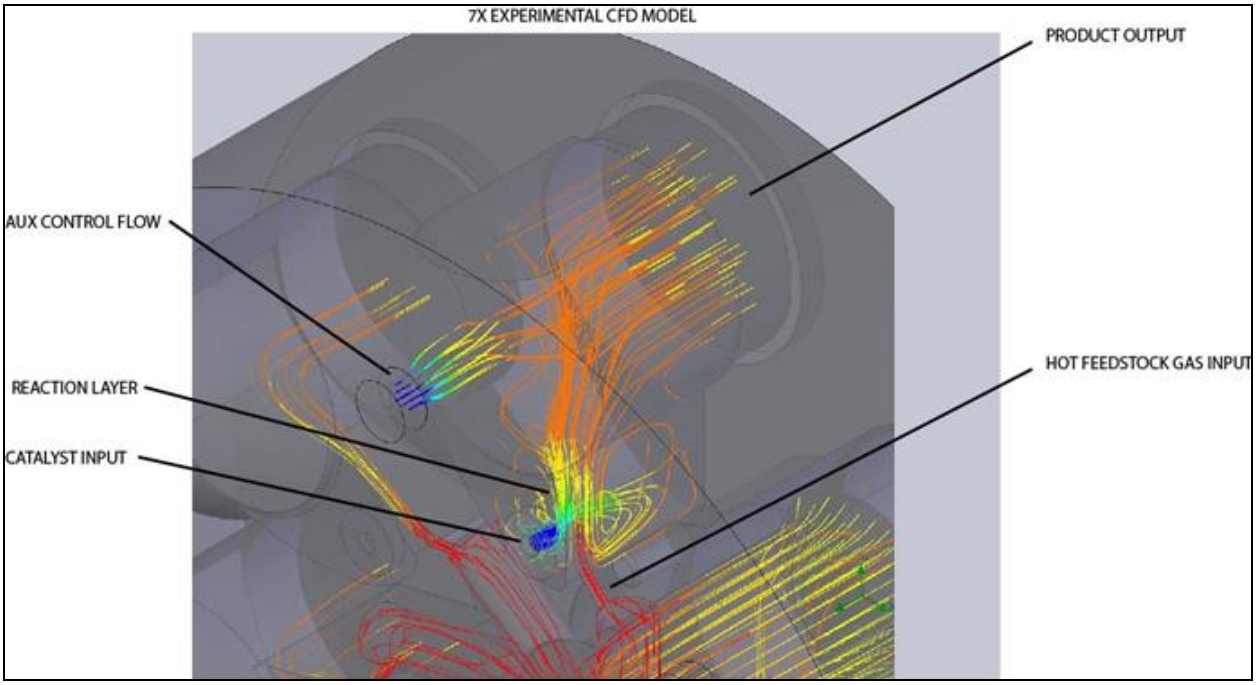

Figure 54. Computational Fluid Dynamics Diagram – 7x Reactor Core

Dramatically reduce the cost of producing high-quality SWNTs through HiPco
Using the reaction chamber from above, further manipulation of the shape of each reaction zone was performed to enable a further multiplication of SWNT production versus resources used. The nozzle settings were changed to produce a flat, or spatular reaction zone, in contrast to the balloon-shaped zone in the present system. This will allow us to lengthen the reaction zone, and by manipulating flow rates, to increase the time available to each catalyst particle for growing its SWNT. This also relies heavily on the process software improvements and inline sample collection improvements from the previous objectives: the former is part of what allows for manipulating the conditions of the reaction zone, and the latter enables rapid experimental iteration. All of the ideas we will pursue are supported by the Computational Fluid Dynamics analysis done to date.

Success in this effort is expected to result in a multiple in process efficiency of between ten and 100 versus today's HiPco process – hence our reference to it as the 10x – 100x effort. The rationale is as follows:

- The two gas flows differ greatly in temperature, which dramatically reduces the possible geometries of mixing that can create a functional reaction zone.
- The primary hot gas flow is limited to a cylindrical or semi-cylindrical shape, which limits the active reaction zone to the exposed surface area of the flow column.
- If the secondary flow is assumed to completely surround the primary flow, the process will only scale linearly as the surface area of the primary flow increases.

However, the flow – and the amount of energy and system support – increases by the square of the primary flow diameter (the area). Simply increasing the size of the flow does not provide a viable path to large-scale improvements. However, if we optimize the flow/surface area problem and repeat the solution with the same reactor core, we expect to find a much more viable path to large-scale improvements in the HiPco process. Current data suggests that the optimized configuration of the reaction zone would be a much smaller physical design requiring much less input energy. The remaining available energy would be then be used for additional instances of the same new reaction zone.

Result: The team was unable to complete any work on this due to insufficient time and funds.

Enhance HiPco's ability to tailor SWNT production toward specific characterisitics, particularly in diameter and length

The objectives here are to manipulate the catalyst and reaction conditions to yield additional SWNT specificity, extend the previous efforts toward increasing catalyst utilization and SWNT length by lengthening the residence time of the catalyst particles in the reaction zone, and reducing the rate of particle collisions that lead to catalyst death. Experiments have already been conducted in HiPco and results reviewed from the literature indicate that the distribution of SWNT type and size may be manipulated by catalyst particle size and composition. The expected outcome of this work is an ability to increase the proportions of targeted types and sizes within the SWNT production.

Result: The team was unable to complete any work on this due to insufficient time and funds.

Slipstream Sample Port

The planned changes in reactor geometry and methods of catalyst injection will lead to changes in SWNT diameters and lengths, total SWNT yields and residual catalyst content – all of which will require rapid characterization that can be tied to experimental changes in operational parameters. Previous research into the HiPco process has required samples to be sourced from the bulk collection chambers, which has made the process of testing slow and batch-oriented. Moreover, there was no reliable or precise way to measure the results of variables changed in midstream.

The re-designed collection system will provide for non-interruptive, rapid, repeated sample collection, while the remaining bulk of the SWNT production is funneled to the main collectors. This rapid collection will allow both for speedier experimental iteration and for significantly improved correlation of sample changes to specific changes in operational parameters. In-house TGA, TEM, SEM, AFM, Raman, fluorescence and UV-vis-NIR absorption spectroscopy will be used for rapid product characterization, with immediate feedback for guidance.

Result: Sample port designed but not executed due to lack of time and resources.

Q.2.2. Research Objective 2: Alignment and Characterization of SNWT-based Armchair Quantum Wire: contributions, by group

Q.2.2.1. Ajayan Group

Achievements during the period of 2011 to present and during the project overall

During the report period, carbon nanotubes were synthesized in a home built floating catalyst chemical vapor deposition system. Single-wall carbon nanotube (SWNT) films and double-wall carbon nanotube (DWNT) materials were synthesized for carbon fiber spinning/pulling. Methane and xylene were used as carbon sources and ferrocene and ferrocene/sulfur as catalysts for the single walled and double walled nanotube growth, respectively. Carbon nanotube growth on substrates was also carried out; in this case alumina and Fe/Co catalyst layers were deposited on silicon wafers and ethylene and ethyl alcohol were used as carbon sources. Both the floating catalyst and substrate based methods resulted in materials on the 100 mg scale which could be appropriately proper for spinning short (several ten cm) fibers for further tests. Nanotube fibers with dry and wet spinning methods were spun and studied for mechanical and electrical properties of the fibers. In the wet spinning processes acetone was used for densification during spinning. Characterization of the fibers showed potential for applications as sensors, unique burnout shape and high specific conductivity exceeding the value of the practically used metals. Three papers published in this period are listed in the report.

Summary for the whole project

Carbon nanotube synthesis was investigated for standalone and co-catalyst arrangements for both predeposited and the floating catalyst CVD methods. For predeposited the catalysts were optimized successfully for single and doublewalled carbon nanotube growth resulting in aligned nanotube forests with height on several hundred micrometer scale. The floating catalyst method was successful for growth of measurable amount of nanotubes (100 mg scale) with different carbon sources and various dopants, sulfur, nitrogen and water. Fibers were pulled and spin-pulled from the carbon nanotube materials and characterized; electrical and electromechanical properties measured showed potential for upscaling and applications.

Publications:

1. L. Song, G. Toth, J. Q. Wei, Z. Liu, W. Gao, L. J. Ci, R. Vajtai, M. Endo, and P. M. Ajayan, "Sharp Burnout Failure Observed in High Current-Carrying Double-Walled Carbon Nanotube Fibers", Nanotechnology, 23(1)(2012).

2. Y. Zhao, J. Q. Wei, R. Vajtai, P. M. Ajayan, and E. V. Barrera, "Iodine Doped Carbon Nanotube Cables Exceeding Specific Electrical Conductivity of Metals", Scientific Reports, 1(2011).

3. R. K. Srivastava, V. S. M. Vemuru, Y. Zeng, R. Vajtai, S. Nagarajaiah, P. M. Ajayan, and A. Srivastava, "The Strain Sensing and Thermal-Mechanical Behavior of Flexible Multi-Walled Carbon Nanotube/Polystyrene Composite Films", Carbon, 49(12), 3928-3936 (2011).

Q.2.2.2. Barron Group

SWNT separations summer 2011 research project

Prior work has shown that separations are possible using known techniques such as precipitation using NaCl solutions, but the product yield was always minimal, and it has not previously been considered that the product yield is a function of total volume tested. In other words, it was suggested that a fixed amount of material contributes to poor product yield, but if the total

amount reacted is increased dramatically then the net effect of the fixed amount becomes increasingly less important. In this way by doing reactions on a larger scale, some portions tend to crap out regardless, then that becomes less important as the total scale increases.

Results and Discussion

Selective precipitation using NaCl solutions

Samples of SWNT/SDS solutions were mixed with varying concentrations of NaCl solutions and left to equilibrate for a week. Figure 55 shows the effect of the SWNT/SDS suspension after the time period of one week. Bundles began settling to the bottom after the addition of a 0.1 molar NaCl solution. With increasing concentration of NaCl solution the precipitate shows more compressed bundle layer. However at >0.4 M NaCl some white precipitate was noted also, that we suggest is the SDS, that results from excessive Na+ cation concentration.

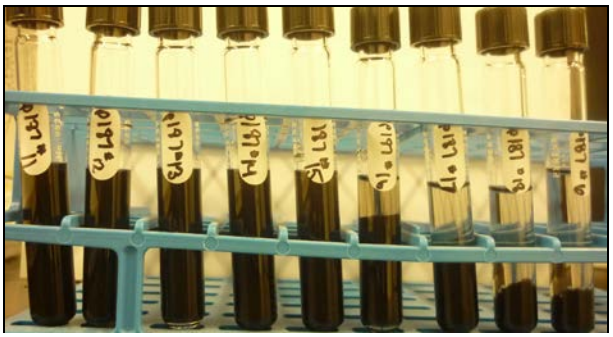

Figure 55. Showing the effect of salt addition to SWNT/SDS suspension. From left to right the salt concentration is increasing from 0 to 0.2 M NaCl

Centrifugation could be used to accelerate the settling process. The samples were all placed back in the centrifuge. Supernatants of concentrations > 0.1 M NaCl came out completely clear. Figure 56 shows typical photoluminescence data of SWNT/SDS solutions upon the addition of NaCl solutions with concentrations varying from 0 – 0.2 M NaCl.

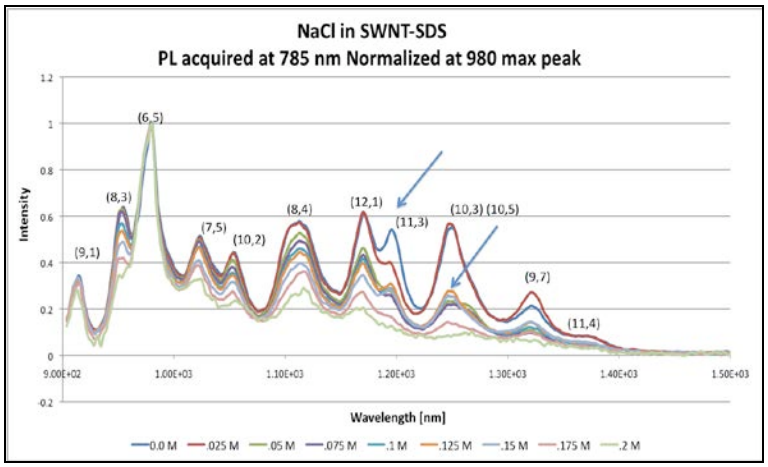

Figure 56. Showing PL data from the addition of NaCl with concentrations ranging from 0 – 0.2 Molar.

Selective aggregation was noted for SWNTs (10,5) and (9,7) as these were found to crash out of solution fast, this was consistent with the work of Niyogi et al. It was also observed that the intensity for the SWNTs (8,4) (12,1) (11,3) decreased incrementally. This suggests that there might be some diameter dependence in the selective precipitation of SWNTs due to the electrostatic repulsion between the sulfur head groups of SDS as they assemble about the surface of the SWNTs. This can be seen particularly when higher concentrations of NaCl are used as is evident in Figure 56, where the peaks at higher wavelengths decrease in intensity due to the bundling, the intensity of these tubes decreases much greater than those of the tubes with lower wavelengths.

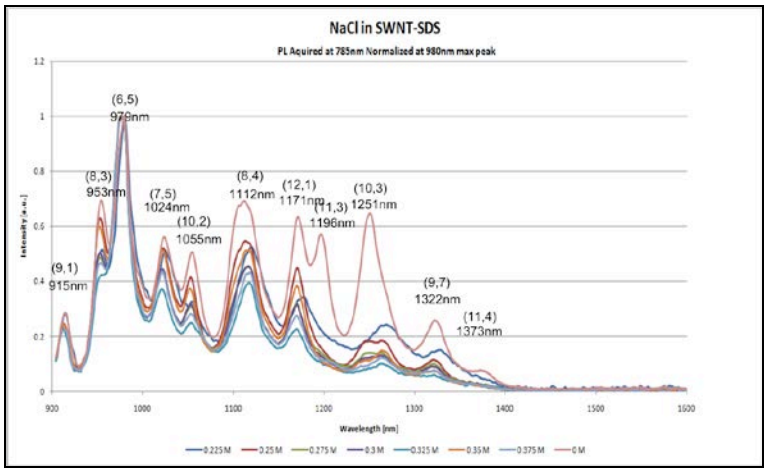

Figure 57. Showing PL data from the addition of NaCl with concentrations ranging from 0.2 – 0.4 Molar.

Conclusions:
By the addition of NaCl it was found that (10,5) or (10,3) aggregation was highest, effectively meaning they were precipitated quickest. As such the addition of electrolytes coupled with centrifugation can be used as bundling technique to quickly separate S-SWNTs from solution.

Further work to be carried out would explore differences in surfactant packing and how this influences the bundling rate, and hence the rate of precipitation. Thus finding the electrolyte balances that bundles semiconducting tubes and decreases metallic tubes density is sought after, so it can be used to eliminate need of ultracentrifuge. This would enable large volume separation.

References
[1] S Niyogi, S Boukhalfa, S.B Chikkannanavar, T.J McDonald, M.J Heben, S.K Doorn, Selective aggregation of single-walled carbon nanotubes via salt addition, J. Am. Chem. Soc. (2007) vol. 129 (7) pp. 1898-1899.

Q2.2.3. Hauge Group
Developing Scalable Technology for CVD Growth of SWNTs
The primary effort has been focused on the development of a scalable technology for the CVD growth of single wall carbon nanotubes. Secondary goals have focused on exploring the effects of temperature, gas composition and catalyst preparation on the yields and diameter distribution of the SWNTs that are grown and the optical and electrical characteristics of the aligned SWNT

forests.

An important component of a scalable technology for CVD growth of SWNTs is the way in which a surface catalyst is applied to the growth substrate. We have explored wet methods that distribute nanoparticles of alumina or clay uniformly on a support that can be scaled to large area supports. We have also designed and built a growth reactor that permits the safe use of hydrazine as a growth catalyst activator. This is currently being tested as a means for catalyst activation over large areas. Plans are also in place to explore the repeated use of a catalyst by detaching and removing grown nanotube forests with a high gas flow to a filter downstream and reactivating the catalyst for further growth. These achievements are expected to allow the production of SWNTs at the rate of grams/day.

We have also explored the electrical, thermal and photovoltaic behavior of HiPco grown SWNTs. We have shown that sidewall functionalized nanotubes can be partially separated into metallic and semiconductor types by heating to temperatures that primarily defunctionalize semiconductor tubes. Photovoltaic studies of aligned CVD grown SWNTs have demonstrated signal generation via the Seebeck effect with signal level generation sufficient to allow their potential use detectors in the mid-infrared.

Publications:

1. Alvarez, N. T.; Li, F.; Pint, C. L.; Mayo, J. T.; Fisher, E. Z.; Tour, J. M.; Colvin, V. L.; Hauge, R. H., Uniform Large Diameter Carbon Nanotubes in Vertical Arrays from Premade Near-Monodisperse Nanoparticles. *Chemistry of Materials* 2011, 23, 3466-3475.

2. Amama, P. B.; Pint, C. L.; Mirri, F.; Pasquali, M.; Hauge, R. H.; Maruyama, B., Catalyst-support interactions and their influence in water-assisted carbon nanotube carpet growth. *Carbon* 2012, 50, 2396-2406.

3. Green, M. J.; Young, C. C.; Parra-Vasquez, A. N. G.; Majumder, M.; Juloori, V.; Behabtu, N.; Pint, C. L.; Schmidt, J.; Kesselman, E.; Hauge, R. H.; Cohen, Y.; Talmon, Y.; Pasquali, M., Direct imaging of carbon nanotubes spontaneously filled with solvent. *Chemical Communications* 2011, 47, 1228-1230.

4. Haroz, E. H.; Duque, J. G.; Lu, B. Y.; Nikolaev, P.; Arepalli, S.; Hauge, R. H.; Doorn, S. K.; Kono, J., Unique Origin of Colors of Armchair Carbon Nanotubes. *Journal of the American Chemical Society* 2012, 134, 4461-4464.

5. Pint, C. L.; Nicholas, N. W.; Xu, S.; Sun, Z.; Tour, J. M.; Schmidt, H. K.; Gordon, R. G.; Hauge, R. H., Three dimensional solid-state supercapacitors from aligned single-walled carbon nanotube array templates. *Carbon* 2011, 49, 4890-4897.

6. Pint, C. L.; Sun, Z.; Moghazy, S.; Xu, Y.-Q.; Tour, J. M.; Hauge, R. H., Supergrowth of Nitrogen-Doped Single-Walled Carbon Nanotube Arrays: Active Species, Dopant Characterization, and Doped/Undoped Heterojunctions. *Acs Nano* 2011, 5, 6925-6934.

7. Pint, C. L.; Sun, Z.; Moghazy, S.; Xu, Y.-Q.; Tour, J. M.; Hauge, R. H., Supergrowth of Nitrogen-Doped Single-Walled Carbon Nanotube Arrays: Active Species, Dopant Characterization, and Doped/Undoped Heterojunctions. *Acs Nano* 2011, 5, 6925-6934.

8. Zhang, C.; Bets, K.; Lee, S. S.; Sun, Z.; Mirri, F.; Colvin, V. L.; Yakobson, B. I.; Tour, J. M.; Hauge, R. H., Closed-Edged Graphene Nanoribbons from Large-Diameter Collapsed Nanotubes. *Acs Nano* 2012, 6, 6023-6032.

9. Zhang, C.; Li, J.; Liu, E.; He, C.; Shi, C.; Du, X.; Hauge, R. H.; Zhao, N., Synthesis of hollow carbon nano-onions and their use for electrochemical hydrogen storage. *Carbon* 2012, 50, 3513-3521.

Q.2.2.4. Kono Group

Report on DC transport studies of carbon nanotube networks for the AQW program, by Xuan Wang: Introduction

The transport of an electron through a carbon nanotube (CNT) network consists of "fast" intratube transport, yielding the intrinsic resistance (R_{in}), and "slow" intertube transport, yielding the junction resistance (R_j). Given the mean free path L_e, R_{in} of each metallic CNT can be evaluated by:

$$R_{in} = \frac{h}{4e^2}\left(1+\frac{L}{L_e}\right) \text{ or } \rho_{in\_1d} = \frac{R_{in}}{L} = \frac{h}{4e^2}\left(\frac{1}{L}+\frac{1}{L_e}\right) \quad (10)$$

where L is the tube length, ρ_{in_1d} is the one-dimensional resistivity of a single tube, which is related to the three-dimensional resistivity as $\rho_{in\_3d} = S \times \rho_{in\_1d}$, where S is the cross-section of the nanotube.

In the diffusive transport regime, L_e will decrease with increasing temperature due to the increasing electron-phonon scattering rate with temperature. Therefore, R_{in} will increase as a function of temperature. In particular, when electron-acoustic phonon scattering is dominant, R_{in} can be written as a linear function of temperature (T) as

$$R = R_r + \alpha T \quad (11)$$

where α is the temperature coefficient and R_r is the residual resistance due to impurities and defects. The corresponding temperature range where this formula is valid is typically from several tens to several hundreds Kelvin depending on the CNT type. At higher temperatures, where optical phonons are excited, higher-order terms should be added and R_{in} will increase faster with increasing T. Theoretical calculations show that α/L ~ 107 ohm/Km for CNTs, yielding L_m ~ 500 nm to 1um at room temperature, consistent with experimental results. By using such L_e and ~2 nm as the diameter (d) of the tube, the ideal ρ_{in_3d} for one CNT is ~2×10^{-8} ohm-m. However, the observed ρ_{in_3d} is usually much higher than this value in CNT bundles or networks. This is because the length of each individual CNT is usually too short to connect two terminals, and hence, carriers must transport from one tube to another, making intertube transport, characterized by R_j, important.

There are mainly two mechanisms for intertube transport. The first is variable range hopping (VRH) in which electron hops incoherently between two electronic states of two tubes. When VRH is dominant, R_j is related to the temperature as:

$$R_j = R_h \exp\left(\frac{T_0}{T}\right)^{\gamma} \quad (12)$$

where T_0 is the characteristic temperature, R_h is the saturation resistance, and γ ranges from 0.25 to 0.5 , depending on the number density of CNT. Given the same γ, a smaller R_h and a lower T_0 indicate better coupling between two CNTs. The second mechanism is the fluctuation-induced tunneling (FIT), in which carriers can tunnel coherently between two electronic states of two tubes. In this case, R_j is related to the temperature as:

$$R_j \propto R_t \exp\left(\frac{T_t}{T+T_s}\right) \tag{13}$$

where R_t is the saturation resistance, T_t characterizes the tunneling barrier, and T_s characterizes the scale of energy fluctuation needed to tunnel. Generally to speak, FIT yields a smaller Rj than VRH.

Although in many experiments, R_j limits the overall resistivity, R_j can, in principle, be reduced to zero. This is because the overlapping area for R_j is proportional to *d X L*. Given the same tube-to-tube coupling, increasing the tube length could decrease R_j without alternating R_{in}.

Single CNT also shows high saturation current density limit $j>10E^{+9}$ A/cm^2 , which is 3 orders of the electromigration current limit of copper. However, in many applications, deterioration induced by joule heating prevents CNT device from achieving such limit. In this case, the current carrying capacity (CCC) of CNT device not only depends on the intrinsic properties of CNT, but also on its environment characterized by ambient temperature (T_{am}), temperature change (ΔT) and so on. Particularly, the power transmission current density limit (j_p) defines the maximum current density that an infinite long suspended wire can achieve with its surface temperature increasing to Tam+ ΔT. Given that only the surrounding gas dissipates heat from CNT through its surface area, j_p can be evaluated by:

$$j_p = \sqrt{\frac{4g\Delta T}{\rho D}} \tag{14}$$

Where D is the cross section of the CNT wire, ρT is the three dimensional resistivity at Tam+ ΔT. g is the heat coefficient of the gas surrounding the wire, which is a function of gas specie , T_{am} and ΔT.

DC transport study of density gradient ultracentrifugation (DGU) films

The resistivity of DGU films generally increases with decreasing temperature, mainly arising from intertube transport (see Figure 58).

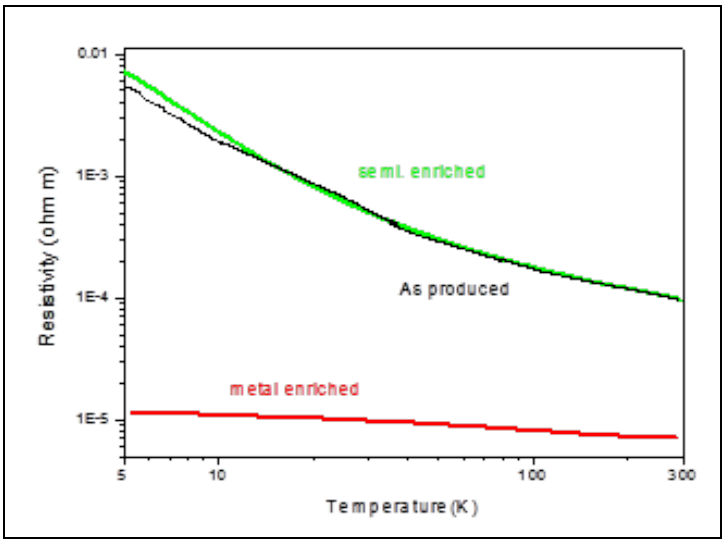

Figure 58. Resistivity as a Function of Temperature for DGU Films

The resistivity of a metal enriched film is well fitted by FIT model, while the resistivities of semiconductor enriched films and as-produced film can be fitted by the VRH model. The fitting parameters are listed in Table 17.

Table 17. Fitting Parameter for Resistivity of DGU Film

Sample	Resistivity at 285K (Ω m)	Hopping model fitting	Tunneling fitting
Semicond. enriched annealed	9.4 E-5	γ=0.337 T_0=941.076	Not good
As-produced	9.65 E-5	γ=0.339 T_0=807.592	Not good
Metal enriched annealed	7.09 E-6	Not good	T_c=50.4K T_s=70.7K

The resistivity of a metallic enriched DGU film is typically one order smaller than that of a semiconductor enriched DGU film, consistent with the fact that FIT should prevail over VRH if the sample is more conductive. A subtle issue to note is that semiconductor enriched films is unintentionally doped by residual impurities or gas molecules. Although the resistivity of as-produced films is close to that of semiconductor enriched films at room temperature, such a comparison is not meaningful because as-produced samples contain more impurities than DGU films, which increases the resistivity, while it is made by longer CNTs, which decreases the resistivity.

In all DGU films, contribution from R_{in} is not observed. This is because the changing rate of R_j (~ $-2.5E^{-9}$ ohm m/K from fitting) is still much higher than that of R_{in} (~$10E^{-11}$ ohm m/K estimated from α).

DC transport study of CNT fibers

The resistivity of a CNT fiber usually shows tunneling-like (or hopping-like) resistivity at low temperatures and metallic-like resistivity at high temperatures, which can be modeled by a

heterogeneous model as:

$$\rho(T) = f_1 \rho_t \exp\left(-\frac{T_t}{T+T_s}\right) + f_2\left(R_r + \alpha T\right) \tag{15}$$

Or

$$\rho(T) = f_1 \rho_h \exp\left(\frac{T}{T_0}\right) + f_2\left(R_r + \alpha T\right) \tag{16}$$

Here, the first equation is for FIT and phonon scattering, while the second is for VRH and phonon scattering, and f_1 and f_2 are the geometric factors, which can be written as

$$f_{i=1,2} = \frac{L_i S}{L S_i} \tag{17}$$

where L and S are the fiber length and cross section area, respectively, and L_i and S_i are the effective length and cross section area that conduct current. In the ideal case when each single tube is long enough to connect both terminals, $f_1 = 0$ and $f_2 = 1$ and so the current goes through each individual tube without passing through inter-tube junctions. This sets the lower limit for the resistivity. Further improvement will rely on better CNTs. In other cases, $f_1 > 0$ and $f_2 > 1$ yields higher resistivity. Also the two terms in the equation above are not independent to each other, because the relation between R_{in} and R_j is not really in series. f_2 will increase as f_1 increases. As a result, the second term in the equation (FIT and phonon scattering) will increase through f_2, even though R_{in} remains unchanged.

The resistivity of a CNT fiber strongly depends on the level of doping level and alignment (see Figure 59).

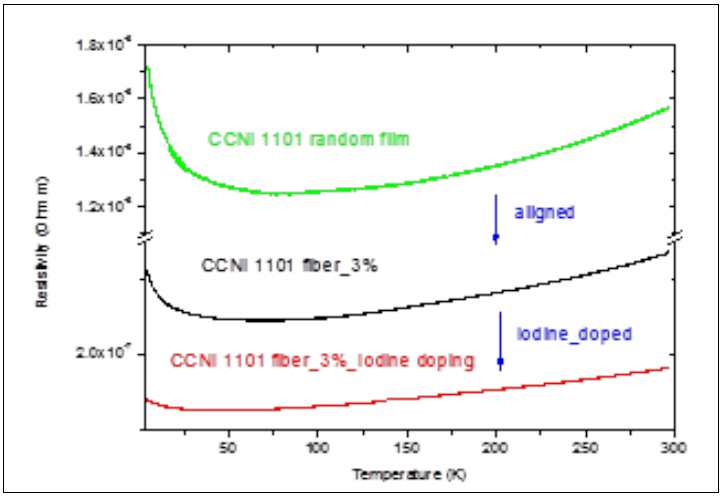

Figure 59. Effect of Alignment and Doping on the Resistivity of CNT Fiber

A comparison between annealed fiber and superacid-doped fiber shows that superacid-doping decreases resistivity by one order. In addition, iodine-doping further decreases it by half. However, such significant effect on resistivity by doping is not fully understood. Doping can reduce R_{in} by adding charge carriers to semiconductor tubes. Since more carriers are available to hop or tunnel, R_j will also decrease. Some theoretical studies also suggest that impurities may help conserve momentum during intertube transport. Studies are being carried out now in Kono's lab to further understand doping process.

Alignment also drastically decreases the resistivity by a factor of five, which can be seen by comparing the random film and fiber. Since the random film has a higher doping level (due to more porous structure) than the fiber, an extra mechanism to decrease the resistivity, the real improvement due to alignment should be larger than this value. Better alignment decreases the resistivity because it increases the overlapping area, reduces intertube distance, and increases the density of tubes.

We also notice that as the overall resistivity decreases, weights from the first term in the aforementioned equation (characterized by $f_1\rho_t$) decreases, an indication of approaching the resistivity limit determined by Rin (characterized by $f_2\alpha$). For the best iodine-doped fiber, $f_2\alpha$ is still one order larger than the ideal value for metallic tubes (~$10E^{-11}$ ohm m/K). This may be because that doped semiconductor tubes may suffer from more scattering than metallic tubes due to interband transitions. Theoretical studies show that α can be one order larger in doped semiconductor tubes than that in metallic tubes. If this is true, then the resistivity of fibers may be close to the resistivity limit for doped semiconductor bundles. However, this potential advantage of metallic tubes over doped semiconductor tubes requires further experimental proofs. Another possible explanation is the junction resistance is still relatively large so that the resistivity limit ($f_1 = 0$ and $f_2 = 1$) is not achieved yet.

Comparison between DGU films and CNT fibers:

Table 18 shows a comparison between the metallic enriched DGU film and CNT fiber. The number density and tube length of DGU films are estimated values. The average tube length in fiber is around 2 um with a fairly broad distribution. As shown in Table 18, the resistivity of the fiber is more than one order smaller than the metallic enriched DGU film. This is because the number density of tubes in the fiber is higher than that of the DGU film, so more tubes are contributing to current transport. On the other hand, the tube length in the fiber is about 1 order longer than that in the DGU film. As a result, the number of junctions per length is about 1 order less in the fiber than in the DGU film. After normalization in terms of number density and length, the resistivity of the DGU film is only 0.24 of the resistivity of the fiber. This means if 2 um long metallic carbon nanotubes are used to replace the CCNI 1101 batch CNT to spun fiber, even without improving R_j, the resistivity would be ~$5E^{-8}$ ohm m. Alignment and doping should further decrease R_j to reach the ideal limit.

Table 18. Normalized Resistivity of Metal Enriched Film and Fiber

Sample	Resistivity around RT (Ω m)	Length of CNT	Density of CNT	Normalized Resistivity
Metal enriched annealed	70.9 E-7	~100nm	10%	0.24
Fiber material film	16 E-7	~2um	10%	~1.1
Iodine doped fiber	1.83E-7	~2um	80%	1

Current Carrying Capacity (CCC) of CNT fibers

The break-down current (or fuse current) of super acid doped fiber (CCNI 1001 wt. 6% draw ratio: 13.3 m/min vs 0.05 ml/min) under various experimental condition is shown in Figure 60.

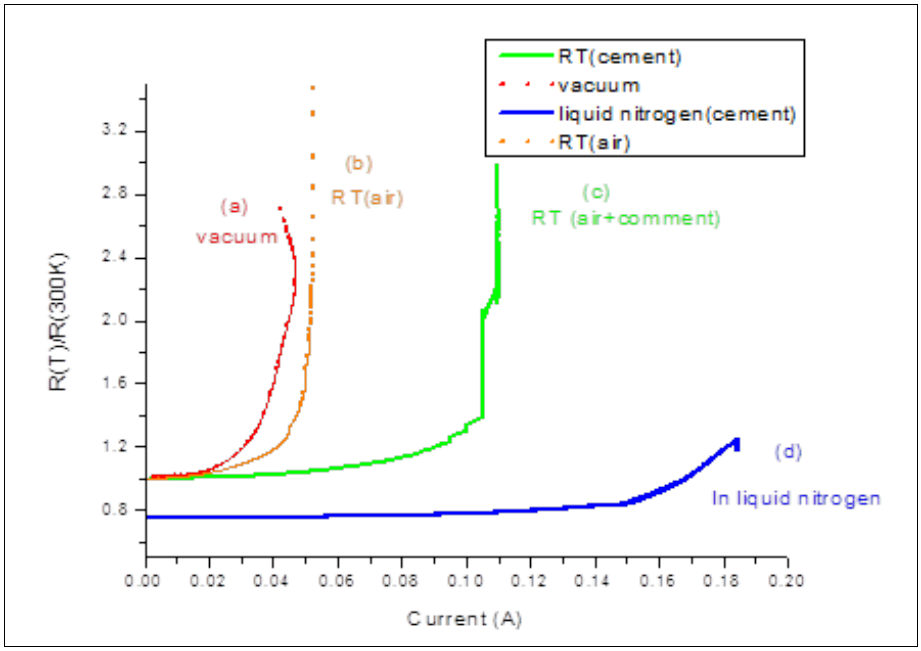

Figure 60. Fuse Current of CNT Fiber Under Various Testing Conditions.

(a) Fiber is suspended in vacuum, (b) Fiber is suspended in air, (c) Fiber is laid on a substrate and is covered by isolation cement to enhance heat exchange at room temperature, and (d) same as (c) but in liquid nitrogen.

The fact that fuse current strongly depends on the heat exchange medium and ambient temperature indicates that the break-down is triggered by joule heating. Before break-down takes place, there also exists a current region when irreversible damage appears. Then depending on the current training process, fibers could either keep a resistivity several folds of the original value, or slowly break.

The power transmission current density limits j_p) of CNT fiber (CCNI 1101wt. 3% draw ratio:0.16 ml/mm vs 5ml/mm, D=20 um) ,and a pure copper wire (purchased from Nilaco corporation, D=25um) is shown in Table 19.

Table 19. Power Transmission Current Density Limit for CNT Fiber and Copper Wire

Unit : 10^4 A/cm^2

	Helium	argon	Air
CNT fiber (CCNI 1101)	3.2	1.08	1.32
Copper *	3.9	3.4	

$T_{am} = 300K$, $\Delta T = 60degree$

In this test, no irreversible damage is observed up to 363K. First, j_p of CNT fiber in helium gas is much higher than in the other two gases, which contradicts to previous studies on single CNT, where jp in helium gas is the lowest of the three. This may be because that helium gas can penetrate the porous structure of CNT such that the effective surface area for heat exchange increases. In this case, the j_p equation doesn't hold. j_p of CNT fiber in argon is about 1/3 of that of copper wire. Based on that equation, such difference is mainly due to the difference in resistivity. By further decreasing the resistivity, j_p of CNT could surpass pure copper wire.

Summary:
We have studied the resistivity of CNT networks. In DGU films, the resistivity is still limited by the large junction resistance due to shorter tube lengths and random network structure. By improving alignment and doping, the resistivity should drastically decrease, as observed in the CNT fiber. The resistivity of CNT fibers could be further improved, close to the resistivity of copper, if longer metallic enriched tubes are used. The CCC of CNT fiber is limited by joule heating and by reducing the resistivity of fiber, the CCC could exceed copper wire.

Undergraduate Research Project on Separations – Summer 2011 – Managed by Erik Haroz:
One of the main limitations with the successful enrichment of armchair carbon nanotubes via density gradient ultracentrifugation is the overall mass yield and lack of scalability. Only ~1 microgram of enriched SWNT material is produced for every milligram of as-produced SWNT material put into the centrifuge. As a result, the current DGU process for electronic-type-enriched SWNT material production is insufficient for fiber spinning or large scale-up.

To that end, we chose to investigate a different separation approach (developed by the Kataura group, AIST) with the potential for scalability based on gel column chromatography. Specifically, SWNTs suspended in aqueous surfactant (sodium dodecyl sulfate) are passed through an agarose gel column under gravity and separated by electronic type due to an electronic-type-specific difference in binding affinity of the SWNTs for the agarose gel over the mobile phase consisting of aqueous surfactant. This results in retention of semiconducting SWNTs in the column while allowing metallic SWNTs to pass. The semiconducting SWNTs are then separated from the column by passing a second surfactant (sodium deoxycholate) through the column that has a stronger binding affinity for the SWNTs than the agarose gel column.

Using another type of gel column material, an acrylamide-dextran gel, it was shown by the same group (Kataura group, AIST) that single-chirality separation of semiconducting species was

possible. With our group of summer students, we attempted to reproduce the results from both works, improve upon it, and increase the scale. Unfortunately, we could not reproduce the results described in the Kataura group papers using their written procedures for both type- and chirality-separation with their stated separation purities.
Our results always yielded lower separation purities than those stated in the reference papers. The students' work identified several important factors that affect the separation efficiency of both gel column approaches including column orifice size, gel packing density, SWNT loading amount, and elutant flow rate and composition. While studies of such parameters led to improvement of our separation yields, we could never achieve the stated separation yields, pointing to other important parameters not identified in the referenced papers or in our own studies. These studies were useful for understanding the mechanism behind surfactant-based separations, however, they did not ultimately prove a route towards scalable separations.

Publications:

1. N. Behabtu, C. C. Young, D. E. Tsentalovich, O. Kleinerman, X. Wang, A. W. K. Ma, E. A. Bengio, R. F. ter Waarbeek, J. J. de Jong, R. E. Hoogerwerf, S. B. Fairchild, J. B. Ferguson, B. Maruyama, J. Kono, Y. Talmon, Y. Cohen, M. J. Otto, and M. Pasquali, "Strong, Light, Multifunctional Fibers of Carbon Nanotubes with Ultrahigh Conductivity," *Science* **339**, 182 (2013).

2. E. H. Hároz, J. G. Duque, X. Tu, M. Zheng, A. R. Hight Walker, R. H. Hauge, S. K. Doorn, and J. Kono, "Fundamental Optical Processes in Armchair Carbon Nanotubes" (invited feature article), *Nanoscale*, in press.

3. S. Nanot, E. H. Hároz, J.-H. Kim, R. H. Hauge, and J. Kono, "Optoelectronic Properties of Single-Wall Carbon Nanotubes" (invited review article), *Advanced Materials* **24**, 4977 (2012).

4. B. Dan, A. W. K. Ma, E. H. Hároz, J. Kono, and M. Pasquali, "Nematic Like Alignment in Transparent Conductive Single-Walled Carbon Nanotube Thin Films from Aqueous Colloidal Suspensions," *Industrial & Engineering Chemistry Research* **51**, 10232 (2012).

5. W. D. Rice, R. T. Weber, A. D. Leonard, J. M. Tour, P. Nikolaev, S. Arepalli, V. Burka, A.-L. Tsai, and J. Kono, "Enhancement of the Electron Spin Resonance of Single-Walled Carbon Nanotubes by Oxygen Removal," *ACS Nano* **6**, 2165 (2012).

6. E. H. Hároz, J. G. Duque, B. Y. Lu, P. Nikolaev, S. Arepalli, R. H. Hauge, S. K. Doorn, and J. Kono, "The Unique Origin of Colors of Armchair Carbon Nanotubes," *Journal of the American Chemical Society* **134**, 4461 (2012).

7. E. H. Hároz, J. G. Duque, W. D. Rice, C. G. Densmore, J. Kono, and S. K. Doorn, "Resonant Raman Spectroscopy of Armchair Carbon Nanotubes: Absence of Broad G^- Peak," *Physical Review B Rapid Communications* **84**, 121403R (2011).

Presentations:

1. "Light Absorption in Metallic Carbon Nanotubes: UV to THz," *221st Meeting of the Electrochemical Society*, Seattle, Washington, USA, May 6-11, 2012.

2. "Enrichment of Armchair Carbon Nanotubes via Density Gradient Ultracentrifugation: Raman Population Mapping," *Rice Quantum Institute Symposium*, Rice University, Houston, TX, USA, August 5, 2011.

3. "Spectroscopy of Metallic Carbon Nanotubes," *219th Meeting of the Electrochemical Society*, Montreal, Quebec, Canada, May 1-5, 2011.

4. "The Colors of Armchair Carbon Nanotubes," *15th International Conference on Modulated Semiconductor Structures (MSS 15)*, Tallahassee, Florida, USA, July 25-29, 2011.

5. "Resonant Raman Scattering of Armchair Carbon Nanotubes: Absence of "Metallic" Signature," *March Meeting of the American Physical Society*, Dallas, TX, USA, March 21-25, 2011.

Degrees Awarded:

1. William D. Rice, Ph.D., May 2012, "Low-Energy Charge and Spin Dynamics in Quantum Confined Systems"
2. Erik H. Hároz, M.S., December 2012, "Curvature Effects in the Optical Transitions of Single-Wall Carbon Nanotubes"

Q.2.2.5. Pasquali Group

Contributors:
Natnael Behabtu
Colin Young
Tiffany Li-Ling
Vishnu Kumar
Shannon Eichmann
Dmitri Tsentalovich
Matteo Pasquali

SWNT Length and Chirality Separations (2011):

The goal of this study was to separate metallic and semiconducting HiPco SWNTs by tuning the protonation of the SWNTs in superacid solutions. Since metallic SWNTs are more strongly protonated by superacids than semiconducting SWNTs, at a critical acid strength semiconductors form a liquid crystalline phase, while metallics will remain predominantly in the isotropic phase. The two phases can then be separated by centrifugation. We determined that after quenching SWNTs from acid, it is possible to redisperse the SWNTs in aqueous surfactant solutions to measure their fluorescence in order to characterize whether the separation procedure was effective. Because longer CNTs transition into a liquid crystalline phase at lower concentrations and can crash out of solution when the solvent quality is changed, SWNT samples that are monodisperse in length are required to separate metallics from semiconductors with superacids. Therefore, a necessary first step of this study was to demonstrate a method to separate SWNTs by length. We attempted to use a column packed with 10 μm diameter silica particles to separate SWNTs by length with size-exclusion chromatography. However, the acid did not elute at all from the column as the pore size in the column was too small, even when pressure was applied with a syringe pump. In the future, the pore size of the column can be tuned by using polydisperse samples of larger beads to provide a variety of pore sizes for the acid to flow through. After obtaining a SWNT sample that is monodisperse in length, we will disperse the SWNTs in superacids of varying strength to separate the metallics from the semiconductors.

Q.2.2.6. Tour Group

The goal of our research was to pursue the synthesis of multifunctional fibers using graphene nanoribbons or graphene oxide. The fiber spinning goal of this project has been reached, producing fibers with promising mechanical performance. The next step is high temperature

annealing (over 2000 °C) to convert these highly aligned graphene layers into graphitic structures.

General description and research achievements
We were able to show that graphene oxide nanoribbons (GONRs) are advanced precursors for making carbon fibers, by subjecting GONR fibers to 1600 °C treatments to achieve comparable mechanical performance as commercial carbon fibers for general purpose applications. In addition, we were also able to make highly aligned graphene oxide (GO) fibers by applying a drawing force during the spinning process. A record high tensile modulus was obtained from these highly aligned as-spun GO fibers.

We also made conductive graphene nanoribbon-coated Kevlar fiber; this multifunctional fiber has much better flexibility as compared to commercial carbon fibers, which makes it a viable component in applications such as wearable electronics and in conductive wires for LED arrays.

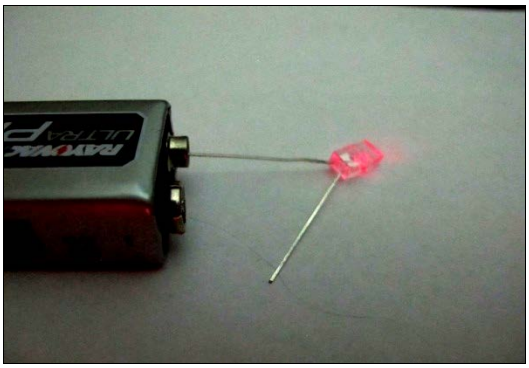

Figure 61. Graphene Nanoribbon fiber attached to rightmost connection of LED

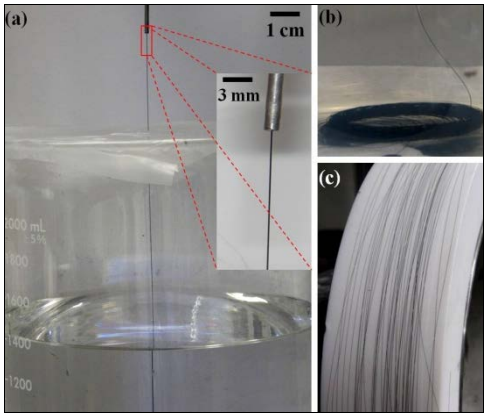

Figure 62. Graphene nanoribbon: a) exiting spinner and entering quenching bath; b) coiling at bottom of bath; c) rolled up on drum

Publications:

1. Xiang, C.; Lu, W.; Zhu, Y.; Sun, Z.; Yan, Z.; Hwang, C. "Carbon Nanotube and Graphene Nanoribbon-Coated Conductive Kevlar Fibers" ACS Appl. Mater. Interfaces 2012, 4, 131–136.

2. Xiang, C.; Behabtu, N.; Liu, Y.; Han, C.; Young, C.; Genorio, B.; Tsentalovich, D.; Kosynkin, D.; Lomeda, J.; Kumar, S.; Pasquali, M.; Tour, J. M. "Graphene Nanoribbons as an

Advanced Precursor for Making Carbon Fiber" ACS Nano submitted and in final revision.

3. Xiang, C; Young, C.; Wang, X.; Yan, Z.; Hwang, C.; Ceriotti, G.; Lin, J.; Pasquali, M.; Tour, J.M. "Highly Aligned Graphene Oxide Fibers and Its Unconventional Knot Efficiency" in preparation.

Collaborations:
Prof. Matteo Pasquali (Rice) and Prof. Satish Kumar (Georgia Tech) groups.

Q.2.2.7. Wong Group

Group members involved:
Prof. Michael S. Wong
Varun Shenoy Gangoli
Juyan Azhang (Undergrad, not funded by AQW)
Taryn T. Willett (Undergrad, not funded by AQW)
Sean A. Gelwick (Summer visiting student working on separations, funded by AQW)

Selective SWNT Growth using Growth Modulators

Work goal was to identify catalyst "poisons" in order to selectively poison growth of non-armchair SWNTs. We identified selenium, sulfur and phosphorous as potential growth modulators of SWNT growth from Fe catalyst. The term "poison" is improper here in that we do not poison SWNT growth and so the term "growth modulator" is to be used henceforth. We demonstrated the effect of Se and P on SWNTs grown from Fe catalyst in the Barron reactor. This was done by using controlled amounts of Se in TOP (Trioctyl phosphene) and also just TOP to see effect of just P. We were able to achieve localized growth based on location of growth modulator, i.e., SWNTs grew as usual where the growth modulator was not applied and grew selectively where it was applied. The selectively grown SWNTs were nearly double in average length as compared to the control. However, chiral selectivity could not be tested owing to limitations in growth reactor and the need for a new dedicated CVD system was recognized. We therefore planned and constructed a new CVD system capable of vertically aligned nanotube array (VANTA) growth. We demonstrated VANTA growth from Fe catalyst with and without Se. The growth substrates were from Benji Maruyama's group at AFRL of the type Fe/Al2O3/Si and Se was incorporated in controlled amounts using octadecene (ODE) as a carrier which in itself does not influence SWNT growth.

Scale-up of SWNT growth

New CVD system built uses C_2H_4 as the carbon source at atmospheric conditions, making this highly conducive for scale-up. We are able to produce ~400 $\mu g/cm^2$ substrate/h of growth.

Summer 2011 and beyond -Metal/Semiconductor SWNT separation from Agarose Gel Column Chromatography

- Developed a 3-step separation protocol for separating metal and semiconductor enriched samples
- Sodium dodecylsulfate elutes out metals, nonionic surfactants such as Pluronics and Tetronics elute out semiconductors and sodium deoxycholate elutes out the rest of the SWNTs from the agarose column

- Separation successfully demonstrated to work across various SWNT sources such as HiPco and laser ablation SWNTs
- Metal enriched HiPco sample ~75-80% pure, metal enriched laser ablation sample ~85-90% pure
- Semiconductor enriched HiPco sample ~92-97% pure, semiconductor enriched laser ablation sample ~85-90% pure

Patent filed:
- Method to produce highly enriched semiconductor single wall carbon nanotubes (2012).

Publication:
- Journal article: V.S. Gangoli et al., "Chromatographic Production of Semiconductor-type Carbon Nanotubes by using Nonionic Surfactants", *J. Nanoparticle Res.*, 2013 (Under review).

Presentations:
- Conference talk: V.S. Gangoli et al., "Using Nonionic Surfactants for improved Semiconductor Enrichment of Single Wall Carbon Nanotubes from Agarose Gel Column Chromatography", ACS National Meeting and Expo, Spring 2012- San Diego.

Posters presented :
- Optimizing Column Chromatography Separation of Metallic/Semiconductor Single Wall Carbon Nanotubes (J. Azhang et al., Rice Quantum Institute Symposium, 2011).
- Using Nonionic Surfactants Towards Highly Enriched Semiconductor SWNTS By Agarose Gel Column Chromatography (T.T. Willet et al., Rice Undergraduate Research Symposium, 2012).
- Using Nonionic Surfactants for improved Semiconductor Enrichment of Single Wall Carbon Nanotubes from Agarose Gel Column Chromatography (V.S. Gangoli et al., Transatlantic Science Week, 2012).
- Demonstrating efficient Metal/Semiconductor separation of various types of Single Wall Carbon Nanotubes Using Agarose Gel Column Chromatography (J. Azhang et al., Rice Undergraduate Research Symposium, 2012).

Q.2.2.8. Yakobson Group
Boris I. Yakobson, Fangbo Xu, and Arta Sadrzadeh

Quantum Conductance Computations:
We derived and coded an algorithm which computes the position-resolved current on individual atomic sites so as to visualize the current distribution of any given atomistic structure, and calculate the associated magnetic field more efficiently than conventional methods. As both a test and important physics phenomenon study, we applied this algorithm to graphite screw dislocation and therefore revealed its considerably high inductance and Q-factor as a promising nanoscale electronic device. (Manuscript ready for submission [1].)

Further, we computed and visualized the current distribution across the junctions (Figure 63) of two armchair nanotubes, and found and explained the two coexisting oscillating behaviors of

conductance of a single junction as the junction length increases. We also investigated the conducting properties of junctions constituted by metallic armchair and/or zigzag nanotubes (Figure 64). (Manuscript ready for submission [2].)

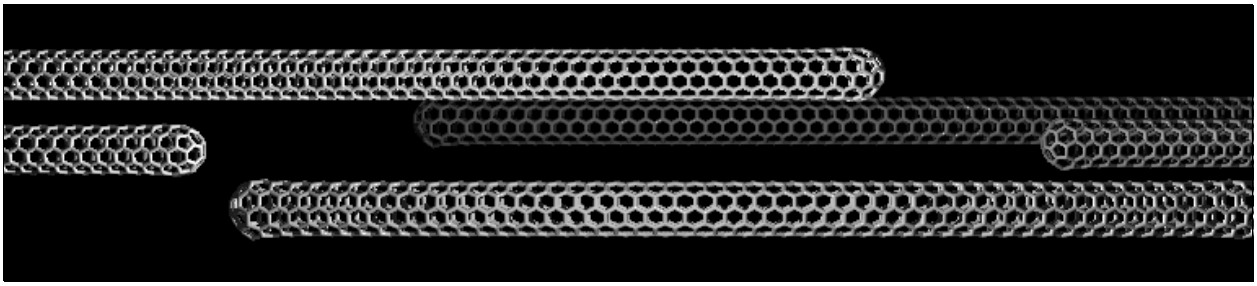

Figure 63. Current Distribution Across the Junctions of Two Armchair Nanotubes

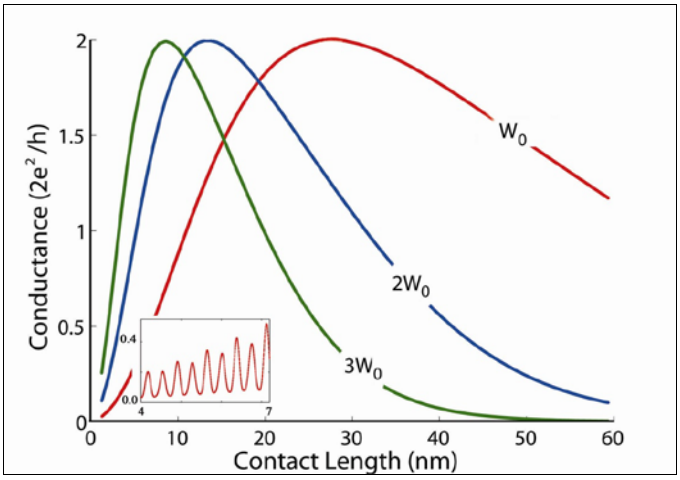

Figure 64. Conducting Properties of Junctions Constituted by Metallic Armchair and/or Zigzag Nanotubes

We developed a full open-source package which computes electronic structure and conductance of atomistic systems with helical symmetry. The code works for conventional translational symmetry as well. With this package we studied the electronic properties of twisted graphene nanoribbons and had it published [3].

There are also another two aspects in which we spent time but no valuable outcome; listed here for completeness:

AC conductance: we derived and coded an algorithm for calculation of quantum AC conductance of any given atomistic structure under alternating voltages. By this approach we revealed the stability of conductance in a carbon nanotube with respect to varying frequency up to GHz, and also investigated the AC electron transport in various junctions of nanotubes or nanoribbons.

Doping of nanotubes: we derived and coded an algorithm for calculation of quantum AC conductance of any given atomistic structure under alternating voltages. By this approach we revealed the stability of conductance in a carbon nanotube with respect to varying frequency up

to GHz, and also investigated the AC electron transport in various junctions of nanotubes or nanoribbons.

Percolation Assessment
We also proposed a lattice structure to model the most close-packing nanotube bundle (Figure 65), and proposed and coded a more efficient algorithm for searching for the percolation threshold. We not only worked out the percolation threshold of infinite lattice structure, but also obtained and verified the formula for the percolation threshold as a function of the diameter and length of the nanotube bundle. (Manuscript In preparation)

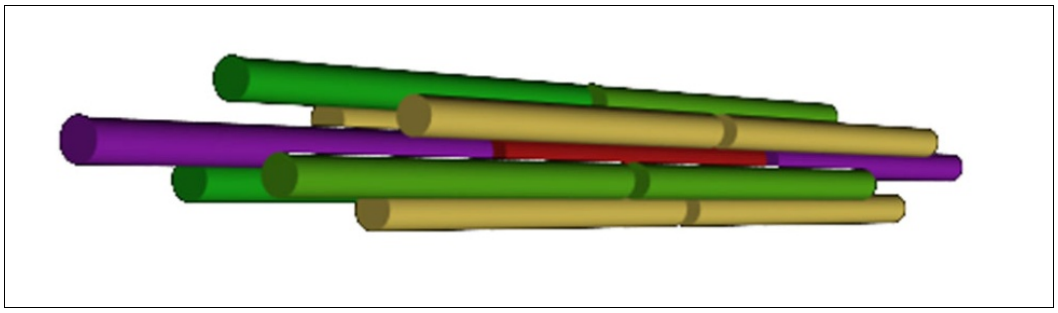

Figure 65. Lattice Structure to Model the Most Close-Packing Nanotube Bundle

Theory of CNT growth, with the emphasis on chiral selectivity
Here the first breakthrough was the dislocation-growth theory and its prediction that the abundance of tubes type must be proportional to their chiral angles. Indeed, the periodic makeup of carbon nanotubes suggests that their formation should obey the principles established for crystals. Nevertheless, this important connection remained elusive for decades and no theoretical regularities in the rates and product type distribution have been found. Here we contend that any nanotube can be viewed as having a screw dislocation along the axis. Consequently, its growth rate is shown to be proportional to the Burgers vector of such dislocation and therefore to the chiral angle of the tube. This is corroborated by the ab initio energy calculations, and agrees surprisingly well with diverse experimental measurements, which shows that the revealed kinetic mechanism and the deduced predictions are remarkably robust across the broad base of factual data [5].

Further collaboration with French researchers also revealed apparent CNT rotation which also requires step-kink (dislocation) growth mechanism for explanation of the facts [6].

Important theoretical step was in finding a way to compute the graphene edge energy at arbitrary slanted angle. This is exact analog of chirality in the CNT and therefore important for prediction the chiral selection at nucleation stage. The energy of an arbitrary graphene edge, from armchair (A) to zigzag (Z) orientation, is derived in analytical form. It contains a ‘‘chemical phase shift’’ determined by the chemical conditions at the edge. Direct atomistic computations support the universal nature of the relationship, definitive for graphene formation, and shapes of the voids or ribbons. It has further profound implications for nanotube chirality selection and possibly control by chemical means, at the nucleation stage [7].

Latest important collaborative work (with AFRL) provided direct evidence for chirality controlling growth rate. Chiral-selective growth of SWNTs remains a great challenge that hinders their use in applications such as electronics and medicine. Recent experimental and theoretical reports have begun to address this problem by suggesting that selectivity may be achieved during nucleation by changing the catalyst composition or structure. Nevertheless, to establish a rational basis for chiral-selective synthesis, the underlying mechanisms governing nucleation, growth, and termination of SWNTs must be better understood. To this end, we report the first measurements of growth rates of individual SWNTs through in situ Raman spectroscopy and correlate them with their chiral angles. Our results show that the growth rates are directly proportional to the chiral angles, in agreement with recent theoretical predictions. Importantly, the evidence singles out the growth stage as responsible for the chiral distribution—distinct from nucleation and termination which might also affect the final product distribution. Our results suggest a route to chiral-selective synthesis of SWNTs through rational synthetic design strategies based on kinetic control [8].

Publications:

1. F. Xu, A. Sadrzadeh and B.I. Yakobson, Graphite Solenoid: A Promising Nanoscale Inductor

2. Sadrzadeh, F. Xu, Z. Xu, and B.I. Yakobson, XTRANS: Transport in Nano-Scale Devices and Implementation of Helical Symmetry, Current Density and Inductance Calculation.

3. A. Sadrzadeh, M. Hua, and B.I. Yakobson, *Electronic properties of twisted armchair graphene nanoribbons*, Appl. Phys. Lett. 99, 013102 (2011).

4. F. Xu, A. Sadrzadeh, Z. Xu, and B.I. Yakobson, Contact Resistance in Carbon Nanotube based Conducting Wires.

5. "Dislocation theory of chirality-controlled nanotube growth", F. Ding, A.R. Harutyunyan, and B. I. Yakobson, Proc. Natl. Acad. Sci., 106, 2506-2509 (2009). -- Cover Article.

6. "Growing a carbon nanotube atom by atom: 'And yet it does turn'", M. Marchand, C. Journet, D. Guillot, J.-M. Benoit, B. I. Yakobson, and S.T. Purcell, Nano Lett., 9, 2961-2966 (2009).

7. "Graphene edge from A to Z—and the origins of nanotube chirality", Y. Liu, A. Dobrinsky, and B.I. Yakobson, Phys. Rev. Lett. 105, 235502 (2010).

8. "In situ evidence for chirality-dependent growth rates of individual carbon nanotubes", R. Rao, T. Cherukuri, B.I. Yakobson, and B. Maruyama, Nature Materials, 11, 213-216 (2012).

Length and diameter effects:

We have continued efforts in understanding the fundamentals of lateral load transfer, and consequently how the length of the CNT-segments determines and limits the overall expacted strength of the AQW-assembly. The Figure 66 shows the schematic of the capillary and traction force distribution, and the resulting overall cable-strength S relaticve to the ideal strength of a constituent sebment S_i, as a function of segments length L/d (relative to their diametr d ~ 1-2 nm).

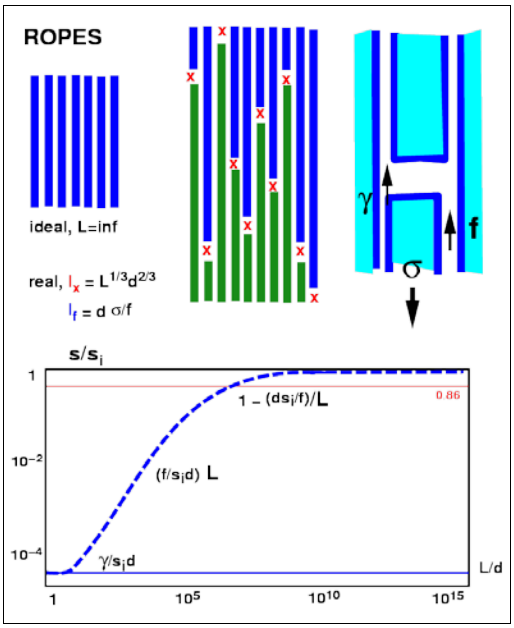

Figure 66. Schematic of the Capillary and Traction Force Distribution, and the Resulting Overall Cable-Strength

An important study within the recent period was concerned with the diameter role on stability of individual CNT, and how it determines the CNT collapse-flattening, essentially into a bilayer graphene ribbons. The Figure 67 shows the result of computations for (a) uncollapsed and collapsed SWNTs with different diameters in free space generated by LAMMPS molecular dynamics simulation. The geometry of a collapsed SWNT consists of two highly strained bulbs on the two edges and a collapsed region where the two opposing walls are flattened and stabilized due to the Van der Waals interaction, leaving the interlayer distance as 3.4 Å. The heights of the two edged bulbs are found to be a constant around 4.9 Å independent of initial diameter of the nanotube. The height of the bulb is comparable in size to C_{60} molecular, as is shown. (b) The linear relationships between measured width (W) and original cylindrical diameter (D) for uncollapsed and collapsed structures in free space ((SWNT, DWCNT), (CE2GNR) and (CE4GNR)) and on a substrate ((SWNT on substrate) and (CE2GNR on substrate)) are shown by the straight lines and their corresponding equations. For simple comparison, a conversion equation of $W=\pi D/2$ is given if the formation of highly strained bulbs is not taken into account. Details are in the paper [9], collaborative with other co-PIs (Hauge, Tour, Colvin).

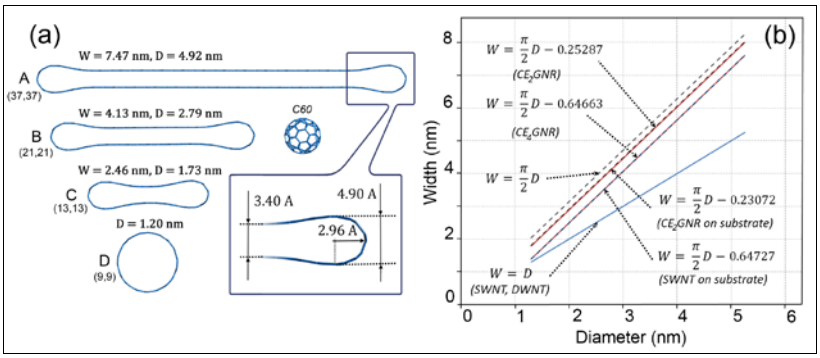

Figure 67. Result of Computations for (a) Uncollapsed and Collapsed SWNTs with Different Diameters in Free Space Generated by LAMMPS Molecular Dynamics Simulation, and (b) the Linear Relationships Between Measured Width and Original Cylindrical Diameter for Uncollapsed and Collapsed Structures in Free Space

Publications:

1. "Atomistic Theory of Mechanical Relaxation in Fullerene Nanotubes", B.I.Yakobson, G.Samsonidze, G.G.Samsonidze, Carbon 38, 1675 (2000). Presently further developed.

2. "Closed-edged graphene nanoribbons from large diameter collapsed nanotubes", Ch. Zhang, K. Bets, S.-S. Lee, V. Colvin, B.I. Yakobson, J. Tour, and R. Hauge, ACS Nano, in press (2012).

Q.2.2.9. Carter Kittrell – Research Scientist:

This aim involved CVD system construction projects and constructing tunable resonance Raman spectrometer.

Four major projects:

1. Redesigning and upgrading a general purpose CVD system for Jim Tour's graphene growth. This has been highly productive for nearly two years. Reference (Youtube cookie growth)

2. Construction of a new CVD system, emphasizing the highest purity, and capable of annealing the copper substrate at two atmospheres absolute at 1050C. This has proved crucial for growth of large single domain graphene sheets.

3. Constructing a new CVD system from scratch for Mike Wong, as described in th Wong Group section. The purpose was growth of CNT with partially poisoned catalyst particles to control diameter and chirality.

4. Constructing a tunable laser resonance Raman spectrometer for positive identification of metallic SWNT chirality.

1. CVD system (with Jim Tour):

The primary goal of this CVD apparatus is ultra-low oxygen contamination, and easy, swapping of the quartz tube to allow for rapid succession of multiple users with different growth methods, including doping the sample with boron or nitrogen by atom substitution. Since deposits in the quartz tube proved the biggest cause of cross-contamination, designing for one minute removal/installation reliably leak free allows for cleaning or switching furnace tubes. High purity gas filters on all gas supplies are incorporated to minimize contamination from oxygen and are fitted with electronic flow controllers. A bubbler system provided volatile nitrogen containing compounds for atom substitution. The vacuum system incorporates liquid nitrogen

and metal wool oil traps, in addition to a modified vacuum pump to minimize oil volatility.

2. Annealing system (with Jim Tour):
This is a new system similar to the CVD system except with the emphasis on maintaining the highest purity and zero contamination. Only inert gases and hydrogen are used, to avoid any contamination of samples being annealed. Samples can be annealed to 1100C under inert or reducing conditions. It also has a high quality vacuum system, electronic flow controllers and Baratron pressure gauges.

3. CVD system (with Mike Wong):
The new CVD system is very versatile, with four gas flow channels and one vapor channel that uses a fritted bubbler to introduce vapor into a carrier gas from a volatile liquid. This approach, rather than having simple evaporation from the neat liquid, allows operating at up to atmospheric pressure and provides a highly reproducible concentration of vapor. The combination of a temperature regulated bath and flow controlled dilution stream provides essentially any desired concentration of the vapor. The gas supply bottles are fitted with oxygen scrubbers, and heated transfer lines to degas moisture and any other contaminants. The supply system with 5 electronic flow controllers is connected to a welded manifold with hard metal seal VCR fittings. A custom design input connector to the 25 mm quartz tube eliminates chipping that often plagues quartz tube CVD systems. In addition to the gas inlet port, it has a port for a movable thermocouple, which allows checking the temperature inside the quartz tube, and at multiple locations, rather than the temperature of the external furnace heater. The exhaust has a custom modified fitting also designed to prevent chipping of the quartz tube. Electronic Baratron pressure gauges monitor pressures from 0.1 mTorr to 1000 Torr. A downstream bubbler may be valved into the exhaust line to provide a scrubber for sulfur or selenium containing compounds that may be used to poison the catalyst.

4. Tunable laser resonance Raman spectrometer (Carter Kittrell with Jun Kono):
This system has been constructed to use a tunable dye laser for the excitation source. Since SWNTs have relatively narrow absorption bands, it is necessary to tune the excitation source to the peak for any particular SWNT chirality. In particular, most of the armchair SWNTs do not correspond to the standard commercial Raman instruments, and hence are essentially invisible, and cannot be observed by either fluorescence or Raman detection, and overlapping absorption bands of families of the metallic SWNTs, and higher excitations of the semiconductor SWNTs often yield ambiguous results. Hence there is no other simple method to characterize an armchair separated sample.

Dye laser excitation sources are an Nd:YAG laser frequency doubled to 532 nm, and an argon ion laser. The ring dye laser produces sub-wavenumber linewidths. Recently, a second dye laser was assembled by combining components from old dye lasers. This is important, due to the limited tuning range of any one dye. By having a second dye laser, two different families from one sample, such as one green dye (8,8) family and one orange dye (9,9) family, can be explored without needing to change dyes or optics, which considerably increases the versatility of the instrument. The Raman scattering from the SWNT sample passes into a double grating spectrometer fitted with an astronomical-type CCD camera, thermoelectrically cooled to -90C for very low noise. The instrument linewidth is a wavenumber, compared to typical 5

wavenumber resolution of commercial systems. Hence the highest resolution is available, and is always sample limited, not instrument limited. One drawback to this approach is the very high dispersion used to limit the observable range to about 70 wavenumbers. Although the grating could be repositioned for any Raman shift frequency, collecting in such multiple steps was tedious and made amplitude comparisons more difficult. The spectrometer was modified by adding a demagnifying telescope in front of the CCD camera, which doubled the observing range to 160 wavenumbers, without any reduction in the sub-wavenumber instrument resolution.

In addition, tunability provides Raman excitation profiles for positive identification of chirality, and optimizing excitation wavelengths for the particular chirality. This adds a second adjustable experimental parameter so that when the Raman emission of two chiralities overlap, they may be distinguished by using different excitation wavelengths, and the relative intensities of adjacent Raman lines will move up or down. Combined with the highest resolution, this provides positive identification of individual chirality.

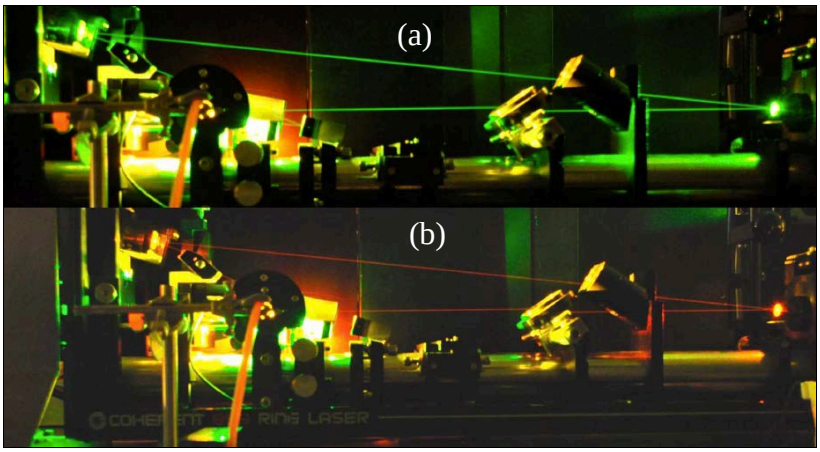

Figure 68. Narrow Bandwidth Tunable Ring Dye Laser: (a) Operating at the Shortest Wavelength of the Dye, (b) Operating at the Longest Wavelength of the Dye

The orange tube to left of center rising up from the pump below contains the rhodamine 6G dye. The output is attenuated to a constant 100 mW for all wavelengths, and scatters from the SWNT into the spectrometer, out of view to the right of the picture.

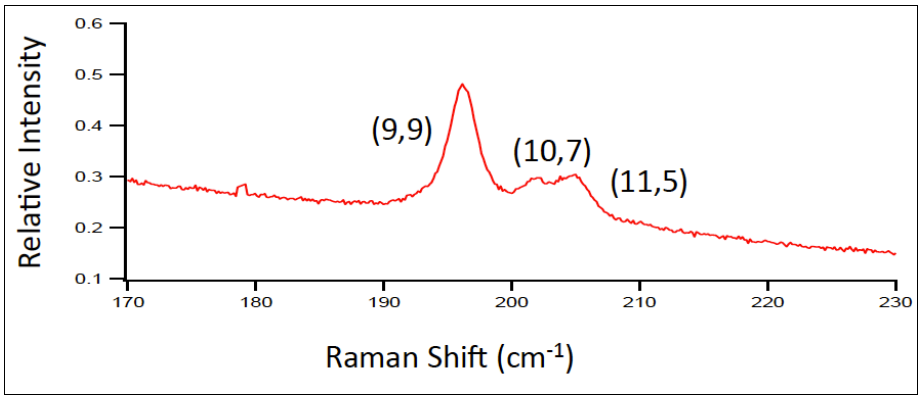

Figure 69. Conventional Raman Emission Spectrum with dye laser tuned to 596 nm, or 2.08eV, near the peak of (9,9) absorption band. This enhances the (9,9) intensity of the DGU enriched sample.

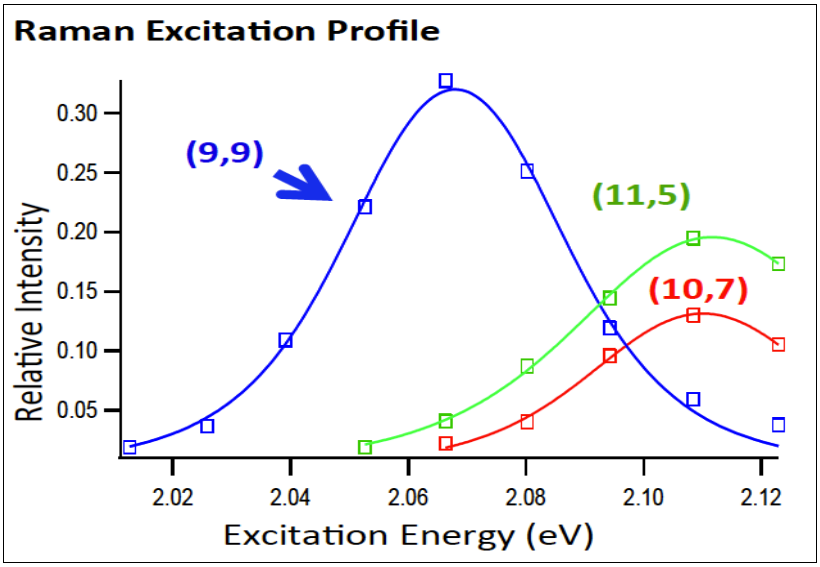

Figure 70.Raman Excitation Profiles

These REPs were obtained by changing the dye laser wavelength and measuring the Raman amplitude for each of three Raman emitting species. In each case, the laser power was adjusted to be about 100 mW, and measured to be sure that all intensities were normalized. The width of the REP for the (9,9) armchair is the narrower than any reported in the literature, showing that this system has the ability to provide a sample-limited profile linewidth, that is likely to represent homogeneous broadening, and hence provides a measure of the excited state lifetime of the (9,9) armchair, as well as that of the (11,5) and the (10,7). The fits are remarkably good, showing the inherent stability of this system of obtaining REPs.

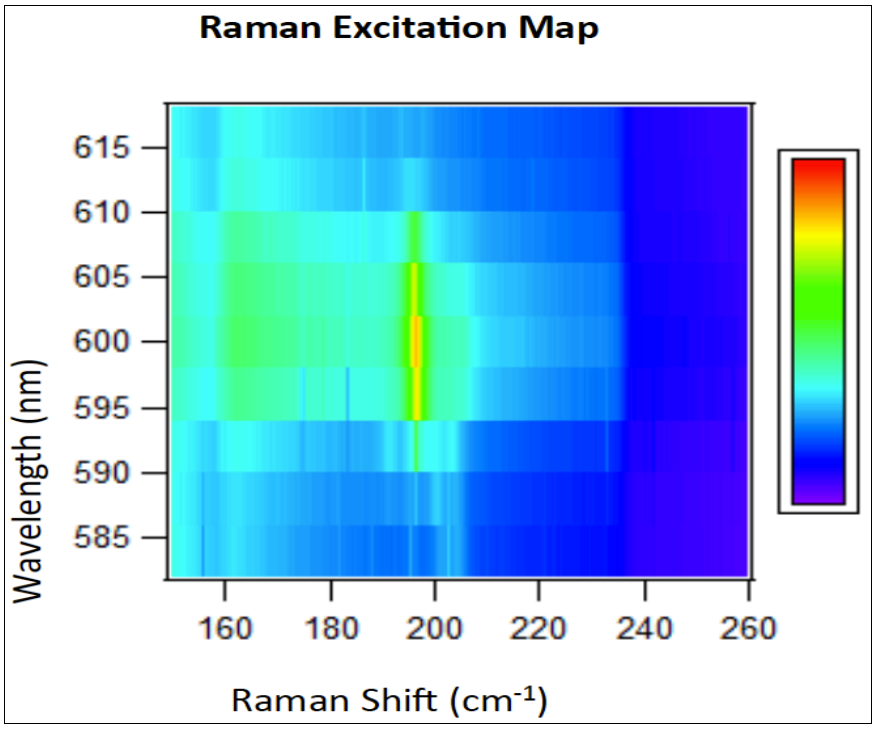

Figure 71. Raman excitation map which provides a 3D plot of the excitation profile, with color representing the intensity at every point in the 2D excitation-emission matrix.

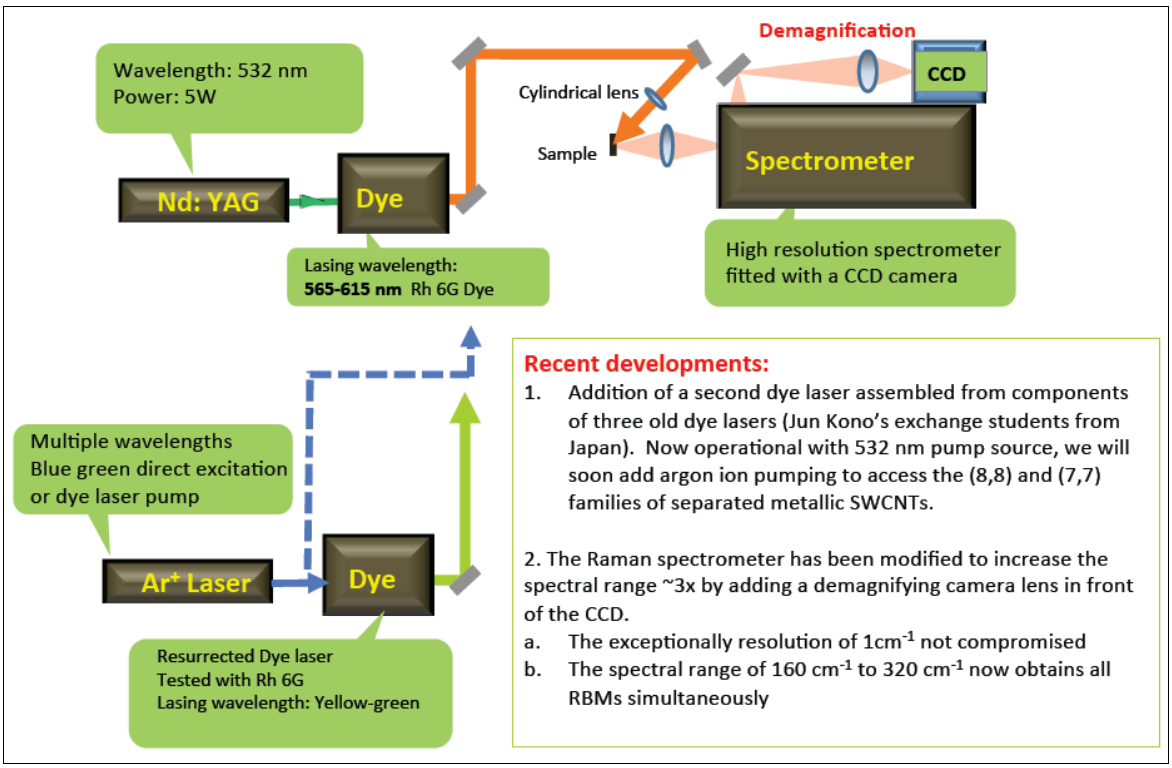

Figure 72. Schematic of the Tunable Laser Raman System

Figure 72 shows the newly added 2x demagnification in front of the CCD camera and provides a sufficiently wide range that the radial breathing modes in the Raman emission spectrum can be captured in a single exposure of the CCD in a matter of seconds, without needing to change the position of the grating. The grating is moved when the dye laser wavelength is changed to again place the desired emission range on the CCD camera.

Presentation:

- Alice Jeng[1], H. Sugahara[2], P. Yu[3], C. Kittrell[4], E. Haroz[5], J. Kono[5], Population Analysis of Different Chiralities in the (8,8) & (9,9) Families in Armchair-"Enriched Single-Walled Carbon Nanotube Samples via Resonant Raman Spectroscopy".

Rice University Summer Research Colloquium, August 11, 2011:

1. NanoJapan Program, Rice University and Department of Chemical Engineering, University of Oklahoma (alice.jeng@ou.edu)
2. Department of Physics, Hokkaido University
3. University of North Texas
4. Department of Chemistry, Rice University
5. Department of Electrical & Computer Engineering, Rice University

Q.3. Conclusions

The goal is to develop a sample of metallic SWNTs with sufficient length, purity and concentration to spin a stable, aligned fiber. This team has produced a fibril from a 99% pure metallic sample. However, the fiber fell apart during conductivity testing, because the SWNTs were too short (Pasquali's group). Films made from a 99% sample were demonstrated to be structurally sound but not very conductive; they were non-aligned by its nature (Kono's group). All separation techniques, so far, have resulted in CNTs too short for well-aligned fibers (Kono, Wong, and Barron's groups).

Good alignment for strength and conductivity is critical. Currently no separation techniques appear to be very scalable yet. No selective-growth mechanism has been identified with confidence (Yakobson's group). Results seem to point toward pursuing amplification of short tubes (Barron's group), but possible routes still exist in acid-selectivity (Pasquali's group), or functionalization selectivity (Hauge's group). Strong fibers are being spun from as-produced SWNTs with good conductivity - close to copper by weight (Ajayan and Pasquali's groups). Progress in understanding how conductivity works has also been reported (Kono and Yakobson's groups).

Recommendations:

Longer, high quality nanotubes can be made available through HiPco synthesis, provided that work can be successfully completed on HiPco modifications. Scalable separations may be possible with either acid solubility or functional group solubility processes. The team feels that success is likely with further funding. Theory has greatly aided nucleation and growth research such that it is also believed possible to achieve chirality growth control with further research. Amplification growth from seeds has been demonstrated, but further research will be needed to demonstrate scalability.

LIST OF ACRONYMS, ABBREVIATION, AND SYMBOLS

Acronym	Definition
CONTACT	Consortium for Nanomaterials for Aerospace Commerce and Technology
AFRL	Air Force Research Laboratory
THz	Terahertz
ID	Identification
ISR	Intelligence, Surveillance, and Reconnaissance
NSMMS	National Space Missile Materials Symposium
UTPA	University of Texas at Pan American
UTB	University of Texas at Brownsville
HESTEC	Hispanic Engineering, Science and Technology Week
CNFs	Carbon Nanofibers
SEM	Scanning Electron Microscope
HRTEM	High Resolution Transmission Electron Microscope
GNRs	Graphene Nanoribbons
PVDF	Polyvinylidene Fluoride
P3HT	Poly-3-hexylythiophene
PEO	Polyethylene Oxide
PbS	Lead Sulphide
ITO	Indium-tin-oxide
SHPE	Society of Hispanic Professional Engineers
PCE	Power Conversion Efficiency
PREM	Partnership for Research and Education in Materials
FRA	Faculty Research Award
NEC	Nanoscale Engineering Concentration
QDs	Quantum Dots
THz	Terahertz
SWCNW	Single Wall Carbon Nano Wires
MMS	Method of Multiple Scales
ROM	Reduced Order Method
FDTD	Finite-Difference Time-Domain
Si-MR	Silicon Membrane Reflector
SLs	Superlattices
IR	Infrared
CIS	$CuInSe_2$
CNT	Carbon Nanotube
SAMs	Self Assembled Monolayers
OSC	Organic Solar Cells
CCL	Charge Collecting Layer
FTS	Fluoro-alkyl-trichlorosilanes

LIST OF ACRONYMS, ABBREVIATION, AND SYMBOLS Cont'd

Acronym	Definition
PCBM	[6,6]-phenyl-C61 Butyric Acid Methyl Ester
PEDOT:PSS	Poly(3,4-ethylenedioxythiophene):poly(4-syrenesulfonate)
OSC	Organic Solar Cell
CuPc	Copper Phthalocyanine
CN	Chloronapthalene
CB	Chlorobenzene
QE	Quantum Efficiency
PV	Photovoltaic
SCs	Solar Cells
SR	Spectral Response
IPCE	Incident Photon to Current Conversion Efficiency
OPV	Organic/Polymeric Photovoltaic
SWNT	Single Wall Carbon Nanotube
6FDA	2,4,6-trimethyl-1,3-hexafluoroisopropylidene Diphthalic Anhydride
DAM	2,4,6-trimethyl-1,3-phenylenediamine
DABA	3,5-diaminobenzoic Acid
NMP	1-methyl-2-pyrrolidinone
DMAc	Dimethylacetamide
PSCs	Polymer Solar Cells
BDT	Benzo [1,2-b: 4,5-b']dithiophene
V_{oc}	Open-Circuit Voltage
AQW	Armchair Quantum Wire
CFD	Computational Fluid Dynamics
DWNT	Double-wall Carbon Nanotube
R_j	Junction Resistance
T	Temperature
FIT	Fluctuation-Induced Tunneling
CCC	Current Carrying Capacity
T_{am}	Ambient Temperature
ΔT	Temperature Change
DGU	Density Gradient Ultracentrifugation
GONRs	Graphene Oxide Nanoribbons
GO	Graphene Oxide
VANTA	Vertically Aligned Nanotube Array
ODE	Octadecene